3-Deoxyanthocyanins : Chemical synthesis, structural transformations, affinity for metal ions and serum albumin, antioxidant activity

Sheiraz Al Bittar

ACADÉMIE D'AIX-MARSEILLE

UNIVERSITÉ D'AVIGNON

Ecole Doctorale 536 Agrosciences & Sciences

THESE

présentée pour l'obtention du

Diplôme de Doctorat

Spécialité: **chimie**

par

Sheiraz AL BITTAR

le 17 juin 2016

3-Deoxyanthocyanins : Chemical synthesis, structural transformations, affinity for metal ions and serum albumin, antioxidant activity

Composition du jury:

Victor DE FREITAS	Professeur Faculté des Sciences - Université de Porto	Rapporteur
Cédric SAUCIER	Professeur Faculté de Pharmacie - Université de Montpellier I	Rapporteur
Hélène FULCRAND	Directrice de Recherche à l'INRA Montpellier - SupAgro	Examinatrice
Olivier DANGLES	Professeur UFR STS - Université d'Avignon	Directeur de thèse
Nathalie MORA-SOUMILLE	Maître de Conférences UFR STS - Université d'Avignon	Co-Encadrante

A Alma & Jana…

Remerciements

Difficile d'être exhaustive dans ces remerciements tant les rencontres, échanges et soutiens ont été nombreux durant ces cinq années.

Tout d'abord, je tiens à remercier l'université d'Avignon pour m'accueillir dans ces locaux et de m'offrir le nécessaire pour acomplir ce travail.

Je remercie également l'université Al-Baath en Syrie pour la bourse d'étude qui m'a permis de venir en France et Campus Farnce pour l'accueil et la direction en France.

Toute ma gratitude va aux membres du jury Victor DE FREITAS, Cédric SAUCIER et Hélène FULCRAND d'avoir accepté d'évaluer ma thèse. Je remercie encore une fois Hélène FULCRAND tant que membre de mon comité de thèse, pour les discussions constructives et ses conseils pendant ma thèse.

Je tiens à remercier infiniment mon directeur de thèse Olivier DANGLES. Merci d'accepter de m'accueillir dans votre équipe sans me connaitre il y a 6 ans. J'ai eu beaucoup de chance d'être encadré par vous et de profiter de vos larges connaissances et compétences scientifiques. Merci pour votre patience infinie et votre disponibilité malgré vos larges occupations. Grâce à vous, ma petite famille est à mon côté en toute sécurité ce jour-ci. Votre positivisme contagieux m'a beaucoup aidée aux moments difficiles de la thèse même aux difficultés personnelles. Votre passion pour la science, vos capacités pédagogiques incroyables, votre efficacité et votre manière de voir toujours le bon côté des choses me seront une référence dans la vie.

Je remerie également ma co-encadrante de thèse Nathalie MORA-SOUMILLE qui m'a accompagné pas à pas au laboratoire. Merci de me passer tes connaissances et ton expérience en synthèse chimique. Merci de m'apprendre les vocabulaires chimiques ainsi que les citations connues en France. Ta disponibilité et ta présence à la paillasse m'aidé à m'adapter et d'avancer ainsi. Merci de nous accueillir chez toi seule et avec ma famille. Merci pour ta confiance et ton amitié.

Merci à notre équipe sur le site INRA pour votre accueil chaleureux pendant mes manips. Un merci spécial à Michèle LOONIS pour ta collaboration, ta disponibilité, ton efficacité, tes explications très enrichissant en analytiques.

Je tiens à remercier également Maxence ROSA pour les premiers résultats obtenus dans ce sujet, de ta disponibilité et tes discussions. Je remercie également tous les stagiaires : Nadia, Arno, Aurélia, Benjamin, Ketty et Mathieu et Siobhan qui ont participé à affiner les résultats de synthèse pendant leurs semaines de stages.

Un grand merci à l'équipe GREEN dirigé par Farid CHEMAT, Je vous remercie d'avoir m'accepter en Master 2 et de m'accueillir en stage au sein de votre équipe. Merci à Sandrine de m'encadrer pendant le stage, pour ton amitié et ton aide pour démarrer mon travail de recherche en France qui a abouti à mon premier article. Merci à Manu, Karine, Daniella, Céline et Tamara pour votre amitié dans les moments difficiles.

Je tiens à remercier l'équipe IBMM dirigé par Gregory DURAND pour m'accueillir avec mes échantillons RMN (qui ne finissent jamais). Je remercie également Ange Polidori pour son soutien et sa confiance. Merci à Simon pour ton bon humour et tonaide au laboratoire, à Stéphane pour tes explications et pour passer mes tubes RMN tard le soir.

Merci à Njara pour ta présence avec moi au laboratoire, tes réponses, tes regards positives et tes initiatives quand je pensais d'être seule. (La première à rencontrer ma famille à la gare TGV Avignon). Merci à Valérie pour ta présence au bureau pendant quatre ans, nos papotages ainsi que nos discussions scientifiques étaient enrichissant et parfois rassurantes. Merci à Cathy VIEILLESCASE pour votre confiance et votre soutien.

Merci à Aurélia, Marie, Gildas, Christophe et encore Stéphane. J'ai eu de la chance de partager avec vous le bureau, pour l'ambiance et les sorties restos. Merci à Salma pour ton amitié et pour l'entraide pendant la préparation des cours. Merci à Katérina, Sabiha, Amra pour votre amitié.

Merci à tous les amis qui m'ont soutenue pendant cette thèse. Merci à mes amies d'enfance Kinana, Rasha, vous êtes un trésor. Merci à mes collègues syriens qui ont gardé les contacts et les liens bien forts malgré la distance et la pression de la situation. Merci Wissam, Loubab, Ramia et Saeid.

Merci à tous les amis de tous les coins du monde que j'ai eu l'occasion et la chance de rencontrer durant mon séjour en France. Merci à Mounia, Mijou, Bassam pour les super-soirées libano-syriennes, j'ai de la chance de vous avoir à côté, vous étiez notre famille en France. Merci spécial à Zeid, mon cousin, pour ton amitié, ton aide quand j'étais seule, pour les petites sorties (mon bon voisin).

Un énorme merci à mes parents à qui j'ai confié mes filles pendant deux ans (C'était une grande responsabilité), ma sœur Shirin, mon beau-frère et mon ami d'étude Kamel pour votre accueil et votre soutien. Merci à ma belle-famille de m'encourager à prendre ce chemin même s'il paraissait impossible au début. Avec vous tous, je suis arrivée au bout.

Enfin, un grand merci aux plus chers à mon cœur Bahaa, de ton amour infini, de ta confiance, de supporter la distance et le stress de thèse et de me suivre à l'autre bout de monde. Mes deux bougies Alma et Jana, merci de me soutenir dans mon rêve même sans conscience, de comprendre mon départ quand vous avez besoins de moi, d'adapter une nouvelle vie pour rester à mes côtés, de supporter d'avoir une maman fatiguée, peu disponible et énervée parfois. Votre présence à côté de moi était mon énergie et ma motivation.

C'est grâce à vous trois que j'écris ces lignes. Je vous aime infiniment……

Sheiraz

Scientific communications

Publications:

S. Al Bittar, N. Mora, M. Loonis, O. Dangles

"Chemically synthesized glycosides of hydroxylated flavylium ions as suitable models of anthocyanins: binding to iron ions and human serum albumin, antioxidant activity in model gastric conditions"

Molecules, **2014**, *19*, 20709-20730.

S. Al Bittar, S. Périno-Issartier, O. Dangles, and F. Chemat,

"An innovative grape juice enriched in polyphenols by microwave-assisted extraction"

Food Chem., **2013**, *141*, 3268–3272.

V. Petrov, R. Gavara, O. Dangles, **S. Al Bittar**, N. Mora-Soumille, and F. Pina,

"Flash photolysis and stopped-flow UV-visible spectroscopy study of 3',4'-dihydroxy-7- O-β-D-glucopyranosyloxy-flavylium chloride, an anthocyanin analogue exhibiting efficient photochromic properties"

Photochem. Photobiol. Sci., **2013**, *12*, 576–581.

N. Mora-Soumille, **S. Al Bittar**, M. Rosa, and O. Dangles,

"Analogs of anthocyanins with a 3', 4'-dihydroxy substitution: Synthesis and investigation of their acid-base, hydration, metal binding and hydrogen-donating properties in aqueous solution"

Dyes & Pigments, **2012**, *96*, 7-15.

S. Al Bittar, N. Mora, M. Loonis, and O. Dangles

"A simple synthesis of 3-deoxyanthocyanidins and their O-glucosides"
Submitted (in revision)

Oral communications:

1. International Workshop of Anthocyanins IWA, 16-18 September **2015**, Montpellier, France

2. International Workshop of Anthocyanins IWA, 6-9 September **2013**, Proto, Portugal

3. Quatrième journée of Groupe Métabolites Secondaires (pole PHI), 28 mars **2013**, INRA, Avignon, France.

4. European Summer School sur les microondes et les ultrasons, 6-11 juin **2011**, Avignon, France.

Posters:

1. Journée TERSYS, le 12 Septembre **2013**, CERI, Avignon, France

2. International Congress of Green Extraction of Natural products, avril **2013**, Avignon, France.

3. Journée Franco-Italienne de Chimie (JFIC), le 16 -17 avril **2012**, Marseille, France

''Les hommes éprouvent une grande joie à la vue de couleur, l'œil en a besoin comme il a besoin de lumière.''

Goethe, 1810

Thesis Content

Général Introduction

Anthocyanins :

the colored polyphenols

Anthocyanins are a major flavonoids subclass widely distributed in the plant kingdom, some examples are presented in Figure 1. In Greek, *anthos* means a flower and *kyanos* means dark blue. Through proton transfer and interactions with metal ions and copigments, anthocyanins are able to change their color expression from red to blue. Moreover, they are present in various gymnosperms, ferns and some bryophytes [1]. They are responsible for the colors of beverages made from fruit, notably red wine, fruit juices and pink ciders (examples in Figure 2). In spite of their high water solubility, anthocyanins are commonly called 'pigments' in food and plant sciences ('pigment' is usually the term for non-soluble coloring agents in biology).

Figure 1. Anthocyanin-colored fruits and vegetables

Figure 2. Red to violet food bevereges made from fruits rich in anthocyanins.

These pigments mainly exist as aqueous solution in the vacuoles of plant cells although anthocyanin-based crystals have been also observed in plants (see image at right).

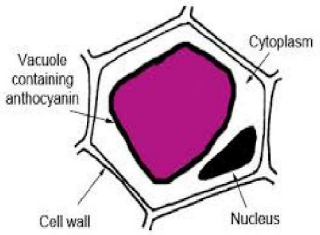

Anthocyanins are secondary metabolites in plants and have different roles due to their location. While anthocyanins display an attractive role in flower petals for better insect fecundation, bright red to blue pigments in berries are food indicator for birds and other animals. Anthocyanins are also protective agents against sunlight in green leaves. They become visible in autumn upon chlorophyll degradation (Figure 3).

Figure 3. Some of anthocyanins color roles in plant royal.

On the other hand, cereal pigments are phytoalexins, which accumulate after fungal infections, e.g. by *Colletotrichum sublineolum* [2][3]. At the site of fungal infection, reddish-brown pigments can be observed in the leaf epidermal cells. These compounds accumulate in intracellular insertion bodies, which migrate toward the site of fungal penetration and release their contents, killing both the fungus and the cells that synthesize them. As seen in the image at left, high concentrations of red pigments accumulate in the red and black sorghum brans [4][5]. A mass spectrometry identification of these colored phytoalexins showed that luteolinidin and apigeninidin are the major antifungal agents induced. For instance, a quantity of 70 µg/g fresh weight of luteolinidin was produced 72 hours after fungal inoculation of one-week-old seedlings [6].

1. Chemical structure of anthocyanins:

Anthocyanins have a C6-C3-C6 skeleton typical of flavonoids. More definitely, anthocyanins are glycosylated, polyhydroxylated and/or polymethoxylated derivatives of the 2-phenylbenzopyrylium cation (flavylium cation). The main part of anthocyanins is its aglycone, called anthocyanidin, which absorbs light around 500 nm due to extended π-conjugated system causing the pigments color recognition to human eye. This maximum absorption band shows a bathochromic effect (blue) when the solvent polarity decreases while a hypsochromic effect (orange) has been detected as the 3, 3' and 5' positions are glycosylated or methylated. Glycosylation of anthocyanidins enhances their water solubility and stability.

Today, 23 different anthocyanidins are identified in fruits and vegetables, only six of them are abundant: pelargonidin, cyanidin, peonidin, delphinidin, malvidin, and petunidin (see Figure 4). They differ in the number of hydroxyl and methoxyl groups on the B-ring of the flavylium cation [7]. Aglycones rarely exist in vivo while glycosides are ubiquitous in nature [8]. The most common sugar moiety is D-glucose and, less frequently, L-rhamnose, D-xylose, D-galactose, arabinose, and fructose as well as rutinose (6-*O*-α-L-rhamnosyl-D-glucose), sophorose (2-*O*-β-D-xylosyl-D-glucose), gentiobiose (6-*O*-β-D-glucosyl-D-glucose), sambubiose (2-*O*-β-D-xylosyl-D-glucose), xylosylrutinose, and glycosylrutinose [9]. Anthocyanins from flowers tend to have a higher degree of glycosylation and acylation compared to those derived from fruit and vegetables.

On the other hand, anthocyanins in cereals as sorghum, named 3-deoxyanthocyanins, are characterized by the lack of hydroxyl group at C3. In 1969, they were firstly identified in red sorghum by Nip and Brun [10]. They have planar structure due to a hydrogen bond between the oxygen atom in C-ring and some hydrogen atoms in B-ring [11].

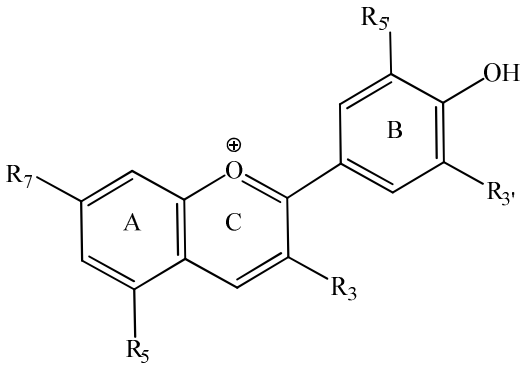

	Natural pigment	R_3	R_5	R_7	$R_{3'}$	$R_{5'}$
anthocyanidins	Cyanidin	OH	OH	OH	OH	H
	Pelargonidin	OH	OH	OH	H	H
	Peonidin	OH	OH	OH	OCH_3	H
	Malvidin	OH	OH	OH	OCH_3	OCH_3
	Delphinidin	OH	OH	OH	OH	OH
	Petunidin	OH	OH	OH	OCH_3	OH
3-deoxyanthocyani(di)ns	Apigeninidin	H	OH	OH	H	H
	Apigeninidin-5-*O*-glucoside	H	OGlc	OH	H	H
	7-*O*-Methylapigeninidin	H	OH	OCH_3	H	H
	7-*O*-Methylapigeninidin-5- *O*-glucoside	H	OGlc	OCH_3	H	H
	5-*O*-Methylapigeninidin	H	OCH_3	OH	H	H
	Luteolinidin	H	OH	OH	OH	H
	Luteolinidin-5- *O* -glucoside	H	OGlc	OH	OH	H
	5-*O*-Methylluteolinidin	H	OCH_3	OH	OH	H
	5- *O* -Methylluteolinidin-7- *O* -glucoside	H	OCH_3	OGlc	OH	H
	7- *O*-Methylluteolinidin	H	OH	OCH_3	OH	H

Figure 4. Chemical structure of natural anthocyanidins (R_3 = OH) and 3-deoxyanthocyani(di)ns (R_3 = H).

2. Anthocyanin biosynthesis:

The condensation of *p*-coumaroyl-Co-A with three malonyl-Co-A units represent the first step of flavonoid biosynthesis in cereals. It is first catalyzed by the enzyme of chalcone synthase (CHS), then, the chalcone thus formed is converted into the corresponding flavanone by chalcone isomerase (CHI). Next, a sequence catalyzed by dihydroflavonol reductase (DFR) and anthocyanidin synthase (ANS), with early or final hydroxylation catalyzed by flavonoid-3'-hydroxylase (F3'H), produces the 3-deoxyanthocyanidins; apigeninidin and luteolinidin.

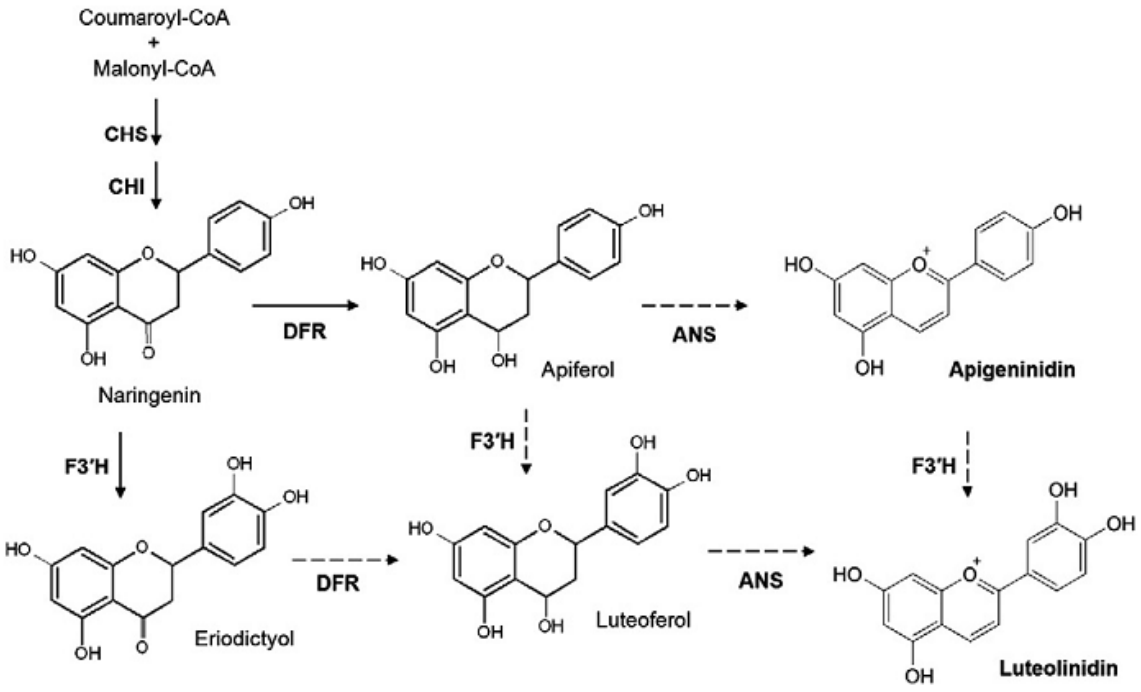

Scheme 1. Proposed biosynthesis of 3-deoxyanthocyanins ; CHS, chalcone synthase ; CHI , chalcone isomerase ; DFR, dihydroflavonol reductase ; ANS, anthocyanidin synthase ; F3'H, flavonoid-3'-hydroxylase [5].

Anthocyanidins biosynthesis described in scheme below, showed that they have common precursors and certain steps with 3-deoxyanthocyanidins. But, flavonoid-3-hydroxylase (F3H) represents the key enzyme shifting the biosynthesis from 3-deoxyanthocyanidins to anthocyanidins (Scheme 2).

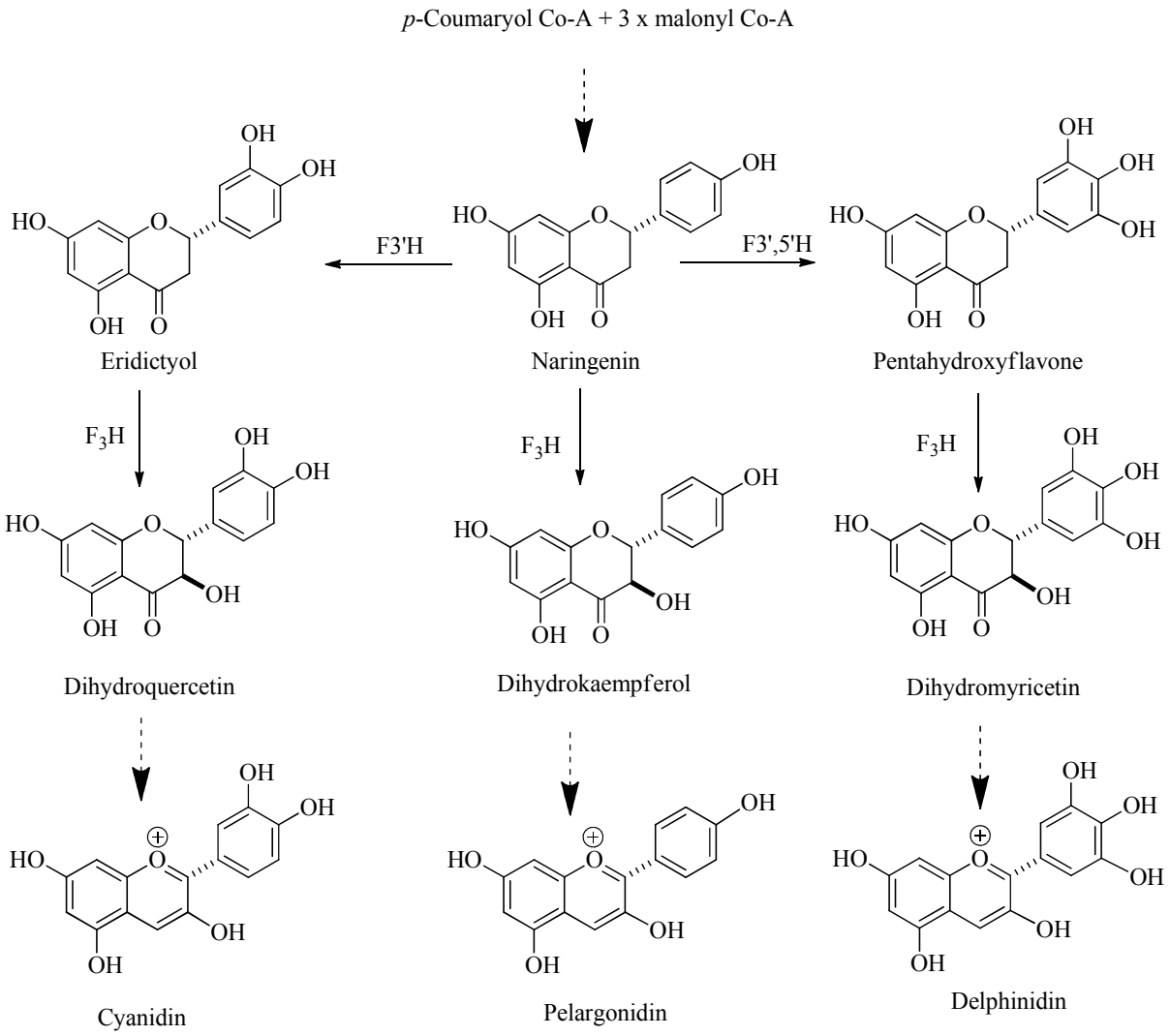

Scheme 2. Anthocyanidin biosynthesis and the key-role of flavonoid-3-hydroxylase (F3H), scheme inspired from [12].

Anthocyanin chemistry can be briefly explained trough next plan:

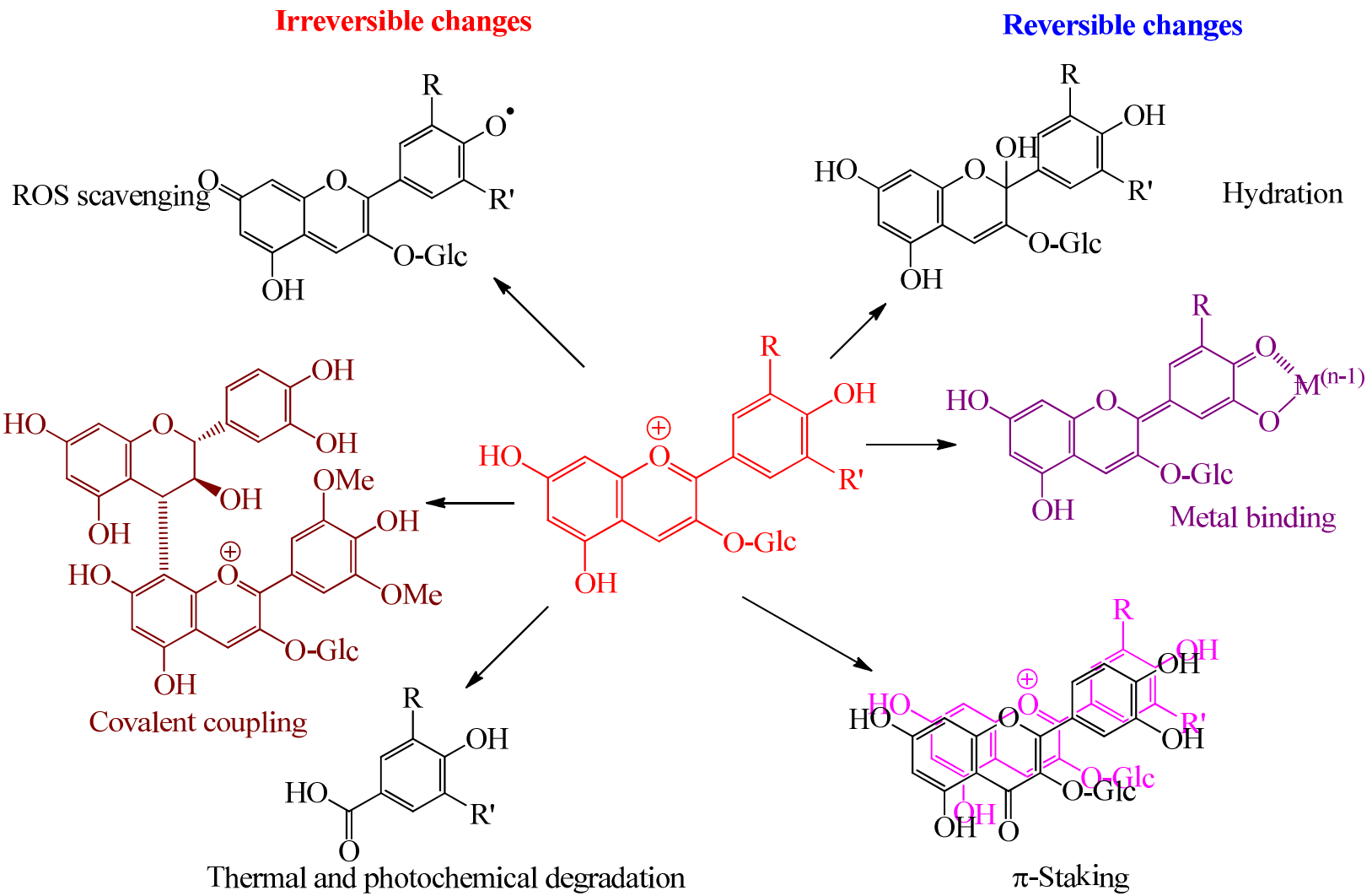
Irreversible changes
Reversible changes
ROS scavenging
Hydration
Metal binding
Covalent coupling
Thermal and photochemical degradation
π-Staking

3. The reversible chemistry of anthocyanins: the different equilibria in aqueous solution as a function of pH:

The pH value is a very important factor in anthocyanin stability; they are more stable in acidic media than in alkaline solutions [13]. According to the aqueous solutions acidity, anthocyanins exist as four main species (Scheme 3): the flavylium cation AH^+, the neutral and anionic quinonoidal bases A and A^-, the hemiketal B, and the *cis*- and *trans*-chalcones [8][14]. The red flavylium cation is the only form in a very acidic media (pH < 2). When the pH increases, the more the color intensity and the concentration of the flavylium cation decrease and the blue-violet quinonoidal form appears due to a rapid proton loss from the flavylium cation (microsecond timescale) (Figure 5). The flavylium cation also undergoes the nucleophilic attack of water at C2. The colorless hemiketal thus formed gives (by fast ring opening) the pale yellow *cis*-chalcone, in slow equilibrium with the corresponding *trans*-chalcone. The neutral quinonoidal bases are the main colored forms between pH 4 and 7 but their concentration is usually low as the hemiketal is more stable [15].

In equilibrated mildly acidic solution, the hemiketal is the major equilibrium form of common anthocyanins *vs.* *trans*-chalcone for 3-deoxyanthocyanins [16].

As mentioned before, the glucose moiety at C3-OH in anthocyanins enhances their color stability. Indeed, anthocyanidin chalcones are very prone to chemical degradation. 3-Deoxyanthocyanidins (*e.g.* luteolinidin) are less prone to water addition than anthocyanins (*e.g.* malvidin-3-glucoside = oenin), probably because the B-ring of 3-deoxyanthocyanis flavylium ions lies in the plane of the A- & C-rings, thereby allowing extensive electron delocalization (thermodynamic values are shown in Table 1). Anthocyanins can express relatively persistent blue-purple color around pH 8-9 as water addition to the chromophore is very slow in such conditions [17].

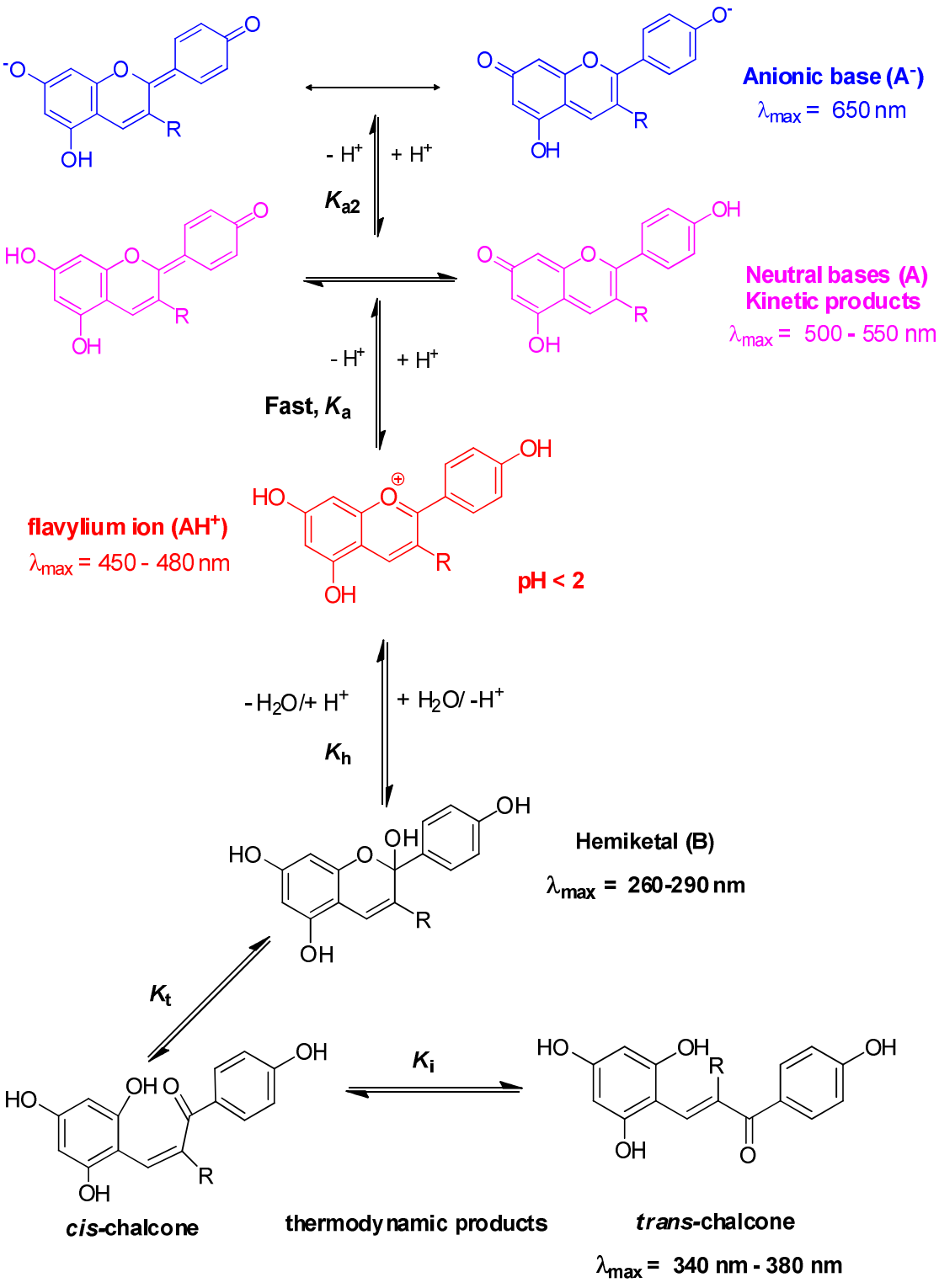

Scheme 3. structural transformations of anthocyanins as a function of pH.

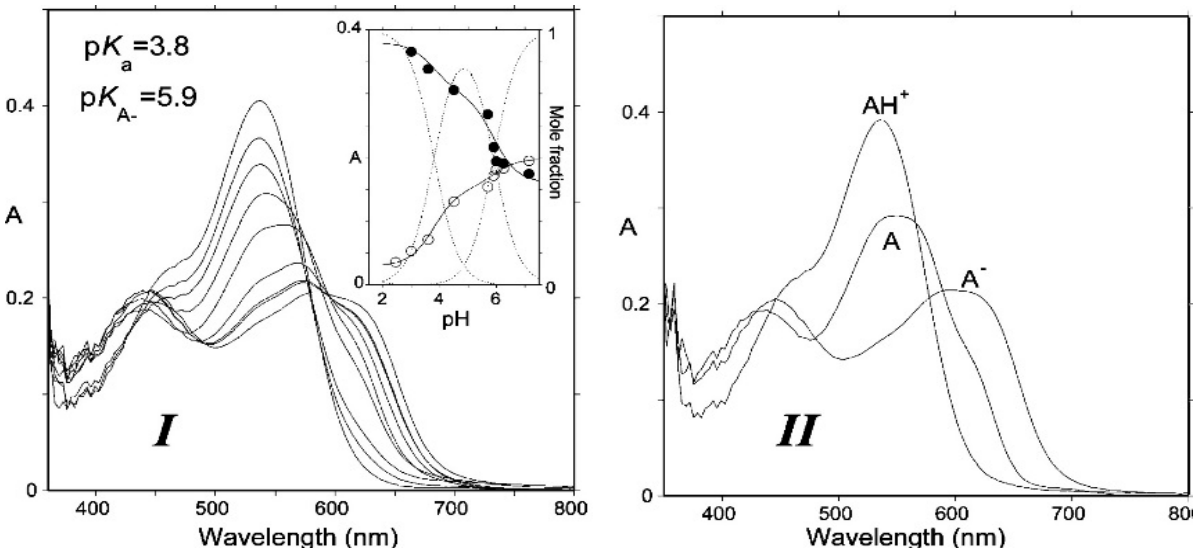

Figure 5. Typical visible spectra of the colored forms [18]. **Part I:** experimental spectra in the pH range 2 – 7. **Part II:** spectra of individual forms (spectra of A and A^- are obtained after mathematical deconvolution of experimental spectra in mildly acidic or neutral conditions).

Table 1. Thermodynamic constants oenin (malvidin 3-glucoside) and luteolinidin.

Compound	**pK$_a$**	***K*$_h$ (M)**	**K$_t$**	**K$_i$**	**p*K*'$_h$** *	**Ref.**
Oenin**	3.8	3.4×10^{-3}	0.12	2.4	2.3	[18]
Luteolinidin**	4.1	3.3×10^{-8}	0.8	6.5×10^{3}	3.8	[19]

* $K'_h = K_h\,[1 + K_t(1 + K_i)] = [H^+]([B] + [C_c] + [C_t])/[AH^+]$ (overall hydration constant)

** *Experiments in methanol/water* (3:1) for luteolinidin and in water for oenin.

4. The natural mechanisms of color stabilization & variation: metal complexation & copigmentation:

Copigmentation is the noncovalent π-stacking interaction between anthocyanins and colorless phenols [9]. This phenomenon represents the main mechanism for color stabilization in plant cell vacuoles where free anthocyanins ought to be colorless given the prevailing mildly acidic to neutral pH conditions. The copigmentation was observed first in grape by Willstätter and Zollinger in 1913 who noticed that the natural grape pigment oenin (malvidin 3-glucoside) changes its color hue toward purple (bathochromic shift) by the addition of tannins or gallic acid. Copigmentation theory was then developed though many researches leading to better understanding of this natural phenomenon [9,20–23].

Thousands of natural phenols are potential copigments [24]. Copigments are characterized by their (i) extended π-conjugated systems which favors π−π stacking interactions (ii) hydrogen bond donor/acceptor groups such as OH and C=O groups [9]. The major natural copigments are hydrolysable tannins, flavonoids (including flavonols, flavanones, flavanols and dihydroflavonols) and phenolic acids (such as hydroxycinnamic acids) (Figure 6). Flavonols, such as quercetin, kaempferol and rutin are the most efficient copigments because of the extension of electron delocalization over the entire tricyclic structure (rings A, B, and C).

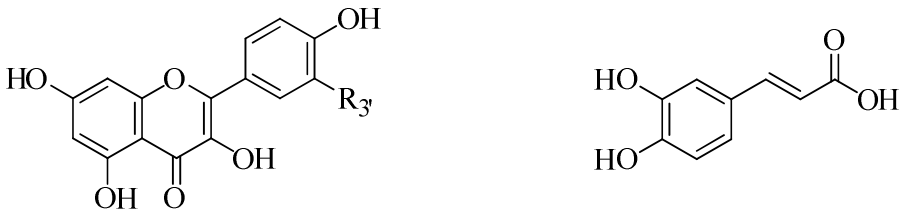

Flavonol
Quercetin $R_{3'}$= OH
Kaempferol $R_{3'}$= H

Hydroxycinnamic acid
Caffeic acid

Figure 6. Chemical structures of copigments.

Generally, copigmentation can take place through several mechanisms as self-association, intermolecular or intramolecular copigmentation (with or without metals) (Figure 7).

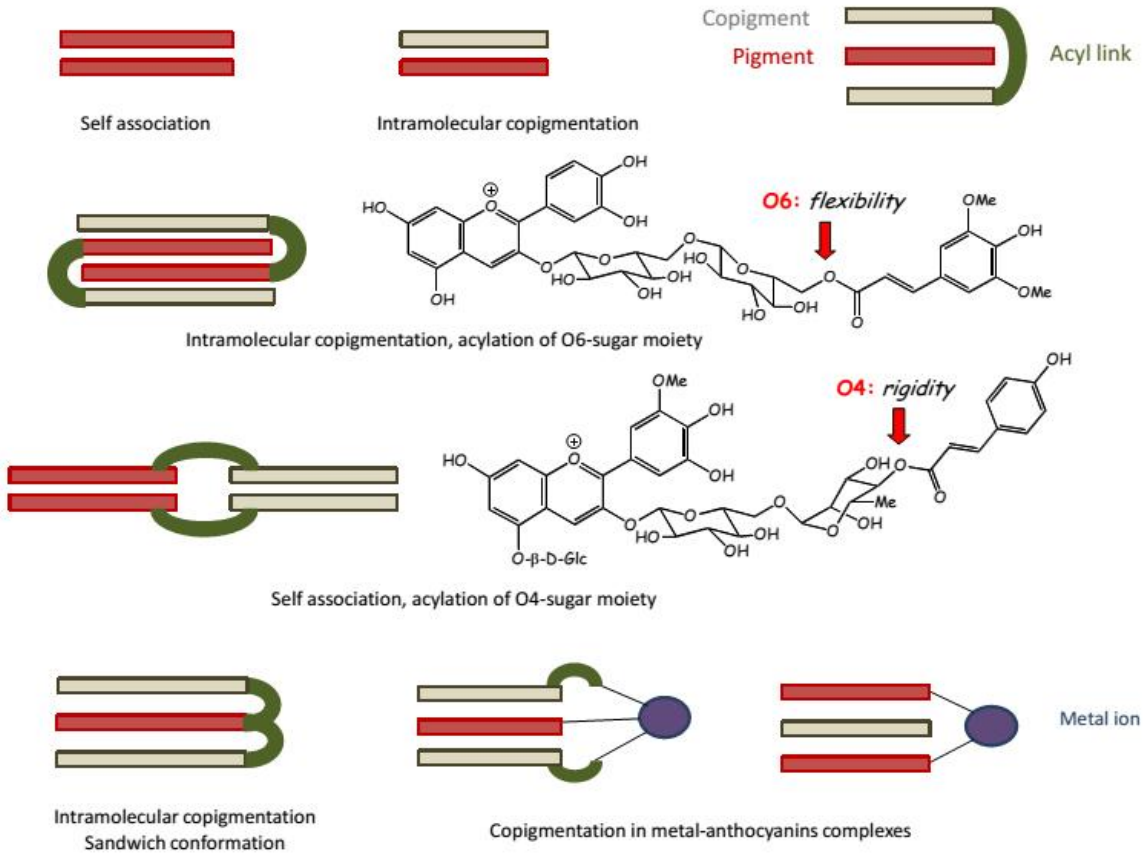

Figure 7. Examples of supramolecular assemblies involving anthocyanins and copigments [9] [25] [26].

- *Intermolecular interaction*

The mechanism of intermolecular copigmentation was defined by Brouillard in 1983 as a noncovalent bonding between a colored anthocyanin and a colorless copigment in aqueous solution. Copigmentation can occur with both the flavylium cation and the quinonoidal bases where delocalized π-electrons in the planar colored forms favor vertical stacking interactions with the phenolic nuclei of copigments. Dispersion interactions strengthened by the hydrophobic effect have been suggested as the main driving forces in intermolecular copigmentation [27].

Copigmentation opposes the nucleophilic attack of water onto the anthocyanin molecule and thus stabilizes its color [28]. The hyperchromic effect reflects a shift of the flavylium – hemiketal equilibrium toward the flavylium ion due to its specific affinity for the copigment. The visual or spectroscopic manifestations of copigmentation are much weaker at very low pH values where the flavylium cation dominates than in mildly acidic solutions where colorless forms are abundant (Figure 8).

Higher temperature tends to dissociate the copigmentation complexes, meaning that the binding is exothermic (Figure 8). The solvent composition affects copigmentation as the structure of water largely controls the pigment – copigment molecular association though the hydrophobic effect [24]. Hence, the addition of organic cosolvents (e.g., methanol, formamide) or salts weakens copigmentation [29].

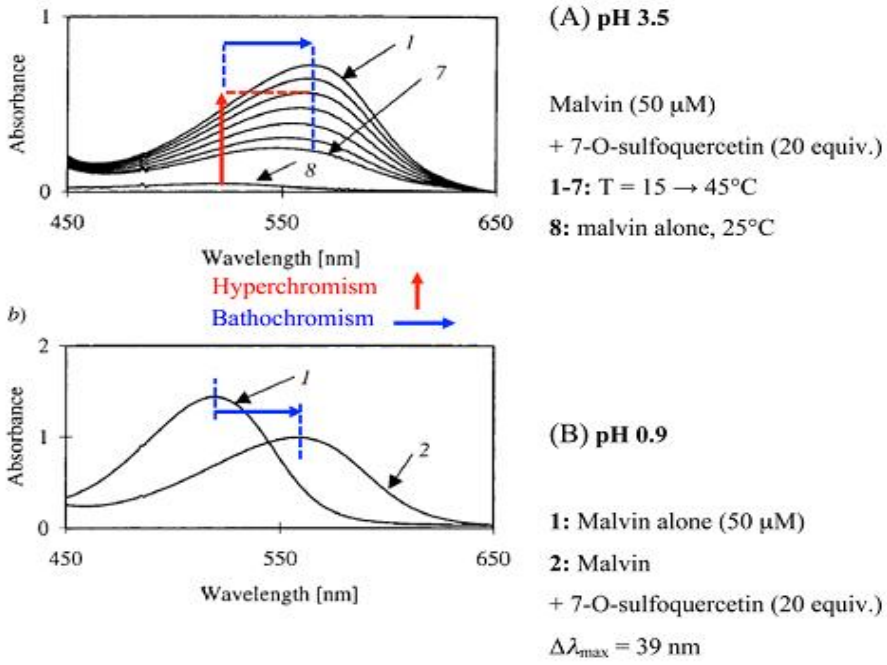

Figure 8. Copigmentation of malvidin 3,5-di-O-β-D-glucoside by 7-O-sulfoquercetin [30].

- *Intramolecular copigmentation*

Intramolecular copigmentation is responsible for the exceptional stability and variability of flower colors. Indeed, anthocyanins in flowers are generally acylated on their sugar residues. Intramolecular copigmentation occurs also in black carrot and other edible plants rich on acylated anthocyanins [31]. In intramolecular copigmentation, the copigment is a part of the pigment structure that favors a folded conformer in aqueous solutions in which the chromophore and phenolic acyl group are stacked on one another. Acylation occurs with hydroxycinnamic and hydroxybenzoic acids. Anthocyanins acylated by aliphatic acids, such as malonic, acetic, malic, succinic or oxalic acids, are also known but the role of these acyl groups in color expression is marginal. The number of acyl groups, their structure, their position on the glycosyl residues (usually at O6), as well as the structure and number of glycosyl moieties affect intramolecular copigmentation [32]. When the protective stacking occurs with two phenolic acyl groups and takes place on both sides of the anthocyanin aglycone, a so-called "sandwich" conformation is formed [33]. Depending on their structure, acylated anthocyanins can be more prone to noncovalent dimerization than to intramolecular copigmentation (Figure 7).

- *Self-association:*

In concentrated solution, self-association of anthocyanins can be evidenced by UV-visible spectroscopy, circular dichroism (CD) and NMR [34]. For instance, increasing the anthocyanin concentration from 10^{-4} to 10^{-2} M causes a change of maximum absorption wavelength from 507 to 520 nm (bathochromic effect) with an increase in color intensity (hypochromic effect) [21]. This phenomenon is responsible of color enhancement in young red wines and can be in competition with intermolecular copigmentation [35]. CD is very efficient for discriminating the two phenomena.

- *Anthocyanin-metal binding:*

After copigmentation, metal - anthocyanin complexation is the main mechanism of color diversification in plants. It was first mentioned by Shibata & coll. as the reason of blue-colored flowers [20]. Indeed, in pH 3 - 6, anthocyanins exist mostly as quinonoidal bases. So, they can bind various metal ions, most importantly Al^{III}, Fe^{III} and Mg^{II}. This binding is manifested by a bathochromic shift due to the replacement of the phenolic protons by the metal ion, with the additional contribution of anthocyanin-to-metal charge transfer with metal ion. The reaction between flavonoids and multivalent metal ions has been largely studied by UV-visible spectroscopy [36][37]. The chelating capacity of anthocyanins depends on the pH and on the anthocyanin structure as a 3',4'-dihydroxy substitution on the B-ring (catechol) is required. Moreover, blue metalloanthocyanins are supramolecular assemblies of pigment, copigment and metal ions in 6:6:2 stoichiometry involving intermolecular copigmentation, pigment and copigment self-association as well as metal - pigment complexation [22] (Figure 9).

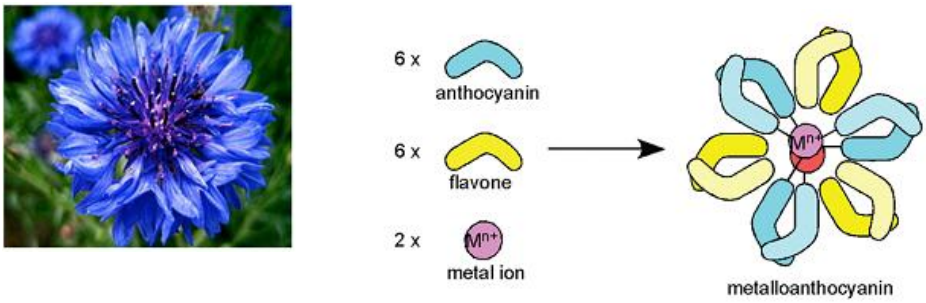

Figure 9. Structure of metalloanthocyanins example showing the two metal ions Fe^{III} and Mg^{II} in the center of the supramolecular assembly [24].

5. The irreversible chemistry of anthocyanins

Anthocyanins rapidly evolve during food processing or storage. Colorless products but also new pigments can be produced. This chemistry can impact the food color, taste, odor as well as the nutritional properties [38]. Many researches were carried out to control processing and storage conditions such as temperature, pH and dioxygen to preserve the original color as long as possible [39]. On the contrary, the changes in wine color upon aging can be regarded as a factor of quality.

- *Wine aging:*

The evolution of the original color of grape juice during wine making is the key-step toward more stable dark red wines. It's important to indicate that color modification is accompanied by organoleptic changes [40]. For instance, anthocyanin concentration was proposed as a key-component for increasing tannin solubility and transfer into wine via the formation of polymeric pigments [41]. Copigmentation was confirmed as an essential mechanism leading to stable color in red wines. As grape juice contains anthocyanins, flavonoids, phenolic acids and their derivatives (e.g., caftaric acid), copigmentation can easily occurs. Anthocyanin self-association explains color enhancement in young red wines (before the decay in anthocyanin concentration) [35]. Either in bottles or barrels aged wines, copigmentation is just the first step and is followed by the formation of covalent linkages between pigment, copigment and other wine components. For example, the A-rings of anthocyanins (hemiketal form) and flavanols are nucleophilic and can react with acetaldehyde formed by EtOH oxidation, thus yielding the specific wine pigments catechin-methylmethine-anthocyanins [42]. The C-ring of anthocyanins (flavylium form) is electrophilic and can react with wine nucleophiles such as 4-vinylphenols and carbonyl compounds (enol forms), thus yielding pyranoanthocyanins, e.g., vitisins A & B [43], oxovitisins, pyranoanthocyanin-phenols, pyranoanthocyanin-flavanols, bluish vinylpyranoanthocyanin-flavanol portisin, and pyranoanthocyanin dimers [44] (see structures in Figure 10). These new pigments induce color shifts to orange or purple/blue. They are more resistant to water and sulfite addition and so to color loss. Moreover, they display extended π-conjugated systems with self-association capacity, which allows colored forms to remain stable at higher pH values.

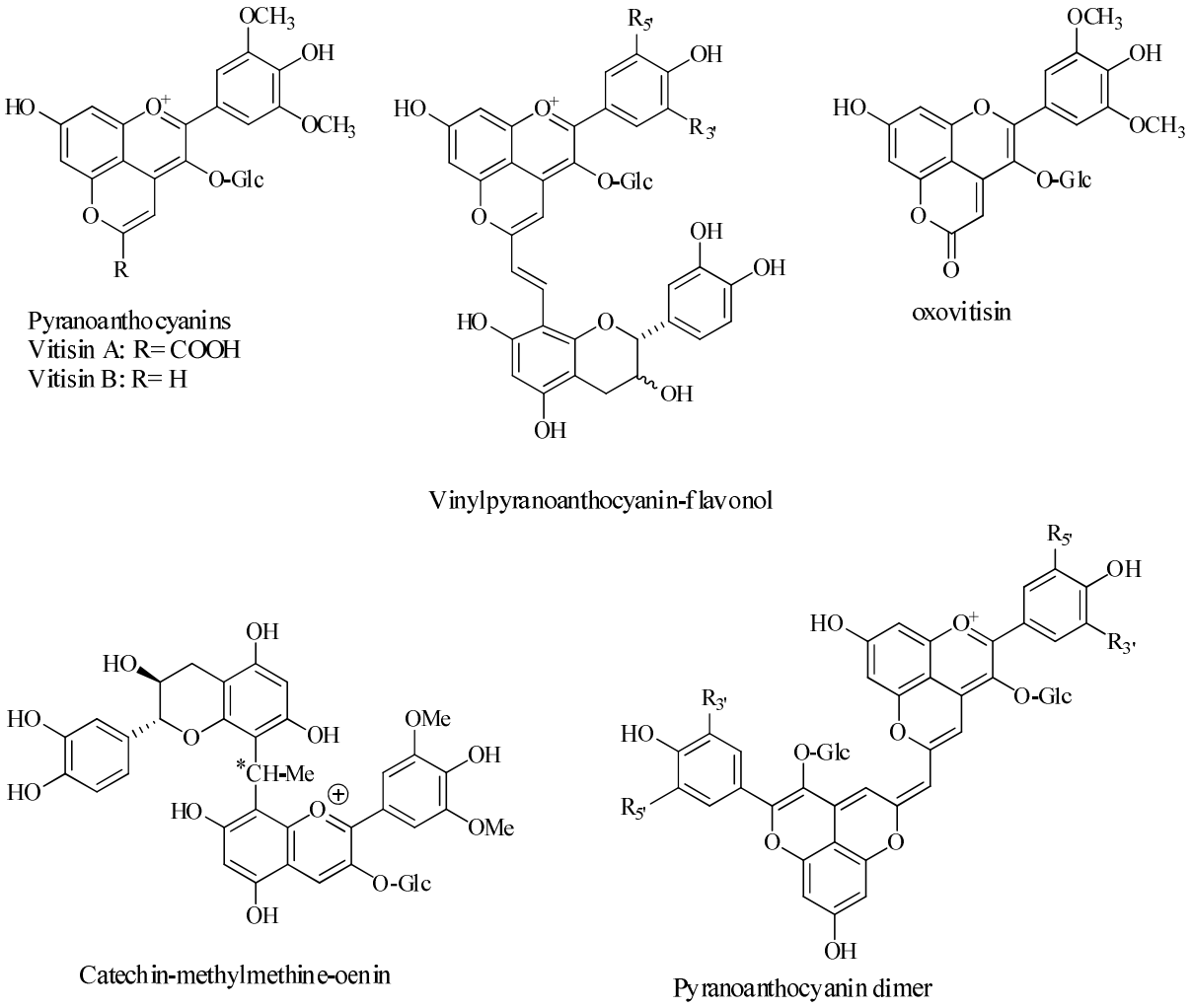

Figure 10. Covalent linkage and pyranoanthocyanin formation in aged wines.

- *Anthocyanin degradation:*

Heating is the main cause of irreversible degradation of anthocyanins [45]. The higher the temperature, the faster the anthocyanin degradation occurs especially in the presence of oxygen [46] [47]. High temperature at pH 2 - 4 cause glycosidic bond hydrolysis producing instable anthocyanidins and so color loss [29]. The formation of chalcones represents the first step in thermal degradation of anthocyanins, which follows first-order kinetics [28]. In a thermal and photochemical degradation study carried out over four anthocyanidins: pelargonidin, delphinidin, malvidin and cyanidin [48], 2,4,6-trihydroxybenzaldehyde (originated from ring A) was detected for all pigments studied. Moreover, 3,4,5-trihydroxybenzoic acid was detected from delphinidin, 4-hydroxy-3,5-dimethoxybenzoic acid from malvidin, 3,4-dihydroxybenzoic acid from cyanidin, and 4-hydroxybenzoic acid from pelargonidin (all originated from ring B) (Scheme 4). Upon irradiation, the excitation of the flavylium cation led to the same final products as for the thermal degradation.

It was reported that bond cleavage between the C- and B-rings is also possible and leads to coumarins [49].

Contrarily, 3-deoxyanthocyanins showed an overall thermal stability and a good resistance of C-ring fission (a color retention from 39% at pH 7 to 87% at pH 3), which indicates a good potential for food applications [50].

On the other hand, anthocyanins can be easily oxidized and oxidation products can accumulate in foods exposed to oxygen during processing or storage. It was reported that anthocyanidins are more oxidable than their glycosides [51]. Anthocyanone A results from the oxidative degradation of maldivin 3-*O*-glucoside was identified in a wine model solution heated to 90°C (Scheme 4). The key-step of its formation is the nucleophilic attack of hydrogen peroxide to maldivin 3-*O*-glucoside followed by a Baeyer−Villiger rearrangement [52].

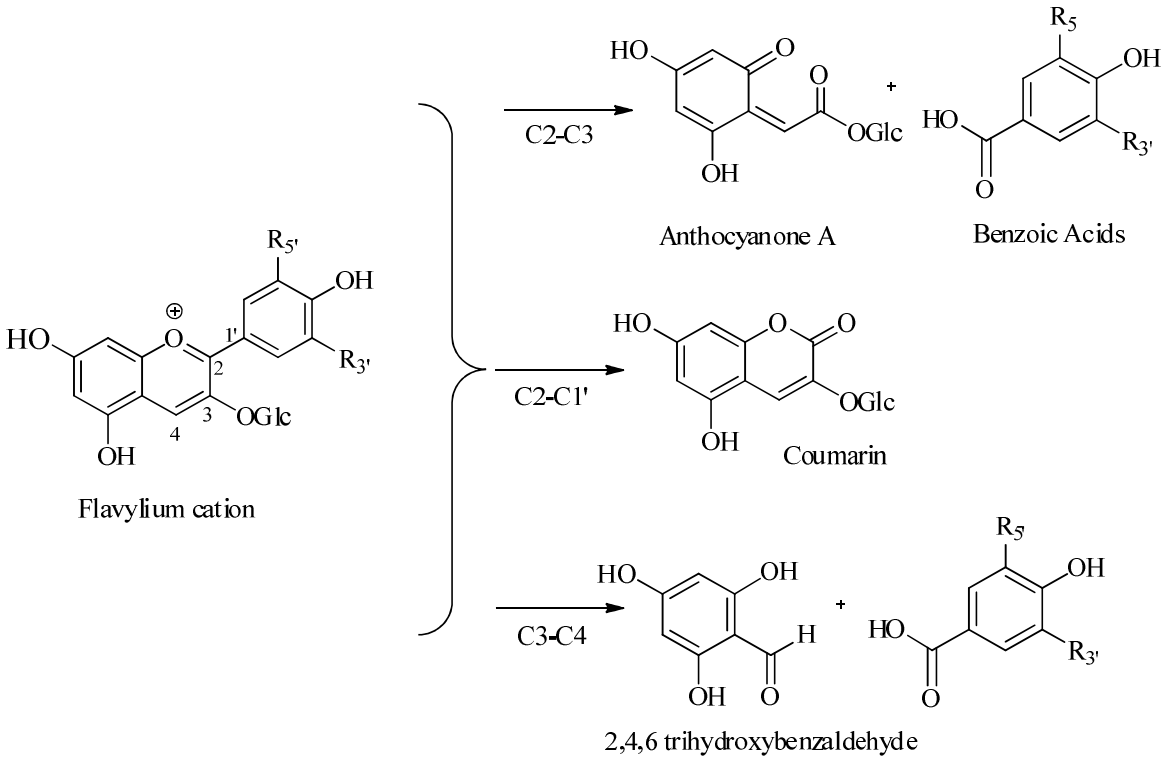

Scheme 4. Typical degradation products of anthocyanins [52] [53].

6. Anthocyanin extraction:

In fruits and berries, anthocyanins are mainly located in the peel [54]. However, they can be found in the pulp as in the case of cherries or blue berries. Conventional solid-liquid phase extraction is an efficient technique of anthocyanin extraction [55]. However, the toxicity of organic solvents used in extraction procedures limits the potential use of these extracts in food applications.

Recently, innovative and clean extraction methods as Superheated Liquid Extraction (SHLE) [56], Ultrasound-Assisted Extraction (UAE) [49], Microwave-Assisted Extraction (MAE) [57] and Micro-Hydrodiffusion and Gravity (MHG) [58] have been proposed as efficient methods of anthocyanin extraction. However, high cost and low extraction yields have limited the use of these clean methods. Low yields can be explained by anthocyanin degradation and transformation during extraction conditions as time, light, temperature, pH, oxygen, ascorbic acid and many others. So, the chemical synthesis of anthocyanins keeps a possible way to obtain them in acceptable quantities and purity.

Black sorghum brans are a very good source of pigments (up to 19 mg/g bran) compared to other natural sources (for example, *ca.* 1 mg/g fresh weight in the *Cabarnet Sauvignon* grape variety [59]). Black sorghum has the highest 3-deoxyanthicyanins content (4.0-9.8 mg luteolinidin equivalents/g) [60]. Moreover, sorghum is harvested at lower moisture levels (13 - 15%) relative to fruits and vegetables (80%), thus shorter drying periods and lower energy input are needed [11].

The conventional extraction of 3-deoxyanthocyanins from sorghum bran used acidified methanol (1% HCl) or water / acetone (3:7) [4]. Accelerated solvent extraction (ASE) gave acceptable yields of colorants from red sorghum [61]. Sorghum genotypes were developed to enhance their pigment content. However, sorghum hybrids were characterized by higher tannin but lower 3-deoxyanthocyanin content [4].

7. Chemical synthesis:

In the early period of 20th century, the acid-catalyzed condensation of phloroglucinol with benzoylacetone and benzoylpyruvic acid was developed by Bülow to produce the respective 4-methyl and 4-carboxylflavylium salts in good yields (Scheme 5) [62].

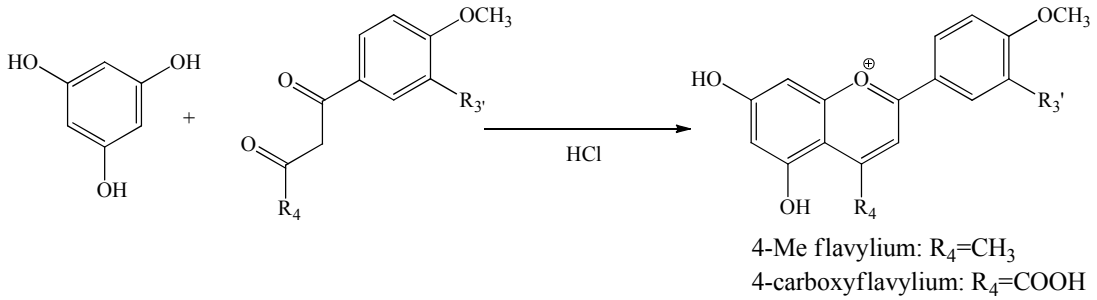

Scheme 5. Bülow's synthesis of anthocyanins.

Later, natural 3-deoxyanthocyanidins; apigeninidin and luteolinidin, were firstly synthesized by Sweeny & *coll.* who based on the oxidation of the 4-carboxyflavenes as prepared by Bülow (Scheme 6) [63].

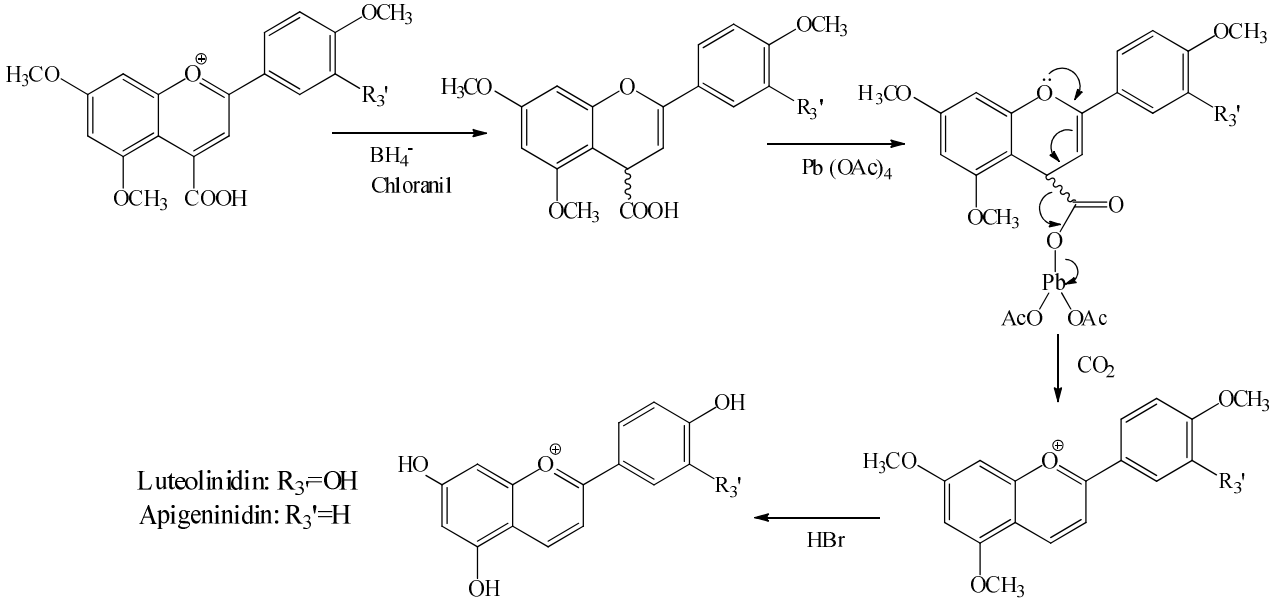

Scheme 6. Sweeny's synthesis of 3-deoxyanthocyanidins.

Benzopyrylium salts and 3-deoxyanthocyanidins were also prepared by the reaction of phenols and arylethynylketones in the presence of acids (Scheme 7) [64].

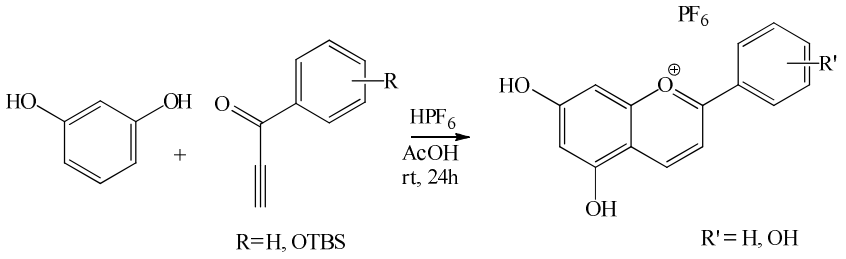

Scheme 7. Chassaing's synthesis of 3-deoxyanthocyanidins.

More recent research reported that 3-deoxyanthocyanins can be synthesized by the reaction of phloroglucinol with coniferaldehyde and sinapaldehyde at 35°C (Scheme 8) [65]

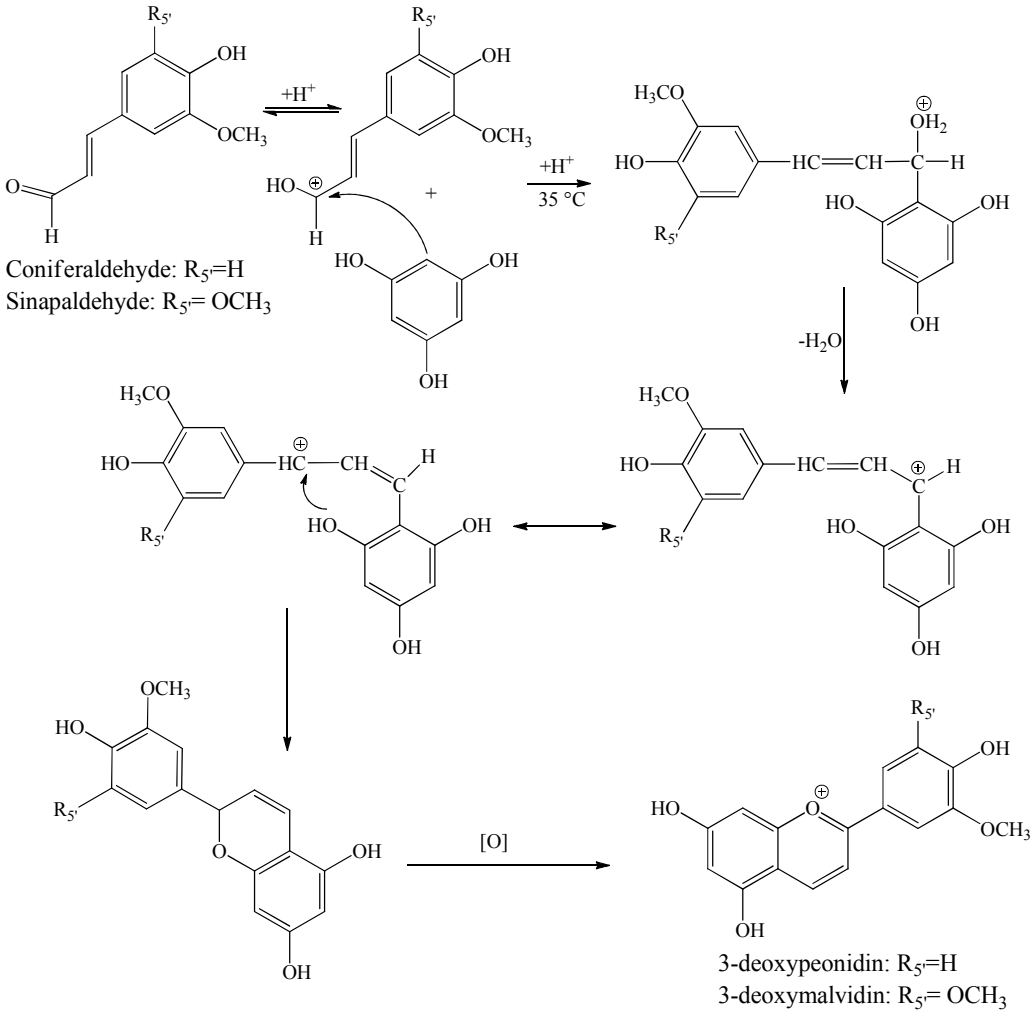

Scheme 8. De Freitas's synthesis of 3-deoxyanthocyanidins.

The first works on the synthesis of natural anthocyanins were developed by Robinson. It based on an acid-catalyzed aldol condensation and led to anthocyanidin mono- and di-glucosides but in very low yields (Scheme 9)[66].

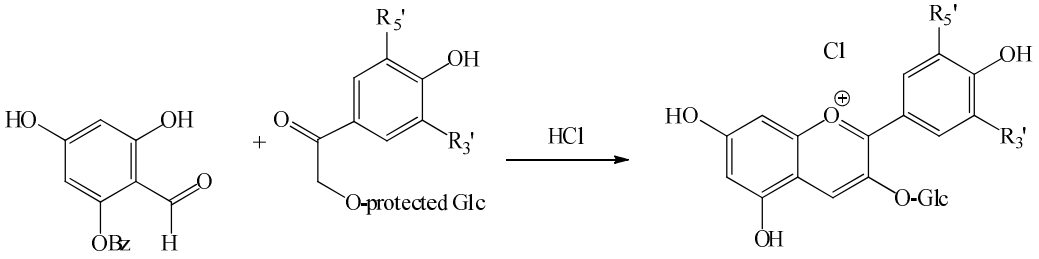

Scheme 9. Robinson's synthesis of anthocyanins.

In the last 2 decades, Dangles & *coll.* applied Robinson's route and 3-methoxy- and 3-(β-D-glycopyranosyloxy)flavylium ions were successfully obtained (Scheme 10)[67]. The same method yielded 3'-(β-D-glycopyranosyloxy)flavylium ions and luteolinidin[68].

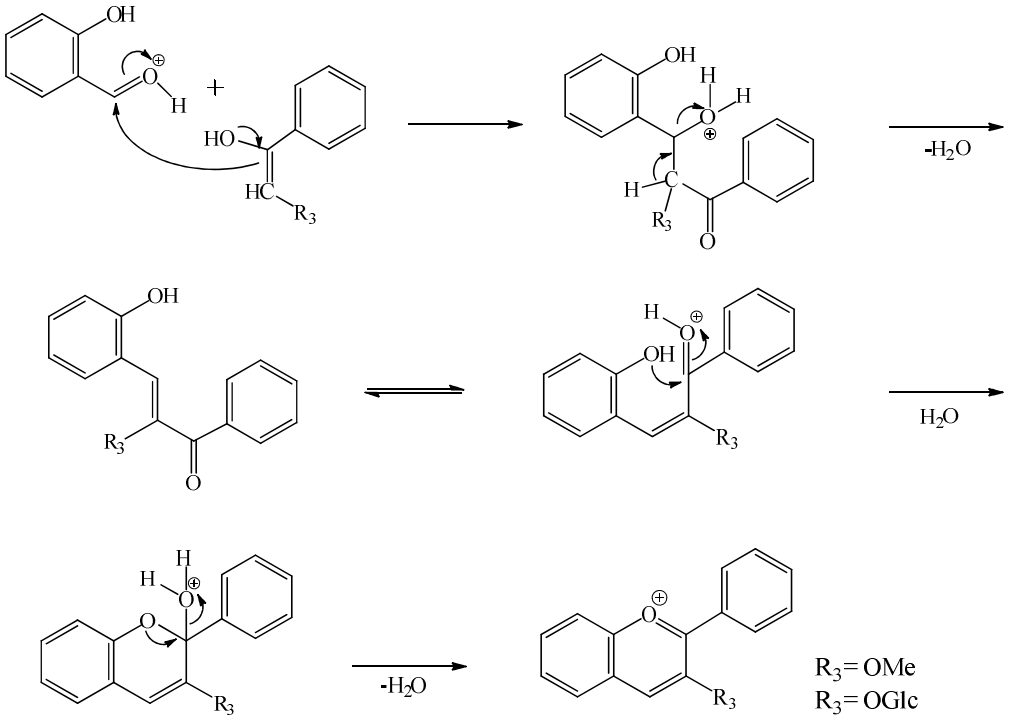

Scheme 10. Aldol condensation of benzaldehyde and acetophenone in acidic conditions for anthocyanin synthesis.

Recently, cyanidin-3-glucoside was obtained by glucosidation of C3-OH of (+)-catechin, then its hydroxylation at C4 and subsequent dehydration give the 5,7,3',4'-tetra-*O*-(t-butyldimethylsilyl) flav-3-en-3-ol-3-*O*-glucoside as a key intermediate. The latter is deprotected and oxidized under air in hydrogen chloride/MeOH to give cyanidin-3-glucoside (Scheme 11) [69]. Similarly, pelargonidin-3-*O*-6''-*O*-acetyl-β-glucopyranoside was synthesized via the corresponding kaempferol glucoside [70].

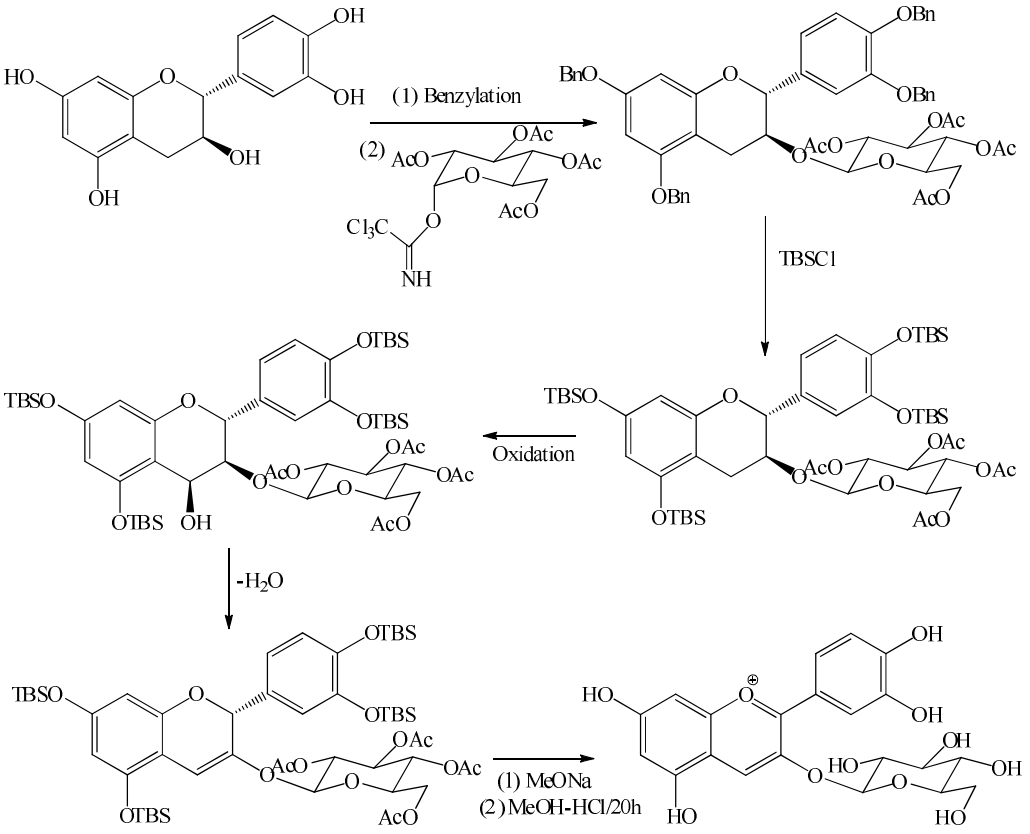

Scheme 11. Kondo's synthesis of anthocyanins.

Another way of anthocyanin synthesis via flavone or flavonol reduction by metals was described. C-glycosylanthocyanidins were synthesized from their respective C-glycosyloxyflavones by Clemmensen reduction using zinc-amalgam (Scheme 12)[71].

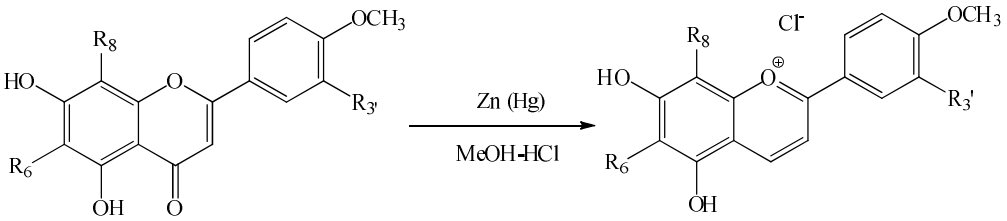

Scheme 12. Andersen's synthesis of 3-deoxyanthocyanidins (R_6 and/or R_8 = Glc, $R_{3'}$ = H, OH).

8. Anthocyanins in humans:

Besides their importance as potential food colorants, many researches have outlined the health benefits of anthocyanins [72]. The regular consumption of anthocyanins and other polyphenols in fruit, vegetables and (in moderation) red wines is associated with reducing the risk of chronic diseases [73]. In particular, markers of oxidative stress are found inversely related to our intake of polyphenol-rich foods [74]. In vitro studies have shown that anthocyanins display antioxidant, anti-inflammatory, anti-mutagenic, chemo- and radio-protective activities [75][59]. They may also have an important role in enhancing sight acuteness, in controlling diabetes [76] and in fighting against cardiovascular diseases [77]. Examples of cardiovascular protective mechanisms are the inhibition of ROS-forming enzymes, platelet aggregation and leukocyte activation, as well as the promotion of vasodilation [78]. Anthocyanins also combat various blood circulation disorders originated by capillary fragility and help maintain a normal vascular permeability [79]. Concerning 3-deoxyanthocyanidins, luteolinidin (200 µM) decreases the viability of human leukemia HL-60 and hepatoma HepG2 cells by 90 and 50% respectively [80]. It was reported that luteolinidin inhibits colon cancer stem cell proliferation more efficiently than apigeninidin [81]. It was also proved that the cytotoxicity of apigeninidin was higher in malignant cells than in normal ones [82]. Moreover, the anti-proliferative activity of a 3-deoxyanthocyanin extract on human breast cancer cell line MCF 7 was evidenced [83].

9. Bioavailability in humans:

Over the last 2 - 3 decades, many studies have been conducted on the bioavailability of polyphenols [84] and anthocyanins [85] in humans. The maximal plasma concentrations of polyphenols and their conjugated forms don't exceed 1 μM and are actually less than 50 nM for anthocyanins [86]. The latter value is *ca.* 3 orders of magnitude smaller than that of the typical hydrophilic antioxidant ascorbate. So, the *in-vivo* antioxidant activity of anthocyanins after intestinal absorption is proposed to be minimal.

The low absorption of anthocyanins from the gastrointestinal tract may be due to their poor gastrointestinal stability and active efflux from the intestinal cells [87]. Depending on their rapid appearance in blood stream, early anthocyanins absorption from the stomach had been approved through a moderately differentiated adenocarcinoma stomach cells (MKN-28) as gastric barrier [88]. To evaluate their absorption from small intestine, we distinguish two cases: (i) it was proved that hydrophobic aglycones can passively diffuse through biological membranes, (ii) the absorption of anthocyanins requires either a specific active transport mechanism or enzymatic hydrolysis of the glycosyl bonds before absorption [85]. Consequently, we can say that glycosylation is key step in anthocyanins absorption in small intestine. In large intestine, they are exposed to the multi-enzymatic activity of the colonic microbiota before entering in blood circulation as smaller phenolic acid and aromatic catabolites (Figure 11) [89]. Indeed, large intestine is the main pass for parent compounds as well as their metabolites in considerable quantities to blood circulation. Certain studies suggest that anthocyanidins share common metabolic fate with other flavonoids in humans and undergo extensive glucuronidation and methylation during further phase II metabolism and enterohepatic recirculation in the liver [90]. Metabolites can be subjected to a back recycling to the small intestine through bile excretion [91].

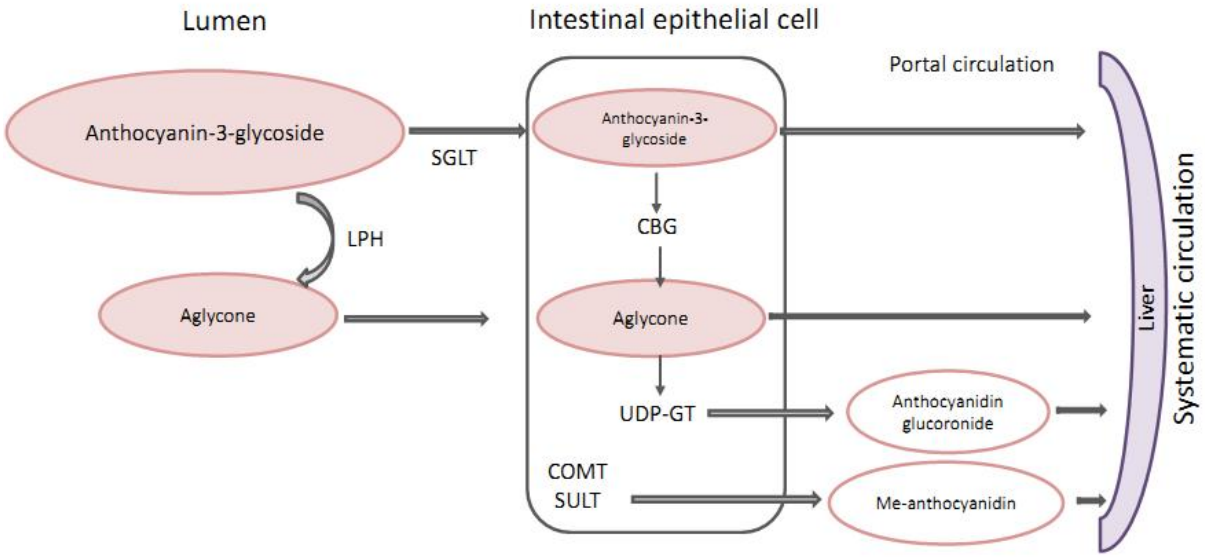

Figure 11. Potential mechanisms of anthocyanins absorption proposed by Kay & coll. [85], SGLT; sodium-glucose co-transporter, CBG; cytosolic β-glucoside, LPH; lactate phlorizin hydrolase, UDP-GT; UDP-glucuronosyltransferase, COMT; catechol-O-methyltransferase, SULT; sulfotransferase.

We can conclude that anthocyanins are underestimated regarding our knowledge of their benefices to human health. Several hypotheses were proposed to understand the mechanisms of their evidenced biological effects in spite of their low bioavailability. Kay & coll reported that anthocyanin metabolites are present in the blood circulation in higher concentration and for a longer time than their parents, so, metabolites are proposed as the real active molecules [92]. It was reported that protocatechuic acid (3,4-dihydroxybenzoic acid) is the principal catabolite of cyanidin-3-*O*-glucoside in humans [93]. Consequently, it's useless to estimate anthocyains activity by a simple quantification of native anthocyanins or their aglycones in blood samples after anthocyanin intake while their metabolites should be identified and controlled. Indeed, recent study proposes quantitative and qualitative methods for anthocyanin metabolite estimation in clinical samples [94].

In correspondence with this hypothesis, *in-vitro* studies were carried out to prove the biological effect of detected metabolites. For instance, apoptotic effects of protocatechuic has been evidenced on human gastric adenocarcinoma and HepG2 hepatoma cells [95].

It was also reported that phenolic metabolites modulate vascular endothelial cell function through alternative mechanisms to those previously described for cyanidin-3-glucoside that stimulat of endothelial NO synthase expression. By contrast, both of its degradation product, protocatechuic acid and its phase II metabolite vanillic acid, significantly reduce endothelial superoxide level and maintain vascular homeostasis [96].

In another hypothesis, the gastrointestinal (GI) tract has been suggested as an important site where native polyphenols can be available in much higher concentrations than in blood circulation. In this site, parent anthocyanins may act as true antioxidants by protecting dietary polyunsaturated fatty acids (PUFAs) against oxidation initiated by dietary pro-oxidant species such as heme iron (the red meat pigment) [97] [86] [98]. This method is used in later sections to estimate the antioxidant activity of 3-deoxyanthocyanidins and their chalcones.

10.Food applications:

In our days, color is still playing very important role in the acceptability of foods as it's the consumer's first judge of the food quality. Food industry used colorants to enhance foods quality, restore their original appearance or to ensure uniformity [99]. However, during last decades, the safety of synthetic colorants used in food applications was questioned leading to restrictions in their use. For instance, recent studies had showed a significant increase of the attention deficit hyperactivity disorder (ADHD) in children after consumption of drinks containing artificial dyes [100]. As a consequence, since July 2010, European Commission Directive 1333/2008 (EC) imposes the labeling of food containing synthetic colorants with warning notices.

Currently, there is a great interest in food colorants from natural sources in order to address the consumer's mistrust of synthetic food additives as well as to comply with a legislation becoming more stringent. So, anthocyanins are proposed as alternative natural colorants in food, pharmaceutical and cosmetic industries. Moreover, many studies have demonstrated other potential applications for these colorants such as their use as hair dyes, laser dyes, sensitizers for solar cells, and molecular-level memory systems [65]. In food processing, the chelation of transition metal traces by natural ligands such as anthocyanins represents an additional antioxidant mechanism as bound metal ions are no longer active in the Fenton reaction [101].

Actually, used E163 is a natural anthocyanin extract from grapes, red berries and red cabbage co-products widely commercialized as a food colorant. The extraction is carried out by methanol, sulfited water, ethanol or carbon dioxide. Then, the extract is concentrated, purified or atomized. The resulted extracts contain anthocyanins, organic acids, tannins, sugars and inorganic salts, etc. in different proportions comparing to the plant material. Nevertheless, this industrial colorant of natural origin is not really safe and must not be confused with natural anthocyanins obtained by consuming fresh fruits (cherries, grapes, berries….) and vegetables (onions, eggplant…). In reality, E163 contains high levels of sulfites and different auxiliary additives as phosphates. Moreover, high levels of ethanol could be reached in the extract after the maceration process. Consequently, *according to Directives et Règlements de l'Union Européenne relatifs aux additifs alimentaires (Règlement 231/2012),* E163 is authorized in the European Union with accepted daily intake *(DJA_{E163ii}= 0.25 mg / Kg / Day)* in jellies, jams, milk products, conserved berries, ice creams and energy drinks.

A major limitation to the use of anthocyanins in the food industry is their relative low stability to processing, formulation and storage conditions. Generally, their degradation is manifested by a color loss [27] and may impart undesirable odor or flavor to food formulations [31]. The stability of anthocyanins is affected by different parameters such as; their structure and concentration, pH, temperature, oxygen, light, in addition to the presence of other compounds such as flavonoids, proteins, enzymes, ascorbic acid, sugars and metal ions.

Unlike fruits and vegetables, cereals have been less regarded as valuable anthocyanin sources. Nowadays, there is a considerable interest in sorghum, millets and pseudo-cereals for their phytochemical content, their nutritional potential in addition to their use in gluten-free formulations [102]. Sorghum Bicolor (L.) Moench is traditionally used in some African cultures because of its food coloring properties and the traditional belief in its benefits. Nowadays, sorghum crops are used in China and in the south of the USA for the coloration of syrups and the production of bioethanol. However, in the rest of the occidental world, pigmented sorghum is not used in the food industry and innovative attempts were made to incorporate it in our daily diets. Thus, various food products such as breads, cakes, cookies, and tortillas can use red sorghum flour instead of common wheat flour.

The relative stability of sorghum pigments (3-deoxyanthocyani(di)ns) in mildly to neutral aqueous solutions present their potential use an alternative colorant in food industry, pharmaceutics and cosmetics.

11.References:

1. Wallace, J. W. Special Issue Chemosystematics of the Pteridophytes Chemosystematic implications of flavonoids and C-Glycosylxanthones in “ferns.” *Biochem. Syst. Ecol.* **1989**, *17*, 145–153.

2. Lo, S.; Verdier, K.; Nicholson, R. L. Accumulation of 3-deoxyanthocyanidin phytoalexins and resistance to Colletotrichum sublineolum in sorghum. *Physiol. Mol. Plant Pathol.* **1999**, *55*, 263–273.

3. Boddu, J.; Svabek, C.; Sekhon, R.; Gevens, A.; Nicholson, R. L.; Jones, A. D.; Pedersen, J. F.; Gustine, D. L.; Chopra, S. Expression of a putative flavonoid 3′-hydroxylase in sorghum mesocotyls synthesizing 3-deoxyanthocyanidin phytoalexins. *Physiol. Mol. Plant Pathol.* **2004**, *65*, 101–113.

4. Dykes, L.; Rooney, W. L.; Rooney, L. W. Evaluation of phenolics and antioxidant activity of black sorghum hybrids. *J. Cereal Sci.* **2013**, *58*, 278–283.

5. Ejike, C. E. C. C.; Gong, M.; Udenigwe, C. C. Phytoalexins from the Poaceae: Biosynthesis, function and prospects in food preservation. *Food Res. Int.* **2013**, *52*, 167–177.

6. Devi, P. S.; Saravanakumar, M.; Mohandas, S. Identification of 3-deoxyanthocyanins from red sorghum (Sorghum bicolor) bran and its biological properties. *Afr. J. Pure Appl. Chem.* **2011**, *5*, 181–193.

7. Kong, J.-M.; Chia, L.-S.; Goh, N.-K.; Chia, T.-F.; Brouillard, R. Analysis and biological activities of anthocyanins. *Phytochemistry* **2003**, *64*, 923–933.

8. Brouillard, R. chemical structure of anthocyanins. *Acad. Press Inc* **1982**, 1–40.

9. Trouillas, P.; Sancho-Garcia, J. C.; De Freitas, V.; Gierschner, J.; Otyepka, M.; Dangles, O. Stabilizing and modulating color by copigmentation: insights from theory and experiment. *Chem. Rev.*

10. Nip; Bruns pigments characterization in grain sorghum. *Cereal Chem.* 1969, 490–495.

11. Awika, J. M.; Rooney, L. W.; Waniska, R. D. Anthocyanins from black sorghum and their antioxidant properties. *Food Chem.* **2005**, *90*, 293–301.

12. Petrussa, E.; Braidot, E.; Zancani, M.; Peresson, C.; Bertolini, A.; Patui, S.; Vianello, A. Plant Flavonoids—Biosynthesis, Transport and Involvement in Stress Responses. *Int. J. Mol. Sci.* **2013**, *14*, 14950–14973.

13. Torskangerpoll, K.; Andersen, Ø. M. Colour stability of anthocyanins in aqueous solutions at various pH values. *Food Chem.* **2005**, *89*, 427–440.

14. Melo, M. J.; Moura, S.; Maestri, M.; Pina, F. Micelle effects on multistate/multifunctional systems based on photochromic flavylium compounds. The case of luteolinidin. *J. Mol. Struct.* **2002**, *612*, 245–253.

15. Pina, F. Chemical Applications of Anthocyanins and Related Compounds. A Source of Bioinspiration. *J. Agric. Food Chem.* **2014**, *62*, 6885–6897.

16. V. Petrov; R. Gavara; O.Dangles; S. Al-bittar; N.soumille-Mora; F.Pina Flash photolysis and stopped-flow UV-visible spectroscopy study of 3’,4’-dihydroxy-7-O-β-D-glucopyranosyloxy-flavylium chloride, an anthocyanin analogue exhibiting efficient photochromic properties. *Photochem. Photobiol. Sci.* **2013**, *12*, 576–581.

17. Cabrita, L.; Fossen, T.; Andersen, Ã. M. Colour and stability of the six common anthocyanidin 3-glucosides in aqueous solutions. *Food Chem.* **2000**, *68*, 101–107.

18. The effect of self-aggregation on the determination of the kinetic and thermodynamic constants of the network of chemical reactions in 3-glucoside anthocyanins http://buproxy.univ-avignon.fr:2083/science/article/pii/S0031942212003007 (accessed Mar 27, 2016).

19. Melo, M. J.; Moura, S.; Maestri, M.; Pina, F. Micelle effects on multistate/multifunctional systems based on photochromic flavylium compounds. The case of luteolinidin. *J. Mol. Struct.* **2002**, *612*, 245–253.

20. Shibata, K.; Shibata, Y.; Kasiwagi, I. Studies in anthocyanins variations in blue flowers. *J. Am. Chem. Soc.* **1919**, *41*, 208–220.

21. Asen, S.; Stewart, R. N.; Norris, K. H. Co-pigmentation of anthocyanins in plant tissues and its effect on color. *Phytochemistry* **1972**, *11*, 1139–1144.

22. Goto, T.; Kondo, T. Structure and Molecular Stacking of Anthocyanins—Flower Color Variation. *Angew. Chem. Int. Ed. Engl.* **1991**, *30*, 17–33.

23. Yoshida, K.; Mori, M.; Kondo, T. Blue flower color development by anthocyanins: from chemical structure to cell physiology. *Nat. Prod. Rep.* **2009**, *26*, 884–915.

24. Mazza G; Brouillard, R. The mechanism of co-pigmentation of anthocyanins in aqueous solutions. *Phytochemistry* **1990**, *29*, 1097–1102.

25. Yoshida, K.; Kondo, T.; Goto, T. *Tetrahedron Lett.* 1991, 5579–5580.

26. Nerdal, W.; Andersen, O. M. *Phytochem. Anal.* 1992, 182–189.

27. Brouillard, R. The in vivo expression of anthocyanin colour in plants. *Phytochemistry* **1983**, *22*, 1311–1323.

28. Cavalcanti, R. N.; Santos, D. T.; Meireles, M. A. A. Non-thermal stabilization mechanisms of anthocyanins in model and food systems—An overview. *Food Res. Int.* **2011**, *44*, 499–509.

29. Mazza, G.; Brouillard, R. Recent developments in the stabilization of anthocyanins in food products. *Food Chem.* **1987**, *25*, 207–225.

30. B. Alluis; O. Dangles Quercetin (=2-(3,4-Dihydroxyphenyl)-3,5,7-trihydroxy-4H-1-benzopyran-4-one) Glycosides and Sulfates: Chemical Synthesis, Complexation, and Antioxidant Properties. *Helv. Chim. Acta* **2001**, *84*, 1133–1156.

31. Giusti, M. M.; Wrolstad, R. E. Acylated anthocyanins from edible sources and their applications in food systems. *Biochem. Eng. J.* **2003**, *14*, 217–225.

32. Dangles, O.; Saito, N.; Brouillard, R. The International Journal of Plant BiochemistryAnthocyanin intramolecular copigment effect. *Phytochemistry* **1993**, *34*, 119–124.

33. Brouillard, R. Origin of the exceptional colour stability of the Zebrina anthocyanin. *Phytochemistry* **1981**, *20*, 143–145.

34. González-Manzano, S.; Dueñas, M.; Rivas-Gonzalo, J. C.; Escribano-Bailón, M. T.; Santos-Buelga, C. Studies on the copigmentation between anthocyanins and flavan-3-ols and their influence in the colour expression of red wine. *Food Chem.* **2009**, *114*, 649–656.

35. Boulton, R. The copigmentation of anthocyanins and its role in the color of red wine: a critical review. *Am. J. Enol. Vitic.* **2001**, *52*, 67–87.

36. El hajii, H.; Nkhili, E.; Tomao, V.; Dangles, O. interaction of quercetin with iron and copper ions. *Free Radic. Res.* **2006**, 303–320.

37. E. Nkhili; M. Loonis; S. Mihai; H. El HAjji; O. Dangles Reactivity of food phenols and copper ions: binding dioxygen activation and oxidation mechanisms. *Food Funct.* **2014**.

38. Wrolstad, R. E.; Durst, R. W.; Lee, J. Tracking color and pigment changes in anthocyanin products. *Trends Food Sci. Technol.* **2005**, *16*, 423–428.

39. Cavalcanti, R. N.; Santos, D. T.; Meireles, M. A. A. Non-thermal stabilization mechanisms of anthocyanins in model and food systems—An overview. *Food Res. Int.* **2011**, *44*, 499–509.

40. McRae, J. M.; Kennedy, J. A. Wine and grape tannin interactions with salivary proteins and their impact on astringency: a review of current research. *Molecules* **2011**, *16*, 2348–2364.

41. Timberlake, C. F.; Bridle, P. Interactions Between Anthocyanins, Phenolic Compounds, and Acetaldehyde and Their Significance in Red Wines. *Am. J. Enol. Vitic.* **1976**, *27*, 97–105.

42. Brouillard, R.; Dangles, O. Anthocyanin molecular interactions: the first step in the formation of new pigments during wine aging? *Food Chem.* **1994**, *51*, 365–371.

43. Oliveira, J.; Mateus, N.; Silva, A. M. S.; de Freitas, V. Equilibrium Forms of Vitisin B Pigments in an Aqueous System Studied by NMR and Visible Spectroscopy. *J. Phys. Chem. B* **2009**, *113*, 11352–11358.

44. Fulcrand, H.; Atanasova, V.; Salas, E.; Cheynier, V. The fate of anthocyanins in wine: Are there determining factors? *ACS Symp. Ser.* **2004**, *886*, 68–88.

45. Hellström, J.; Mattila, P.; Karjalainen, R. Stability of anthocyanins in berry juices stored at different temperatures. *J. Food Compos. Anal.* **2013**, *31*, 12–19.

46. Markakis, P. Stability of anthocyanins in food. *Acad. Press Inc* **1982**, 163–178.

47. Cavalcanti, R. N.; Santos, D. T.; Meireles, M. A. A. Non-thermal stabilization mechanisms of anthocyanins in model and food systems—An overview. *Food Res. Int.* **2011**, *44*, 499–509.

48. Furtado, P.; Figueiredo, P.; Neves, H. C. das; Pina, F. Photochemical and thermal degradation of anthocyanidins. *J. Photochem. Photobiol. Chem.* **1993**, *75*, 113–118.

49. Tiwari, B. K.; Patras, A.; Brunton, N.; Cullen, P. J.; O'Donnell, C. P. Effect of ultrasound processing on anthocyanins and color of red grape juice. *Ultrason. Sonochem.* **2010**, *17*, 598–604.

50. Yang, L.; Dykes, L.; Awika, J. M. Thermal Stability of 3-Deoxyanthocyanidin Pigments. *Food Chem.* **2014**.

51. Kähkönen, M. P.; Heinonen, M. Antioxidant Activity of Anthocyanins and Their Aglycons. *J. Agric. Food Chem.* **2003**, *51*, 628–633.

52. Lopes, P.; Richard, T.; Saucier, C.; Teissedre, P.-L.; Monti, J.-P.; Glories, Y. Anthocyanone A: A Quinone Methide Derivative Resulting from Malvidin 3-O-Glucoside Degradation. *J. Agric. Food Chem.* **2007**, *55*, 2698–2704.

53. Fleschhut, J.; Kratzer, F.; Rechkemmer, G.; Kulling, S. E. Stability and biotransformation of various dietary anthocyanins in vitro. *Eur. J. Nutr.* **2006**, *45*, 7–18.

54. Muñoz, S.; Mestres, M.; Busto, O.; Guasch, J. Determination of some flavan-3-ols and anthocyanins in red grape seed and skin extracts by HPLC-DAD: Validation study and response comparison of different standards. *Anal. Chim. Acta* **2008**, *628*, 104–110.

55. Denev, P.; Ciz, M.; Ambrozova, G.; Lojek, A.; Yanakieva, I.; Kratchanova, M. Solid-phase extraction of berries' anthocyanins and evaluation of their antioxidative properties. *Food Chem.* **2010**, *123*, 1055–1061.

56. Luque-Rodríguez, J. M.; Castro, M. D. L. de; Pérez-Juan, P. Dynamic superheated liquid extraction of anthocyanins and other phenolics from red grape skins of winemaking residues. *Bioresour. Technol.* **2007**, *98*, 2705–2713.

57. Liazid, A.; Guerrero, R. F.; Cantos, E.; Palma, M.; Barroso, C. G. Microwave assisted extraction of anthocyanins from grape skins. *Food Chem.* **2011**, *124*, 1238–1243.

58. Al Bittar, S.; Périno-Issartier, S.; Dangles, O.; Chemat, F. An innovative grape juice enriched in polyphenols by microwave-assisted extraction. *Food Chem.* **2013**, *141*, 3268–3272.

59. Orak, H. H. Total antioxidant activities, phenolics, anthocyanins, polyphenoloxidase activities of selected red grape cultivars and their correlations. *Sci. Hortic.* **2007**, *111*, 235–241.

60. Awika, J. M.; McDonough, C. M.; Rooney, L. W. Decorticating Sorghum To Concentrate Healthy Phytochemicals. *J. Agric. Food Chem.* **2005**, *53*, 6230–6234.

61. Barros, F.; Dykes, L.; Awika, J. M.; Rooney, L. W. Accelerated solvent extraction of phenolic compounds from sorghum brans. *J. Cereal Sci.* **2013**, *58*, 305–312.

62. Bülow; Wagner, H. *Ber Dtsch Chem* **1901**, *Ges 34*, 1782.

63. Sweeny, J. G.; Iacobucci, G. A. Synthesis of anthocyanidins-III: Total synthesis of apigeninidin and luteolinidin chlorides. *Tetrahedron* **1981**, *37*, 1481–1483.

64. Chassaing, S.; Kueny-Stotz, M.; Isorez, G.; Brouillard, R. Rapid Preparation of 3-Deoxyanthocyanidins and Novel Dicationic Derivatives: New Insight into an Old Procedure. *Eur. J. Org. Chem.* **2007**, *2007*, 2438–2448.

65. Sousa, A.; Mateus, N.; de Freitas, V. A novel reaction mechanism for the formation of deoxyanthocyanidins. *Tetrahedron Lett.* **2012**, *53*, 1300–1303.

66. Robertson, A.; Robinson, R. *J Chem Soc* **1927**, 242–247.

67. Dangles, O.; El Hajji, H. synthesis of 3-methoxy- and 3-(β-D-Glycopyransyloxy)flavilium Ions: Influence of the flavilium subtitution Pattern on the reactivity of Anthocyanins in Aqueous Solutions. *Helv. Chim. Acta* **1994**, *77*, 1595–1610.

68. El Hajji, H.; Dangles, O.; Figueiredo, P.; Brouillard, R. 3'-(β-D-Glycopyransyloxy)flavilium Ions: Synthesis and Investigation of Their Properties in Aqueous Solutions. Hydrogen Bonding as a Mean of Colour Variation. *Helv. Chim. Acta* **1997**, *80*, 398–413.

69. Kondo, T.; Oyama, K.; Nakamura, S.; Yamakawa, D.; Tokuno, K.; Yoshida, K. Novel and Efficient Synthesis of Cyanidin 3-O-β-d-Glucoside from (+)-Catechin via a Flav-3-en-3-ol as a Key Intermediate. *Org. Lett.* **2006**, *8*, 3609–3612.

70. Oyama, K.; Kawaguchi, S.; Yoshida, K.; Kondo, T. Synthesis of pelargonidin 3-O-6″-O-acetyl-β-d-glucopyranoside, an acylated anthocyanin, via the corresponding kaempferol glucoside. *Tetrahedron Lett.* **2007**, *48*, 6005–6009.

71. BjorØy, Ø.; Rayyan, S.; Fossen, T.; Kalberg, K.; Andersen, Ø. M. C-glycosylanthocyanidins synthesized from C-glycosylflavones. *Phytochemistry* **2009**, *70*, 278–287.

72. Kong, J.-M.; Chia, L.-S.; Goh, N.-K.; Chia, T.-F.; Brouillard, R. Analysis and biological activities of anthocyanins. *Phytochemistry* **2003**, *64*, 923–933.

73. Marfella, R.; D'Onofrio, N.; Sirangelo, I.; Rizzo, M. R.; Capoluongo, M. C.; Servillo, L.; Paolisso, G.; Luisa Balestrieri, M. Chapter 15 - Polyphenols, Oxidative Stress, and Vascular Damage in Diabetes. In *Diabetes: Oxidative Stress and Dietary Antioxidants*; Preedy, V. R., Ed.; Academic Press: San Diego, 2014; pp. 145–156.

74. Hermsdorff, H.; Barbosa, K.; Volp, A.; Puchau, B.; Bressan, J.; Zulet, M. Vitamin C and fibre consumption from fruits and vegetables improves oxidative stress markers in healthy young adults. *Br J Nutr* **2012**, *107*, 1119–1127.

75. Wang, H.; Nair, M. G.; Strasburg, G. M.; Chang, Y.-C.; Booren, A. M.; Gray, J. I.; DeWitt, D. L. Antioxidant and Antiinflammatory Activities of Anthocyanins and Their Aglycon, Cyanidin, from Tart Cherries. *J. Nat. Prod.* **1999**, *62*, 294–296.

76. Guo, H.; Xia, M. Chapter 8 - Anthocyanins and Diabetes Regulation. In *Polyphenols in Human Health and Disease*; Watson, R. R.; Preedy, V. R.; Zibadi, S., Eds.; Academic Press: San Diego, 2014; pp. 83–93.

77. Speciale, A.; Virgili, F.; Saija, A.; Cimino, F. Chapter 72 - Anthocyanins in Vascular Diseases. In *Polyphenols in Human Health and Disease*; Watson, R. R.; Preedy, V. R.; Zibadi, S., Eds.; Academic Press: San Diego, 2014; pp. 923–941.

78. Mladěnka, P.; Zatloukalová, L.; Filipský, T.; Hrdina, R. Cardiovascular effects of flavonoids are not caused only by direct antioxidant activity. *Free Radic. Biol. Med.* **2010**, *49*, 963–975.

79. Jiménez, J. P.; Serrano, J.; Tabernero, M.; Arranz, S.; Díaz-Rubio, M. E.; García-Diz, L.; Goñi, I.; Saura-Calixto, F. Effects of grape antioxidant dietary fiber in cardiovascular disease risk factors. *Nutrition* **2008**, *24*, 646–653.

80. Shih, C.-H.; Siu; Ng, R.; Wong, E.; Chiu, L. C. M.; Chu, I. K.; Lo, C. Quantitative Analysis of Anticancer 3-Deoxyanthocyanidins in Infected Sorghum Seedlings. *J. Agric. Food Chem.* **2007**, *55*, 254–259.

81. Massey, A. R.; Reddivari, L.; Vanamala, J. The Dermal Layer of Sweet Sorghum (Sorghum bicolor) Stalk, a Byproduct of Biofuel Production and Source of Unique 3-Deoxyanthocyanidins, Has More Antiproliferative and Proapoptotic Activity than the Pith in p53 Variants of HCT116 and Colon Cancer Stem Cells. *J. Agric. Food Chem.* **2014**, *62*, 3150–3159.

82. Woo, H. J.; Oh, I. T.; Lee, J. Y.; Jun, D. Y.; Seu, M. C.; Woo, K. S.; Nam, M. H.; Kim, Y. H. Apigeninidin induces apoptosis through activation of Bak and Bax and subsequent mediation of mitochondrial damage in human promyelocytic leukemia HL-60 cells. *Process Biochem.* **2012**, *47*, 1861–1871.

83. Suganyadevi, P.; Saravanakumar, K. M.; Mohandas, S. The antiproliferative activity of 3-deoxyanthocyanins extracted from red sorghum (Sorghum bicolor) bran through P53-dependent and Bcl-2 gene expression in breast cancer cell line. *Life Sci.* **2013**, *92*, 379–382.

84. Day, A. J.; Gee, J. M.; DuPont, M. S.; Johnson, I. T.; Williamson, G. Absorption of quercetin-3-glucoside and quercetin-4′-glucoside in the rat small intestine: the role of lactase phlorizin hydrolase and the sodium-dependent glucose transporter. *Biochem. Pharmacol.* **2003**, *65*, 1199–1206.

85. Colin D. Kay Aspects of anthocyanin absorption, metabolism and pharmacokinetics in humans. *Nutr. Res. Rev.* **2006**, *19*, 137–146.

86. Dangles, O. Antioxidant activity of plant phenols: chemical mechanisms and biological signficance. *Curr. Org. Chem.* **2012**, *16*, 1–23.

87. Li, Z.; Jiang, H.; Xu, C.; Gu, L. A review: Using nanoparticles to enhance absorption and bioavailability of phenolic phytochemicals. *Food Hydrocoll.* **2015**, *43*, 153–164.

88. Fernandes, I.; de Freitas, V.; Reis, C.; Mateus, N. A new approach on the gastric absorption of anthocyanins. *Food Funct.* **2012**, *3*, 508- 516.

89. Del Rio, D.; Rodriguez-Mateos, A.; Spencer, J. P. E.; Tognolini, M.; Borges, G.; Crozier, A. Dietary (Poly)phenolics in Human Health: Structures, Bioavailability, and Evidence of Protective Effects Against Chronic Diseases. *Antioxid. Redox Signal.* **2012**, *18*, 1818–1892.

90. Mazza G,; Kay CD; Cottrell T; Holub BJ Absorption of anthocyanins from blueberries and serum antioxidant status in human subjects. *J. Agric. Food Chem.* **2002**, *50*, 7731–7737.

91. Del Rio, D.; Rodriguez-Mateos, A.; Spencer, J. P. E.; Tognolini, M.; Borges, G.; Crozier, A. Dietary (poly)phenolics in human health: structures, bioavailability, and evidence of protective effects against chronic diseases. *Antioxid. Redox Signal.* **2013**, *18*, 1818–1892.

92. de Ferrars, R. M.; Czank, C.; Zhang, Q.; Botting, N. P.; Kroon, P. A.; Cassidy, A.; Kay, C. D. The pharmacokinetics of anthocyanins and their metabolites in humans. *Br. J. Pharmacol.* **2014**, *171*, 3268–3282.

93. Vitaglione, P.; Donnarumma, G.; Napolitano, A.; Galvano, F.; Gallo, A.; Scalfi, L.; Fogliano, V. Protocatechuic Acid Is the Major Human Metabolite of Cyanidin-Glucosides. *J. Nutr.* **2007**, *137*, 2043–2048.

94. de Ferrars, R. M.; Czank, C.; Saha, S.; Needs, P. W.; Zhang, Q.; Raheem, K. S.; Botting, N. P.; Kroon, P. A.; Kay, C. D. Methods for Isolating, Identifying, and Quantifying Anthocyanin Metabolites in Clinical Samples. *Anal. Chem.* **2014**, *86*, 10052–10058.

95. Lin, H.-H.; Chen, J.-H.; Huang, C.-C.; Wang, C.-J. Apoptotic effect of 3,4-dihydroxybenzoic acid on human gastric carcinoma cells involving JNK/p38 MAPK signaling activation. *Int. J. Cancer* **2007**, *120*, 2306–2316.

96. Edwards, M.; Czank, C.; Woodward, G. M.; Cassidy, A.; Kay, C. D. Phenolic Metabolites of Anthocyanins Modulate Mechanisms of Endothelial Function. *J. Agric. Food Chem.* **2015**, *63*, 2423–2431.

97. Goupy, P.; Vulcain, E.; Caris-Veyrat, C.; Dangles, O. Dietary antioxidants as inhibitors of the heme-induced peroxidation of linoleic acid: Mechanism of action and synergism. *Free Radic. Biol. Med.* **2007**, *43*, 933–946.

98. Charlotte Sy; Catherine Caris-Veyrat; Claire Dufour; Malika Boutaleb; Patrick Borelcd; Olivier Dangles Inhibition of iron-induced lipid peroxidation by newly identified bacterial carotenoids in model gastric conditions: comparison with common carotenoids. *Food Funct.* **2013**, *4*, 698–712.

99. Giusti, M. M.; Wrolstad, R. E. Acylated anthocyanins from edible sources and their applications in food systems. *Biochem. Eng. J.* **2003**, *14*, 217–225.

100. McCann, D.; Barrett, A.; Cooper, A.; Crumpler, D.; Dalen, L.; Grimshaw, K.; Kitchin, E.; Lok, K.; Porteous, L.; Prince, E.; others Food additives and hyperactive behaviour in 3-year-old and 8/9-year-old children in the community: a randomised, double-blinded, placebo-controlled trial. *The Lancet* **2007**, *370*, 1560–1567.

101. Smyk, B.; Pliszka, B.; Drabent, R. Interaction between Cyanidin 3-glucoside and Cu(II) ions. *Food Chem.* **2008**, *107*, 1616–1622.

102. Taylor, J. R. N.; Belton, P. S.; Beta, T.; Duodu, K. G. Increasing the utilisation of sorghum, millets and pseudocereals: Developments in the science of their phenolic phytochemicals, biofortification and protein functionality. *J. Cereal Sci.* **2013**.

Objective of Thesis

Our research work is focused on 3-deoxyanthocyanins (3-DAs), as natural or bio-inspired colorants and antioxidants, which are both more stable and of easier access by chemical synthesis than anthocyanins.

The present work is developed along two axes:

1- *The chemical synthesis of artificial and natural 3-deoxyanthocyanidins and their O-glucosides by simple procedures*

The simplest route to natural 3-DAs and analogs is the acid-catalyzed aldol condensation between 2-hydroxybenzaldehyde and acetophenone derivatives. This strategy will be applied to the synthesis of various flavylium ions substituted by OH, OMe and β-D-glucosyloxy groups. The series will also include the sorghum pigments luteolinidin and apigeninidin. Special attention will be devoted to optimizing the condensation step (solvent composition, reaction time, temperature, proton donor) and finding the most efficient sequence (sugar deprotection – condensation *vs*. condensation - sugar deprotection).

The organic synthesis of pigments **P1** (3',4',7-trihydroxyflavylium chloride) and **P2** (3',4'-dihydroxy-7-β-D-glucopyranosyloxyflavylium chloride) is reported in **Article I**. The organic synthesis of the other pigments is reported in **Article III**. Each pigment is carefully characterized by NMR and ultrafast UPLC-DAD-MS analyses (*see Appendix II*).

2- *The physicochemical properties of the synthesized pigments*

Our synthetic work provides a good opportunity to investigate the influence of common anthocyanin substituents on the reactivity of the chromophore. In that respect, pigments **P1** and **P2** are especially interesting as they possess a catechol B-ring, which allows metal binding and

efficient electron donation (reducing capacity). The physical chemistry of **P1** and **P2** is described in **Article I** and **Article II**. It includes:

- their structural transformation in aqueous solution: proton transfer, water addition and subsequent isomerization steps,

- their interaction with aluminum and iron ions and its impact on color,

- their affinity for serum albumin, the typical carrier of flavonoids in the blood circulation,

- their radical-scavenging activity (DPPH test) and capacity to inhibit the heme-induced peroxidation of linoleic acid in mildly acidic micelle solution (a simple model of antioxidant activity in the gastric compartment).

A special attention will be devoted to discriminating the reactivity of the colored *vs*. colorless forms, a point typically neglected in the literature.

As part of an ongoing collaboration with the team of Pr. Fernando PINA (Lisbon University) specialized in the physical chemistry of anthocyanins, a detailed work on the structural transformations of **P2** (making use of its remarkable photochromic properties) is also provided as *Annex publication*. This work has been recently extended to the other glucosides (**P3**, **P4**, **P5**, **P6**). The corresponding article is in preparation.

Article I

Analogs of anthocyanins with a 3',4'-dihydroxy substitution: Synthesis and investigation of their acid-base, hydration, metal binding and hydrogen-donating properties in aqueous solution

Nathalie Mora-Soumille, Sheiraz Al Bittar, Maxence Rosa, Olivier Dangles*

Published in *Dyes and Pigments*, **2012**

Abstract

Glycosides of hydroxylated flavylium ions are proposed as pertinent analogs of anthocyanins, a major class of polyphenolic plant pigments. Anthocyanins with a 3',4'-dihydroxy substitution on the B-ring (catechol nucleus) are especially important for their metal chelating and electron-donating (antioxidant) capacities. In this work, an efficient chemical synthesis of 3',4'-dihydroxy-7-*O*-*β*-D-glucopyranosyloxyflavylium chloride (**P2**) and its aglycone (**P1**) is reported. Then, the ability of the two pigments to undergo proton transfer (formation of colored quinonoid bases) and add water (formation of a colorless chalcone) is investigated: at equilibrium the colored quinonoid bases (kinetic products) are present in very minor concentrations (< 10% of the total pigment concentration) compared to the colorless chalcone (thermodynamic product). **P2** appears significantly less acidic than **P1**. The thermodynamics of the overall sequence of flavylium – chalcone conversion is not affected by the *β*-*D*-glucosyl moiety while the kinetics appears slower by a factor *ca*. 8. Although **P1** and **P2** display similar affinities for Al^{3+}, the Al^{3+}-**P2** complex is more stable than the Al^{3+}-**P1** complex due to the higher sensitivity of the latter to water addition and conversion into the corresponding chalcone. Finally, **P1** and **P2** are compared for their ability to reduce the DPPH (1,1-diphenyl-2-picrylhydrazyl) radical in a mildly acidic water/MeOH (1:1) mixture as a first evaluation of their antioxidant activity. Glycosidation at C_7-OH results in a lower rate constant of first electron transfer to DPPH and a lower stoichiometry (total number of DPPH radicals reduced per pigment molecule).

Anthocyanins are difficult to extract from plants in substantial amount. However, the analogs investigated in this work are of easy access by chemical synthesis and express the physico-chemical properties typical of anthocyanins. They can thus be regarded as valuable models for investigating the coloring, metal-binding and antioxidant properties of these important natural pigments.

Keywords: anthocyanin, flavylium, glycoside, synthesis, aluminium, antioxidant

1. Introduction

Polyphenols with a 1,2-dihydroxybenzene (catechol) group are common in plants and in our diet. This is for instance the case of caffeic acid (3,4-dihydroxycinnamic acid) and 3',4'-dihydroxyflavonoids such as quercetin, (epi)catechin, cyanidin and their derivatives (O-glycosides, esters, oligomers) [1,2]. Those polyphenols are of special interest for their ability to bind metal ions and readily transfer electrons or H-atoms to radicals. As such, they are typically strong in vitro antioxidants. Although the relatively poor bioavailability and extensive metabolism of polyphenols in humans [3] severely restrict the biological significance of in vitro antioxidant tests, it is reasonable to assume that polyphenols with a catechol group may be very important antioxidants in plant and food, and possibly in the digestive tract [4,5].

Anthocyanins are naturally occurring glycosides of flavylium (2-phenyl-1-benzopyrylium) ions substituted by hydroxyl and methoxyl groups [6]. As most polyphenols, they are mainly stored in the mildly acidic aqueous environment of vacuoles within plant cells. Anthocyanins constitute one of the major classes of plant pigments, typically responsible for a wide variety of red to blue colors [7]. One important mechanism of color stabilization and variation is metal – anthocyanin binding, a phenomenon restricted to 3',4'-dihydroxyflavylium ions. In particular, most blue colors found in Nature are complexes of anthocyanins with magnesium, aluminium or iron ions. On the other hand, anthocyanins are also one of the most ubiquitous polyphenol classes in foods, *e.g.* berries and their products (juices, jams, red wine), red cabbage, red onion and eggplant [2]. As such, anthocyanins may contribute to the protective effects of diets rich in plant products [8]. However, investigating the chemical properties of anthocyanins in line with their activity in plant, food and in humans is somewhat impeded by their difficult extraction and purification from plants and their limited access from commercial sources. Hence glycosides of hydroxylated flavylium ions can be proposed as pertinent anthocyanin analogs. In this work, an efficient chemical synthesis of 3',4'-dihydroxy-7-*O*-*β*-D-glucopyranosyloxyflavylium chloride and its aglycone is reported as well as the ability of the two pigments to undergo proton transfer, add water with subsequent conversion into chalcones, bind Al^{3+} and deliver electrons to the DPPH (1,1-diphenyl-2-picrylhydrazyl) radical.

2. Experimental

2.1. Materials and instruments

All starting materials were obtained from commercial suppliers and were used without purification. Purifications were performed by column chromatography on Merck Si60 silica gel (40-63 μm) and by elution on Varian bond elut C18 silica gel cartridges.

^{1}H and ^{13}C NMR spectra were recorded on an Advance DPX300 Bruker apparatus at 300.13 MHz (^{1}H) or 75.46 MHz (^{13}C). Chemical shifts (δ) in ppm relative to tetramethylsilane, ^{1}H-^{1}H coupling constants (J) in Hz. High-resolution mass spectrometry (HRMS) analyses were carried out on Qstar Elite instrument (Applied Biosystems SCIEX). Mass detection was performed in the positive electrospray ionization mode. HPLC analyses were performed on a Waters HPLC system consisting of a 600E pump, a 717 autosampler, a 2996 photodiode array detector, an in-line AF degasser and a Millenium workstation. A LichroCart 250-4 Lichrospher 100 RP18e column (250x4.6 mm, 5 μm particle size) was used for chromatographic separations at 25 °C. The solvent system was a gradient of A (5% HCO_2H in MeCN/H_2O 1/1) and B (5% HCO_2H in H_2O) with 10% A at 0 min and 100% A at 60 min (flow rate = 1 ml min^{-1}). UV-Vis absorption spectra were recorded on a Agilent 8453 diode array spectrometer equipped with a magnetically stirred quartz cell (optical pathlength = 1 cm). The temperature in the cell was controlled by means of a water-thermostated bath at 25 ± 0.1 °C.

2.2. Chemical syntheses

2.2.1. 3,4-Dihydroxyacetophenone

A mixture of activated zinc powder (5 g, 76 mmol), ω-chloro-3,4-dihydroxyacetophenone (5 g, 27 mmol), THF (120 ml) and acetic acid (30 ml) was vigorously stirred for 2 days at room temperature. After filtration and concentration under reduced pressure, 100 ml of EtOAc were added. The organic layer was washed with water (3x100 ml),

dried over Na_2SO_4 and evaporated. The crude product was purified by column chromatography (SiO_2, cHex/EtOAc, 1:1 v/v) to give compound 3,4-dihydroxyacetophenone as a white amorphous powder (3.7 g). Yield 90%. ^{1}H NMR [$CDCl_3$]: δ = 2.53 (s, 3H, $COCH_3$), 5.99 (1H, s, OH), 6.19 (1H, s, OH), 6.96 (1H, d, J = 8.3, H_5), 7.55 (1H, dd, J = 2.0 and 8.3, H_6), 7.67 (1H, d, J = 2.0, H_2). ^{13}C NMR [$CDCl_3$]: δ = 24.9 (CH_3), 114.4, 114.6 (C_1, C_5), 122.2 (C_2), 129.2 (C_6), 145.0 (C_3), 150.9 (C_4), 198.4 (C=O). HPLC-UV/Vis t_R = 14.2 min, λ_{max} = 276 nm.

*2.2.2. 3',4',7-Trihydroxyflavylium chloride (**P1**)*

A solution of equimolar amounts (4 mmol) of 2,4-dihydroxybenzaldehyde and 3,4-dihydroxyacetophenone in distilled EtOAc (10 ml) was cooled to 0°C. Gaseous HCl (generated by action of 98% H_2SO_4 on solid NaCl) was gently bubbled through the solution for 90 min. The mixture was kept at 4°C for 3 days, then filtered. More precipitate was collected after evaporation of the filtrate and addition of diethyl ether (Et_2O). After precipitation in EtOAc, **P1** was obtained as a red powder (0.651 g, yield 56%). The purity of **P1** was carefully checked by reversed-phase HPLC. ^{1}H NMR [0.2 M TFA-d in CD_3OD]: δ = 7.08 (1H, d, J = 8.8, $H_{5'}$), 7.40 (1H, dd, J = 2.2 and 8.8, H_6), 7.46 (1H, d, J = 2.2, H_8), 7.84 (1H, d, J = 2.2, $H_{2'}$), 8.00 (1H, dd, J = 2.2 and 8.8, $H_{6'}$), 8.11 (1H, d, J = 8.8, H_5), 8.24 (1H, d, J = 8.8, H_3), 8.99 (1H, d, J = 8.8, H_4). ^{13}C NMR [0.2 M TFA-d in CD_3OD]: δ = 103.0 (C_8), 112.9 (C_3), 115.7 ($C_{2'}$), 117.3 ($C_{5'}$), 119.0 (C_{10}), 121.0 ($C_{1'}$), 121.5 (C_6), 125.7 ($C_{6'}$), 133.1 (C_5), 147.8 ($C_{3'}$), 153.1 (C_4), 156.7 ($C_{4'}$), 159.4 (C_9), 169.3 (C_7), 173.1 (C_2). HRMS m/z = 255.0652 (M^+, 255.0652 calculated for $C_{15}H_{11}O_4^+$). UV/Vis (0.13 M aqueous HCl): ε(470 nm) = 38400 M^{-1} cm^{-1}. HPLC-UV/Vis t_R = 24.1 min, λ_{max} = 472 nm.

2.2.3. 4-(2',3',4',6'-Tetra-O-acetyl-β-D-glucopyranosyloxy)-2-hydroxybenzaldehyde

A solution of tetra-*O*-acetyl-α-D-glucopyranosylbromide (9.25 g, 1.5 equiv.) in CH_2Cl_2 (25 ml) was added to a solution of 2,4-dihydroxybenzaldehyde (2.07 g, 15 mmol) and tris(2-(2-methoxyethoxy)ethyl)amine (7.20 ml, 1.5 equiv.) in 1 M $NaHCO_3$ / 1 M KCl (25 ml, 1/1, v/v). The mixture was refluxed for 48 h. After the addition of H_2O (100 ml) and extraction with CH_2Cl_2 (3 x 100 ml), the combined organic phases were successively washed with 1 M HCl (2 x 100 ml) and H_2O (2 x 100 ml), dried over Na_2SO_4 and concentrated. The residue was purified

on silica gel (eluent EtOAc/ cyclohexane (3/7, v/v)) to afford the target compound as a white powder (5.62 g, yield 80%). ^{1}H NMR [$CDCl_3$]: δ = 2.08 (12H, s, 4 CH_3 of Ac groups), 3.95 (1H, m, $H_{5'}$), 4.17-4.33 (2H, 2dd, J = 12.4 and 5.8, J = 12.4 and 2.3, $H_{6'}$), 5.14-5.32 (4H, m, $H_{1'}$, $H_{2'}$, $H_{3'}$, $H_{4'}$), 6.54 (1H, s, H_3), 6.59 (1H, d, J = 8.5, H_5), 7.47 (1H, d, J = 8.5, H_6). ^{13}C NMR [$CDCl_3$]: δ = 20.6 (4 CH_3 of Ac groups), 61.8 ($C_{6'}$), 68.1 ($C_{4'}$), 70.8 ($C_{2'}$), 72.3 ($C_{5'}$), 72.5 ($C_{3'}$), 97.6 ($C_{1'}$), 103.5 (C_3), 109.6 (C_5), 116.6 (C_6), 135.4 (C_1), 163.1 (C_2), 164.0 (C_4), 169.2-170.6 (4 C=O of Ac groups), 194.9 (CHO).

*2.2.4. 3',4'-Dihydroxy-7-O-β-D-glucopyranosyloxyflavylium chloride (**P2**)*

Equimolar amounts (1 mmol) of 3,4-dihydroxyacetophenone and 4-(2',3',4',6'-tetra-O-acetyl-β-D-glucopyranosyloxy)-2-hydroxybenzaldehyde were dissolved in dry EtOAc (10 ml) and cooled to 0°C. Gaseous HCl was gently bubbled through the solution under stirring during 60 min. The deep-red solution was then allowed to stay at -18°C for 6 days and filtered. Et_2O was added to the filtrate to ensure complete precipitation. The solid was dissolved in MeOH (20 ml) under Ar and a solution of MeONa in MeOH was added until pH 9 (wet pH paper). After stirring for 1.5 h at room temperature, 1 M HCl was added until pH 1 (wet pH paper). The mixture was kept at 4°C for 12 h, then concentrated under reduced pressure. The residue was dissolved in 0.01M HCl (2 mL) and loaded on a C18 cartridge. After elution with 100 ml of 0.01 M HCl to remove contaminating NaCl, **P2** was eluted with 70 ml of 0.2 M HCl in MeOH. After evaporation of solvent under reduced pressure, **P2** was obtained as a red powder (0.34 g, yield 75%). The purity of **P2** was carefully checked by reversed-phase HPLC. ^{1}H NMR [0.2 M TFA-d in CD_3OD]: δ = 3.47 (1H, t, J = 9.2, $H_{4''}$), 3.55-3.61 (2H, m, $H_{3''}$, $H_{2''}$), 3.69-3.79 (2H, m, $H_{5''}$, $H_{6''}$), 3.99 (1H, m, $H_{6''}$), 5.37 (1H, d, J = 6.7, $H_{1''}$), 7.11 (1H, d, J = 8.8, $H_{5'}$), 7.63 (1H, dd, J = 2.2 and 8.9, H_6), 7.91 (1H, d, J = 2.2, H_8), 7.95 (1H, d, J = 2.2, $H_{2'}$), 8.12 (1H, dd, J = 2.2 and 8.8, $H_{6'}$), 8.24 (1H, d, J = 8.9, H_5), 8.42 (1H, d, J = 8.9, H_3), 9.08 (1H, d, J = 8.9, H_4). ^{13}C NMR [0.2 M TFA-d in CD_3OD]: δ = 62.5 ($C_{6''}$), 71.2 ($C_{4''}$), 74.6 ($C_{2''}$), 77.8 ($C_{5''}$), 78.7 ($C_{3''}$), 101.9 ($C_{1''}$), 105.0 (C_8), 109.3 (C_3), 115.5 ($C_{2'}$), 116.9 ($C_{5'}$), 118.3 (C_{10}), 121.6 ($C_{1'}$), 122.3 (C_6), 127.5 ($C_{6'}$), 133.0 (C_5), 148.7 ($C_{3'}$), 153.8 (C_4), 158.6 ($C_{4'}$), 159.2 (C_9), 167.0 (C_7), 175.0 (C_2). HRMS m/z = 417.1178 (M^+, 417.1180 calculated for $C_{21}H_{21}O_9^+$). UV/Vis (0.13 M aqueous HCl): ε(466 nm) = 14300 M^{-1} cm^{-1}. HPLC-UV/Vis t_R = 15.3 min, λ_{max} = 467 nm.

2.3. Spectroscopic measurements

2.3.1. Proton transfer and hydration reactions

To 2 ml of a 0.05 M acetate buffer (pH 3 – 6) containing 0.5 M NaCl and placed in the spectrometer cell was added a small volume (20 – 40 µl) of a concentrated solution of pigment in acidified MeOH (0.2 M HCl). The pigment concentration in the cell was 50 µM. A first UV-visible spectrum was recorded immediately for pK_a determination. A second UV-visible spectrum was recorded after overnight equilibration in the dark for pK'_h determination. For investigating the kinetics of flavylium – chalcone conversion, UV-visible spectra were recorded at regular time intervals (90 s) over 2h following pigment addition. Each experiment was repeated three times at different pH.

2.3.2. Aluminium complexation

To 2 ml of a 0.1 M acetate buffer (pH 4) placed in the spectrometer cell were successively added 50 µl of Al^{3+} solution (prepared from $Al_2(SO_4)_3$, 18 H_2O, concentration range: 1 – 10 mM) in 0.05 M aqueous HCl and 50 µl of a freshly prepared 2 mM pigment solution in acidified MeOH (0.1 M HCl). Spectra were typically recorded every 0.5 s over 1 min or every 15 s over 15 min. Spectra were also recorded after overnight equilibration.

2.3.3. Hydrogen abstraction by DPPH

To 1 ml of a freshly prepared 0.2 mM solution of DPPH in MeOH was added 1 ml of 0.1 M acetate buffer (pH 3.5) in the spectrometer cell (final pH *ca*. 4.4). Aliquots (20 - 60 µl) of a freshly prepared 0.1 mM solution of the antioxidant in acidified MeOH (0.01 M HCl). Spectra were recorded every 0.5 s over 2 min for the determination of rate constants and partial stoichiometries. Kinetic runs over 60 min were used for the determination of total stoichiometries.

2.4. Data analysis

All calculations were carried with the Scientist program (MicroMath, Salt Lake City, USA). Curve-fittings were achieved through least square regression and yielded optimized values for the parameters (rate constants, thermodynamic constants, molar absorption coefficients, stoichiometries, *see eqs in text*). Standard deviations are reported. Good (> 0.99) to excellent (> 0.999) correlation coefficients were typically obtained.

3. Results and discussion

3.1. Synthesis of pigments

The route for the synthesis of 3',4'-dihydroxy-7-*O*-*β*-D-glucopyranosyloxyflavylium chloride (**P2**) was adapted from one of our previous work [9] reporting the synthesis of 3',7-dihydroxy-4'-*O*-*β*-D-glucopyranosyloxyflavylium chloride (Scheme 1). Due to the strong hydrogen bond between the carbonyl group and C_2-OH of 2,4-dihydroxybenzaldehyde, the latter group is probably much less acidic than C_4-OH. Consequently, glycosidation under mildly alkaline phase transfer conditions regioselectively took place at C_4-OH. The flavylium chromophore was then constructed via acid-catalyzed aldol condensation followed by cyclization and subsequent dehydration. Methanolysis of the acetate protecting groups, acidification and purification afforded pigment **2** in good yield.

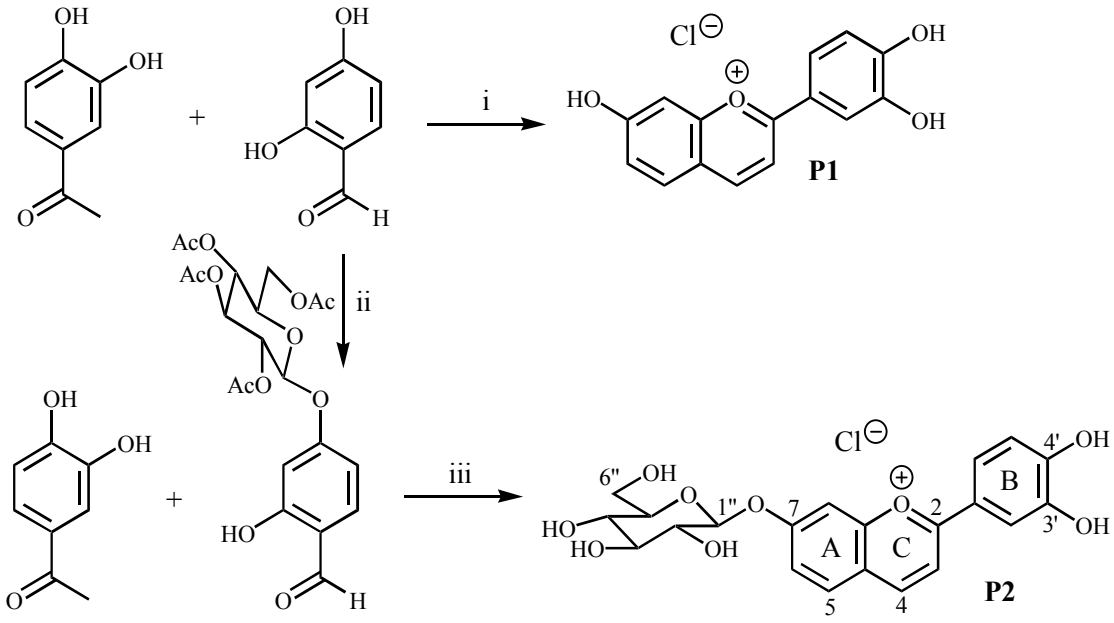

Scheme 1. Chemical synthesis of **P1** and **P2**: (i) Gaseous HCl, AcOEt. (ii) tetra-*O*-acetyl-α-D-glucopyranosylbromide, tris(2-(2-methoxyethoxy)ethyl)amine in CH_2Cl_2 / H_2O (1 M $NaHCO_3$, 1 M KCl). (iii) Gaseous HCl, AcOEt, then MeONa, MeOH, then aq. HCl.

3.2. Structural transformations in water

When the pH is increased from 2 to 6, flavylium ions (AH^+) are typically converted into neutral quinonoid bases (A, kinetic products) by proton transfer (thermodynamic constant K_a) and in a mixture of colorless forms (thermodynamic products) by the following sequence (Scheme 2): water addition at C_2 yielding hemiketal B (thermodynamic constant K_h), cycle-chain tautomerization of B into (*Z*)-chalcone C_Z (thermodynamic constant K_t) and isomerization of C_Z into (*E*)-chalcone C_E (thermodynamic constant K_i) [6,10,11]. Due to their planarity and extensive electron delocalization over the 3 rings, flavylium ions lacking a O-glycosyloxy group at C_3 are less prone to water addition than natural anthocyanins. Consequently, the flavylium ions of **P1** and **P2** are slowly converted into C_E with no significant accumulation of hemiketal B and C_Z.

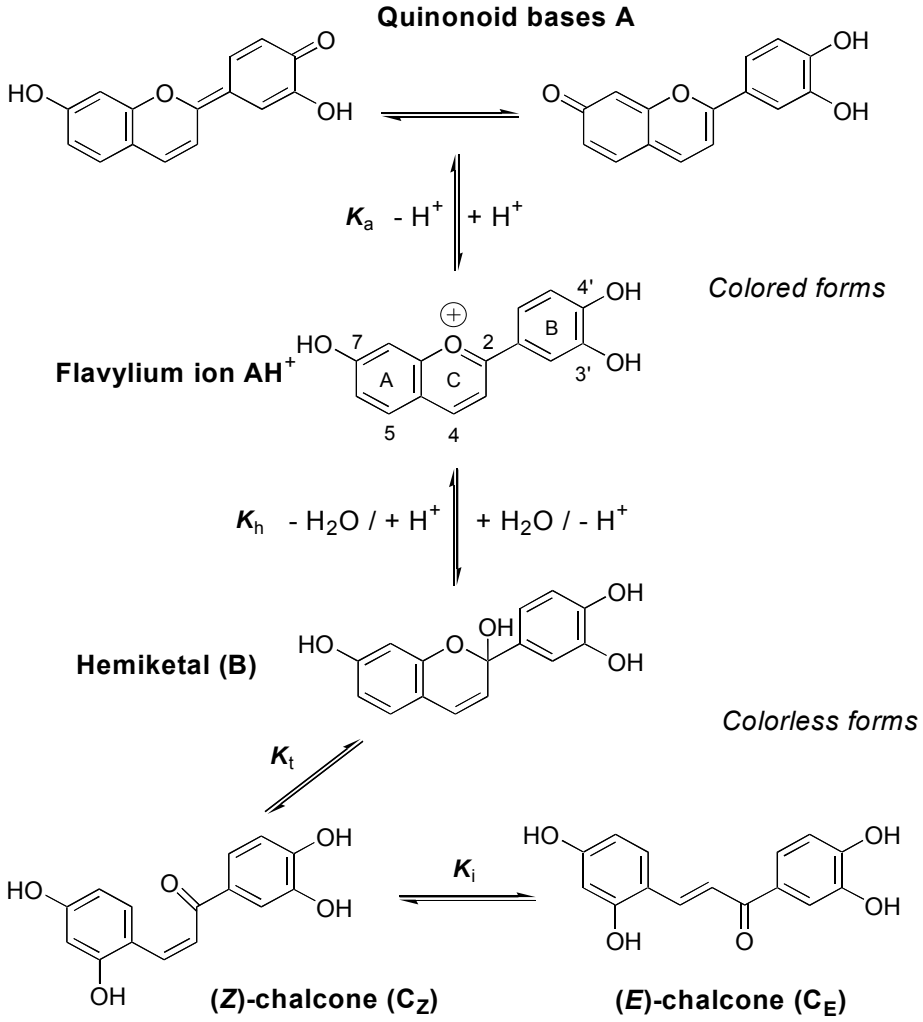

Scheme 2. Structural transformations of 3',4',7-trihydroxyflavylium ion (**P1**) in mildly acidic aqueous solution.

This particular behavior makes it possible to independently investigate proton transfer and chalcone formation. Thus, addition of a strongly acidic concentrated solution of **P1** or **P2** in MeOH to aqueous buffers at pH 3 – 6 with immediate recording of the UV-visible spectra permits the determination of the thermodynamic constant of proton transfer (K_a = $[H^+][A]/[AH^+]$) while the UV-visible spectra recorded after overnight equilibration give access to the overall thermodynamic constant of water addition ($K'_h = K_h K_t K_i = [H^+][C_E]/[AH^+]$). The typical UV-visible spectra of AH^+, A and C_E are shown in Fig. 1.

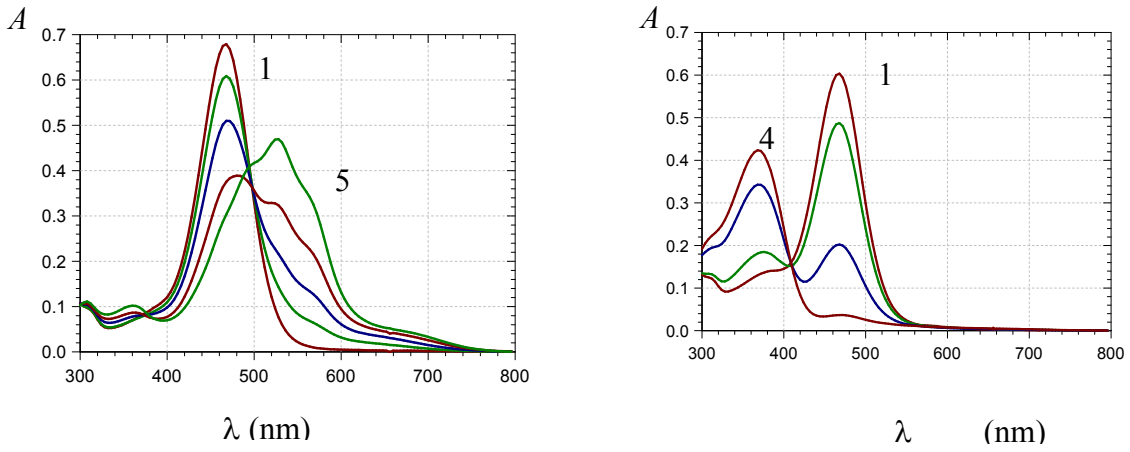

Figure 1. pH-Dependence of the UV-visible spectra of **P2**. *Left*: Spectral measurements immediately after addition of pigment to buffer (**1**: pH 2.0, **2**: pH 4.0, **3**: pH 4.4, **4**: pH 5.0, **5**: pH 6.0). *Right*: Spectral measurements on solutions equilibrated overnight (**1**: pH 2.0, **2**: pH 3.0, **3**: pH 3.5, **4**: pH 4.0).

Combining the Beer's law, the expressions of the thermodynamic constants K_a and K'_h and the equation of pigment conservation readily permits the derivation of the changes in visible absorbance as a function of pH for freshly prepared pigment solution (eq 1, water addition neglected) and solutions equilibrated overnight (eq 2).

$$A_0 = A_{AH}\frac{1+r_A K_a 10^{pH}}{1+K_a 10^{pH}} \quad (1)$$

$$A_f = A_{AH}\frac{1+r_A K_a 10^{pH}}{1+(K_a+K'_h)10^{pH}} \quad (2)$$

$A_{AH} = \varepsilon_{AH} C$ (absorbance of a strongly acidic pigment solution containing the sole flavylium ion, C: total pigment concentration), $r_A = \varepsilon_A/\varepsilon_{AH}$ (ratio of the molar absorption coefficients of quinonoid bases and flavylium ion).

Eqs 1 and 2 were used in the curve-fitting analyses for pK_a and pK'_h determination, respectively (Fig. 2, Table 1).

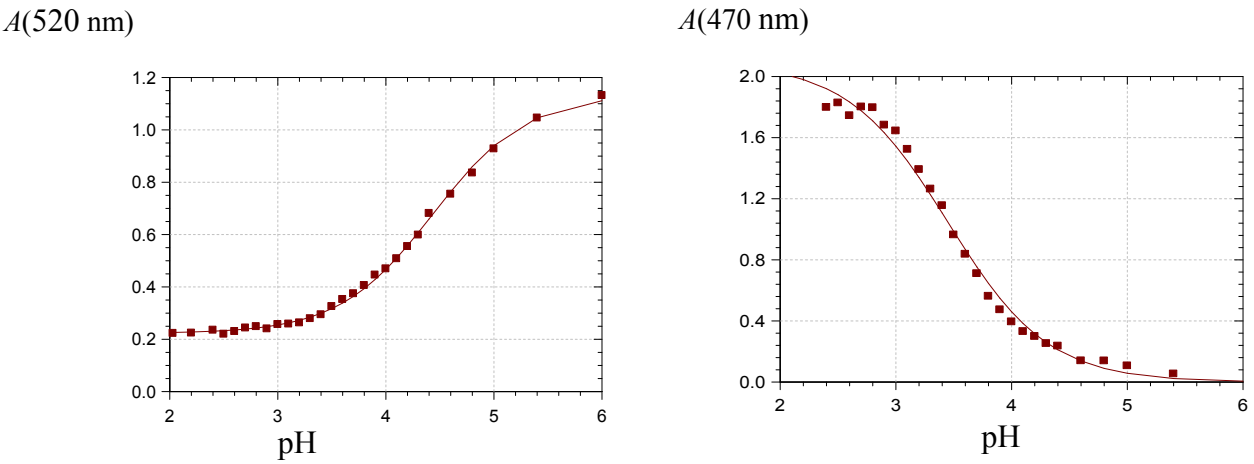

Figure 2. pH dependence of the visible absorbance of **P1**. *Left*: Spectral measurements immediately after addition of pigment to buffer (the solid line is the result of the curve-fitting according to eq 1). *Right*: Spectral measurements on solutions equilibrated overnight the solid line is the result of the curve-fitting according to eq 2).

Table 1. Thermodynamic constants of water addition and proton transfer

Pigment	pK_{obs}	A_{AH}, $r_A = \varepsilon_A/\varepsilon_{AH}$	λ (nm), r (number of points)
P1 [a]	4.44 (± 0.01)	0.22 (± 0.01), 5.1 (± 0.1)	520, 0.9992 (28)
P1 [b]	3.45 (± 0.03)	2.09 (± 0.04), 0	470, 0.996 (25)
P2 [a]	4.72 (± 0.02)	0.085 (± 0.002), 5.64 (± 0.15)	526, 0.998 (26)
P2 [b]	n.a. [c]	-	-

[a] Spectral measurements immediately after addition of pigment to buffer: $K_{obs} = K_a$. Curve-fitting according to eq 1.

[b] Spectral measurements on solutions equilibrated overnight: $K_{obs} = K'_h + K_a \approx K'_h$. Curve-fitting according to eq 2.

[c] Not applicable because of insufficient chemical stability (*see section 3.2.*).

Combining eqs 1 and 2 gives eq 3, which can also be used for the estimation of K'_h from the amplitude $\Delta A = A_0 - A_f$ of the time-dependence of the visible absorbance during water addition (Fig. 3, Table 2).

$$K'_h = (10^{-pH} + K_a)\frac{A_0 - A_f}{A_f} = (10^{-pH} + K_a)\frac{\Delta A}{A_0 - \Delta A} \qquad (3)$$

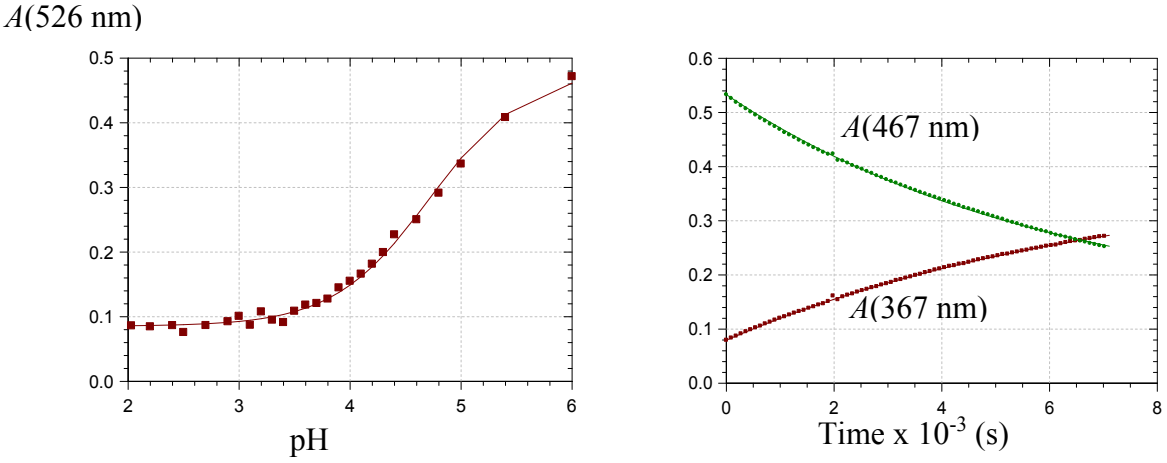

Figure 3. *Left* pH-dependence of the visible absorbance of **P2**. Spectral measurements immediately after addition of pigment to buffer (the solid line is the result of the curve-fitting according to eq 1). *Right*: Time-dependence of the UV-visible absorbance of **P2** at pH 4.0 (the solid lines are the result of exponential curve-fittings).

Unexpectedly, with both **P1** and **P2**, when the observed rate constant of flavylium hydration k_h^{obs} is plotted as a function of the proton concentration, a monotonous increase is observed (Fig. 4), which is in sharp contrast with the usual behavior [6].

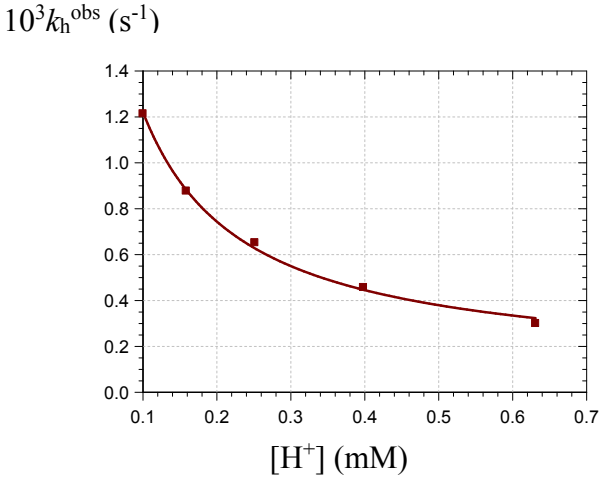

Figure 4. Dependence of the apparent rate constant of flavylium **P1** hydration as a function of the proton concentration. The solid line is the result of the curve-fitting according to eq 5: k'_h = 15.4 (± 0.4) x10^6 M^{-1} s^{-1}, k'_{-h} = 9.3 (± 2.0) x10^{-5} s^{-1} (r = 0.999).

Indeed, quinonoid bases are less electrophilic than the flavylium ion and do not undergo water addition in mildly acidic solution. Hence, k_h^{obs} normally decays when the pH increases as a consequence of less flavylium ion and more quinonoid bases being present in solution. One has: $k_h^{obs} = k'_h x_{AH} + k'_{-h}[H^+]$ (k'_h: overall rate constant for the flavylium to chalcone conversion, k'_{-h}: overall rate constant for the chalcone to flavylium conversion) with $x_{AH} + x_A = 1$, $K_a = [H^+]x_A/x_{AH}$. Combining these equations yields eq 4.

$$k_h^{obs} = \frac{k'_h}{1 + \frac{K_a}{[H^+]}} + k'_{-h}[H^+] \quad (4)$$

Obviously, eq 4 does not hold with **P1** and **P2**. Unlike natural anthocyanins, those flavylium ions are strongly conjugated as no substituent at C_3 restricts the planarity of the 3 rings. Hence, conjugation of $O_{4'}$ and O_7 with the pyrylium C-ring must be very strong and this may lower the positive charge at C_2 to the point that hydration only takes place via the minor hydroxide ion. If so, the observed rate constant of flavylium hydration can be rewritten as: $k_h^{obs} = k'_h x_{AH}[HO^-] + k'_{-h}$. Consequently, eq 4 is changed into eq 5 (K_w: ionic product of water):

$$k_h^{obs} = \frac{k'_h K_w}{[H^+] + K_a} + k'_{-h} \quad (5)$$

Eq 5 actually permits a good curve-fitting of k_h^{obs} *vs*. proton concentration curve (Fig. 4).

With $K_a << K'_h$ for both pigments, it can be concluded that the quinonoid bases (kinetic products) are present in very minor concentrations at equilibrium (< 10% of the total pigment concentration) compared to the chalcone (thermodynamic product) (Fig. 5). **P2** appears significantly less acidic than **P1** as a consequence of the replacement of the acidic proton at C_7-OH by the *β-D*-glucosyl moiety. Unexpectedly, **P2** turned out to be rather unstable in mildly

acidic conditions (pH > 4 – 5), thereby complicating the determination of pK'_h from fully equilibrated solutions. This instability may reflect its sensitivity to autoxidation (initiated by unidentified metal traces). The close pK'_h values deduced from the amplitude of the time-dependence of the visible absorbance during water addition (Table 2) show that the thermodynamics of the overall hydration-ring opening-(*Z*,*E*) isomerization process is not affected by the *β*-*D*-glucosyl moiety.

Surprisingly, this is not so with the corresponding kinetics. Indeed, at pH 4.0, glycosidation at C_7-OH lowers the rate constant of flavylium consumption by a factor *ca*. 8 (Table 2). As the observed kinetics is governed by the step of chalcone (*Z*,*E*) isomerization, it may be suggested that the +M effect of O_7 weakens the C_3=C_4 double bond by enhancing the conjugation with C_4=O and that this effect is strongly decreased by glycosidation of O_7, thereby making the chalcone (*Z*,*E*) isomerization much slower for **P2** than for **P1** with no impact on the thermodynamics of the reaction.

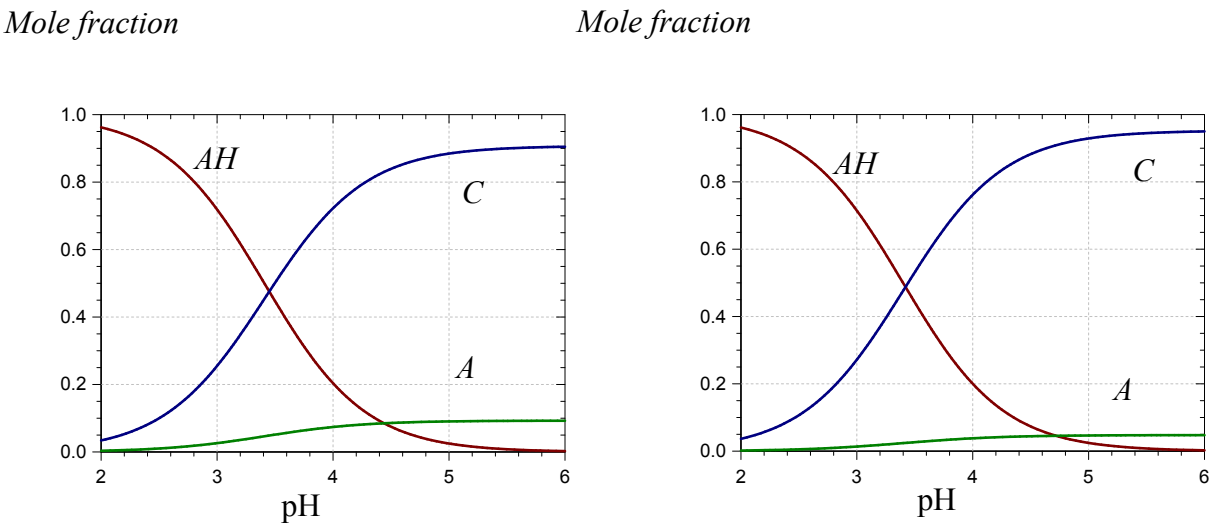

Figure 5. Speciation diagrams of **P1** (*Left*) and **P2** (*Right*) at equilibrium.

Table 2. Kinetics of flavylium – chalcone conversion at pH 4.0

Pigment	$10^5 k_h^{obs}$ (s^{-1})	A_0, ΔA	pK'_h [a]	λ (nm), r
P1	121.3 (± 0.1)	1.70, 1.28	3.38	470, 0.99999
	134.1 (± 0.3)	0.225, 0.693		377, 0.99995
P2	16.5 (± 0.2)	0.533, 0.405	3.42	467, 0.9998
	15.7 (± 0.2)	0.072, 0.295		367, 0.9998

[a] Calculated according to eq 3.

3.3 Aluminium complexation

Anthocyanins having a 1,2-dihydroxy substitution in their B-ring can bind hard metal ions such as Al^{3+} and Fe^{3+} with concomitant removal of the phenolic protons [7,12]. The corresponding chelates display a quinonoid structure that is much more stable than in the absence of metal ions. Consequently, metal binding is a powerful mechanism of color variation and stabilization in plants. In this work, **P1** and **P2** were compared for their ability to bind Al^{3+} in mildly acidic aqueous solutions mimicking their natural medium (vacuoles of plant cells).

When **P1** and **P2** are added to a Al^{3+} solution in a pH 4 acetate buffer, a relatively fast binding of the colored form is observed which is manifested by a decay of the visible absorption band at *ca*. 470 nm (free ligand *L*, a mixture of flavylium and quinonoid bases) and a building-up of a broader absorption band at *ca*. 525 nm characteristic of the metal complex (*ML*) (Fig. 6). Interestingly, the Al^{3+} complex of **P1** appeared much less stable than the one of **P2** as judged from the subsequent decay of *A*(525 nm) and concomitant increase of the absorbance at 370 - 380 nm featuring free chalcone accumulation (Fig. 7). However, after overnight equilibrium, accumulation of free chalcone was observed with both **P1** and **P2** although in much lower concentration with the glucoside (Fig. 6).

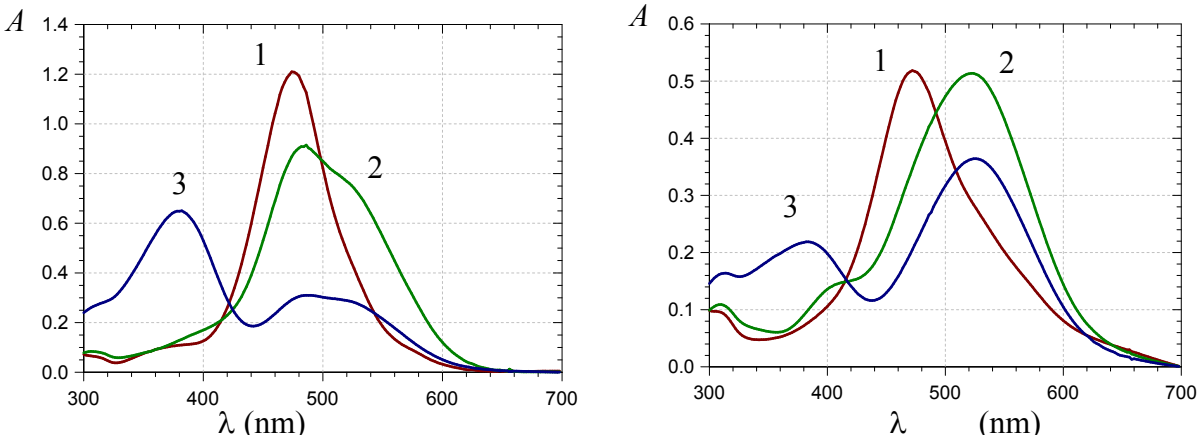

Figure 6. UV-visible spectra of **P1** (*Left*) and **P2** (*Right*) in the presence of Al^{3+} (4 equiv.) at pH 4. **1**: free ligand, **2**: time of maximal Al^{3+} complexation, **3**: after equilibration overnight.

The absorbance – time curves for free ligand consumption and complex and chalcone formation could be analyzed simultaneously according to a simplified mechanism assuming irreversible metal binding (rate constant k_M) and water addition on both the free ligand and its complex (respective rate constants k_h^{obs} and k_h^M). In addition to the Beer's law for the different pigment species (L, ML, C), eqs 6-9 were used in the curve-fittings:

$$-d[L]/dt = k_M[M][L] + k_h^{obs}[L] \quad (6)$$

$$-d[M]/dt = k_M[M][L] - k_h^M[ML] \quad (7)$$

$$d[ML]/dt = k_M[M][L] - k_h^M[ML] \quad (8)$$

$$d[C]/dt = k_h^{obs}[L] + k_h^M[ML] \quad (9)$$

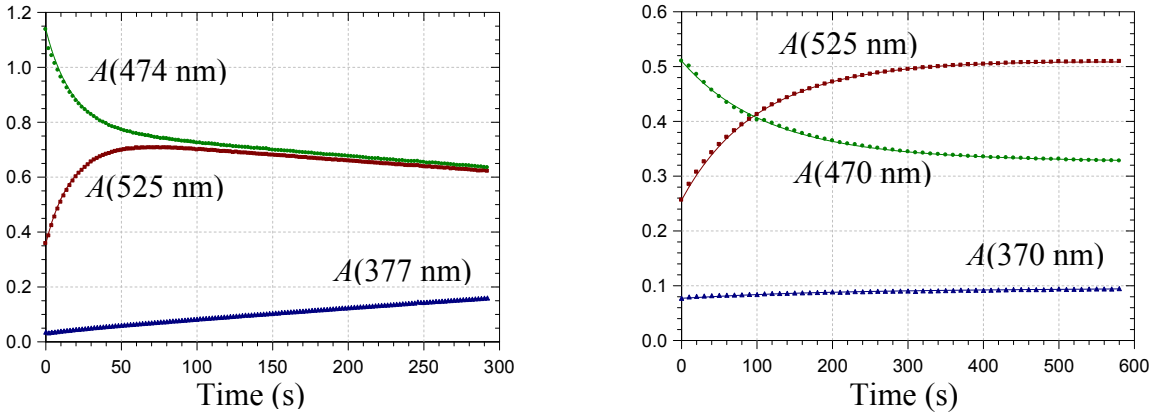

Figure 7. Time-dependence of the UV-visible absorbance of **P1** (*Left*) and **P2** (*Right*) after addition of Al^{3+} (4 equiv.) at pH 4.0. The solid lines are the result of the curve-fittings according to eqs 6-9.

The optimized values of the observed rate constants are collected in Table 3. It is noteworthy that no satisfactory curve-fitting could be achieved without the hypothesis of water addition onto the complex. In particular, the slow decay of the absorption band of the Al^{3+} - **P1** complex could not be accounted for by assuming reversible metal binding and water addition on the free ligand only.

From this kinetic analysis, it is also clear that Al^{3+} binding is faster with **P1** than with **P2** but that the Al^{3+} - **P1** complex is much more prone to water addition than the Al^{3+} - **P2** complex. From this viewpoint, glycosidation at C_7-OH can be regarded as an efficient way to increase the stability of the Al^{3+} complex in mildly acidic aqueous solution. Surprisingly, the values of the observed rate constant for free flavylium hydration (k_h^{obs}) are higher than those estimated in the absence of Al^{3+} (Table 2), especially for **P2**. It is unclear why the free flavylium - chalcone conversion is faster in the presence of Al^{3+}.

It can however be noted that C_E itself probably binds Al^{3+} as evidenced by the weak bathochomic shift (ca. 10 nm) observed when comparing Fig. 1 (lower part, free C_E) and Fig. 6 (lower part). As the kinetics of the overall flavylium - chalcone conversion is governed by the slow step of (*Z*)-(*E*) chalcone isomerization, it can be suggested that Al^{3+} - chalcone binding accelerates the latter step.

Table 3. Kinetic analysis of Al^{3+} binding and water addition at pH 4.0 [a]

Pigment	Al^{3+} (equiv.)	k_M (M^{-1} s^{-1})	$10^5 k_h^{obs}$, $10^5 k_h^M$ (s^{-1})	ε_{ML} [b] (ε_C [c]) (M^{-1} cm^{-1})
P1	2	486 (± 3)	302 (± 7), 82 (± 1)	19990, 27980 (21920)
	4	288 (± 1)	324 (± 6), 64 (± 1)	21290, 21850 (20480)
	6	257 (± 2)	341 (± 14), 54 (± 1)	24690, 20550 (21960)
	8	195 (± 1)	614 (± 23), 38 (± 1)	23000, 17400 (19950)
	10	161 (± 1)	467 (± 26), 29 (± 1)	27550, 18840 (22390)
P2	2	23.2 (± 1.0)	284 (± 9), 6.3 (± 0.2)	25520, 20600 (4340)
	4	37.3 (± 1.3)	226 (± 22), 3.2 (± 0.3)	16240, 10420 (8140)
	6	41.3 (± 1.4)	284 (± 36), 2.5 (± 0.2)	16550, 9200 (10440)
	8	40.3 (± 1.1)	315 (± 36), 1.8 (± 0.2)	16430, 8970 (11990)
	10	12.6 (± 0.1)	182 (± 6), 3.7 (± 0.1)	15890, 10020 (9250)

[a] **P1**: simultaneous curve-fitting of the absorbance curves at 525, 474 and 377 nm (Δt = 2 s, t_f = 5 min) according to eqs 6-9. **P2**: simultaneous curve-fitting of the absorbance curves at 525, 470 and 370 nm (Δt = 10 s, t_f = 15 min).

[b] First value at 525 nm, second value at 474 nm (**P1**) or 470 nm (**P2**).

[c] At 377 nm (**P1**) or 370 nm (**P2**).

The maximal absorbance amplitude at 525 nm (ΔA) was also plotted as a function of the total metal concentration (M_t) and the corresponding curve analyzed by assuming pure 1:1 binding and negligible chalcone formation (eqs 10 and 11, K_M: metal – pigment binding constant, L_t: total ligand concentration, $\Delta\varepsilon = \varepsilon_{ML}^{525} - \varepsilon_L^{525}$).

$$\Delta A = \Delta\varepsilon(M_t - [M]) \qquad (10)$$

$$M_t = [M](1 + \frac{K_M L_t}{1 + K_M [M]}) \qquad (11)$$

The following K_M values were thus obtained: for **P1**, K_M = 8.9 (± 1.3) x10^3 M^{-1} (r = 0.997), for **P2**, K_M = 19 (± 8) x10^3 M^{-1} (r = 0.98).

Alternatively, for **P2**, the observed first-order rate constant of metal binding (k_M^{obs}) was found to vary linearly with the total metal concentration (Fig. 8, r = 0.998). From $k_M^{obs} = k_M M_t + k_{-M}$, estimates for the rate constants of complex formation and dissociation were obtained: k_M = 44 (± 2) M^{-1} s^{-1}, k_{-M} = 20 (± 4) x10^{-4} s^{-1}, from which one deduces: $K_M = k_M/k_{-M}$ = 22 x10^3 M^{-1}.

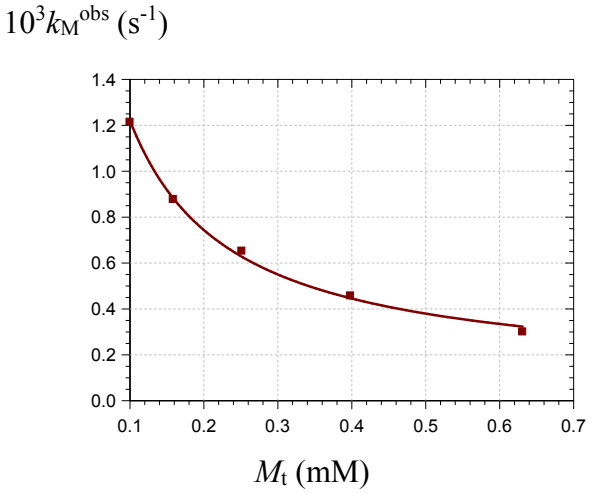

Figure 8. Plot of the apparent first-order rate constant of Al^{3+} - **P2** binding as a function of the total metal concentration (pH 4.0).

Finally, for **P1**, the overall first-order rate constant of flavylium – chalcone conversion was plotted as a function of M_t and the corresponding curve analyzed according to eqs 11 and 12 (Fig. 9, $r = 0.996$).

$$k_h^{overall} = \frac{k_h^{obs} + k_h^M K_M[M]}{1 + K_M[M]} \qquad (12)$$

Thus, one obtains estimates for the binding constant as well as for the rate constants of chalcone formation from the free flavylium and its complex: $k_h^{obs} = 195\ (\pm 12)\ x10^{-5}\ s^{-1}$, $k_h^M = 45\ (\pm 1)\ x10^{-5}\ s^{-1}$, $K_M = 9.8\ (\pm 3.5)\ x10^3\ M^{-1}$.

In summary, **P1** and **P2** display similar affinities for Al^{3+} ($K_M = 1 - 2\ x10^4\ M^{-1}$) but the complex of **P2** is more stable as its conversion into the corresponding chalcone is slower.

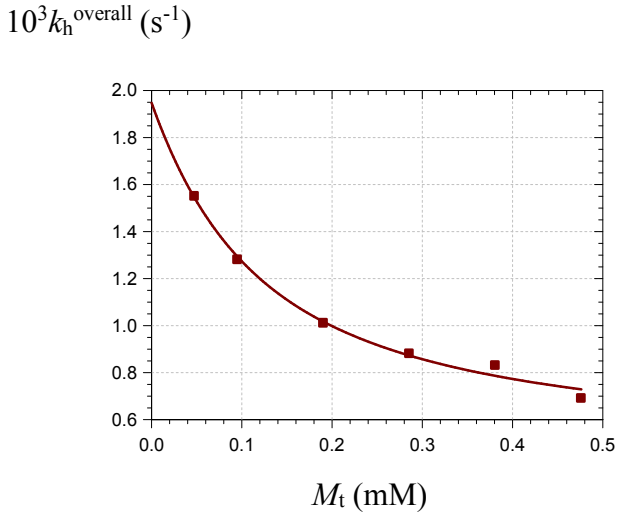

Figure 9. Plot of the apparent first-order rate constant of flavylium – chalcone conversion for **P1** as a function of the total metal concentration (pH 4.0). The solid line is the result of the curve-fitting according to eq 12.

3.4. Scavenging of the DPPH radical

Polyphenols with a catechol group are potent electron or H-atom donors to radicals due to the relatively stability of the semiquinone radicals thus formed (a combination of electronic and intramolecular hydrogen bonding effects). Semiquinone radicals derived from polyphenols are however rapidly converted into *o*-quinones by disproportionation or scavenging of a second radical. From these reactive intermediates, different pathways (oligomerization, solvent addition, ring cleavage) typically ensue, ultimately giving a complex set of oxidation products [4]. Such reactions may take place in plants where polyphenols act as electron donors for the enzymatic reduction of hydrogen peroxide in vacuoles but also in food and in the digestive tract where polyphenols may protect polyunsaturated lipids from oxidation and/or regenerate the potent phenolic antioxidant α-tocopherol (vitamin E) by H-atom or electron transfer to its aryloxyl radical. Whether in plants, food or the digestive tract, anthocyanins typically experience a mildly acidic aqueous environment. Hence, investigating their electron-donating capacity toward the stable radical DPPH (1,1-diphenyl-2-picrylhydrazyl) in a MeOH / pH 3.5 acetate buffer (1:1) mixture (final pH *ca*. 4.4) is a first acceptable approach to assess their antioxidant activity.

When the pigment is added to the DPPH solution, a fast decrease of the DPPH visible absorption band is observed featuring the transfer of the labile H-atoms of the catechol OH groups. Then, a slower decay follows that reflects the residual H-donating activity of some oxidation products. From the total absorbance amplitude over 1h (ΔA^{515} = A^{515}(t = 1h) - A^{515}(t = 0, *i.e*. before pigment addition)), the total number of DPPH radicals reduced to the corresponding hydrazine per pigment molecule (total stoichiometry n_{tot}) can be deduced from the following relationship: $n_{tot} = \Delta A^{515}/(\varepsilon^{515}_{DPPH}\,[\text{pigment}]_0)$ (Table 4) with ε^{515}_{DPPH} = 11240 M^{-1} cm^{-1} [13].

The fast step was kinetically analyzed according to a model developed in details in our previous works [13,14] and permitting the estimation of the rate constant of first H-atom transfer (k_1) and the partial stoichiometry n (number of DPPH radicals reduced per pigment molecule during the fast step) (Table 4). It is noteworthy that the kinetic analysis had to be conducted at 600 nm so as to avoid interference with the visible absorption of the pigment at the onset of the reaction.

Table 4. DPPH scavenging by P1 and P2 in MeOH / pH 3.5 acetate buffer (1:1)

Pigment, conc. (μM)	DPPH conc. (μM)	k_1 (M^{-1} s^{-1}) [a]	n [a]
P1, 10	77.0	4305 (± 64)	2.22 (± 0.01)
P1, 15	83.8	4290 (± 160)	2.09 (± 0.03)
P1, 15	77.4	5354 (± 70)	2.67 (± 0.01)
P2, 15	64.6	1426 (± 37)	0.85 (± 0.01)
P2, 15	64.8	1355 (± 48)	0.70 (± 0.01)
P2, 25	70.8	1368 (± 32)	0.91 (± 0.01)
P2, 25	66.5	1363 (± 11)	0.93 (± 0.01)
P2, 30	65.9	1066 (± 10)	0.82 (± 0.01)

[a] Curve-fitting of A^{600} *vs*. time curves (see model in text) over the 40 first seconds following pigment addition: k_1: rate constant of first H-atom abstraction, n: number of DPPH radicals reduced per pigment molecule.

[b] From the absorbance amplitude at 515 nm over 1h: total number of DPPH radicals reduced per pigment molecule n_{tot} = 4.0 (± 0.2) for **P1**, 1.38 (± 0.04) for **P2** (means from triplicates).

As the catechol group is the critical determinant of the H-donating activity of polyphenols, it may be anticipated that **P2** be as good at scavenging the DPPH radical as **P1**. Surprisingly, this is not so. Not only does **P1** transfer a first H-atom to DPPH *ca*. 4 times as rapidly as **P2**, but also the total number of DPPH radicals reduced by **P1** is *ca*. 3 times as high as by **P2**. As DPPH is a rather bulky radical, part of the lower reactivity of **P2** could be attributed to the steric hindrance brought about by the glucose moiety. It is also important to keep in mind that **P2** is less acidic than **P1**. As the flavylium ion (because of its positive charge) is expected to be a poor electron or H-atom donor and as the kinetic of flavylium – chalcone conversion is much slower than the DPPH-scavenging reaction, rate constant k_1 must essentially reflect the ability of the quinonoid bases to transfer an H-atom to DPPH. Moreover, **P1** can form both $A_{4'}$ and A_7 tautomers whereas A4' is the only possible quinonoid base for **P2**. Overall, it could be suggested that A_7 makes a major contribution to the radical-scavenging activity of **P1** via H-transfer from $C_{4'}$-OH. Alternatively, the anionic quinonoid base $A_{4',7}$, although in minor concentration, could be the true electron-donor due to the extended electron-delocalization on the chromophore. Indeed, upon deprotonation, $A_{4'}$ and A_7 merge into a single π-electron-rich

anion with a concomitant spectacular rise of the HOMO by *ca*. 4 eV (HyperChem software, AM1 parametrization).

On the other hand, the total stoichiometry value is defined by the fate of the antioxidant during oxidative degradation. In a previous work [15], we showed that upon two-electron oxidation **P1** forms an *o*-quinone that undergoes water addition on the C- and A-rings. The quinonoid bases thus formed display an additional OH groups and must also participate in radical-scavenging, thereby prolonging the activity. It is possible that glycosidation at C_7-OH somehow hinders these sequences of oxidation / water addition, thus resulting in lower n_{tot} values.

4. Conclusion

3',4'-Dihydroxy-7-*O*-*β*-D-glucopyranosyloxyflavylium chloride (**P2**), which has been synthesized in this work at a scale of several hundreds of mg, is a valuable model of natural anthocyanins. Its glucose moiety improves the water solubility while only moderately affecting the acid-base and hydration properties of the chromophore. Due to its catechol group, **P2** can be used to investigate the affinity of anthocyanins for metal ions and their ability to deliver electrons to radicals, two characteristics that have a strong impact on the pigmentation and nutritional properties of anthocyanins.

References

[1] Quideau S, Deffieux D, Douat-Casassus C, Pouysegu L. Plant polyphenols: chemical properties, biological activities, and synthesis. Angew Chem Int Ed **2011**;50:586-621.

[2] Perez-Jimenez J, Neveu V, Vos F, Scalbert A. Systematic analysis of the content of 502 polyphenols in 452 foods and beverages: an application of the phenol-explorer database. J Agric Food Chem **2010**;58:4959-4969.

[3] Crozier A, Jaganath I B, Clifford MN. Dietary phenolics: chemistry, bioavailability and effects on health. Nat Prod Rep **2009**;26:1001-1043.

[4] Dangles O. Antioxidant activity of plant phenols: chemical mechanisms and biological significance. Curr Org Chem **2012**;16:692-714.

[5] Frankel EN, Finley JW. How to standardize the multiplicity of methods to evaluate natural antioxidants. J Agric Food Chem **2008**;56:4901-4908.

[6] Pina F, Melo MJ, Laia CAT, Parola AJ, Lima JC. Chemistry and applications of flavylium compounds: a handful of colours. Chem Soc Rev **2012**;41:869-908.

[7] Yoshida K, Mori M, Kondo T. Blue flower color development by anthocyanins: from chemical structure to cell physiology. Nat Prod Rep **2009**;26:857-964.

[8] Tsuda T. Dietary anthocyanin-rich plants: Biochemical basis and recent progress in health benefits studies. Mol Nutr Food Res **2012**;56:159-170.

[9] El Hajji H, Dangles O, Figueiredo P, Brouillard R. 3'-(*β*-D-Glycopyranosyloxy)flavylium ions: synthesis and investigation of their properties in aqueous solution. Hydrogen bonding as a mean of colour variation. Helv Chim Acta **1997**;80:398-413.

[10] Dangles O, Saito N, Brouillard R. Kinetic and thermodynamic control of flavylium hydration in the pelargonidin-cinnamic acid complexation. Origin of the extraordinary flower color diversity of *Pharbitis nil*. J Am Chem Soc **1993**;115:3125-3132.

[11] Nave F, Petrov V, Pina F, Teixeira N, Mateus N, de Freitas V. Thermodynamic and kinetic properties of a red wine pigment: catechin-(4,8)-malvidin-3-*O*-glucoside. J Phys Chem B **2010**;114:13487-13496.

[12] Dangles O, Elhabiri M, Brouillard R. Kinetic and thermodynamic investigation of the aluminium-anthocyanin complexation in aqueous solution. J Chem Soc Perkin Trans 2 **1994**;2587-2596.

[13] Goupy P, Loonis M, Dufour C, Dangles O. A quantitative kinetic analysis of hydrogen transfer reactions from dietary polyphenols to the DPPH radical. J Agric Food Chem **2003**;51:615-622.

[14] Goupy P, Bautista-Ortin AB, Fulcrand H, Dangles O. Antioxidant activity of wine pigments derived from anthocyanins: hydrogen transfer reactions to the DPPH radical

and inhibition of the heme-induced peroxidation of linoleic acid. J Agric Food Chem **2009**;57:5762-5770.

[15] Dangles O, Fargeix G, Dufour C. Antioxidant properties of anthocyanins and tannins: a mechanistic investigation with catechin and the 3',4',7-trihydroxyflavylium ion. J Chem Soc Perkin Trans 2 **2000**;1653-1663.

Article II

Chemically Synthesized Glycosides of Hydroxylated Flavylium Ions as Suitable Models of Anthocyanins: Binding to Iron Ions and Human Serum Albumin, Antioxidant Activity in Model Gastric Conditions

Sheiraz Al Bittar, Nathalie Mora-Soumille, Michèle Loonis, Olivier Dangles*

Published in *Molecules*, **2014**

Abstract:

Polyhydroxylated flavylium ions, such as 3',4',7-trihydroxyflavylium chloride (P1) and its more water-soluble 7-*O*-β-D-glucopyranoside (P2), are readily accessible by chemical synthesis and suitable models of natural anthocyanins in terms of color and species distribution in aqueous solution. Owing to their catechol B-ring, they rapidly bind Fe^{III}, weakly interact with Fe^{II} and promote its autoxidation to Fe^{III}. Both pigments inhibit heme-induced lipid peroxidation in mildly acidic conditions (a model of postprandial oxidative stress in the stomach), the colorless (chalcone) forms being more potent than the colored forms. Finally, P1 and P2 are moderate ligands of human serum albumin (HSA), their likely carrier in the blood circulation, with chalcones having a higher affinity for HSA than the corresponding colored form

Keywords: anthocyanin; 3-deoxyanthocyanidin; flavylium; chalcone; iron; lipid peroxidation; serum albumin.

1. Introduction

Anthocyanins are responsible for the colors of numerous flowers, fruits, vegetables and even cereals. Colors expressed by anthocyanins vary from red to blue depending on pH, self-association (especially, in the case of acylated anthocyanins) and interactions with metal ions (Al^{3+}, Fe^{3+}, Mg^{2+}) and phenolic copigments, such as flavones, flavonols and hydroxycinnamic acids [1–5]. Through their coloring properties, anthocyanins strongly contribute to food quality and appeal to consumers. They may also contribute to the health benefits of diets rich in plant products [6]. For instance, anthocyanins with an electron-rich B-ring, in particular an *o*-dihydroxylated B-ring (catechol), are intrinsically good antioxidants, either by acting as electron donors to reactive oxygen species or by chelating transition metal ions (potential inducers of oxidative stress) as inert complexes [7,8].

Dietary anthocyanins can be partly absorbed along the gastrointestinal (GI) tract (from stomach to colon) [9] but have an overall poor bioavailability in humans, at least based on the very low circulating concentrations of the native forms and their conjugates [10]. In fact, anthocyanins may be relatively unstable in the intestine [11–14] and, as polyphenols in general [15], undergo an extensive catabolism by intestinal glucosidases and by the enzymes of the colonic microbiota. In particular, hydrolysis of the anthocyanins' glycosidic bond at C3-OH, which releases highly unstable anthocyanidins, must be a critical step toward cleavage of the C-ring. Consequently, a large part of the health benefits of anthocyanins is expected to be mediated by their degradation products and their conjugates [16].

On the other hand, anthocyanins, as ubiquitous dietary polyphenols, can accumulate under their native form in the GI tract and possibly protect dietary lipids and proteins against oxidation. Indeed, in gastric conditions (high O_2 content, acidic pH), lipid peroxidation induced by dietary heme iron could be very significant but efficiently inhibited by polyphenols [17–21]. Through reduction of high-valence heme iron, polyphenols could preserve the nutritional value of the dietary bolus and prevent the formation of toxic lipid peroxidation products. This hypothesis of an early antioxidant protection by dietary polyphenols, including anthocyanins, is gaining evidence from *in vivo* studies [22].

Once in the general blood circulation, polyphenols and their metabolites, typically bound to human serum albumin (HSA) [23,24], are delivered to tissues for specific biological effects

[15]. 3-Deoxyanthocyanidins and their glucosides have been identified in cereals such as red sorghum [25]. Lacking the C3-OH group of anthocyanidins, which is critically involved in their degradation, 3-deoxyanthocyanidins express more stable colors [26]. They are also promising pigments in terms of potential health benefits, expressed by antioxidant and cell-specific effects [27–29]. So far, little is known about their bioavailability but it may be speculated that it is higher than that of anthocyanins, as 3-deoxyanthocyanidins are probably less prone to catabolism in the GI tract. For future development as food ingredients, it is also noteworthy that mutagenesis-assisted breeding can dramatically increase 3-deoxyanthocyanidin accumulation in sorghum leaves [30].

Interestingly, 3-deoxyanthocyanidins and their glucosides, in particular simplified analogs lacking the C5-OH group, are far more accessible by chemical synthesis than even the simplest anthocyanins. In a previous paper [31], we reported the chemical synthesis, structural transformations, aluminium binding and radical-scavenging (DPPH test) of 3',4',7-trihydroxyflavylium chloride (P1) and its 7-*O*-β-D-glucoside (P2) (Figure 1).

In this work, their capacity to bind iron ions and inhibit heme-induced lipid peroxidation in mildly acidic conditions (a model of postprandial oxidative stress in the stomach) will be quantitatively studied as well as their affinity for HSA, their likely carrier in the blood circulation. In each model, the activity of the colored and colorless forms will be discriminated.

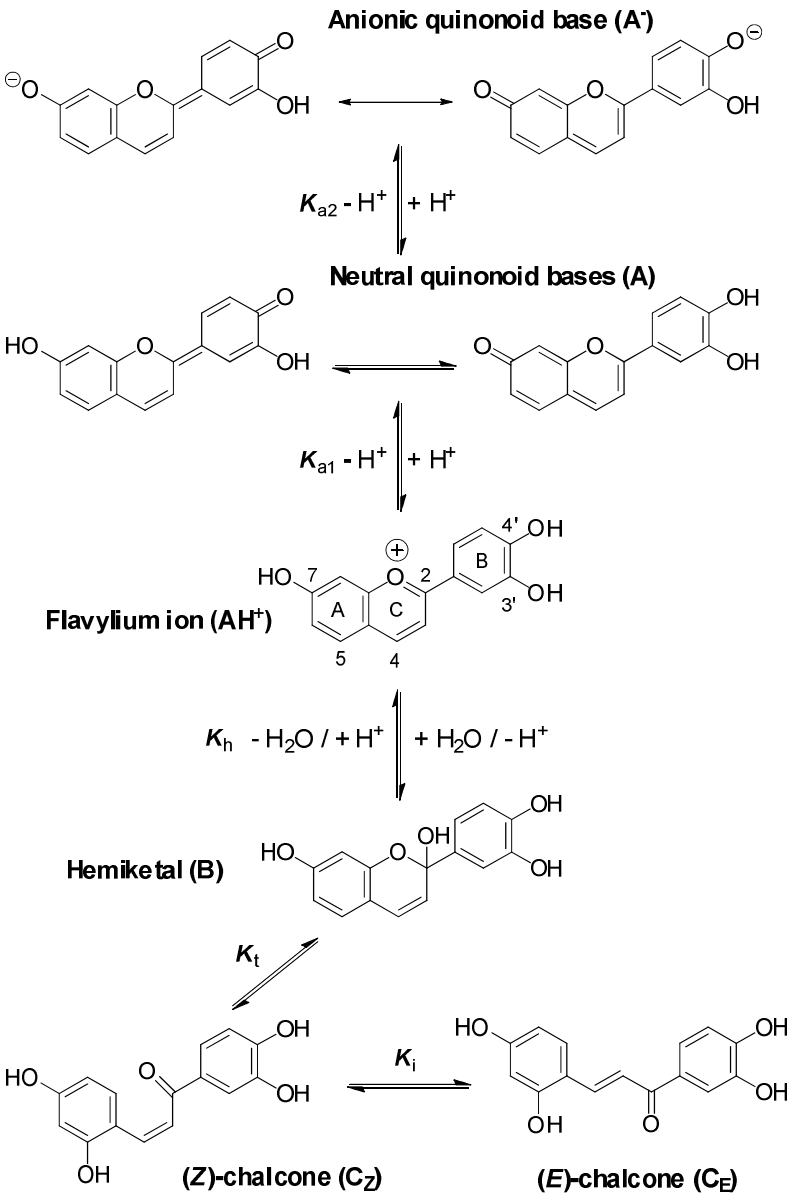

Figure 1. Structural transformations of the 3',4',7-trihydroxyflavyliumion (P1)

The aim of this work is to emphasize, through detailed quantitative physico-chemical analyses, that readily available 3-deoxyanthocyanidins—a relatively overlooked class of natural pigments—are interesting colorants and antioxidants deserving further examination for future applications.

2. Results and Discussion

As a general comment, interpretation of our data rests on the well-established scheme of structural transformation for the flavylium ion of anthocyanins (Figure 1) [32,33]. However, flavylium ions lacking the glycosyloxy substituent of natural anthocyanins at C3 display some peculiarities: dehydration of hemiketal B into the highly planar flavylium ion is faster as well as its sequential conversion into C_Z and C_E. C_E is also much more stable than C_Z ($K_i \approx 75$ for P2 [32]) whereas the two isomers display close stability with natural anthocyanins. Consequently, B and C_Z can be regarded as transient (non-accumulating) intermediates in the overall conversion of the flavylium ion into the corresponding (*E*)-chalcone.

2.1. Iron-Pigment Binding

Together with copigmentation and self-association, metal-anthocyanin binding is one of the most important mechanisms for varying and stabilizing natural colors [1]. In our previous work [31], both P1 and P2 were shown to bind Al^{III} in mildly acidic solutions, thereby forming chelates having a quinonoid chromophore as the result of the simultaneous loss of the two protons at C3'-OH and C4'-OH. Interestingly, the Al^{III}-P2 complex is more resistant than the Al^{III}-P1 complex toward water addition leading to the free (unbound) (*E*)-chalcone.

In this work, P1 and P2 are compared for their ability to bind Fe^{III} and Fe^{II}. As iron ions take part in the production of reactive oxygen species (e.g., via the Fenton reaction [34]), their binding as redox-inert chelates can be considered a potential antioxidant mechanism. Moreover, transition metal ions such as iron and copper ions being present in our diet [35], metal-anthocyanin binding could also take place in the upper GI tract (in mildly acidic conditions) and modulate the properties and stability of anthocyanins in this biological site.

2.1.1. Pigment P1

The successive addition of P1 and Fe^{III} (0.5–5 equiv.) to a pH 4 acetate buffer results in the fast decay of A(470 nm) and the development of a broad visible band in the range 450–750 nm with an absorption maximum at *ca*. 510 nm (Figures 2 and 3). Those spectral changes can be interpreted by the formation of a P1-Fe^{III} complex having a quinonoid chromophore that acts as a donor in a charge transfer interaction with the Fe^{III} empty orbitals.

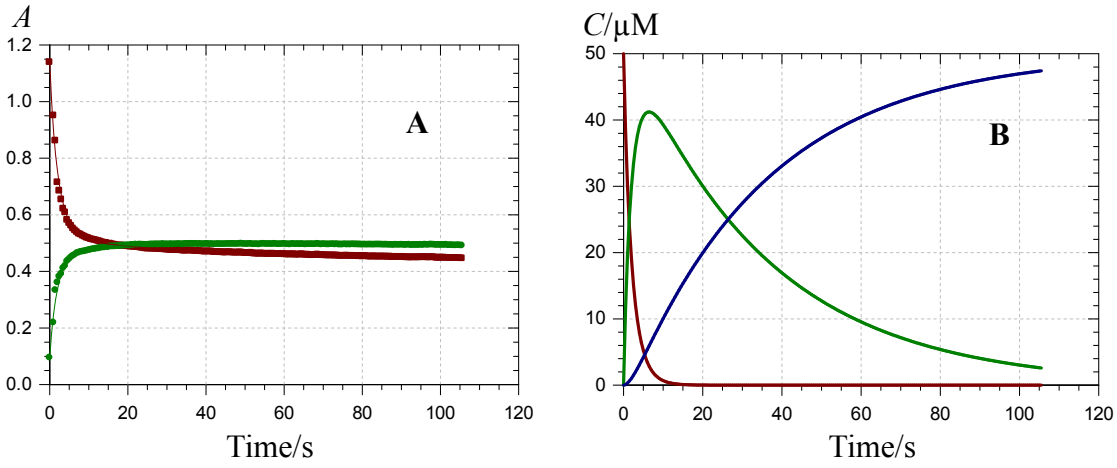

Figure 2. Kinetics of Fe^{III}-P1 binding (pH 4 acetate buffer, 25 °C, 4 equiv. Fe^{III}). (**A**) Time-dependence of the visible absorbance at 470 (■) and 620 nm (●); (**B**) time-dependence of the free pigment (—) and the kinetic (—) and thermodynamic (—) complexes.

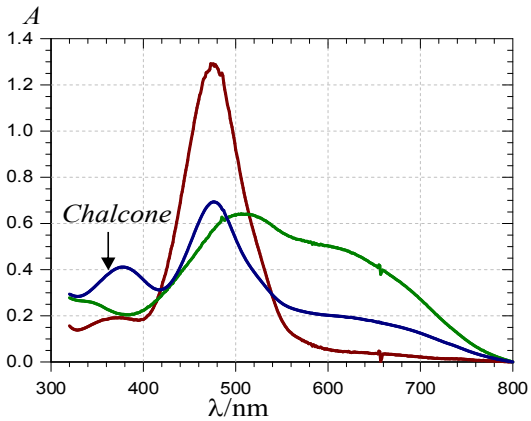

Figure 3. UV-visible spectra of P1 (—), the P1-Fe^{III} complex (—, *ca*. 30 s after addition of 2 equiv. Fe^{III}) and the complex formed *ca*. 400 s after addition of 5 equiv. Fe^{II} (—) (pH 4 acetate buffer, 25 °C, pigment concentration = 50 µM).

Over 2 min, free chalcone formation (typical absorption at λ_{max} = 375 nm) is negligible (confirmed by HPLC-MS analysis), even when P1 is in excess (0.5 equiv. Fe^{III}). When compared with Al^{III}-P1 binding [31], Fe^{III}-P1 binding is much faster and quasi-irreversible as the final maximal absorbance at 620 nm is reached with 1 equiv. Fe^{III}. The time dependence of A(470 nm) and A(620 nm) can be interpreted by the fast formation of a first complex (rate constant of binding k_b) followed by its slower first-order conversion into a second complex (rate constant of rearrangement k_r) (Figure 2).

A simultaneous curve-fitting of both curves (Equations 1–3) gives access to the corresponding rate constants and molar absorption coefficients (Table. 1).

$$-\frac{d}{dt}[Fe^{III}] = -\frac{d}{dt}[L] = k_b[Fe^{III}][L] \quad (1)$$

$$\frac{d}{dt}[Fe^{III}L_1] = k_b[Fe^{III}][L] - k_r[Fe^{III}L_1] \quad (2)$$

$$\frac{d}{dt}[Fe^{III}L_2] = k_r[Fe^{III}L_1] \quad (3)$$

The k_r values, which suggest a quasi-total consumption of the first complex over 2 min, are much higher than those obtained for water addition to free P1 (chalcone formation) and its Al^{III} complex [31]. Moreover, at the end of the kinetics, the broad absorption band, almost covering the visible spectrum and still well visible after several hours, is not compatible with a Fe^{III}-chalcone complex. Addition of Fe^{III} (5 equiv.) to an equilibrated solution of P1 in which C_E is the dominant species shows the binding of the minor colored forms with little impact on the chalcone band over 2 min (data not shown), thus indicating that C_E does not bind Fe^{III} in mildly acidic solution. The hypothesis of Fe^{III} reduction and concomitant oxidation of P1 is also not consistent with the spectrum obtained after acidification to pH < 2 (total recovery of free P1) and the HPLC-MS analysis (no oxidation product detected). Finally, one can propose the formation of a kinetic product (complex 1) evolving into a thermodynamic product (complex 2), possibly by additional coordination of acetate ions. Similar kinetic patterns were previously observed with other phenols in their binding to Fe^{III} [36]. Thus, starting from the flavylium ion, addition of Fe^{III} results in the fast binding of the colored forms (in fast acid-base equilibrium, collectively noted L in Equations 1–3). Concomitantly, the fraction of free flavylium in solution is greatly lowered so that water addition (and subsequent chalcone formation) is quenched.

When Fe^{II} is added in an equimolar concentration, a slow decay of A(470 nm) paralleled by a slow increase of A(375 nm) is observed. As the corresponding absorption bands are not shifted in comparison to free P1, it can be concluded that Fe^{II}-P1 binding is negligible and the spectral changes are fully ascribed to water addition to free P1 with concomitant chalcone formation. A double first-order curve-fitting at 470 and 375 nm yields: k_h^{obs}= 140 (±1) × 10^{-5} s^{-1}, in reasonable agreement with the value in the absence of Fe^{II} (k_h^{obs} ≈ 120 × 10^{-5} s^{-1}, half-life of free P1 at pH 4 ≈ 10 min). However, addition of an excess Fe^{II} (5 equiv.) causes the slow development of a broad visible band in the range 500–750 nm, again with no shift in the band at 470 nm (in contrast to Fe^{III}, see Figures 3 and 4). Moreover, a relatively fast accumulation of free chalcone reaching saturation after 300–400 s is also observed. In a pH 4 acetate buffer, Fe^{II} titration (ferrozine test, data not shown) shows that Fe^{II} autoxidation is negligible. However, the broad visible band appearing in the range 500–750 nm is evidence for the formation of a Fe^{III}-P1 complex [36,37]. Thus, it is proposed that a weak Fe^{II}–P1 binding occurs that promotes a slow Fe^{II} autoxidation (apparent first-order rate constant k_{autox}) without totally quenching water addition to P1. Then, the Fe^{III}–P1 slowly accumulates. Using this kinetic model (detailed below with P2), the corresponding rate constants can be estimated (Table 1) and the different concentrations plotted as a function of time (Figure 4).

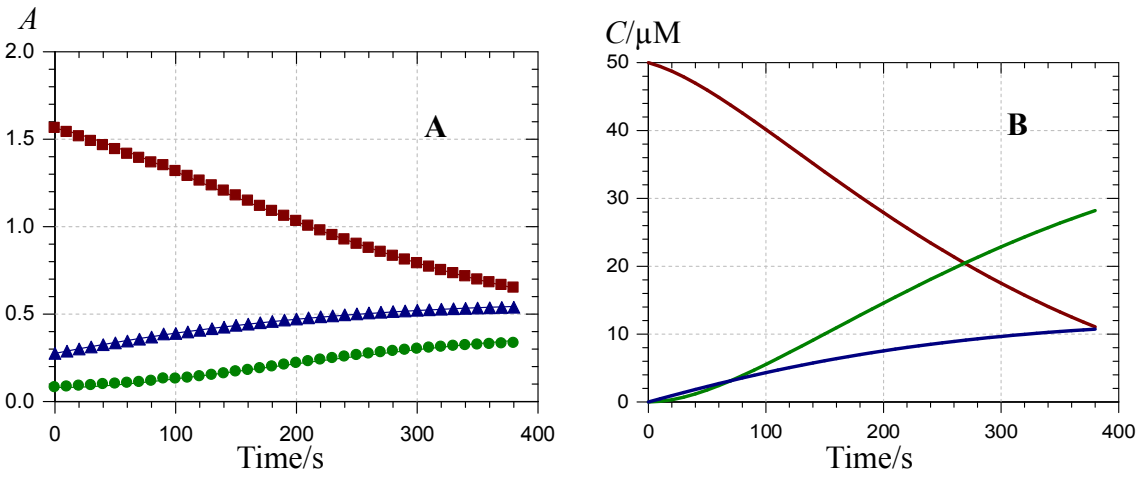

Figure 4. Kinetics of Fe^{II}–P1 binding (pH 4 acetate buffer, 25 °C, 5 equiv. Fe^{II}). (**A**) time-dependence of the visible absorbance at 470 (■), 620 (●) and 375 nm (▲); (**B**) time-dependence of the free pigment (—), the metal complex (—) and the free chalcone (—).

Table 2. Kinetic analysis of P1-Fe^{III} binding. Simultaneous curve-fitting of the A(470 nm) and A(620 nm) *vs.* time curves according to a simple model assuming irreversible 1:1 binding (rate constant k_b) followed by first-order rearrangement of complex 1 into complex 2 (rate constant k_r) (pH 4 acetate buffer, 25 °C, pigment concentration = 50 μM).

M_t/L_t, λ/nm	$k_b/M^{-1}\ s^{-1}$	$10^3 k_r/s^{-1}$	$\varepsilon_1/M^{-1}\ cm^{-1}$	$\varepsilon_2/M^{-1}\ cm^{-1}$
1, 470	17890 (±180)	4 (±2)	10,340	7910
620			12,270	10,810
2, 470	7190 (±250)	44 (±4)	13,190	10,320
620			12,180	12,780
3, 470	4450 (±60)	16 (±3)	12,010	10,300
620			13,160	13,060
4, 470	2670 (±30)	29 (±2)	10,360	8900
620			9710	9930
5, 470	3370 (±50)	59 (±2)	12,830	10,300
620			10,680	11,580
5, 470 [a])			10,700	
630	250 (±30)	-	11,800	-
375			4200	

[a]): Fe^{II}, apparent first-order autoxidation of Fe^{II}: $k_{autox} = 58\ (\pm 6) \times 10^{-5}\ s^{-1}$; chalcone formation: $k_h^{obs} = 95\ (\pm 4) \times 10^{-5}\ s^{-1}$, $\varepsilon_{CE} = 33{,}800\ M^{-1}\ cm^{-1}$ at 375 nm.

2.1.2. Pigment P2

The successive addition of P2 and Fe^{III} (0.5–5 equiv.) to a pH 4 acetate buffer results in spectral changes (Figure 5) that are close to the ones observed with P1. They are consistent with the formation of a P2-Fe^{III} complex having a quinonoid chromophore that acts as a donor in a charge transfer interaction with Fe^{III}.

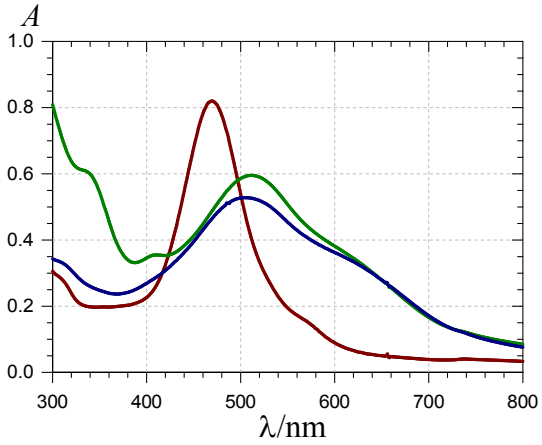

Figure 5. UV-visible spectra of P2 (—), the P2 - Fe^{III} complex (—, *ca*. 10 s after Fe^{III} addition) and the complex formed *ca*. 10 min after addition of Fe^{II} (—) (pH 4 acetate buffer, 25 °C, pigment concentration = 50 µM, iron-P2 molar ratio = 5).

Unlike Al^{III} [31], Fe^{III} binds P2 even more rapidly than P1, so that an accurate kinetic analysis is not possible by conventional UV-visible spectroscopy. However, assuming irreversible 1:1 binding, a lower limit can be proposed for the second-order rate constant of P2-Fe^{III} binding: $k_b > 5 \times 10^3$ M^{-1} s^{-1}. Free chalcone formation is negligible (confirmed by HPLC-MS analysis), even when P2 is in excess (0.5 equiv. Fe^{III}). However, a slight decay of A(650 nm) is observed with 0.5–1 equiv. Fe^{III}. Although fast, Fe^{III}-P2 binding is reversible and the final maximal absorbance at 650 nm is only reached with an excess Fe^{III} (*ca*. 5 equiv.).

The plot of $\Delta A = A_{max} - A_0$ (at 650 nm) as a function of the total metal concentration M_t can be successfully analyzed according to a 1:1 reversible binding model (Equations 4 and 5), thereby allowing the determination of the Fe^{III}-P2 binding constant: K_b = 21 (±6) $\times 10^3$ M^{-1}, $\Delta\varepsilon = \varepsilon_{complex} - \varepsilon_{P2}$ = 6500 (±500) $M^{-1} \cdot cm^{-1}$ (r = 0.995). This K_b value is identical to the one estimated for the Al^{III}-P2 complex [31]. Thus, the two trivalent hard metal cations Fe^{III} and Al^{III} have the same affinity for the P2 catechol nucleus. However, the Fe^{III}-P2 binding is much faster, the equilibrium being reached in a few seconds *vs*. several minutes with Al^{III}.

$$\Delta A = \Delta\varepsilon(Fe^{III}_{total} - [Fe^{III}]) \quad (4)$$

$$Fe^{III}_{total} = [Fe^{III}](1 + \frac{K_b L_{total}}{1 + K_b[Fe^{III}]}) \quad (5)$$

L_{total}: total ligand concentration, Fe^{III}_{total} : total metal concentration, K_b: metal-pigment binding constant, $\Delta\varepsilon = \varepsilon_{FeL}{}^{650} - \varepsilon_{L}{}^{650}$.

The observation that Fe^{III}-P2 binding is faster than Fe^{III}-P1 binding may be ascribed to different binding species in solution at pH 4. Indeed, the higher acidity of the P1 flavylium ion [31] probably indicates that P1 deprotonation at C7-OH is more favorable than at C4'-OH while P2 deprotonation can only occur at C4'-OH (Figure 6). Thus, Fe^{III}-P1 binding probably requires a thermodynamically unfavorable change in quinonoid tautomer that is not needed with P2.

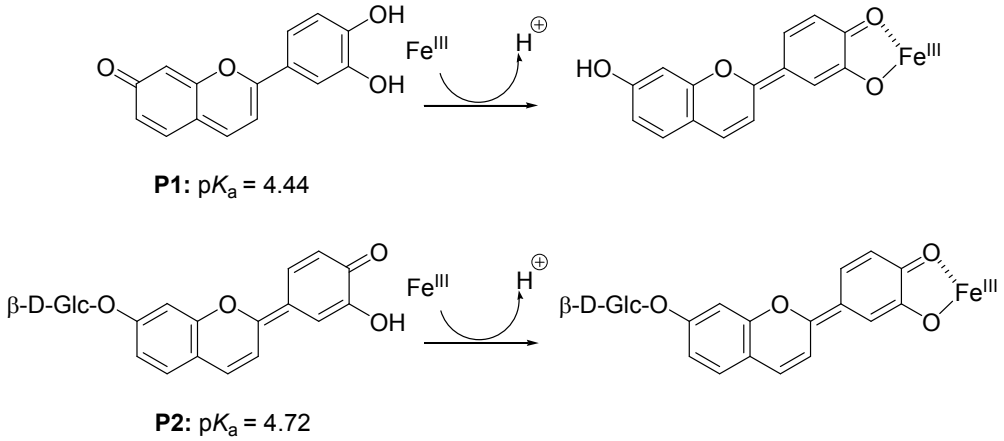

Figure 6. Iron-pigment binding.

Like P1, P2 apparently binds Fe^{II} much more slowly than Fe^{III}. For instance, while Fe^{III}-P2 binding reaches equilibrium in a few seconds, Fe^{II}–P2 binding requires *ca*. 4 min with 5 equiv. Fe^{II} (Figure S1). With 1 equiv. Fe^{II}, the equilibrium is not even achieved after 10 min. Interestingly, with 5 equiv. iron, the final spectra characteristic of the complexes are very close, except for a strong absorption band developing below 360 nm for the Fe^{III}-P2 complex (shoulder at 340 nm) that is characteristic of free Fe^{III} (Figure 4). It can thus be proposed that the same Fe^{III}-P2 complex is ultimately formed after addition of Fe^{III} or Fe^{II}. In other words, Fe^{II} slowly binds P2 with simultaneous conversion into Fe^{III}, while free Fe^{II} in excess remains stable in solution. In

particular, the broad absorption band beyond 600 nm (not observed with the Al^{III}-P2 complex) is characteristic of a catechol-to-Fe^{III} charge transfer interaction.

The curves showing the time dependence of A(470 nm) and A(650 nm) display short lag phases (Figure S1) suggesting that a preliminary slow autoxidation of Fe^{II} (apparent first-order rate constant k_{autox}) must take place to trigger the binding (second-order rate constant k_b).

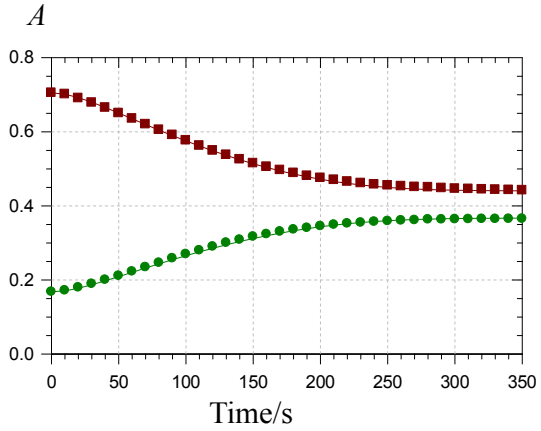

Figure S1. Time dependence of the A(470 nm) (■) and A(650 nm) (●) after addition of Fe^{II} (5 equiv.) to a P2 solution (pH 4 acetate buffer, 25 °C, pigment concentration = 50 µM).

Hence, both curves could be fitted against the following model (Equations 6–10, Table 2).

$$-\frac{d}{dt}[Fe^{II}] = k_{autox}[Fe^{II}] \quad (6)$$

$$\frac{d}{dt}[Fe^{III}] = k_{autox}[Fe^{II}] - k_b[Fe^{III}][L] \quad (7)$$

$$-\frac{d}{dt}[L] = k_b[Fe^{III}][L] + k_h^{obs}[L] \quad (8)$$

$$\frac{d}{dt}[LFe^{III}] = k_b[Fe^{III}][L] \quad (9)$$

$$\frac{d}{dt}[C_E] = k_h^{obs}[L] \quad (10)$$

Table 2. Kinetic analysis of the spectral changes following addition of Fe^{II} to a P2 solution (pH 4 acetate buffer, 25 °C, pigment concentration = 50 μM).

M_t/L_t, λ/nm [a])	$10^5 k_{autox}/s^{-1}$	$k_b/M^{-1}\ s^{-1}$	$\varepsilon_{ML}/M^{-1}\ cm^{-1}$
0.5, 470 (r = 0.9978)	215 (±2)	n.d. [b])	8800 [c])
650 (r = 0.9975)	13.7 (±0.2) [d])		7200 [c])
1, 470 (r = 0.9985)	169 (±1)	n.d. [b])	8800 [c])
650 (r = 0.9985)	13.3 (±0.4) [d])		7200 [c])
2, 470 (r = 0.9992)	181 (±5)	473 (±34)	8870
650 (r = 0.9993)			7320
3, 470 (r = 0.9998)	154 (±2)	663 (±29)	8850
650 (r = 0.9996)			7110
4, 470 (r = 0.9998)	141 (±2)	593 (±23)	8670
650 (r = 0.9999)			7070
5, 470 (r = 0.9988)	163 (±7)	785 (±75)	8810
650 (r = 0.9994)			7340

[a]) Each *A vs.* time curve is a mean of 2 experimental curves; [b]) Steady-state assumed for Fe^{III}; [c]) Set constant; [d]) Apparent rate constant of water addition (k_h^{obs}).

With an excess Fe^{II}, chalcone formation can be neglected with P2 ($k_h^{obs} = 0$), while it is detectable with P1 (Figures 3 and 4).

In summary, Fe^{III} rapidly binds both P1 and P2 in mildly acidic solutions, thereby quenching their conversion into the corresponding chalcones. With P2, the binding is faster but reversible. By contrast, P1 and P2 only weakly interact with Fe^{II}, thereby promoting its autoxidation with subsequent fast binding of Fe^{III}.

2.2. Pigment-Serum Albumin Binding

HSA, the major plasma protein (*ca*. 0.6 mM), is responsible for the transport of a large variety of ligands [38], including drugs and dietary components such as fatty acids and polyphenols [23,24,39]. The heart-shaped structure of HSA consists of three helical domains I (1–195), II (196–383) and III (384–585), each being divided into sub-domains A and B [38]. The main binding sites of drugs and polyphenols are site 1 and site 2 (respectively located in sub-domains IIA and IIIA), which consist in hydrophobic pockets lined by positively charged aminoacid residues (Arg, Lys).

Whereas glycoside hydrolysis prior to intestinal absorption seems the rule with polyphenols in general, native anthocyanins (glycosides) have been detected in the blood circulation, although in very low (sub-micromolar) concentration [10]. Moreover, under physiological conditions, delphinidin, cyanidin and pelargonidin 3-*O*-β-D-glucosides have been reported to bind to HSA site 1 with thermodynamic binding constants in the range 69–144 × 10^3 M^{-1} [40]. So far, no work has discriminated the colored and colorless forms by their affinity for HSA, despite the fact that the colorless forms are expected to largely prevail at equilibrium in neutral conditions.

In this study, pigment–HSA binding was first evidenced by UV-visible spectroscopy. For instance, the visible band of P1 at pH 7.4 shifts from 540–570 nm when an excess HSA (2 equiv.) is added (Figure 7).

However, this is not so with P2 (unchanged λ_{max} = 530 nm). The bathochromic shift specifically observed for P1 suggests a role for the free C7-OH group. At pH 7.4, the anionic quinonoid form makes a substantial contribution. In the case of P1, the binding to HSA could even favor the formation of the anionic quinonoid base, in agreement with the high density of positive charges (protonated Lys and Arg residues) present in sub-domain IIA, the typical binding site of flavonoids [39]. To check this hypothesis, the pH dependence of the visible spectrum of P1 around neutrality was evaluated in the presence and absence of HSA. Very similar titration curves were obtained in agreement with a pK_{a2} value of *ca*. 7.1 (Table 3, Figure S2). Thus, binding to HSA does not significantly shift the equilibrium between the neutral and anionic quinonoid bases. Hence, the HSA-induced bathochromic shift may be rather ascribed to perturbation in the molecular orbitals specifically involved in the visible band, e.g., the HOMO of the anionic quinonoid base (due to possible charge transfer interactions) with no impact on the global stability.

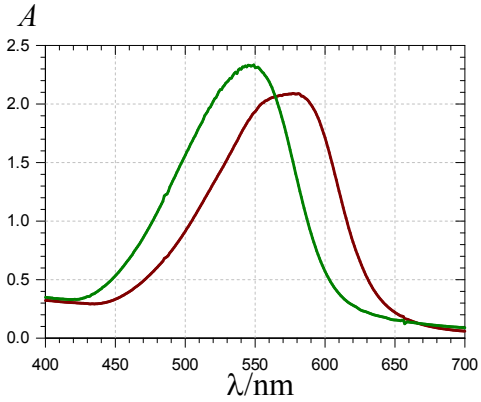

Figure 7. UV-visible spectra of P1 (▬) and the P1-HSA complex (▬) (pH 7.4 phosphate buffer, 25 °C, pigment concentration = 50 µM, HSA-P1 molar ratio = 2).

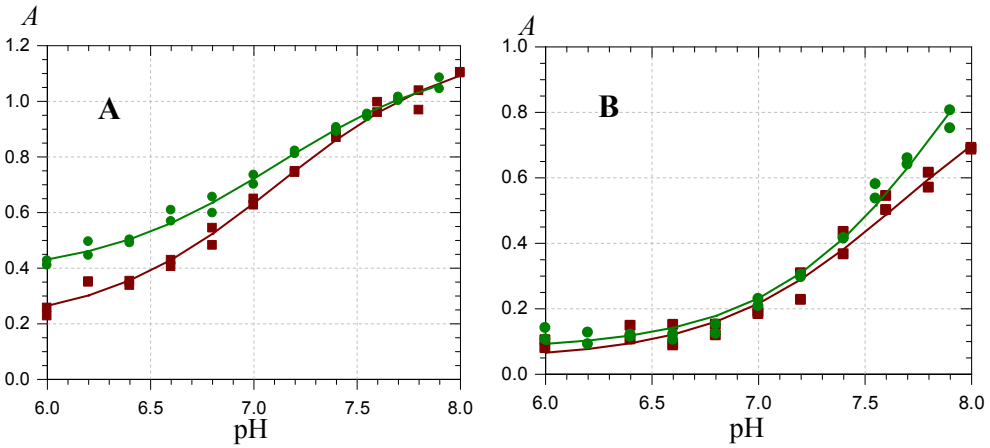

Figure S2. Spectroscopic titration of P1 in the absence (■, 550 nm) or presence (●, 580 nm, 5 equiv.) of HSA. **A:** spectra recorded immediately after P1 addition, **B:** spectra recorded after equilibration over *ca*. 24 h.

Table 3. Kinetic and thermodynamic parameters for the structural transformations of P1 and P2 in neutral conditions with and without HSA.

	P1	**P2**
pK_{a2}, r_a (550 nm), no HSA	7.12 (±0.05), 6.3 (±0.6) [a])	n.a. [b])
pK_{a2}, r_A (580 nm), 5 equiv. HSA	7.11 (±0.04), 3.1 (±0.1) [a])	n.a. [b])
k_h^{obs} (s^{-1}), 530 nm, no HSA	n.a., too slow *ca*. −10% color loss after 45 min	88 (±1) × 10^{-5} [c])
k_h^{obs} (s^{-1}), 530 nm, 2 equiv. HSA	n.a., too slow *ca*. −10% color loss after 45 min	81 (±1) × 10^{-5} [c])

[a]) From the curve-fitting of the *A vs.* pH curves at equilibrium (r_A = ratio of the molar absorption coefficients of the anionic to neutral quinonoid bases); [b]) No proton loss in the pH range 6–8, total conversion of colored forms into chalcone; [c]) From a first-order curve-fitting of the color loss at pH 7.4.

After equilibration for *ca*. 24 h, the titration curves were modified by the gradual appearance of the chalcone (Figure S2). The residual color is approximately the same in the absence or presence of HSA. Thus, HSA has a minor impact on the quinonoid bases-chalcone equilibrium, which is indicative that the different forms have close affinities for the protein. The residual color at pH 7.4 is consistent with a $K_i = (C_E)/(A)$ value *ca*. 10, in agreement with the pK_{a1} and pK'_h values previously determined for P1 ([31], 4.44 and 3.45, respectively). From the K_i and K_{a2} values, a distribution diagram of the different P1 species can be plotted around neutrality in the presence or absence of HSA (Figure S3).

In the case of P2, the situation is simpler as no anionic quinonoid base can form. Monitoring the decay of the color over time shows that the apparent first-order rate constant of water addition (k_h^{obs}) is only weakly affected by HSA (Table 3). Moreover, whether HSA is present or not, the color loss can be considered complete. Thus, the quinonoid base concentration at equilibrium is negligible ($K_i > 10$).

For an accurate estimation of the corresponding binding constants, the pigment-HSA binding was investigated by fluorescence spectroscopy. The intrinsic HSA fluorescence at 340 nm (excitation at 295 nm) is due to its single Trp residue (Trp-214) located in sub-domain IIA. Its

strong quenching by P1, P2 and their chalcones (Figure 8) is evidence that the binding actually takes place to or near this site.

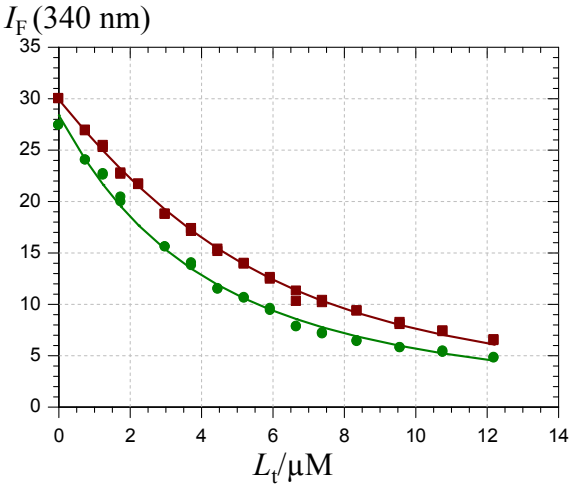

Figure 8. Quenching of the HSA fluorescence by the P1 quinonoid bases (■) and chalcone (●). HSA concentration = 2 µM, pH 7.4 phosphate buffer, 37 °C, excitation at 295 nm.

The excitation wavelength was selected so as to maximize the fluorescence of the single Trp residue of HSA. However, the pigments, especially in their chalcone form, substantially absorb light at the excitation (295 nm) or/and emission (340 nm) wavelengths so that an inner filter correction is necessary. Hence, the protein fluorescence intensity is expressed in Equation (11).

$$I_F = f_P\,[P]\,\exp(-\varepsilon_L\, l\, L_t) \quad (11)$$

$$L_t = [L]\,(1 + K_b[P]) \quad (12)$$

$$P_t = [P]\,(1 + K_b[L]) \quad (13)$$

In Equation (11), f_P is the molar fluorescence intensity of HSA and ε_L stands for the sum of the molar absorption coefficients of the ligand at the excitation and emission wavelengths (Table 4). Its value is determined independently by UV-visible spectroscopy from a Beer's plot. Finally, l is the mean distance travelled by the excitation light at the site of emission light detection. For the spectrometer used in this work, l is estimated to be 0.65 cm. Beside the expression of I_F, the relationships used in the curve-fitting procedures were combinations of the mass law for the complex and mass conservation for the ligand L (pigments) and protein P (Equations (12) and (13), L_t: total ligand concentration, P_t: total protein concentration.

The K_b values (Table 4) illustrate two major points:

(1) The Glc moiety strongly destabilizes the complexes, especially for the colored forms (K_b value reduced by a factor 15–16).

(2) The chalcones, with their open more linear structure, display a higher affinity for HSA (K_b raised by a factor *ca*. 3 for P2) than the corresponding colored forms, although this increase is marginal with P1 in agreement with the investigation by UV-visible spectroscopy. This suggests that the very low circulating concentration of anthocyanins (in comparison to other flavonoids) [10,15] could be partly due to their conversion in colorless forms that may have escaped detection.

Table 4. Binding constant (K_b) of pigments and their chalcones to HSA (2 μM) in a pH 7.4 phosphate buffer at 25 °C (n = 2).

	$10^3 K_b/M^{-1}$	$10^6 f_P/M^{-1}$	$\varepsilon_L/M^{-1}\,cm^{-1}$ [a])	r
P1 colored forms	273 (±7)	15.5 (±0.1)	8900 + 5800	0.998
P1 chalcone	344 (±12) [b])	14.2 (±0.1)	15,800 + 16,400 [b])	0.997
P2 colored forms	17.5 (±0.5)	14.1 (±0.1)	3800 + 2800	0.999
P2 chalcone	58.4 (±1.9)	13.5 (±0.1)	7200 + 7000	0.998

[a]) First value at 295 nm (excitation wavelength), second value at 340 nm (emission wavelength); [b]) Apparent values including a minor contribution of the residual colored forms present at equilibrium. Assuming a 3:1 chalcone-to-colored forms molar ratio (see Figure S3), the true value for the sole chalcone can be estimated: $K_b = 368 \times 10^3\ M^{-1}$.

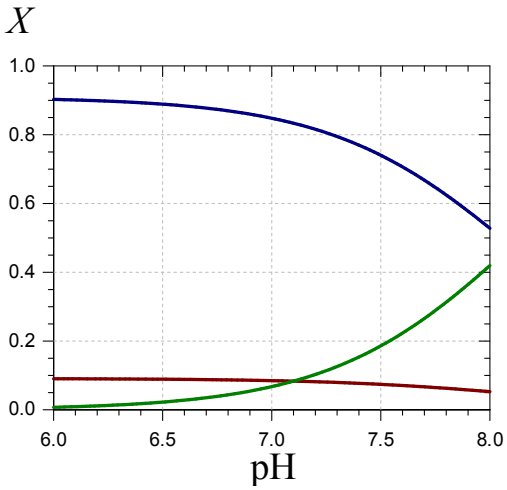

Figure S3. Distribution diagram of P1 species at equilibrium around neutrality (in the presence or absence of HSA): neutral quinonoid bases (—), anionic quinonoid base (—), chalcone (—).

Interestingly, the K_b values for anthocyanidin 3-*O*-β-D-glucosides [40] are intermediates between the values for the P2 and P1 colored forms. Thus, P1 is a better HSA ligand than common anthocyanins, while the reverse is true for P2.

2.3. Inhibition of the Heme-Induced Peroxidation of Linoleic Acid

Given their poor bioavailability and extensive catabolism [10], anthocyanins are expected to exert their antioxidant activity in humans (in the restricted sense of electron donation to reactive oxygen species involved in oxidative stress) prior to intestinal absorption, *i.e.*, in the gastro-intestinal tract, where they can accumulate in substantial concentrations and in their native forms following the consumption of plant products. On the other hand, in the gastric compartment, acidity, dioxygen and pro-oxidant species present in foods (iron, lipid hydroperoxides, H_2O_2) can provide suitable conditions for the oxidation of dietary polyunsaturated acids (PUFAs) in postprandial conditions [17–22]. This oxidation results in a loss of essential lipids and in the accumulation of potentially toxic lipid oxidation products. These lipid hydroperoxides and aldehydes can also alter dietary proteins and may even contribute to increasing the concentration of circulating minimally modified lipoproteins that are more prone to further oxidation and take part in atherogenesis. Based on simple *in vitro* models, our works suggest that heme-induced lipid oxidation is particularly fast in the first period of gastric

digestion (pH 4–6) but efficiently inhibited by plant antioxidants (polyphenols, α-tocopherol, carotenoids) [21,41,42]. Recently, the pertinence of our model was confirmed by gastric fluid analysis in mini pigs [22].

With linoleic acid (LH) as a model of dietary PUFA, conjugated dienes (CDs) are acceptable markers of the early phase of lipid oxidation and can be approximately identified with lipid hydroperoxides (LOOH), the corresponding alcohols (LOH) making only a minor contribution. CD accumulation is easily followed by UV-visible spectroscopy in the presence or absence of antioxidant.

A simple visual comparison of the curves featuring CD accumulation in the presence of a fixed pigment concentration (Figure 9) shows that P2, whether in its colored or chalcone form, is a poorer antioxidant than P1, in agreement with our preliminary investigation of the DPPH radical-scavenging activity [31]. Interestingly, the chalcone forms come up as more potent inhibitors than the corresponding colored forms.

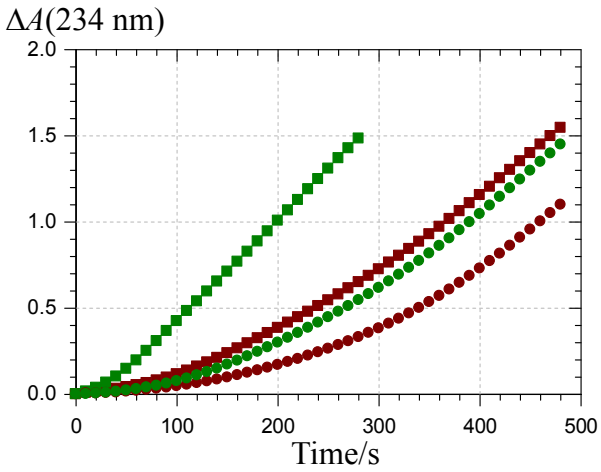

Figure 9. Inhibition of the metmyoglobin-induced peroxidation of linoleic acid. Pigment concentration = 2.5 µM, ■: P1 colored forms, ■: P2 colored forms, ●: P1 chalcone, ●: P2 chalcone (pH 5.8 phosphate buffer + Brij®35, 37 °C).

The metmyoglobin-induced peroxidation of linoleic acid is initiated via a Fe^{III}-Fe^{IV} redox cycle involving small concentrations of PUFA hydroperoxides inevitably contaminating any PUFA sample [43–45]. As hydrophilic antioxidants, polyphenols typically inhibit lipid peroxidation at the initiation stage by reducing hypervalent heme iron (Fe^{IV}), instead of significantly scavenging lipid peroxyl radicals, as lipophilic antioxidants (α-tocopherol, carotenoids) do [21,41,42,46].

The reactions involved in the heme-induced peroxidation of linoleic acid in the presence of an antioxidant are summed up in Figure 10 with the corresponding rate constants.

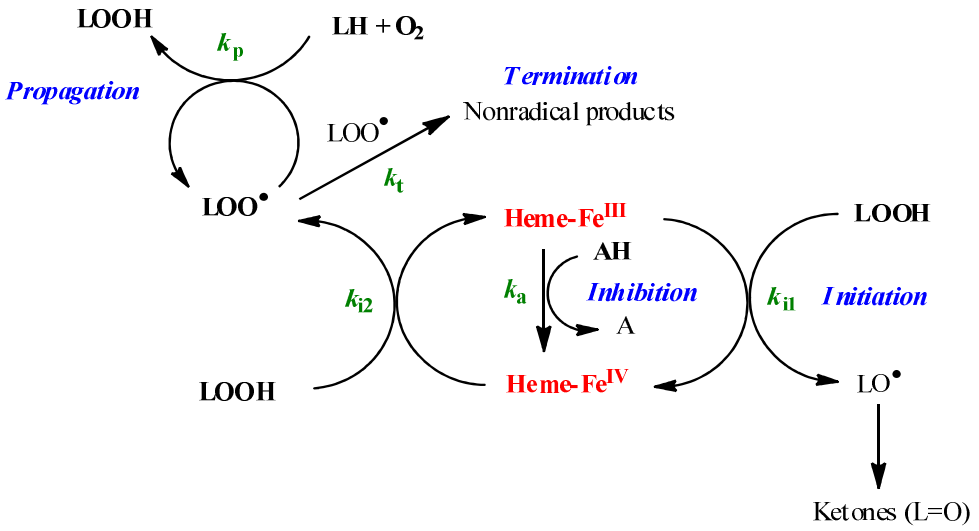

Figure 10. Metmyoglobin-induced peroxidation of linoleic acid and its inhibition by polyphenols (LH: PUFA, LOOH: PUFA hydroperoxide, AH: antioxidant, H^+ and HO^- ions omitted).

In the absence of antioxidant, the short lag phase is better reproduced without assuming a steady-state for Fe^{IV}. On the other hand, the two initiation rate constants can be taken equal ($k_{i1} = k_{i2}$) so as to restrict the total number of adjustable parameters. Thus, in a first step, the curves of uninhibited lipid peroxidation are analyzed so as to estimate a value for k_{i1} (rate constant of LOOH cleavage by low-valence heme) that will be used in all curve-fitting experiments related to inhibited peroxidation with the following adjustable parameters (see Appendix for details): $r_2 = \frac{k_p}{\sqrt{2k_t}}$, a measure of PUFA oxidizability, $AE = \frac{k_a}{k_{i2}}$, the antioxidant efficiency and the antioxidant stoichiometry n, defined as the number of hypervalent iron species reduced per antioxidant molecule. For all four antioxidants (the two pigments and their chalcones), excellent curve-fittings (r>0.999) were obtained.

From the parameter values (Table 5), the following comments can be made:

(1) the antioxidant efficiency, which lies in the range 10–100, does not allow a clear discrimination between antioxidants. Its drift toward lower values when the antioxidant concentration increases suggests that modelling an antioxidant (stoichiometry n) as n independent sub-units, each capable of transferring one electron to Fe^{IV} with the same rate constant (k_a), may be too crude and/or that antioxidant–metmyoglobin binding can take place (resulting in two populations of free and bound antioxidant molecules with distinct reactivities).

(2) the antioxidant stoichiometry suggests that a catechol B-ring favors repeated electron transfer to Fe^{IV} (probably through *o*-quinone intermediates) and thus prolonged inhibition. By contrast, the P2 quinonoid base displays a B-ring that is deactivated by the keto group at C4'.

(3) at high antioxidant concentration, the lipid oxidizability tends to decrease. This drift is ascribed to partial heme degradation and to the accumulation of phenolic oxidation products retaining a weak antioxidant character. The latter point is consistent with the structure of P1 oxidation products already determined by us [47].

Table 5. Kinetic analysis of the metmyoglobin-induced peroxidation of linoleic acid. Curve-fitting of the *A*(234 nm) *vs.* time curves (CD accumulation). Rate constant of lipid hydroperoxide cleavage by metmyoglobin: $k_{i1} = 3 \times 10^3$ M^{-1} s^{-1} (see Figure 10 & Appendix).

Pigment/μM	r_2/$M^{-1/2}$ $s^{-1/2}$	***AE***	***n***
P1, 0.5	2.8 (±0.1)	137 (±16)	3.0 (±0.1)
1	2.6 (±0.1)	40 (±2)	2.5 (±0.1)
1.5	2.3 (±0.1)	38 (±5)	2.5 (±0.1)
2	2.2 (±0.1)	29 (±3)	3.2 (±0.2)
2.5	2.1 (±0.1)	11 (±1)	4.0 (±0.3)
P1-C$_E$, 0.5	2.7 (±0.1)	108 (±6)	4.4 (±0.1)
1	2.4 (±0.1)	59 (±3)	5.6 (±0.1)
1.5	2.3 (±0.1)	40 (±2)	4.3 (±0.1)
2	2.1 (±0.1)	29 (±1)	5.2 (±0.1)
2.5	1.9 (±0.1)	28 (±1)	3.9 (±0.1)
P2, 1.5	2.4 (±0.1)	95 (±6)	0.9 (±0.1)
2.5	2.3 (±0.1)	76 (±14)	0.5 (±0.1)
5	1.9 (±0.1)	15 (±2)	1.4 (±0.1)
6.25	1.6 (±0.1)	17 (±2)	1.2 (±0.1)
7.5	1.0 (±0.1)	24 (±1)	0.9 (±0.1)
P2-C$_E$, 1.25	2.5 (±0.1)	31 (±3)	3.1 (±0.1)
2.5	2.1 (±0.1)	19 (±1)	3.5 (±0.2)
3.75	1.6 (±0.1)	21 (±2)	1.9 (±0.1)
5	1.2 (±0.1)	29 (±2)	1.3 (±0.1)

3. Experimental Section

3.1. Chemicals

$FeSO_4$, $7H_2O$ (98%) and CH_3CO_2Na, $3H_2O$ (99%) were purchased from Alfa-Aesar. Fe $(NO_3)_3$ (99%) was from Acros. HSA (fraction V, 96%–99%, MW = 66,500 g mol^{-1}), Na_2HPO_4, $7H_2O$, NaH_2PO_4, $2H_2O$, polyoxyethyleneglycol 23 lauryl ether (Brij®35), (9Z, 12Z)-octadecadienoic acid (linoleic acid >99%), myoglobin from equine heart (type II, MW ca. 17,600 g mol^{-1}) were from Sigma-Aldrich. Phosphate and acetate buffers were prepared with non-mineralized water C-23597 405 purchased from VWR to limit metal contamination. 3',4',7-Trihydroxyflavylium (P1) and its 7-*O*-β-D-glucoside (P2) were chemically synthesized as described in our previous work [31].

3.2. UV-Spectroscopy

An Agilent 8453 UV-visible spectrometer equipped with a 1024-element diode-array detector was used to record the absorption spectra over the wavelength range 190–1100 nm. A water thermostated bath was used to control the cell temperature with an accuracy of ±0.1 °C. The spectroscopic measurements were carried out with a quartz cell of 1 cm optical path length.

3.3. Fluorescence Spectroscopy

Steady-state fluorescence spectra were recorded on a thermostated *Safas Xenius* fluorimeter. The excitation and emission slit widths were set at 10 nm. All studies were performed at 37 (±1) °C, excitation at 295 nm (HSA Trp residue), emission light collected between 270 and 410 nm.

3.4. Iron-Pigment Binding

To 2 mL of 0.1 M acetate buffer at pH 4.0 placed into the spectrometer cell at 25 °C were successively added 50 µL of a freshly prepared 2 mM pigment solution in acidified MeOH (0.1 M HCl) and 50 µL of freshly prepared iron solution in 0.05 M HCl (concentration range: 1–10 mM). The final iron/pigment molar ratios were in the range 0.5–5. Spectra were typically recorded every 0.5 s over 2 min (binding kinetics) or every 15 s over 15 min (complex stability).

3.5. Inhibition of the Heme-Induced Peroxidation of Linoleic Acid

The experimental conditions used were adapted from an already published procedure [21]. Metmyoglobin (17.6 mg) was dissolved in 20 mL of phosphate buffer (20 mM, pH 6.8). After filtration through 0.45 µm filter, its concentration was standardized at 50 µM using ε = 7700 $M^{-1} \cdot cm^{-1}$ at 525 nm. Given volumes (20 µL) of daily prepared solutions of linoleic acid (70 mM) in MeOH and pigment (0.05–0.25 mM) were added to 2 ml of Brij®35 (4 mM) solution in phosphate buffer (20 mM, pH 5.8). The concentrated solutions of pigments were a) prepared in 0.1 M HCl in MeOH for investigating inhibition by the colored forms or b) incubated in the buffer for 24 h at 37 °C to ensure maximal conversion into the corresponding chalcones. The non-ionic surfactant Brij®35 was chosen for its good stability and very low content of hydroperoxides, which could react with iron. The final concentrations in the cell were 0.7 mM linoleic acid and 0.5–2.5 µM pigment. Oxidation was initiated by adding 20 µL of the 50 µM metmyoglobin solution (final concentration in the cell: 0.5 µM) to the sample under constant magnetic stirring in open air at 37 °C. Each experiment was run in duplicate. Lipid peroxidation was followed by monitoring the concentration of conjugated dienes (CDs) at 234 nm using ε = 24×10^3 $M^{-1} \cdot cm^{-1}$.

3.6. Influence of HSA on the Structural Transformations of Pigments

Aliquots (50 µL) of 2 mM solution of pigments prepared in acidified MeOH (0.1 M HCl) were added to 2 mL of pH 7.4 phosphate buffer (50 mM Na_2HPO_4 + 100 mM NaCl) in the presence or absence of HSA (0–2 equiv.) at 37 °C. Spectra were recorded every 30 s over 7000 s. All experiments were carried out twice.

Similar experiments were also carried out after varying the pH of the phosphate buffer in the range
6–8. The spectra were recorded immediately after pigment addition and after equilibration over *ca*. 24 h.

3.7. Pigment-HSA Binding

Solutions were prepared daily by dissolving HSA in a pH 7.4 buffer (50 mM phosphate + 100 mM NaCl). Aliquots of a 0.5 mM (P1) or 2 mM (P2) solutions were added via syringe to 2 mL of a 2 µM HSA solution placed in a quartz cell (path length: 1 cm) at 37 °C. The concentrated solutions of pigments were (a) prepared in 0.1 M HCl in MeOH for investigating flavylium–

HSA binding (MeOH concentration ≤2.5%) or (b) incubated in the buffer for 24 h at 37 °C to ensure maximal conversion into the corresponding chalcones.

For investigating flavylium-HSA binding, a single addition was carried out with subsequent recording of the fluorescence spectrum and renewal of the sample for the next pigment concentration. In such conditions, the flavylium-to-chalcone conversion is negligible.

3.8. Data Analysis

All curve-fittings were carried out with the Scientist software (MicroMath, Salt Lake City, UT, USA) through least square regression. They yielded optimized values for the parameters implemented in the models (see Text & Appendix). Standard deviations are reported.

4. Conclusions

In this work, 3',4',7-trihydroxyflavylium chloride (P1) and its more water-soluble 7-*O*-β-D-glucopyranoside (P2), come up as suitable models for investigating important properties of anthocyanins: binding of iron ions and serum albumin, inhibition of lipid peroxidation induced by dietary iron in model gastric conditions.

Binding of Fe^{III} is typically fast, especially with the glucoside, and promotes both color variation (due to B-ring deprotonation and additional ligand-to-iron charge transfer) and stabilization (due to the quenching of chalcone formation). Binding of Fe^{II} by itself is not detectable at pH 4 but both pigments promote Fe^{II} autoxidation (followed by the binding of Fe^{III} thus formed), a phenomenon that can be considered protective as Fe^{II} is a potential pro-oxidant through the Fenton reaction. Here again, the glucoside appears superior in accelerating Fe^{II} autoxidation, so that the competing chalcone formation is barely detectable. Binding of serum albumin is weaker with the glucoside, probably because of steric repulsion. It is noteworthy that the chalcone forms a good HSA ligand. In particular, the chalcone glucoside binds HSA three times more tightly than the corresponding colored forms. Consequently, our study suggests that 3-deoxyanthocyanins could partly circulate under their chalcone form in the blood.

Finally, the chalcone forms appear as better inhibitors of heme-induced lipid peroxidation, especially in the case of the glucoside (poorly reactive in its colored form). This prevailing role of the colorless forms in the antioxidant protection afforded by anthocyanins is original and probably important as the physical conditions occurring in the GI tract (temperature, pH, interactions with dietary proteins) could well favor the conversion of the colored forms into the colorless forms.

Overall, 3-deoxyanthocyanins and their chalcones are potentially attractive colorants and antioxidants. Their stability and accessibility by chemical synthesis could foster industrial developments. For instance, iron–3-deoxyanthocyanin chelates could be used in the preparation of colored gels for applications in the food and cosmetic industries [48]. 3-Deoxyanthocyanins could also be developed as natural pH indicators, e.g., for food packaging [49]. They deserve additional

Supplementary Materials

Supplementary materials can be accessed at: http://www.mdpi.com.

Author Contributions

S.A.B., 40% (experimental work & first version of manuscript); N.M, 10% (aid in experimental work); M.L., 10% (aid in experimental work); O.D., 40% (physico-chemical analyses, final version of manuscript and revision).

Appendix

Mathematical Treatment for the Inhibition of Heme-Induced Lipid Peroxidation

The reactions and the corresponding rate constants are displayed in Figure 10.

The peroxidation rate can be written as:

$R_p = d(LOOH)/dt = k_p(LOO^{\bullet})(LH) - k_{i1}(LOOH)(Fe^{III}) – k_{i2}(LOOH)(Fe^{IV}) = R_p − R_{i1} – R_{i2}$

The rate of lipid consumption is: $-d(LH)/dt = R_p$

The rate of antioxidant consumption is: $R_a = −d(AH)/dt$

Assuming a steady-state for the lipid peroxyl radicals, we may write: $R_{i2} = 2k_t(LOO^{\bullet})^2$

We thus deduce: $R_p = r_2(LH)R_{i2}^{1/2} - R_{i1} - R_{i2}$ with $r_2 = k_p/(2k_t)^{1/2}$

Finally, one has: $−d(Fe^{III})/dt = d(Fe^{IV})/dt = R_{i1} − R_{i2} − R_a$

In the absence of antioxidant, the short lag phase is better reproduced without assuming a steady-state for Fe^{IV}. On the other hand, the two initiation rate constants can be taken equal ($k_{i1} = k_{i2}$) so as to restrict the total number of adjustable parameters. We thus estimate k_{i1} (rate constant of LOOH cleavage by low-valence heme): $k_{i1} = 3 \times 10^3\ M^{-1}\ s^{-1}$.

In the presence of an antioxidant, a steady-state for Fe^{IV} can be assumed: $R_{i1} = R_{i2} + R_a$

This relationship can be written as: $k_{i1}(LOOH)(Fe^{III}) = [k_{i2}(LOOH) + k_a(AH)](Fe^{IV})$

We thus deduce: $R_{i2} = \dfrac{R_{i1}}{1 + \dfrac{AE(AH)}{(LOOH)}}$

with $AE = k_a/k_{i2}$ (antioxidant efficiency at inhibiting initiation).

Using the k_{i1} value previously determined, the curves of inhibited lipid peroxidation are analyzed to estimate the oxidizability r_2, antioxidant efficiency AE and stoichiometry n. Parameter n is defined as the number of hypervalent iron species reduced per antioxidant molecule. It is implemented in the program by the following initial condition: AH concentration = n × total antioxidant concentration.

Conflicts of Interest

The authors declare no conflict of interest.

References

1. Yoshida, K.; Mori, M.; Kondo, T. Blue flower color development by anthocyanins: From chemical structure to cell physiology. *Nat. Prod. Rep*. **2009**, *26*, 857–964.
2. Cavalcanti, R.N.; Santos, D.T.; Meireles, M.A.A. Non-thermal stabilization mechanisms of anthocyanins in model and food systems—An overview. *Food Res. Int.* **2011**, *44*, 499–509.
3. Gonzalez-Manzano, S.; Duenas, M.; Rivas-Gonzalo, J.C.; Escribano-Bailon, M.T.; Santos-Buelga, C. Studies on the copigmentation between anthocyanins and flavan-3-ols and their influence in the colour expression of red wine. *Food Chem.* **2009**, *114*, 649–656.
4. Malien-Aubert, C.; Dangles, O.; Amiot, M.J. Color stability of commercial anthocyanin-based extracts in relation to the phenolic composition. Protective effects by intra- and intermolecular copigmentation. *J. Agric. Food Chem.* **2001**, *49*, 170–176.
5. Galland, S.; Mora, N.; Abert-Vian, M.; Rakotomanomana, N.; Dangles, O. Chemical synthesis of hydroxycinnamic acid glucosides and evaluation of their ability to stabilize natural colors via anthocyanin copigmentation, *J. Agric. Food Chem.* **2007**, *55*, 7573–7579.
6. Tsuda, T. Dietary anthocyanin-rich plants: Biochemical basis and recent progress in health benefits studies. *Mol. Nutr. Food Res*. **2012**, *56*, 159–170.
7. Goupy, P.; Bautista-Ortin, A.-B.; Fulcrand, H.; Dangles, O. Antioxidant activity of wine pigments derived from anthocyanins: Hydrogen transfer reactions to the DPPH radical and inhibition of the heme-induced peroxidation of linoleic acid. *J. Agric. Food Chem.* **2009**, *57*, 5762–5770.
8. Deng, J.; Cheng, J.; Liao, X.; Zhang, T.; Leng, X.; Zhao, G. Comparative study on iron release from soybean (glycine max) seed ferritin induced by anthocyanins and ascorbate. *J. Agric. Food Chem*. **2010**, *58*, 635–641.
9. Fernandes, I.; de Freitas, V.; Reis, C.; Mateus, N. A new approach on the gastric absorption of anthocyanins. *Food Funct*. **2012**, *3*, 508–516.
10. Kay, C.D. Aspects of anthocyanin absorption, metabolism and pharmacokinetics in humans. *Nutr. Res. Rev.* **2006**, *19*, 137–146.
11. Bouayed, J.; Hoffmann, L.; Bohn, T. Total phenolics, flavonoids, anthocyanins and antioxidant activity following simulated gastro-intestinal digestion and dialysis of apple varieties: Bioaccessibility and potential uptake. *Food Chem.* **2011**, *128*, 14–21.
12. Fleschhut, J.; Kratzer, F.; Rechkemmer, G.; Kulling, S.E. Stability and biotransformation of various dietary anthocyanins *in vitro*. *Eur. J. Nutr*. **2006**, *45*, 7–18.
13. Vitaglione, P.; Donnarumma, G.; Napolitano, A.; Galvano, F.; Gallo, A.; Scalfi, L.; Fogliano, V. Protocatechuic acid is the major human metabolite of cyanidin-glucosides. *J. Nutr*. **2007**, *137*, 2043–2048.
14. Kay, C.; Kroon, P.; Cassidy, A. The major intestinal metabolites of anthocyanins are unlikely to be conjugates of their parent compounds but metabolites of their degradation products. *Proc. Nutr. Soc*. **2008**, *67*, E309.

15. Del Rio, D.; Rodriguez-Mateos, A.; Spencer, J.P.E.; Tognolini, M.; Borges, G.; Crozier, A. Dietary (poly)phenolics in human health: Structures, bioavailability, and evidence of protective effects against chronic diseases. *Antioxid. Redox Signal.* **2013**, *18*, 1818–1892.
16. Edwards, M.; Czank, C.; Cassidy, A.; Kay, C.D. Vascular bioactivity of anthocyanin degradants: Inhibition of endothelial superoxide production. *Proc. Nutr. Soc*. **2013**, *72*, E228.
17. Kanner, J.; Lapidot, T. The stomach as a bioreactor: Dietary lipid peroxidation in the gastric fluid and the effects of plant-derived antioxidants. *Free Radic. Biol. Med.* **2001**, *31*, 1388–1395.
18. Lapidot, T.; Granit, R.; Kanner, J. Lipid peroxidation by "free" iron ions and myoglobin as affected by dietary antioxidants in simulated gastric fluids. *J. Agric. Food Chem*. **2005**, *53*, 3293–3390.
19. Dangles, O. Antioxidant activity of plant phenols: Chemical mechanisms and biological significance. *Curr. Org. Chem.* **2012**, *16*, 1–23.
20. Lorrain, B.; Dangles, O.; Loonis, M.; Armand, M.; Dufour, C. Dietary iron-initiated lipid oxidation and its inhibition by polyphenols in gastric conditions. *J. Agric. Food Chem.* **2012**, *60*, 9074–9081.
21. Goupy, P.; Vulcain, E.; Caris-Veyrat, C.; Dangles, O. Dietary antioxidants as inhibitors of the heme-induced peroxidation of linoleic acid: Mechanism of action and synergism. *Free Radic. Biol. Med.* **2007**, *43*, 933–946.
22. Gobert, M.; Remond, D.; Loonis, M.; Buffiere, C.; Sante-Lhoutellier, V.; Dufour, C. Fruits, vegetables and their polyphenols protect dietary lipids from oxidation during gastric digestion. *Food Funct*. **2014**, *5*, 2166–2174.
23. Khan, M.K.; Rakotomanomana N.; Dufour, C.; Dangles, O. Binding of flavanones and their glucuronides and chalcones to human serum albumin. *Food Funct.* **2011**, *2*, 617–626.
24. Galland, S.; Rakotomanomana, N.; Dufour, C.; Mora, N.; Dangles, O. Synthesis of hydroxycinnamic acid glucuronides and investigation of their affinity for human serum albumin, *Org. Biomol. Chem.* **2008**, *6*, 4253–4260.
25. Awika, J.M.; Rooney, L.W.; Waniska, R.D. Anthocyanins from black sorghum and their antioxidant properties. *Food Chem.* **2004**, *90*, 293–301.
26. Yang, L.; Dykes, L.; Awika, J.M. Thermal stability of 3-deoxyanthocyanidin pigments. *Food Chem*. **2014**, *160*, 246–254.
27. Awika, J.M.; Rooney, L.W. Sorghum phytochemicals and their potential impact on human health. *Phytochemistry* **2004**, *65*, 1199–1221.
28. Carbonneau, M.-A.; Cisse, M.; Mora-Soumille, N.; Dairi, S.; Rosa, M.; Michel, F.; Lauret, C.; Cristol, J.-P.; Dangles, O. Antioxidant properties of 3-deoxyanthocyanidins and polyphenolic extracts from Cote d'Ivoire's red and white sorghums assessed by ORAC and *in vitro* LDL oxidizability tests. *Food Chem.* **2014**, *145*, 701–709.
29. Taylor, J.R.N.; Belton, P.S.; Beta, T.; Duodu, K.G. Increasing the utilisation of sorghum, millets and pseudocereals: Developments in the science of their phenolic phytochemicals, biofortification and protein functionality. *J. Cereal Sci.* **2014**, *59*, 257–275.
30. Petti, C.; Kushwaha, R.; Tateno, M.; Harman-Ware, A.E.; Crocker, M.; Awika, J.; DeBolt, S. Mutagenesis breeding for increased 3-deoxyanthocyanidin accumulation in leaves of

sorghum bicolor (L.) moench: A source of natural food pigment. *J. Agric. Food Chem*. **2014**, *62*, 1227–1232.
31. Mora-Soumille, N.; al Bittar, S.; Rosa, M.; Dangles, O. Analogs of anthocyanins with a 3',4'-dihydroxy substitution: Synthesis and investigation of their acid-base, hydration, metal binding and hydrogen-donating properties in aqueous solution. *Dyes Pigments* **2013**, *96*, 7–15.
32. Petrov, V.; Gavara, R.; Dangles, O.; al Bittar, S.; Mora-Soumille, N.; Pina, F. Flash photolysis and stopped-flow UV-visible spectroscopy study of 3',4'-dihydroxy-7-*O*-β-D-glucopyranosyloxyflavylium chloride, an anthocyanin analogue exhibiting efficient photochromic properties. *Photochem. Photobiol. Sci.* **2013**, *12*, 576–581.
33. Pina, F. Chemical applications of anthocyanins and related compounds. A source of bioinspiration. *J. Agric. Food Chem*. **2014**, *62*, 6885–6897.
34. Moran, J.F.; Klucas, R.V.; Grayer, R.J.; Abian, J.; Becana, M. Complexes of iron with phenolic compounds from soybean nodules and other legume tissues: Prooxidant and antioxidant properties *Free Radic. Biol. Med*. **1997**, *22*, 861–870.
35. Tokalioglu, S.; Gurbuz, F. Selective determination of copper and iron in various food samples by the solid phase extraction. *Food Chem*. **2010**, *123*, 183–187.
36. Nkhili, E.; Loonis, M.; Mihai, S.; el Hajji, H.; Dangles, O. Reactivity of food phenols with iron and copper ions: Binding, dioxygen activation and oxidation mechanisms. *Food Funct*. **2014**, *5*, 1186–1202.
37. Perron, N.R.; Wang, H.C.; DeGuire, S.N.; Jenkins, M.; Lawson, M.; Brumaghim, J.L. Kinetics of iron oxidation upon polyphenol binding, *Dalton Trans*. **2010**, *39*, 9982–9987.
38. Varshney, A.; Sen, P.; Ahmad, E.; Rehan, M.; Subbarao, N.; Khan, R.H. Ligand binding strategies of human serum albumin: How can the cargo be utilized? *Chirality* **2010**, *22*, 77–87.
39. Dufour, C.; Dangles, O. Flavonoid-serum albumin complexation: Determination of binding constants and binding sites by fluorescence spectroscopy. *Biochim. Biophys. Acta* **2005**, *1721*, 164–173.
40. Tang, L.; Zuo, H.; Shu, L. Comparison of the interaction between three anthocyanins and human serum albumin by spectroscopy. *J. Lumin.* **2014**, *153*, 54–63.
41. Vulcain, E.; Goupy, P.; Caris-Veyrat, C.; Dangles, O. Inhibition of the metmyoglobin-induced peroxidation of linoleic acid by dietary antioxidants: Action in the aqueous *vs.* lipid phase. *Free Radic. Res.* **2005**, *39*, 547–563.
42. Sy, C.; Caris-Veyrat, C.; Dufour, C.; Boutaleb, M.; Borel, P.; Dangles, O. Inhibition of iron-induced lipid peroxidation by newly identified bacterial carotenoids in model gastric conditions. Comparison with common carotenoids. *Food Funct.* **2013**, *4*, 698–712.
43. Roginsky, V.; Zheltukhina, G.A.; Nebolsin V.E. Efficacy of metmyoglobin and hemin as a catalyst of lipid peroxidation determined by using a new testing system. *J. Agric. Food Chem*. **2007**, *55*, 6798–6806.
44. Reeder, B.J.; Wilson, M.T. The effects of pH on the mechanism of hydrogen peroxide and lipid hydroperoxide consumption by myoglobin: A role for the protonated ferryl species. *Free Radic. Biol. Med*. **2001**, *30*, 1311–1318.
45. Baron, C.P.; Skibsted, L.H. Prooxidative activity of myoglobin species in linoleic acid emulsions. *J. Agric. Food Chem*. **1997**, *45*, 1704–1710.

46. Hu, M.; Skibsted, L.H. Kinetics of reduction of ferrylmyoglobin by (−)-epigallocatechin gallate and green tea extract. *J. Agric. Food Chem*. **2002**, *50*, 2998–3003.
47. Dangles, O.; Fargeix, G.; Dufour, C. Antioxidant properties of anthocyanins and tannins: A mechanistic investigation with catechin and the 3',4',7-trihydroxyflavylium ion. *J. Chem. Soc. Perkin Trans.* **2000**, *2*, 1653–1663.
48. Buchweitz, M.; Brauch, J.; Carle, R.; Kammerer, D.R. Application of ferric anthocyanin chelates as natural blue food colorants in polysaccharide and gelatin based gels. *Food Res. Int*. **2013**, *51*, 274–282.
49. Pereira, V.A.; de Queiroz Arruda, I.N.; Stefani, R. Active chitosan/PVA films with anthocyanins from Brassica oleraceae (red cabbage) as time-temperature indicators for application in intelligent food packaging. *Food Hydrocoll.* **2015**, *43*, 180–188.

Sample Availability: Samples of compounds P1 and P2 are available from the authors.

Appendix I

Copper - pigment binding

Introduction

As shown in our precedent works [1][2], 3-deoxyanthocyanidins containing a catechol group are able to chelate aluminum and iron ions and this binding allows color variation and stabilization. 3-Deoxyanthocyanins - Fe^{II} binding is typically followed by autoxidation of Fe^{II} to Fe^{III}. The capacity of 3-deoxyanthocyanins to form inert Fe^{III} chelates is a potential antioxidant mechanism.

Although less abundant than iron, copper is also omnipresent in our diet [3]. Fe^{II}, Cu^{I} can be involved in the production of reactive oxygen species (e.g., via the Fenton reaction [4]). In neutral conditions, polyphenol - Cu^{I} complexes were also found to rapidly transfer two electrons to O_2 with H_2O_2 formation but no change in the copper valence [5] (Scheme 1). The corresponding polyphenol - Cu^{II} complexes can follow the same pathway after (rate-limiting) one-electron reduction of Cu^{II}, for instance by disproportionation of the polyphenol - Cu^{II} complexes [4].

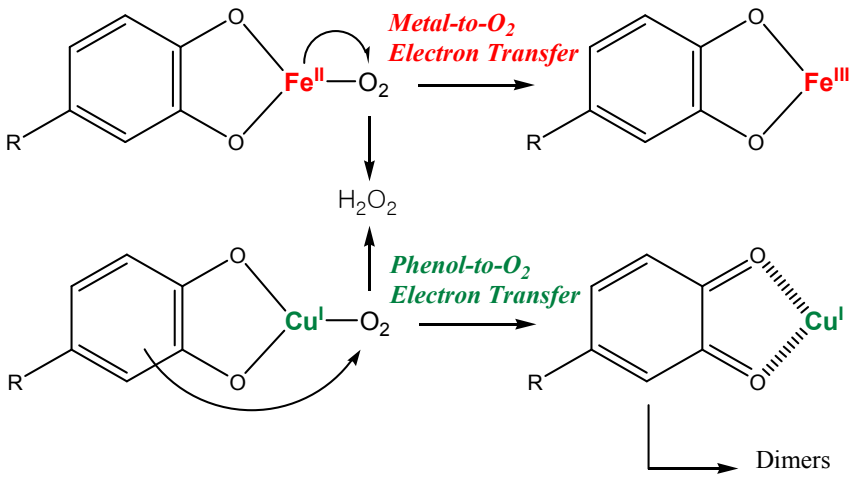

Scheme 1. Mechanism of Fe^{II} and Cu^{I} binding with subsequent hydrogen peroxide formation.

In this section, the binding of copper ions by **P1** and **P2** is briefly studied to appreciate its potential in color variation and its influence on the sensitivity of 3-deoxyanthocyanins to autoxidation.

Materials

$CuCl_2$, $2H_2O$ (99.9 %) and CuCl (99 %) were purchased from Sigma-Aldrich. The buffers used in the experiments are a 0.1 M acetate buffer (pH 5.0) or a 0.1 M phosphate buffer (pH 7.4) prepared with non-mineralized water purchased from VWR C-23597 405 to avoid metal contamination.

Methods

UV-visible spectroscopy. To 2 ml of a pH 5.0 acetate buffer (or pH 7.4 phosphate buffer) placed in the spectrometer cell, 50 µL of a freshly prepared 2 mM pigment solution in acidified MeOH (0.1 M HCl) were added and the spectral monitoring was started. Then, 50 µL of freshly prepared metal solution (Cu^{I} or Cu^{II}) in MeCN - 0.2 M HCl (96:4) (concentration range: 1 – 10 mM) were added. The final metal/pigment ratios in the cell ranged from 0.5 to 5. Spectra were typically recorded every 0.5 s over 2 min (investigation of the binding kinetics) or every 15 s over 15 min (investigation of the chelate stability).

UPLC-DAD-MS analyses were performed on the Acquity Ultra Performance LC™ (UPLC™) apparatus from Waters, equipped with an UV-visible diode array detector (DAD) and coupled with a Bruker Daltonics HCT ultra ion trap mass spectrometer with positive electrospray ionization (ESI) mode. Separation was conducted on a 1.7 µm (2.1- 50 mm) Acquity UPLC BEH C18 column thermostated at 30 °C.

The mobile phase consisted of H_2O / HCO_2H (99:1, v/v) (eluent A) and MeCN / HCO_2H (99:1, v/v) (eluent B). The flow rate was 0.5 mL/min. The elution program was as follows: 10–50% B (0–7.5 min); 50–100% B (7.5–8 min); 100–10% B (8-8.5 min); 10–10% B (8.5–11 min). The mass spectra were generated in the Ultra scan mode in the m/z range 100- 1000. The ion source

parameters were: nebulizer pressure, 50 psi; capillary 2000V, drying gas flow, 9 L min^{-1}; drying gas temperature, 365°C).

Results & Discussion

- *P1-Cu^{I} binding*

The successive addition of **P1** and Cu^{I} (5 equiv.) to a pH 5 acetate buffer results in the fast decay of visible absorbance at 490 nm and the development of a broad visible band in the range 450 – 750 nm with a maximum at *ca*. 640 nm. Then, a slower evolution is observed (Figure 1).

The simultaneous fitting of the A(490 nm) and A(640 nm) *vs*. time curves assuming the formation of a first complex (second-order rate constant k_1) that evolves into a second one (first-order rate constant k_2) gives satisfying results.

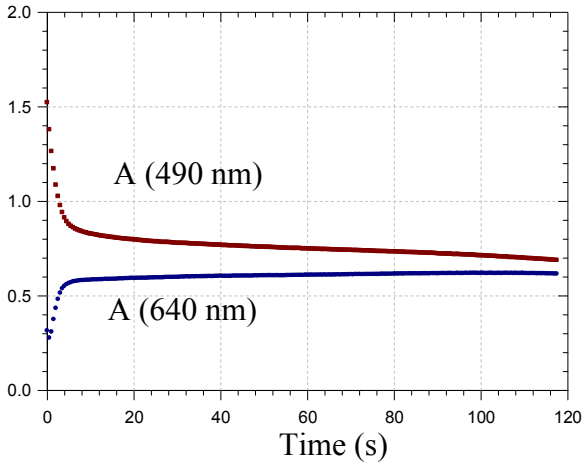

Figure 1. Time-dependence of the UV-visible absorbance in **P1** - Cu^{I} binding (pH 5.0 acetate buffer, 25°C, Cu^{I}/**P1** ratio = 5).

Similar experiments were carried out with Fe^{II} and Fe^{III} in similar conditions for comparison. A fast **P1** - Fe^{III} binding is observed followed by a slow decay. **P1** - Fe^{II} binding is much slower, which is coherent with our results in a pH 4 acetate buffer [2]. The spectral changes are interpreted by a slow autoxidation of Fe^{II} followed by a fast binding of Fe^{III}. Contrary to our observations at pH 4, no chalcone is formed at pH 5 in the presence of Fe^{II} and the final spectra collected with both iron ions are close and attributed to the same **P1** - Fe^{III} complex. **P1** - Cu^{I} binding was also relatively fast, although slower than with Fe^{III}. (Figure 2).

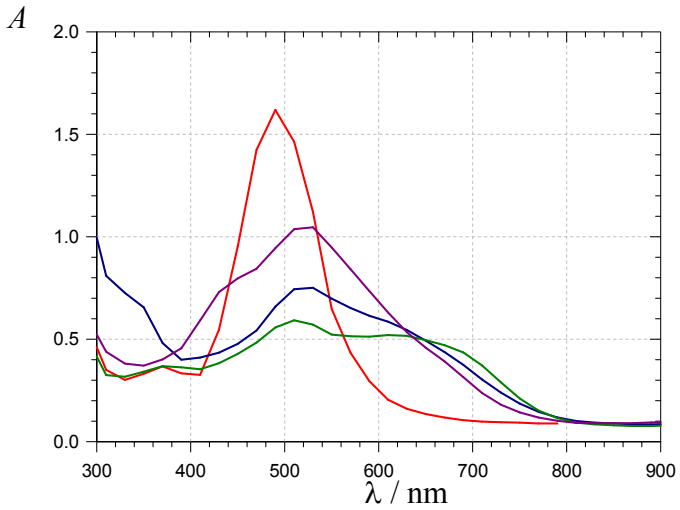

Figure 2. UV-visible spectra of **P1** (red), the **P1** - Fe^{III} complex (green, *ca*. 10 s after Fe^{III} addition), the complex formed *ca*. 10 min after addition of Fe^{II} (blue) and the **P1**-Cu^{I} complex (purple, *ca*. 10 s after Cu^{I} addition) (pH 5 acetate buffer, 25°C, pigment concentration = 50 µM, metal – **P1** molar ratio = 5).

By comparing the A(650 nm)/A(530 nm) ratio for the **P1** - Cu^{I} and **P1** - Fe^{III} complexes at the same pH, it is clear that this ratio is higher with the latter in agreement with a ligand-to-metal charge transfer contribution within the **P1** - Fe^{III} complex (Table 1). Whatever the conditions (metal ion, pH), no **P1** oxidation products were detected (confirmed by UPLC-DAD-MS analysis).

Table 1**.** Kinetic analysis of **P1** - metal binding (pH 5 acetate buffer, 25°C, pigment concentration = 50 µM)

M (5 equiv)	λ / nm	k_1 / M^{-1} s^{-1}	$10^3 k_2$ / s^{-1}	ε_1 / M^{-1} cm^{-1}	ε_2 / M^{-1} cm^{-1}
Cu^{I}	490 (r = 0.999)	1376 (± 14)	18.1 (± 0.8)	12360	10460
	640 (r = 0.996)			6530	7220
Fe^{III}	490 (r = 0.98)	3960 (± 140)	-	10010	-
	620 (r = 0.98)			12290	-
Fe^{II}	490 (r = 0.999)	9610 (± 760)[a]	-	11890	-
	630 (r = 0.999)			10180	-

[a] Rate constant for Fe^{III} binding after rate-limiting first-order autoxidation of Fe^{II}:
k_a = 276 (± 2) x10^{-5} s^{-1}

In neutral conditions (pH 7.4 phosphate buffer), the **P1** - Cu^{I} binding could not be investigated because of instant precipitation of the complex. After re-dissolution by manual stirring, no oxidation products could be evidenced by UPLC-DAD-MS analysis.

- *P1 - Cu^{II} binding*

Consecutive **P1** and Cu^{II} additions to a pH 5 or pH 7.4 buffer were followed by immediate precipitation of the complex. As spectroscopic investigation was impossible, UPLC-DAD-MS analysis was carried out directly after manual stirring to ensure sufficient solubility for detection. However, the sensitivity was poor and allowed only partial product identification.

As shown in Figure 1, the UPLC-DAD-MS analyses suggest that Cu^{II}-induced autoxidation mainly results in oxygenation, which probably occurs through sequences of 2-electron oxidation followed by water addition (Scheme 2). Such sequences were already evidenced in the reaction of **P1** with DPPH and the 3,3',4',7-tetrahydroxyflavylium ion was characterized by NMR after methylation and purification on silica gel [6].

Despite the propensity of the Cu^{II} – **P1** complex for precipitation, the Cu^{II}-induced autoxidation of **P1** seems complete and no residual **P1** could be evidenced (Figure 3).

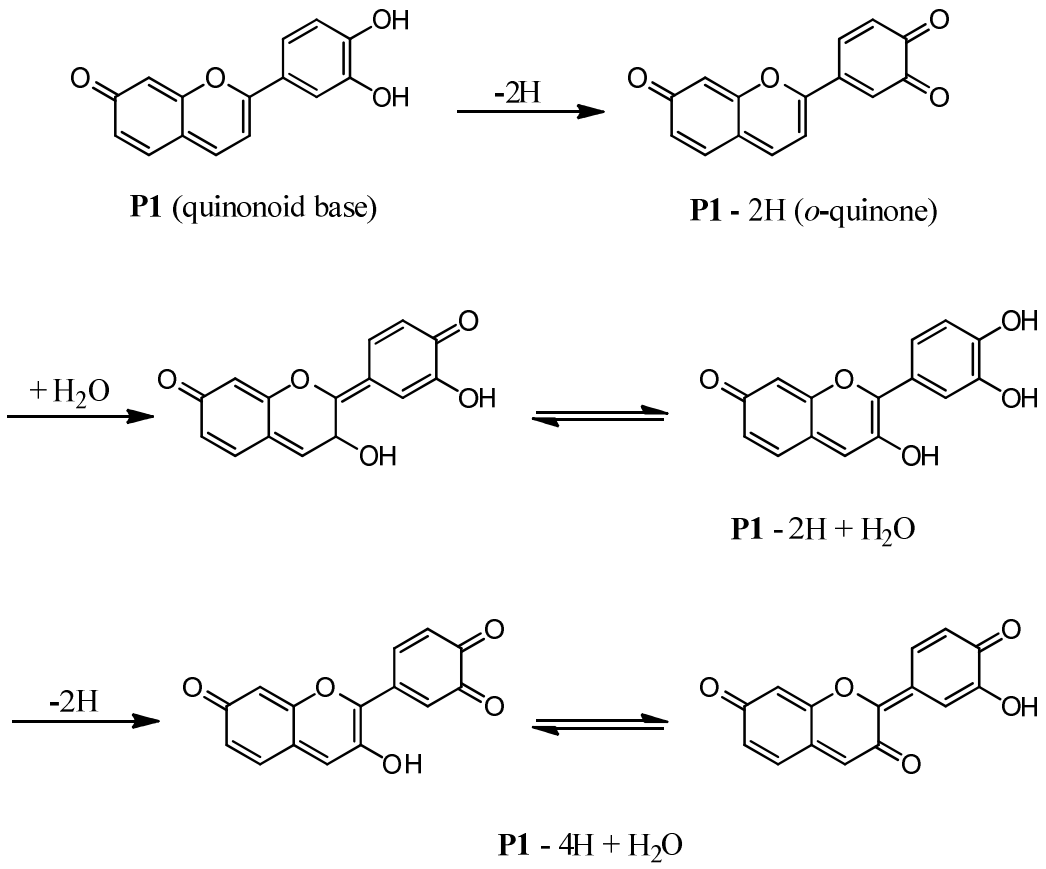

Shceme 2**.** Proposed pathways of two-electron oxidation / water addition for **P1**

- *P2 - Cu binding*

Despite the D-glucose moiety, addition of copper ions to **P2** resulted in instant precipitation, which prevented their spectroscopic investigation.

UPLC-DAD-MS analysis of the **P2** - Cu^{I} mixture confirmed partial water addition to **P2** accompanied by chalcone formation. Surprisingly, **P2** - Cu^{I} doesn't quench chalcone formation as Fe^{III} and Al^{III} did.

UPLC-DAD-MS analysis of the **P2** - Cu^{II} mixture allowed the detection of **P2** and its chalcone as well as two oxidation products (Figure 4, Table 2). While a four-electron oxidized product could be evidenced with **P1**, only two-electron oxidized products were detected with **P2** (with addition of 1 or 3 water molecules), in agreement with **P1** being a better electron-donor than **P2**. With **P2**, oxidation may occur from the chalcone.

A

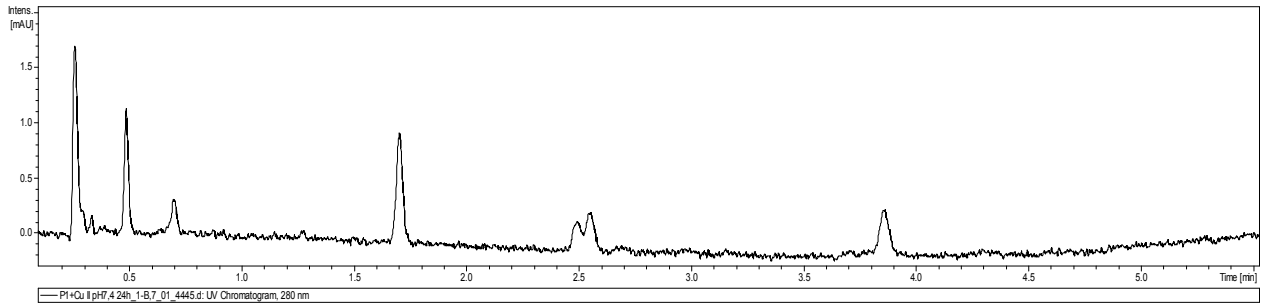

B

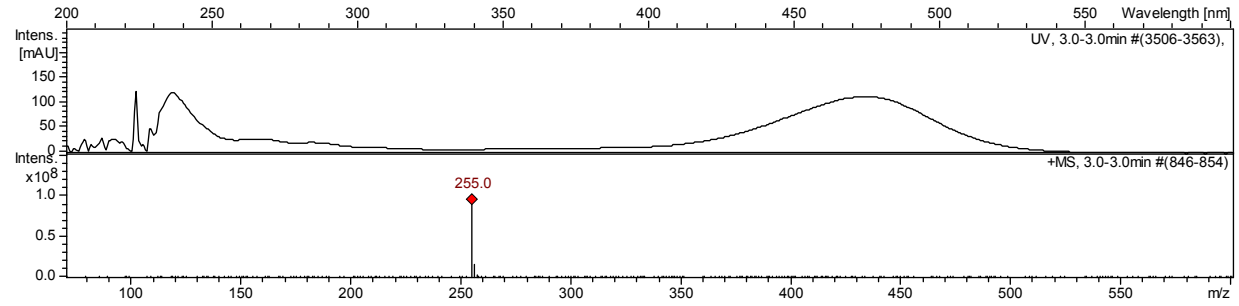

C

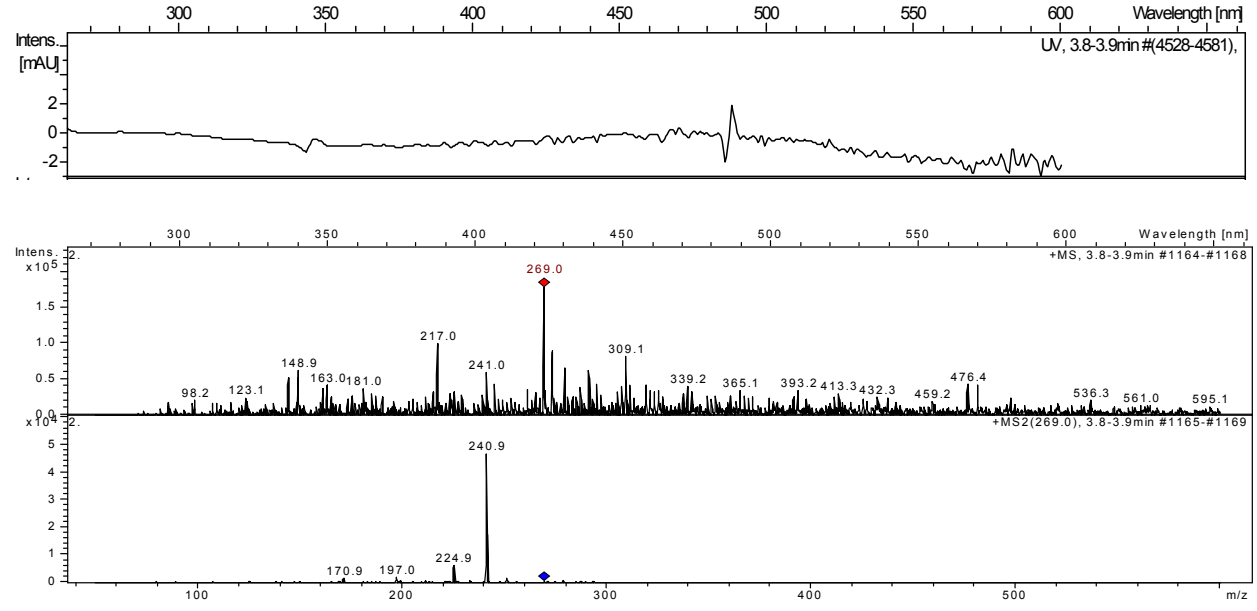

Figure 3. UPLC-DAD-MS analysis of P1 – Cu^{II} binding (incubation for 24 h in a pH 7.4 phophate buffer, 25°C, Cu^{II} / **P1** ratio = 5)

A: Chromatogram (280 nm) of the **P1 -** Cu^{II} mixture

B: UV-vis and mass spectra of **P1** (absent here but detected in iron binding and cited as a control) at t_R = 3.0 min, *m/z* (ES^+) = 255.

C: UV-vis and mass spectra of compound at t_R = 3.85 min, *m/z* (ES^+) = 269.

A

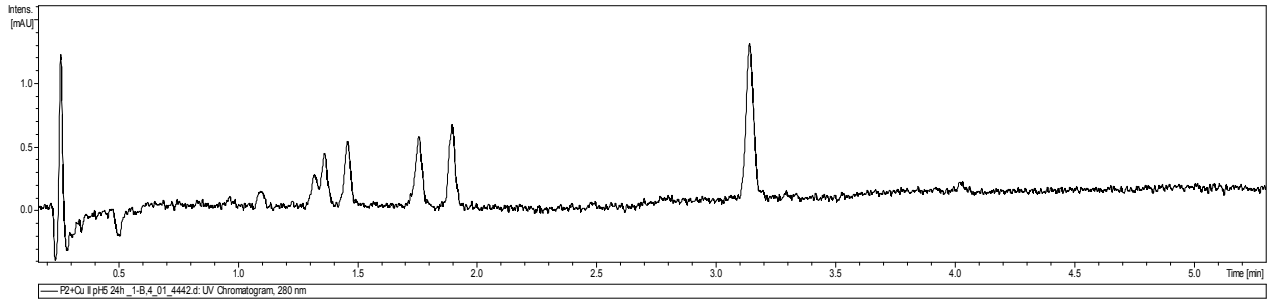
Intens.
[mAU]
1.0
0.5
0.0
0.5
1.0
1.5
2.0
2.5
3.0
3.5
4.0
4.5
5.0
Time [min]
P2+Qu II pH5 24h _1-B,4_01_4442.d: UV Chromatogram, 280 nm

B

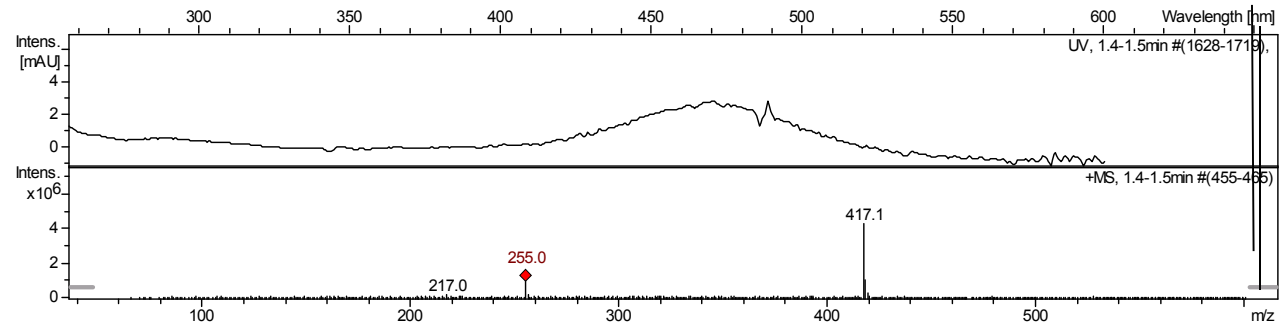
300
350
400
450
500
550
600
Wavelength [nm]
Intens.
[mAU]
UV, 1.4-1.5min #(1628-1719),
+MS, 1.4-1.5min #(455-465)
Intens.
x10^6
417.1
255.0
217.0
100
200
300
400
500
m/z

C

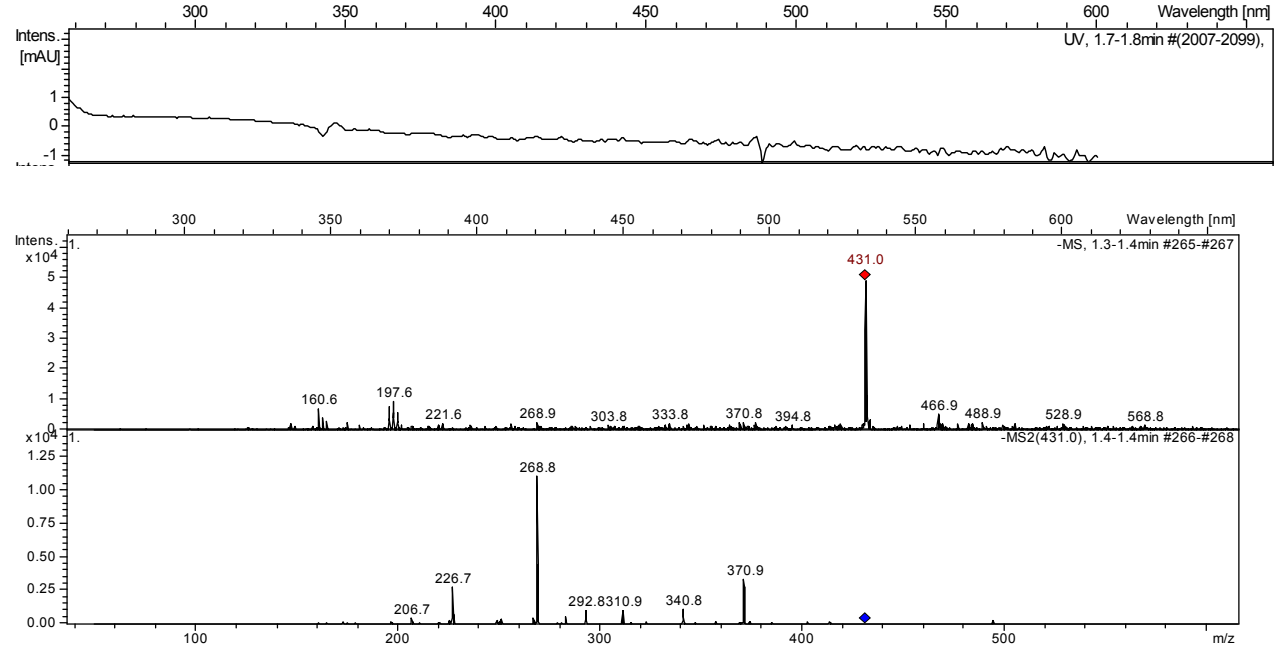
300
350
400
450
500
550
600
Wavelength [nm]
Intens.
[mAU]
UV, 1.7-1.8min #(2007-2099),
-MS, 1.3-1.4min #265-#267
431.0
160.6
197.6
221.6
268.9
303.8
333.8
370.8
394.8
466.9
488.9
528.9
568.8
-MS2(431.0), 1.4-1.4min #266-#268
268.8
226.7
206.7
292.8310.9
340.8
370.9
100
200
300
400
500
m/z

D

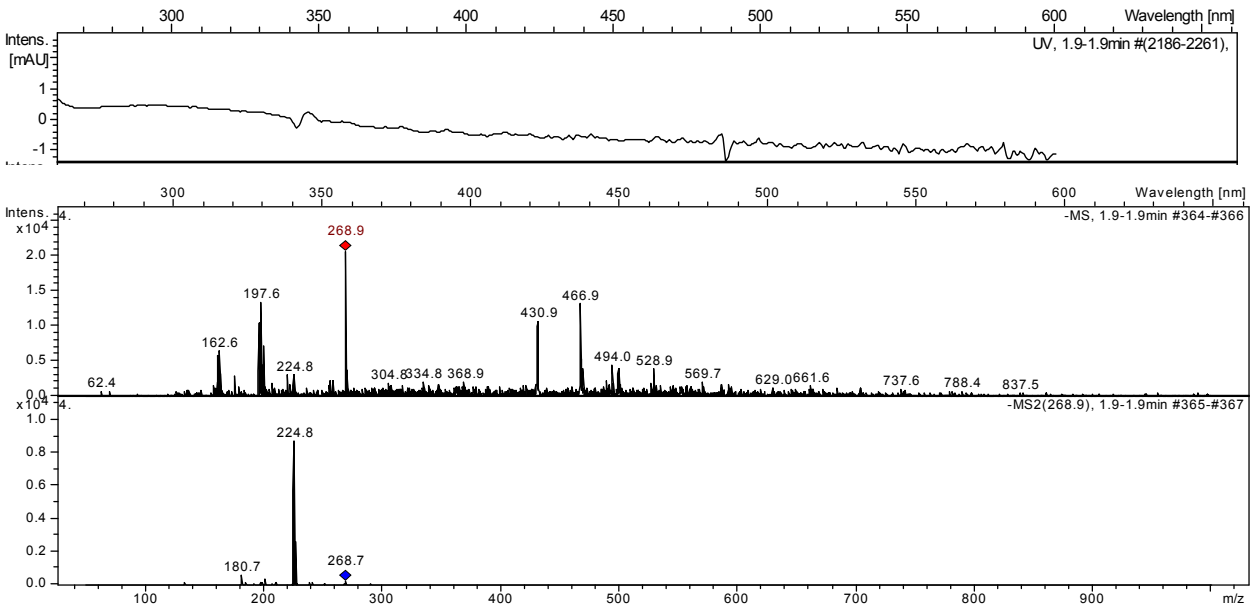

E

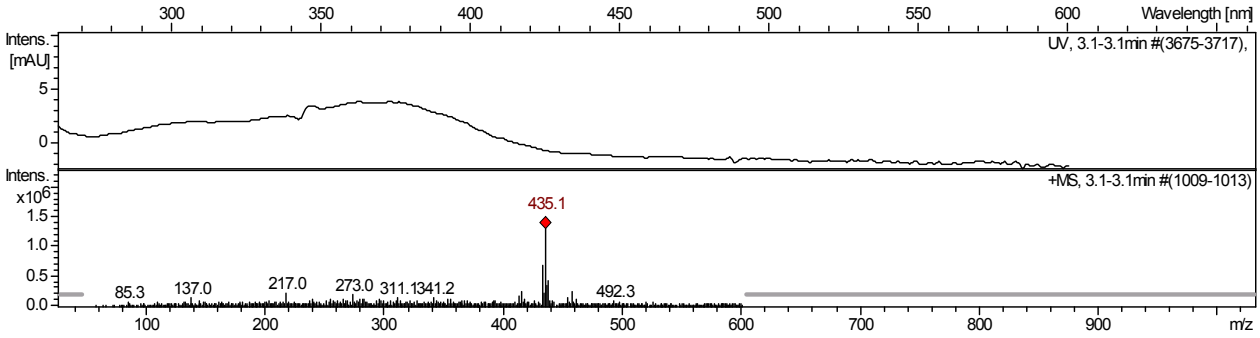

Figure 4. UPLC – DAD – MS analysis of **P2**- Cu^{II} binding (incubation for 24 h in a pH 5.0 acetate buffer, , 25°C, Cu^{II} / **P2** ratio = 5)

A: Chromatogram (280 nm) of the **P2 -** Cu^{II} mixture.

B: UV-vis and mass spectra of compound at t_R = 1.45 min, *m/z* (ES^+) = 417

C: UV-vis and mass spectra compound at t_R = 1.75 min, *m/z* (ES^-) = 431

D: UV-vis and mass spectra of compound at t_R = 1.9 min, *m/z* (ES^-) = 467

E: UV-vis and mass spectra of compound at t_R = 3.15 min, *m/z* (ES^+) = 435

Table 2. UPLC-DAD-MS analyses of products formed in Cu^{II}-induced autoxidation of **P1** and **P2**. (Cu/pigment molar ratio = 5, pH 5.0 acetate buffer, 24h)

Compound	*m/z* (detection mode)	λ (nm)	t_R (min)	*Figure*
P1	255 (ES^+)	470	3.0	3.B
P1 - 4H + H_2O	269, 241 (ES^+)	[a]	3.85	3.C
P2	417 (ES^+)	475	1.45	4.B
P2 chalcone	435 (ES^+)	370	3.15	4.E
P2 – 2H + H_2O	431, 371, 269 (ES^-)	307	1.75	4.C
P2 – 2H + 3H_2O	467, 431, 269, 225 (ES^-)	[a]	1.9	4.D

[a] No value given because of lack of sensitivity

Conclusion

Copper – 3-deoxyanthocyanis binding is generally followed by fast precipitation. Only the **P1** - Cu^{I} complex could be evidenced in solution (pH 5). Despite the fast precipitation of the complexes, 3-deoxyanthocyanins - Cu^{II} binding triggers partial oxygenation of the ligands.

Overall, copper – 3-deoxyanthocyanins binding seems less promising than iron – 3-deoxyanthocyanins binding in the production of stable colors.

Figure 5. shows the variation of **P1** color from orange to different shades of purple – blue in the presence of the metal ions. Over time, a general fading was observed and a color change in the **P1** - Fe^{II} mixture that is ascribed to Fe^{II} autoxidation. However, the colors of the chelates all appeared more stable than that of free **P1**.

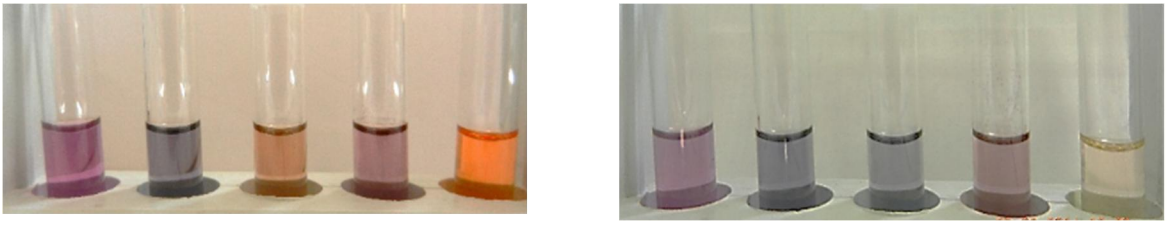

Figure 5. From right to left: **P1**, **P1** - Cu^{I}, **P1** - Fe^{II}, **P1** - Fe^{III}, **P1** - Al^{III}. *Left*: immediately after pigment addition. *Right*: *ca*. 15h after pigment addition. All complexes were prepared in a pH= 5.0 acetate buffer, metal / pigment ratio = 5.

References

1. Soumille, N. M.; Al Bittar, S.; Rosa, M.; Dangles, O. Analogs of anthocyanins with a 3', 4'-dihydroxy substitution: Synthesis and investigation of their acid-base, hydration, metal binding and hydrogen-donating properties in aqueous solution. *Dyes Pigments* **2012**, *96*, 7–15.

2. Al Bittar, S.; Mora, N.; Loonis, M.; Dangles, O. Chemically Synthesized Glycosides of Hydroxylated Flavylium Ions as Suitable Models of Anthocyanins: Binding to Iron Ions and Human Serum Albumin, Antioxidant Activity in Model Gastric Conditions. *Molecules* **2014**, *19*, 20709–20730.

3. Tokalıoğlu, Ş.; Gürbüz, F. Selective determination of copper and iron in various food samples by the solid phase extraction. *Food Chem.* **2010**, *123*, 183–187.

4. Dangles, O. Antioxidant activity of plant phenols: chemical mechanisms and biological signficance. *Curr. Org. Chem.* **2012**, *16*, 1–23.

5. Nkhili, E.; Loonis, M.; Mihai, M.; El Hajji, H.; Dangles, O. Reactivity of food phenols and copper ions: binding dioxygen activation and oxidation mechanisms. *Food Funct.* **2014**, *5*, 1186–1202.

Article III

A simple synthesis of 3-deoxyanthocyanidins and their O-glucosides

Sheiraz Al Bittar, Nathalie Mora-Soumille, Michèle Loonis, Olivier Dangles*

Submitted (in revision)

ABSTRACT

This work deals with the chemical synthesis of simple analogs of anthocyanins, the main class of water-soluble natural pigments. Flavylium ions with hydroxyl, methoxyl and β-D-glucopyranosyloxyl substituents at positions 4' and 7 have been prepared by straightforward chemical procedures. Moreover, the two 3-deoxyanthocyanidins of red sorghum apigeninidin (4',5,7-trihydroxyflavylium) and luteolinidin (3',4',5,7-tetrahydroxyflavylium) were synthesized in a one-step protocol. Attempts to synthesize luteolinidin O-β-D-glucosides resulted in a mixture of the 5-O- and 7-O-regioisomers in low yield. A preliminary study of the 4'-β-D-glucopyranosyloxy-7-hydroxyflavylium and 7-β-D-glucopyranosyloxy-4'-hydroxy-flavylium ions shows that simply changing the glucosidation site can profoundly affect the color intensity and stability.

Keywords: Anthocyanin; 3-Deoxyanthocyanidin; Glycoside; Synthesis; Sorghum; Color

1. Introduction

For centuries, food colorants have been used to attract the consumer's eye, to reproduce color lost during processing and to mask the heterogeneity of food formulations [1]. Chemistry has provided the food industry with diverse, cheap, and stable synthetic colorants. However, during the last decades, the safety of these synthetic colorants has been questioned. For instance, attention deficit hyperactivity disorder (ADHD) was observed in children having consumed red drinks supplemented with azo dyes [2] and products including these synthetic colorants have now to issue specific warnings on their packaging. Overall, natural colorants enjoy a much more positive image to consumers than artificial ones and the search for stable natural colorants remains a current challenge.

Anthocyanins are the most important group of water-soluble plant pigments. Stored in cell vacuoles, they are responsible for most of the red, purple and blue colors found in the plant kingdom [3]. Anthocyanins are generally found in Nature as anthocyanidin O-glycosides and the anthocyanidin aglycone is typically represented by its major colored form in acidic conditions, *i.e*. the 3,4',5,7-tetrahydroxyflavylium ion (pelargonidin) and common parent ions with additional OH or OMe groups at C3' and/or C5'. Among these 6 chromophores, anthocyanidins having a 3',4'-dihydroxy substitution (*e.g*., cyanidin as the simplest) are especially important from two viewpoints: they can bind hard metal ions (Al^{3+}, Fe^{3+}, Mg^{2+}) to form deeply colored chelates, one of the main mechanisms for natural color variation. They are good electron donors (as, more generally, polyphenols and flavonoids bearing catechol nuclei) and thus potential antioxidants [4] [5].

While each anthocyanidin OH group can be potentially glycosylated in anthocyanins, glycosidation at C3-OH suffers no exception. Indeed, a free C3-OH is associated with a high chemical instability (except in highly acidic conditions, pH < 2) and the corresponding C-ring is rapidly cleaved to yield a mixture of simple colorless phenols. Hence, hydrolysis of the glycosidic bond at C3-OH, either chemically during thermal processing, or enzymatically by human or bacterial glycosidases, is rapidly followed by irreversible loss of the typical chromophore [6] [7]. This is one of the main mechanisms underlying the well-known low chemical stability and apparent bioavailability of anthocyanins.

Although much less common than anthocyanins, 3-deoxyanthocyanidins (3-DAs) and their O-glycosides have been found in high concentration in some food sources, especially red sorghum [8] [9] The lack of OH group at C3 makes these pigments much less sensitive to water addition at C2, [10] [11] which reversibly leads to the colorless hemiketal and chalcone forms, and also more resistant to irreversible chemical degradation [12] Thus, in mildly acidic to neutral conditions, 3-DAs express more intense and more stable colors than common anthocyanins. On the other hand, the applications of 3-DAs as food colorants could be limited by their low water solubility, which can be markedly improved by conjugation to D-glucose. Red sorghum actually also contains 3-DA glucosides, such as luteolinidin 5-O-β-D-glucoside [13]

Extraction of anthocyanins from various natural sources typically affords complex extracts combining anthocyanins, colorless polyphenols and other hydrophilic plant components, such as sugars and acids. Hence, the purification of these extracts for the preparation of anthocyanins at the gram scale remains challenging and time-consuming. In this respect, the simple chemical synthesis of anthocyanins and simpler analogs remains interesting, if not for direct industrial application, at least for facilitating the evaluation of their potential as natural colorants for foods and cosmetic products, and as nonessential micronutrients, whose bioavailability and bioactivity are extensively studied [14] [15].

In this present work, we report on the efficient chemical synthesis of 3-DAs and their O-β-D-glucosides (Scheme 1), including the characteristic red sorghum pigments apigeninidin (APN, 4',5,7-trihydroxyflavylium) and luteolinidin (LTN, 3',4',5,7-tetrahydroxyflavylium), as well as a series of simpler analogs. After careful optimization of reaction conditions (time, temperature, solvent composition…), the chemical synthesis of APN and LTN could be achieved in an essentially one-step procedure, *i.e.* via a much simpler route than previously described in the literature [16] [17] A preliminary investigation of the coloring properties of two 3-DA glucosides is also reported, showing the large influence of the sugar position on the resulting color and its stability.

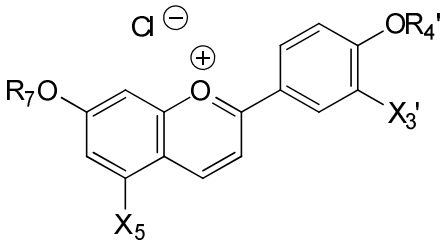

Pigment	$X_{3'}$	$R_{4'}$	X_5	R_7	Yield (%) [a])
P1[18]	OH	H	H	H	56
P2[18]	OH	H	H	β-D-Glc	75
P3	H	H	H	β-D-Glc	42
P4	H	Me	H	β-D-Glc	23
P5	H	β-D-Glc	H	H	77
P6	H	β-D-Glc	H	Me	77
P7	H	H	H	H	45
P8	H	H	H	Me	90
P9	H	Me	H	H	85
APN	H	H	OH	H	34
LTN	OH	H	OH	H	65

[a]) Yield of isolated pigment in the condensation step

Scheme 1. Pigments synthesized in this work (except **P1** and **P2** [18])

2. Results and discussion

The chemical synthesis 3-DAs and analogs has already been described over the last 3 - 4 decades [16-19] The simplest route typically involves the acid-catalyzed aldol condensation of a 2-hydroxybenzaldehyde and an acetophenone bearing additional OH, OMe or O-glycosyl substituents. Using gaseous HCl bubbled into the cooled solution of both reagents in ethylacetate, the corresponding flavylium chloride precipitates and is recovered by simple filtration. Alternatively, 3-DAs were prepared by reduction of the corresponding flavones [20] and from condensation between cinnamaldehyde derivatives and phloroglucinol [21]. Finally, 3-deoxyanthocyanidins can also be prepared by condensation between phenol derivatives and arylethynylketones [22] [23]

As natural anthocyanins all possess a 5,7-dihydroxy substitution (A-ring), aldol condensations involving 2,4,6-trihydroxybenzaldehyde are of particular interest. Unfortunately, 2,4,6-trihydroxybenzaldehyde is poorly soluble in AcOEt and prone to acid-catalyzed dimerization (possibly, oligomerization) by electrophilic aromatic substitution, leading to yellow – orange xanthylium pigments. To circumvent these disadvantages, less simple routes have been devised, some still based on 2,4,6-trihydroxybenzaldehyde but requiring its preliminary partial O-acylation to improve its solubility in weakly polar solvent (convenient for the precipitation of the flavylium salts) and decrease the nucleophilic character of its aromatic ring [17] [24]. In this work, special attention has been devoted to optimizing the direct condensation of (unprotected) 2,4,6-trihydroxybenzaldehyde with an acetophenone to ensure a reasonable yield of flavylium while keeping at a minimum the side-reaction leading to xanthylium pigments. Important factors in the optimization are the solvent composition (ensuring both 2,4,6-trihydroxybenzaldehyde solubility and flavylium precipitation), the temperature, the reagent concentration and the proton donor. For the synthesis of the red sorghum pigments APN and LTN, AcOEt / MeOH (2:1) mixtures were used and gaseous HCl was in situ generated by reaction between MeOH and TMSCl added in controlled excess to a solution of both reagents in a closed flask cooled to 0°C. In such conditions, LTN was formed in 65% yield and isolated after 30 min by simple filtration. LTN was contaminated by small quantities (*ca*. 5%) of 2,4,6,8-tetrahydroxyxanthylium chloride (Scheme 2) characterized by UPLC-MS: t_R = 4.2 min, λ_{max} = 440 nm, *m/z* = 244.9 (M^+) and by a very simple spectrum ^{1}H-NMR (in CD_3OD): δ (ppm) = 6.0

(2H, *s*, H_1, H_9), 6.4 (2H, *s*, H_3, H_7), 9.5 (1H, *s*, H_4).[25] Its formation from 2,4,6-trihydroxybenzaldehyde is not fully clear as it involves a decarbonylation step (CO loss). Solubilization in EtOH and precipitation by AcOEt addition afforded pure LTN.

Remarkably, a similar procedure yielded APN devoid of xanthylium pigment and only contaminated by low amounts of unreacted 2,4,6-trihydroxybenzaldehyde. Repeating the reaction over 60 min with 2 equiv. of 4-hydroxyacetophenone gave pure APN after purification in EtOH / AcOEt.

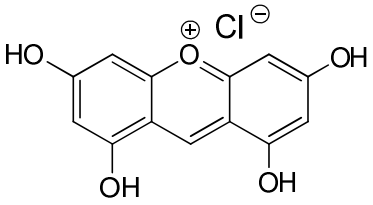

Scheme 2. Structure of 2,4,6,8-tetrahydroxyxanthylium chloride.

Based on this improved procedure, a series of flavylium ions was efficiently prepared with the typical OH and O-β-D-Glc substituents of natural anthocyanins at positions 4' and 7. Although much less common at those positions, the corresponding O-methylethers were also synthesized. The chemical synthesis of aglycones **P7**, **P8** and **P9** was achieved in AcOEt / MeOH (1:1). As neither 2,4-dihydroxybenzaldehyde nor 2-hydroxy-4-methoxybenzaldehyde is prone to competing dimerization, the aldol condensation was prolonged over 3 days at 4°C to ensure total flavylium precipitation and a maximal yield (up to 90% for **P8**).

As for the glucosides, a preliminary glucosidation step of 2,4-dihydroxybenzaldehyde and 4-hydroxyacetophenone was required (Scheme 3). With the former, satisfactory yields were obtained using phase transfer conditions in a 1:1 mixture of saturated aqueous K_2CO_3 (pH 12) and CH_2Cl_2 using 2,3,4,6-tetra-*O*-acetyl-α-D-glucopyranosyl bromide as the glucosyl donor.[18] Due to the strong hydrogen bond between the carbonyl group and C2-OH, the glucosidation of 2,4-dihydroxybenzaldehyde was regioselective and took place at C4-OH. Such strongly alkaline conditions did not allow us to convert 4-hydroxyacetophenone into its glucoside, possibly because of competing enolate formation. A less alkaline aqueous phase ($NaHCO_3$ / KCl (1:1), pH 8.7) was thus used [19] and the glucoside was obtained, although in low yield.

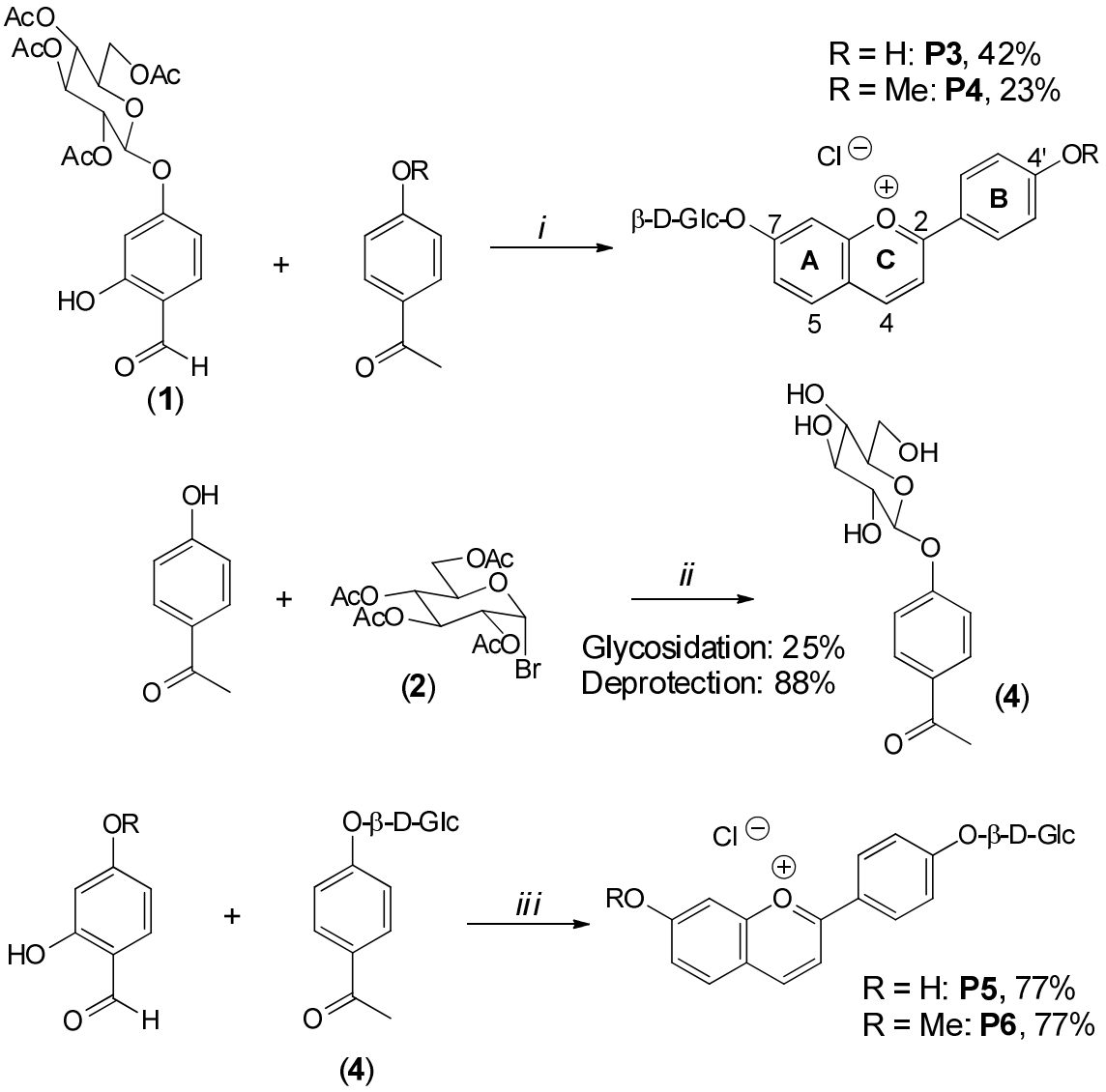

Scheme 3. Chemical synthesis of pigments: (*i*) TMSCl, AcOEt, then MeONa, MeOH, then aq. HCl. (*ii*) tris(2-(2-methoxyethoxy)ethyl)amine in CH_2Cl_2 / 1 M aq. $NaHCO_3$, 1 M aq. KCl, then MeONa, MeOH. (*iii*) TMSCl, AcOEt / MeOH.

To prepare pigments **P3** and **P4**, aldol condensation was achieved in AcOEt / MeOH (4:1) in the presence of TMSCl (10 equiv.) and the mixture kept 3 days at -18°C to minimize possible deglycosidation. A next step of glucose deacetylation was carried out using MeONa in excess (8 equiv.) as part of the reagent is consumed by reversible addition to the pyrylium ring and/or phenolate formation. After acidification, **P3** and **P4** were obtained in moderate over all yields (42% and 23%, respectively).

To prepare pigments **P5** and **P6**, the above-described route was not satisfactory because of incomplete deacetylation of the pigments. Consequently, a preliminary step of glucose deacetylation with traces of MeONa afforded **4** in good yield (≈ 88%). Then, **4** was condensed with 2,4-dihydroxybenzaldehyde or 2-hydroxy-4-methoxybenzaldehyde in MeOH / AcOEt (2:1) (Scheme 3).

Red sorghum contains not only 3-DAs but also some of their glucosides, in particular luteolinidin 5-O-β-glucoside (LTN-5-Glc) [13]. To ensure glucosidation of 2,4,6-trihydroxybenzaldehyde at C2-OH and also lower its hydrophilic character and thus favor its transfer into the organic phase, selective protection at C4-OH was attempted. Benzoylation with benzoylchloride / *t*-BuOK in THF at 0°C afforded an inseparable mixture of 2- and 4-regioisomers along with the dibenzoylated product. Unfortunately, the subsequent step of glucosidation failed because of insufficient stability of the benzoyl groups in the phase transfer conditions. Benzylation with benzyl bromide / K_2CO_3 in DMF turned out to take place mainly at C2-OH, yielding a 4:1 inseparable mixture of 2-benzyloxy-4,6-dihydroxybenzaldehyde and 4-benzyloxy-2,6-dihydroxybenzaldehyde (Scheme 4). It may be speculated that the phenolate anion resulting from deprotonation at C4-OH is stabilized through extensive conjugation with the CHO group while its tautomer formed by deprotonation at C2-OH could bear a larger negative charge on its O-atom, making it more nucleophilic.

Glucosidation of the benzylether regioisomers led to pure 2-benzyloxy-6-hydroxy-4-(2',3',4',6'-tetra-O-acetyl-β-D-glucopyranosyloxy)-benzaldehyde (**6**) in acceptable yield, which suggests that the minor 4-benzyloxy-2,6-dihydroxybenzaldehyde is unreactive in the phase transfer reaction (confirmed by isolation and independent attempt of glycosidation). Then, hydrogenolysis was carried out in soft conditions (30 min, 2 bars of H_2) to avoid aldehyde reduction. Aldol condensation with 3,4-dihydroxyacetophenone gave 7-(2',3',4',6'-tetra-*O*-acetyl-β-D-glucopyranosyloxy)-3',4',5-trihydroxyflavylium. Unfortunately, the final deprotection step turned out to be slow and incomplete even in strongly alkaline conditions (excess MeONa in MeOH or KOH in MeOH/H_2O (1:1) [24]). A possible explanation would be that all phenolic groups are deprotonated in those conditions, so that the nucleophilic attack of methoxide or hydroxide anions onto the acetate groups is impeded by electrostatic repulsion (especially with the nearby C5-O^- group). Overall, despite prolonged reaction time and repeated deprotection, partially protected pigments remained in solution and had to be removed by chromatography on TSK gel.

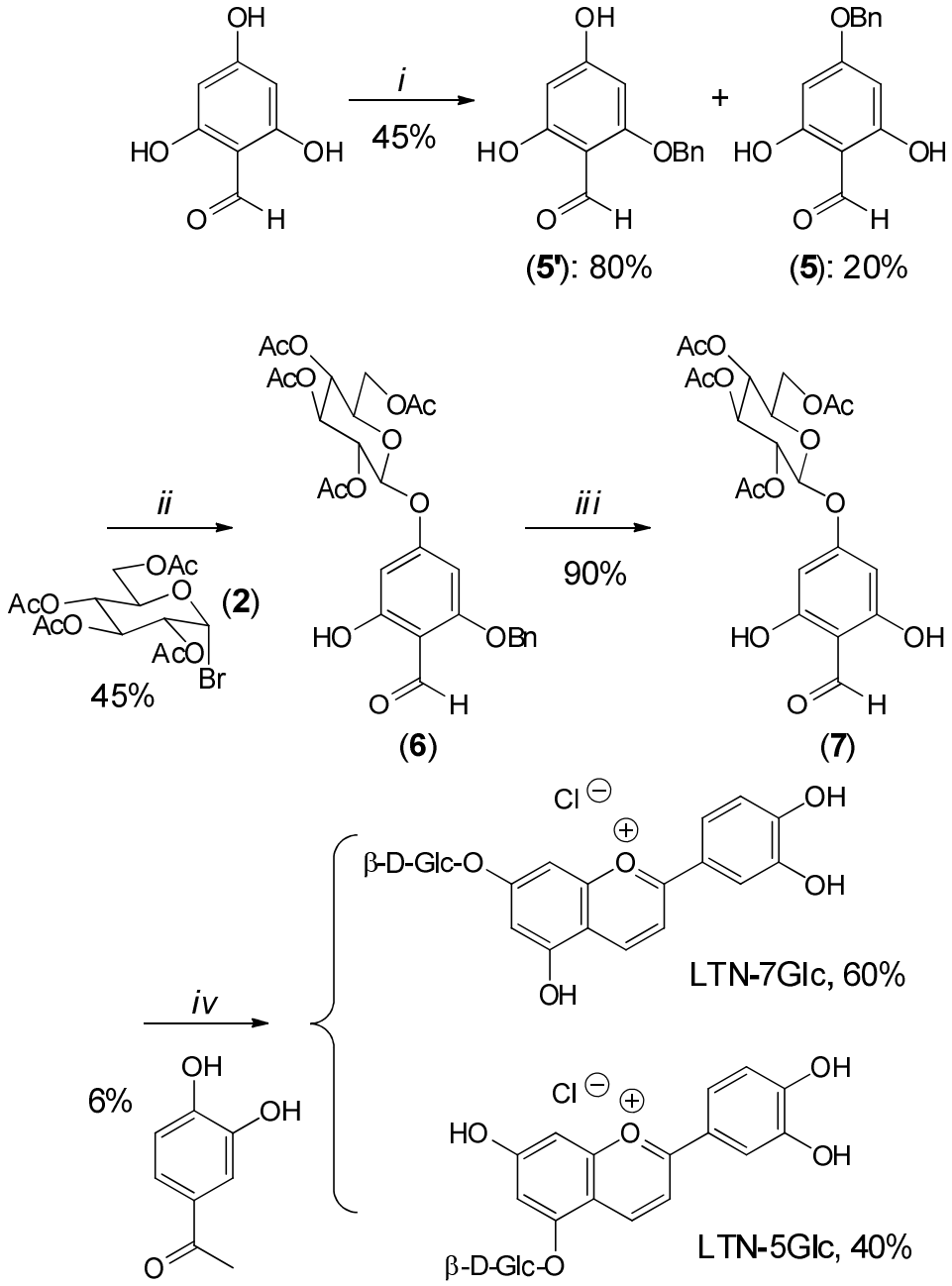

Scheme 4. Chemical synthesis of luteolinidin glucosides: (*i*) BnBr (1 equiv.), K_2CO_3, DMF (*ii*) tris(2-(2-methoxyethoxy)ethyl)amine in CH_2Cl_2 / 1 M aq. $NaHCO_3$, 1 M aq. KCl. (*iii*) H_2, Pd/C, THF - MeOH. (*iv*) TMSCl, AcOEt, then MeONa, MeOH, then aq. HCl.

Surprisingly, UPLC-MS analysis of the deprotected product revealed that it actually was a *ca*. 3:2 mixture of LTN-7-Glc and the naturally occurring LTN-5-Glc. Both were fully characterized by NMR in comparison with the literature [13]. To our knowledge, this unexpected isomerization in alkaline conditions has no equivalent in the literature.

Hydroxylated flavylium ions (AH^+, typically, red) undergo two competitive pathways in mildly acidic solution featuring the natural medium of anthocyanins, [11] [27] *i.e*. the vacuole of plant cells: the first one is fast proton loss and concomitant formation of purple quinonoid bases (A), the second one is the much slower reversible addition of water at the electrophilic C2 center with concomitant proton loss and formation of a colorless hemiketal (B) in fast equilibrium with a *cis*-chalcone (C_c), itself in slow equilibrium with the corresponding *trans*-chalcone (C_t) (Scheme 5).

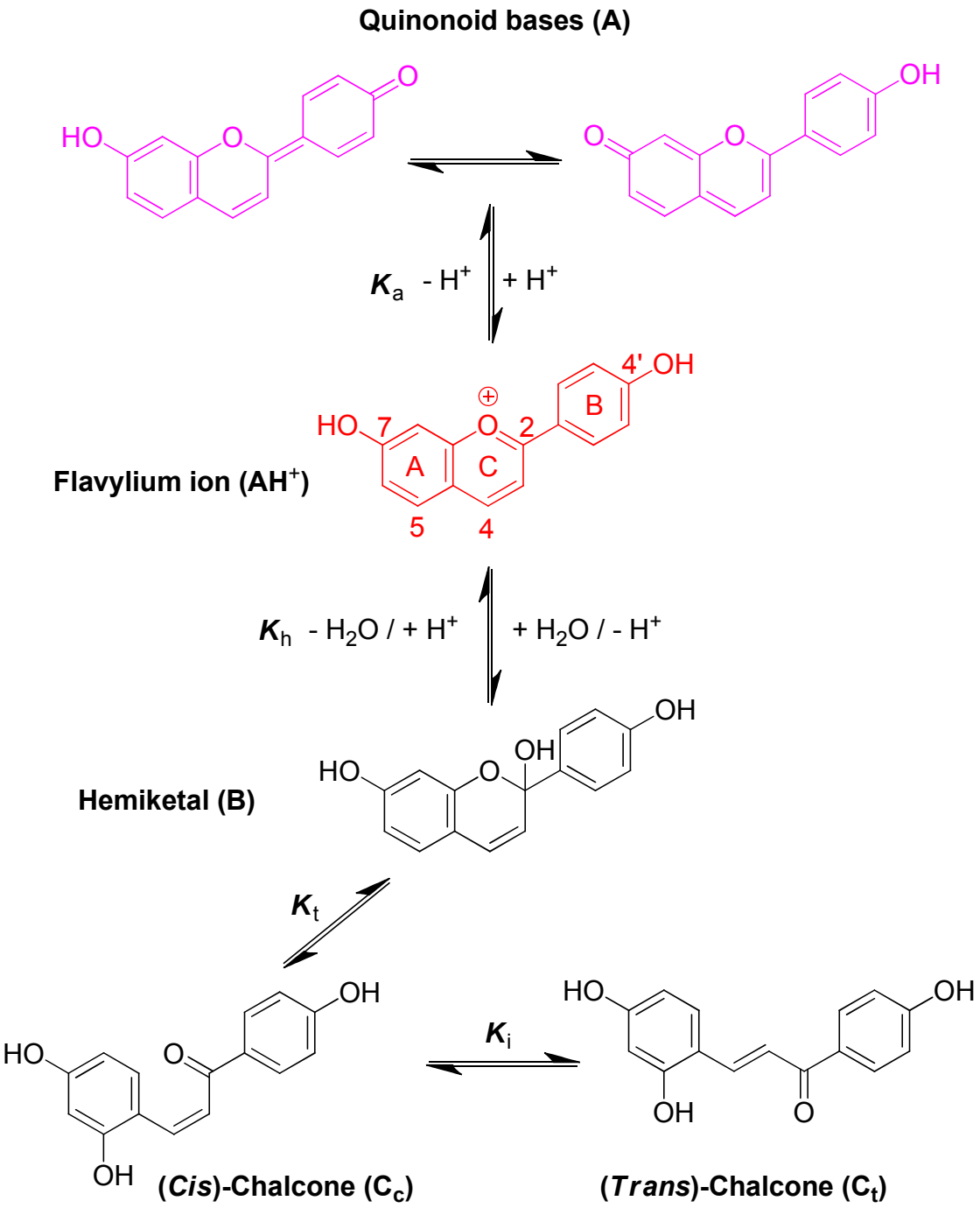

Scheme 5. Structural transformations of flavylium ions in mildly acidic aqueous solution.

With 3-DAs, B and C_c are only transient non-accumulating intermediates and C_t comes up as the only significant colorless form [18] [28]. A simplified scheme can thus be proposed in which A and C_t are respectively the kinetic and thermodynamic products of the concurrent transformations of AH^+ in mildly acidic solution. The set of flavylium ions synthesized in this work offers a good opportunity to investigate the influence on these competitive pathways of the typical substituents of anthocyanins at C4'-OH and C7-OH, in particular the β-D-glucosyl group, and their consequences in terms of color expression and stability. This point will be briefly exemplified with **P3** and **P5**.

When a small volume of pigment solution in acidified MeOH (100% flavylium form) is diluted into a pH 7.4 phosphate buffer, the corresponding quinonoid base is instantaneously formed. **P3** and **P5** bearing only one OH group, a single deprotonation is observed (no further proton loss leading to anionic bases) and a single base is formed (instead of 2 or 3 possible tautomers as with natural anthocyanins). As the first pK_a of flavylium ions is typically in the range 4 - 5, [11] the proton loss can be assumed quantitative. Thus, the spectra recorded immediately after dilution (Fig. 1A) can be ascribed to pure A forms resulting from proton loss at C4'-OH (A4', **P3**) or at C7-OH (A7, **P5**). Interestingly, while both flavylium ions display almost the same λ_{max} in the visible range (*ca*. 450 nm), the visible spectrum of the **P3** base (λ_{max} = 505 nm) is shifted by 20 nm to longer wavelengths, compared to the **P5** base (λ_{max} = 485 nm). Moreover, the higher molar absorption coefficient of the **P3** *vs*. **P5** flavylium ion (*ca*. +70%) is translated and amplified (almost a factor 3) into the corresponding bases. Therefore, although proton loss reduces the HOMO – LUMO gap in both pigments, this decrease and thus the bathochromic shift are larger when deprotonation occurs at C4'-OH. Moreover, the HOMO – LUMO match, which must be mainly responsible for the visible absorption, is better in **P3** than in **P5**, regardless of the acid - base form.

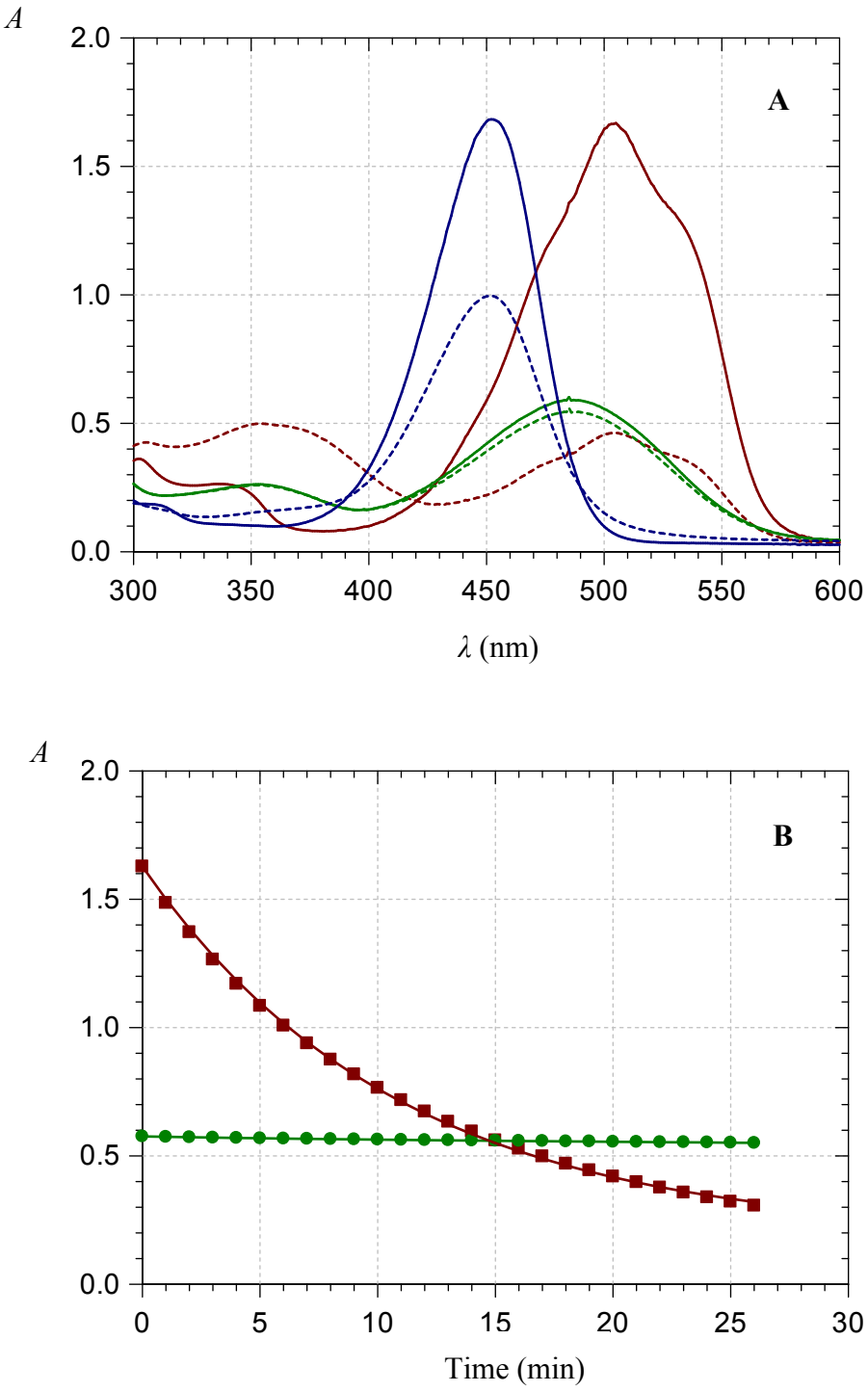

Fig. 1. A: UV-visible spectra (pigment concentration = 50 µM). a) Quinonoid bases (pH 7.4 phosphate buffer, 25°C): **P3** (—) and **P5** (—) immediately after dilution in the buffer, **P3** (---) and **P5** (---) after 30 min. b) Flavylium ions (0.1 M HCl, 25°C): **P3** (—), **P5** (---). **B:** decay of the visible absorbance of the bases at λ_{max}. **P3** (■, detection at 505 nm), **P5** (●, detection at 485 nm). Solid lines result from curve-fitting assuming apparent first-order kinetics: k_{obs}(**P3**) = 15.4 (± 0.2) x10^{-4} s^{-1}, k_{obs}(**P5**) = 19.4 (± 0.2) x10^{-6} s^{-1}, r = 0.9998.

Remarkably, the advantage of **P3** over **P5** in terms of color variation and intensity is not translated in terms of color stability in neutral conditions. Indeed, while the visible spectrum of the **P5** base remains essentially unchanged over 30 min (half-life of **P5** base ≈ 10h based on the observed first-order decay, Fig. 1B), the one of **P3** is markedly weakened (half-life of **P3** base ≈ 7.5 min) with concomitant appearance of a new absorption band around 360 nm featuring the **P3** *trans*-chalcone (Fig. 1A). Thus, **P5** appears as exceptionally resistant to water addition and subsequent fading in neutral conditions.

The color loss features the overall conversion of the colored forms into the *trans*-chalcone. Its rate is governed by the slow step of chalcone *cis – trans* isomerization. Hence, the observed rate constant of fading can be written as Eqn. (1), in which the fraction represents the percentage of *cis*-chalcone at pseudo-equilibrium with the colored forms and hemiketal:[27]

$$k_{obs} = k_i \frac{K_h K_t}{[H^+] + K_a + K_h(1 + K_t)} + k_{-i} \qquad (1)$$

With the 3',4'-dihydroxy-7-O-β-D-glucopyranosyloxyflavylium ion (**P2**), which is closely related to **P3**, the following values were estimated for the different parameters [28]: K_h = 2.5x10^{-5} M, K_a = 1.3x10^{-5} M, K_t = 3.3, k_i = 1.2x10^{-3} s^{-1}, k_{-i} = 1.6x10^{-5} s^{-1}($K_i = k_i / k_{-i} = 75$). At pH 7.4, one has: $[H^+] << K_a + K_h(1 + K_t)$. Moreover, C_t is much more stable than C_c ($k_i << k_{-i}$). Hence, Eqn. (1) can be simplified to give Eqn. (2):

$$k_{obs} = k_i \frac{K_t}{1 + K_t + \frac{K_a}{K_h}} \qquad (2)$$

From Eqn. (2), one obtains: k_{obs} = 8.2x10^{-4} s^{-1}. This value is actually close to our estimate for **P3**: k_{obs} = 15.4 (± 0.2) x10^{-4} s^{-1}. More work is needed to unveil the cause for the much higher stability of **P5**. As there is no reason for K_t and K_h to be dramatically different for **P3** and **P5** or for the *cis-trans* chalcone isomerization barrier to be higher for **P5** than for **P3**, it may be speculated that the very slow fading of **P5** stems from a much higher K_a value due to proton loss being much more favorable from C7-OH than from C4'-OH. Consistently, the pK_a values of the 4'-hydroxyflavylium and 7-hydroxyflavylium ions were reported to be 5.5 and 3.55,

respectively [11]. In other words, in the competition between proton loss and water addition, the quinonoid base of **P5** is probably both the thermodynamic and kinetic product of the flavylium ion ($K_a > K_h$) and the concurrent route leading to the colorless forms is strongly inhibited.

3. Conclusion

Efficient syntheses have been devised for the red sorghum pigments luteolinidin and apigeninidin, as well as for a series of flavylium ions substituted by the typical OH, OMe and O-β-D-Glc groups of naturally occurring anthocyanins. Due to their high water solubility, the glucosides are convenient analogs of natural pigments for systematic investigations of the impact of substitution on color. Based on the preliminary study of two regioisomers, it seems clear that the glucosidation site has a considerable influence on the resulting color and its stability in aqueous solution. The detailed physico-chemical investigation of these pigments is under way.

4. Experimental

4.1. Materials and instruments

All starting materials were obtained from commercial suppliers and were used without purification. 4'-Hydroxyacetophenone, 4'-methoxyacetophenone, 2,4-dihydroxy-benzaldehyde, 2-hydroxy-4-methoxybenzaldehyde and chlorotrimethylsilane were purchased from Aldrich-Sigma (France). 2,4,6-Trihydroxybenzaldehyde was purchased from Extrasynthese (France). 3',4'-Dihydroxyacetophenone and 4-(2',3',4',6'-tetra-O-acetyl-β-D-

glucopyranosyloxy)-2-hydroxybenzaldehyde (**1**) were prepared as already reported.[18] TLC analyses were performed on silica gel 60 F254 or C-18 silica gel F254s. Detection was achieved by UV light (254 nm) and by charring after exposure to a 5% H_2SO_4 solution in EtOH. Purifications of intermediates were performed by column chromatography on silica gel 60 (40-63 µm, from Merck). Pigments were purified by elution on C18 silica gel cartridges (bond elut from Varian).

^{1}H- and ^{13}C-NMR spectra were recorded on an Ascend^{TM}400 Bruker apparatus at 400.18 MHz (^{1}H) or 100.62 MHz (^{13}C). Chemical shifts (δ) are in ppm relative to tetramethylsilane using the deuterium signal of the solvent ($CDCl_3$, CD_3OD) for calibration. ^{1}H-^{1}H coupling constants (J) are in Hz. ^{13}C-NMR signals of the glucosylated pigments were assigned from their HSQC spectra.

HR-MS analysis was carried out on Qstar Elite mass spectrometer (Applied Biosystems SCIEX, Foster City, CA, USA) equipped with API. Mass detection was performed in the positive electrospray ionization mode. UPLC-DAD-MS Analysis was performed on an Acquity Ultra Performance LC™ (UPLC™) apparatus from Waters, equipped with an UV-visible diode array detector (DAD) and coupled with a Bruker Daltonics HCT ultra ion trap mass spectrometer with negative electrospray ionization (ESI) mode. Separation was conducted on a 1.7 µm (2.1 - 50 mm) Acquity UPLC BEH C18 column thermostated at 30°C with an isocratic elution (0.05% aqueous HCO_2H / MeCN (7/3)) at a flow rate of 0.2 mL min^{-1}. Mass spectra were generated in the Ultrascan mode in the *m/z* range 100-900. The ion source parameters were: nebuliser pressure = 40 psi, drying gas flow = 9 L min^{-1}, drying gas temperature = 350°C.

UV-Vis absorption spectra were recorded on an Agilent 8453 diode array spectrometer equipped with a magnetically stirred quartz cell (optical path length = 1 cm). The temperature in the cell was controlled by means of a water-thermostated bath at 25°C.

4.2 Chemical synthesis

These syntheses prolong our previous work[18] about the chemical synthesis of 3',4',7-trihydroxyflavylium chloride (P1) and 3',4'-dihydroxy-7-O-β-D-glucopyranosyloxyflavylium chloride (P2).

4.2.1. 4'-Hydroxy-7-O-β-D-glucopyranosyloxyflavylium chloride (**P3**)

Equimolar amounts (1 mmol) of **1** and 4-hydroxacetophenone were dissolved in 5 mL of AcOEt / MeOH (4/1 v/v) and cooled to 0°C. After addition of TMSCl (0.8 mL, 10 equiv.), the solution was stirred for 10 min and kept for 3 days at -18°C. The pigment was precipitated by adding an access AcOEt. After filtration, the solid was dissolved in MeOH (20 mL) under Ar and MeONa (8 equiv.) was added until pH 9 (wet pH paper). After stirring for 3h at room temperature, 1 M HCl was added (until pH 1). The mixture was kept for 12h at 4°C for complete cyclization, then concentrated under reduced pressure. The residue was dissolved in 0.01 M HCl and loaded on a C18 cartridge. After elution with 100 mL of 0.01 M HCl to remove contaminating NaCl, the compound was eluted with 0.2 M HCl in MeOH. After evaporation, the solid was crystallized in MeOH / AcOEt to give **P3** as a dark red powder. Yield = 42%, R_f = 0.18 (BAW, *i.e.* n-BuOH / AcOH / H_2O, 3/2/1, v/v/v). ^{1}H-NMR (CD_3OD / TFA-d, 95/5): δ = 9.13 (1H, *d*, *J* = 8.8, H_4), 8.51 (2H, *d*, *J* = 8.7, $H_{2'}$, $H_{6'}$), 8.45 (1H, *d*, *J* = 8.8, H_3), 8.20 (1H, *d*, *J* = 8.6, H_5), 7.90 (1H, *d*, *J* = 2.2, H_8), 7.60 (1H, *dd*, *J* = 8.6 and 2.2, H_6), 7.12 (2H, *d*, *J* = 8.7, $H_{3'}$, $H_{5'}$), 5.34 (1H, *d*, *J* = 7.1, $H_{1''}$), 3.98 (1H, broad *d*, *J* = 9.8, $H_{6''B}$), 3.71-3.76 (2H, *m*, $H_{5''}$, $H_{6''A}$), 3.55-3.60 (2H, *m*, $H_{2''}$, $H_{3''}$), 3.45 (1H, broad *t*, *J* = 9.4, $H_{4''}$). ^{13}C-NMR (CD_3OD / TFA-d, 95/5): δ = 175.1 (C_2), 169.0 (C_7), 167.3 (C_9), 159.3 ($C_{4'}$), 154.6 (C_4), 134.9 ($C_{2'}$, $C_{6'}$), 133.1 (C_5), 122.5 (C_6), 121.1 ($C_{1'}$), 121.0 (C_{10}), 118.3($C_{3'}$, $C_{5'}$), 115.3 (C_3), 105.0 (C_8), 101.9 ($C_{1''}$), 78.8 ($C_{5''}$), 77.8 ($C_{3''}$), 74.6 ($C_{2''}$), 71.3 ($C_{4''}$), 62.6 ($C_{6''}$). UV/VIS (0.01M HCl in MeOH): ε(465 nm) = 42800 M^{-1} cm^{-1}. The purity of **P3** was checked by UPLC-DAD-MS, t_R = 2.3 min, λ_{max} = 455 nm, *m*/*z* (M^+) = 401.2.

4.2.2. 4'-Methoxy-7-O-β-D-glucopyranosyloxyflavylium chloride (**P4**)

Equimolar amounts (1 mmol) of **1** and 4-methoxyacetophenone were dissolved in 6 ml of AcOEt/MeOH (1/1, v/v) and cooled to 0°C. After addition of TMSCl (0.8 mL, 10 equiv.), the mixture was stirred for 30 min and kept for 3 days at -18°C. The pigment was precipitated by adding an access of AcOEt. After filtration, the same deacetylation procedure as for **P3** was carried out. **P4** was obtained as a dark red powder after crystallization in MeOH / AcOEt / Et_2O. Yield = 23%, R_f = 0.37 (BAW). ^{1}H-NMR (CD_3OD / TFA-d, 95/5): δ = 9.22 (1H, *d*, *J* = 8.8, H_4), 8.60 (2H, *d*, *J* = 8.8, $H_{2'}$, $H_{6'}$), 8.45 (1H, *d*, *J* = 8.8, H_3), 8.53 (1H, *d*, *J* = 8.8, H_5), 7.96 (1H, *d*, *J* = 2.2, H_8), 7.65 (1H, *dd*, *J* = 8.8 and 2.2, H_6), 7.31 (2H, *d*, *J* =8.8, $H_{3'}$, $H_{5'}$), 5.35 (1H, *d*, *J* = 7.3, $H_{1''}$), 4.04 (3H, s, OCH_3), 3.98 (1H, broad *d*, *J* = 10.0, $H_{6''B}$), 3.68-3.75 (2H, *m*, $H_{5''}$, $H_{6''A}$),

3.53-3.60 (2H, *m*, $H_{2''}$, $H_{3''}$), 3.45 (1H, *t*, *J* = 9.0, $H_{4''}$). ^{13}C-NMR (CD_3OD / TFA-d, 95/5): δ = 175.1 (C_2), 169.4 (C_7), 167.7 (C_9), 159.7 ($C_{4'}$), 155.4 (C_4), 133.3 ($C_{2'}$, $C_{6'}$), 133.2 (C_5), 122.9 (C_6), 122.5 ($C_{1'}$), 121.4 (C_{10}), 117.3, 117.1 ($C_{3'}$, $C_{5'}$), 115.4 (C_3), 105.0 (C_8), 102.0 ($C_{1''}$), 78.8 ($C_{5''}$), 77.9 ($C_{3''}$), 74.6 ($C_{2''}$), 71.2($C_{4''}$), 62.6 ($C_{6''}$), 57.0 (OMe). UV/VIS (0.01 M HCl in MeOH): ε(458 nm) = 35700 M^{-1} cm^{-1}. The purity of **P4** was checked by UPLC-DAD-MS, t_R = 2.2 min, λ_{max} = 455 nm, *m*/*z* (M^+) = 414.9.

4.2.3. 4-(2',3',4',6'-Tetra-O-acetyl-β-D-glucopyranosyloxy)acetophenone (**3**)

A solution of **2** (1.68 g, 4.1 mmol) in distilled CH_2Cl_2 (5 mL) was added to a solution of 4-hydroxyacetophenone (1.49 g, 1.5 equiv.) and tris(2-(2-methoxyethoxy)ethyl)amine (3.52 mL, 1.5 equiv.) in 1 M $NaHCO_3$ / 1 M KCl (1:1) (pH 9, 5 mL). The mixture was refluxed for 72h. After addition of H_2O (10 mL) and extraction with CH_2Cl_2 (3x10 mL), the combined organic phases were successively washed with 1 M HCl (2x10 mL), then with H_2O (2x10 mL), dried over Na_2SO_4 and concentrated. The syrupy residue was purified on silica gel using cHex/ AcOEt (8/2 to 7.5/2.5, then 7/3, v/v). Finally, crystallization in MeOH / H_2O gave **3** as white crystals. Yield = 25%, R_f = 0.21 (cHex / AcOEt, 6/4, v/v). ^{1}H-NMR ($CDCl_3$): δ = 7.87 (2H, *d*, *J* = 8.8, $H_{2'}$, $H_{6'}$), 6.96 (2H, *d*, *J* = 8.8, $H_{3'}$, $H_{5'}$), 5.24 (2H, *m*, $H_{3''}$, $H_{4''}$), 5.12 (2H, *m*, $H_{1''}$, $H_{2''}$), 4.22 (1H, *dd,* *J* = 12.3 and 5.4, $H_{6''B}$), 4.10 (1H, *dd,* *J* = 12.3 and 2.3, $H_{6''A}$), 3.85 (1H, *m*, $H_{5''}$), 2.50 (3H, *s*, OCH_3), 1.99 (12H, broad *s*, 4Ac). ^{13}C-NMR ($CDCl_3$): δ = 196.6 (C=O), 160.2 ($C_{1'}$), 132.5 ($C_{4'}$), 130.5($C_{2'}$, $C_{6'}$), 116.3($C_{3'}$, $C_{5'}$), 98.2 ($C_{1''}$), 72.6 ($C_{3''}$), 72.3 ($C_{5''}$), 71.1 ($C_{2''}$), 68.2 ($C_{4''}$), 61.9 ($C_{6''}$), 20.7 (OMe), 20.6 (Me of Ac).

4.2.4. 4-O-β-D-Glucopyranosyloxyacetophenone (**4**)

Compound **3** (320 mg, 0.69 mmol) was dissolved in dry MeOH (10 mL) and treated with a catalytic amount of MeONa (pH 8-9 using wet pH paper). After stirring for 4 h, total deacetylation was confirmed by TLC (cHex / AcOEt, 3/2, v/v). The mixture was then acidified with ion exchange resin (Amberlite IRC_{50}, H^+ form) to pH 1-2 (wet pH paper), filtered and evaporated. White crystals were obtained after crystallization in MeOH / Et_2O. Yield = 88%, R_f = 0.88 (cHex / AcOEt, 6/4, v/v). ^{1}H NMR (CD_3OD): δ = 8.98 (2H, *d*, *J* = 8.9, $H_{2'}$, $H_{6'}$), 7.17 (2H, *d*, *J* = 8.9, $H_{3'}$, $H_{5'}$), 5.03 (1H, *d*, *J* = 7.5, $H_{1''}$), 3.90 (1H, *dd*, *J* = 12.0 and 2.2, $H_{6''B}$), 3.70 (1H, *dd*, *J* = 12.0 and 5.6, $H_{6''A}$), 3.48-3.50 (3H, *m*, $H_{2''}$, $H_{3''}$,$H_{5''}$), 3.40 (1H, *dd*, *J* = 5.4 and 2.0, $H_{4''}$), 2.56 (3H, *s*, CH_3). ^{13}C-NMR (CD_3OD): δ = 199.4 (C=O), 163.1 ($C_{1'}$), 132.7 ($C_{4'}$), 131.6

($C_{2'}$, $C_{6'}$), 117.3 ($C_{3'}$, $C_{5'}$), 101.6 ($C_{1''}$), 78.3 ($C_{5''}$), 77.3 ($C_{3''}$), 74.8 ($C_{2''}$), 71.3 ($C_{4''}$), 62.5 ($C_{6''}$), 49.5 (OMe), 26.5 (Me of Ac).

4.2.5. 4'-O-β-D-Glucopyranosyloxy-7-hydroxyflavylium chloride (**P5**)

Equimolar amounts (0.5mmol) of **4** and 2,4-dihydroxybenzaldehyde were dissolved in 15 mL of AcOEt / MeOH (1/2, v/v). After addition of TMSCl (1.6 mL, 20 equiv.), the solution was stirred for 30 min at room temperature. The pigment was precipitated by adding AcOEt and isolated as a red powder after filtration. Yield = 77%, R_f = 0.14 (BAW). ^{1}H-NMR (CD_3OD / TFA-d, 95/5): δ = 9.15 (1H, *d*, *J*= 8.9, H_4), 8.48 (2H, *d*, *J* = 9.1, $H_{2'}$, $H_{6'}$), 8.39 (1H, d, *J* = 8.9, H_3), 8.19 (1H, *d*, *J* = 8.9, H_5), 7.54 (1H, *d*, *J* = 2.2, H_8), 7.42 (1H, *dd*, *J* = 8.9 and 2.2, H_6), 7.40 (2H, *d*, *J* = 9.1, $H_{3'}$, $H_{5'}$), 5.17 (1H, *d*, *J* = 7.2, $H_{1''}$), 3.93 (1H, *dd*, *J* = 12.0 and 2.2, $H_{6''B}$), 3.72 (1H, *dd*, *J* = 12.0 and 5.8, $H_{6''A}$), 3.55-3.57 (3H, *m*, $H_{2''}$, $H_{3''}$, $H_{5''}$), 3.45 (1H, *t*, *J* = 9.2, $H_{4''}$).^{13}C-NMR (CD_3OD / TFA-d, 95/5): δ = 173.4 (C_2), 171.0 (C_7), 165.9 (C_9), 160.9 ($C_{4'}$), 155.4 (C_4), 134.2 (C_5), 133.1 ($C_{2'}$, $C_{6'}$), 124.1 ($C_{1'}$), 123.0 (C_6), 120.8 (C_{10}), 119.1 ($C_{3'}$, $C_{5'}$), 113.7 (C_3), 103.7 (C_8), 101.5 ($C_{1''}$), 78.6 ($C_{5''}$), 77.9 ($C_{3''}$), 74.7 ($C_{2''}$), 71.2 ($C_{4''}$), 62.5 ($C_{6''}$). UV/VIS (0.01 M HCl in MeOH), ε(460 nm) = 37600 M^{-1} cm^{-1}. The purity of **P5** was checked by UPLC-DAD-MS: t_R = 1.4 min, λ_{max}= 450 nm, *m/z* (M^+) = 400.9.

4.2.6. 4'-O-β-D-Glucopyranosyloxy-7-methoxyflavylium chloride (**P6**)

Equimolar amounts (1 mmol) of **4** and 2-hydroxy-4-methoxybenzaldehyde were dissolved in 15 mL of AcOEt / MeOH (1/2, v/v). After addition of TMSCl (20 equiv.), the mixture was stirred for 30 min at room temperature. **P6** as a dark red powder was obtained by simple filtration. Yield = 77%, R_f = 0.29 (BAW). ^{1}H-NMR (CD_3OD / TFA-d, 95/5): δ = 9.22 (1H, *d*, *J*= 8.7, H_4), 8.55 (2H, *dd*, *J* = 9.1, $H_{2'}$, $H_{6'}$), 8.50 (1H, *d*, *J*= 8.7, H_3), 8.22 (1H, *d*, *J* = 8.9, H_5), 7.88 (1H, *d*, *J* = 2.2, H_8), 7.56 (1H, *dd*, *J* = 8.9 and 2.2, H_6), 7.42 (2H, *d*, *J* = 9.1, $H_{3'}$, $H_{5'}$), 5.18 (1H, *d*, *J* = 7.4, $H_{1''}$), 4.17 (3H, OCH_3), 3.92 (1H, *dd*, *J* = 12.0 and 2.2, $H_{6''B}$), 3.71 (1H, *dd*, *J* = 12.0 and 5.9, $H_{6''A}$), 3.56-3.60 (3H, *m*, $H_{2''}$, $H_{3''}$, $H_{5''}$), 3.53 (1H, *t*, *J* = 9.2, $H_{4''}$). ^{13}C-NMR (CD_3OD / TFA-d, 95/5): δ = 174.1 (C_2), 171.2 (C_7), 166.2 (C_9), 160.9 ($C_{4'}$), 155.7 (C_4), 133.5 (C_5), 133.2 ($C_{2'}$, $C_{6'}$), 124.0 ($C_{1'}$), 123.1 (C_6), 121.3 (C_{10}), 119.2 ($C_{3'}$, $C_{5'}$), 114.8 (C_3), 101.6

(C_8), 101.5 ($C_{1''}$), 78.6 ($C_{5''}$), 77.9 ($C_{3''}$), 74.7 ($C_{2''}$), 71.2 ($C_{4''}$), 62.5 ($C_{6''}$), 58.1 (OMe). UV/VIS (0.01 M HCl in MeOH): ε(455 nm) = 25400 M^{-1} cm^{-1}. The purity of **P6** was checked by UPLC-DAD-MS: t_R= 1.95 min, λ_{max} = 450 nm, *m/z* (M^+) = 414.9.

4.2.7. 4',7-Dihydroxyflavylium chloride (**P7**)

Equimolar amounts (1 mmol) of 2,4-dihydroxybenzaldehyde and 4-hydroxyacetophenone were dissolved in 5 mL of AcOEt / MeOH (4/1, v/v). After cooling to 0°C, TMSCl (10 equiv.) was added. The mixture was stirred for 10 min, then kept at 4°C for 3 days. Precipitation of pigment was achieved by adding AcOEt. After filtration, **P7** was obtained as a dark red powder. Yield = 45%, R_f = 0.52 (ABFW, *i.e.* AcOH / n-BuOH / HCO_2H / H_2O, 20/2/1/1, v/v/v). ^{1}H-NMR (CD_3OD / TFA-d, 95/5): δ = 9.04 (1H, *d*, *J* = 8.8, H_4), 8.42 (2H, *dd*, *J* = 8.9 and 2.0, $H_{2'}$, $H_{6'}$), 8.30 (1H, *d*, *J* = 8.8, H_3), 8.13 (1H, *d*, *J* = 8.9, H_5), 7.49 (1H, *d*, *J* = 1.9, H_8), 7.40 (1H, broad *d*, *J* = 8.9, H_6), 7.10 (2H, *dd*, *J* = 8.9 and 2.0, $H_{3'}$, $H_{5'}$). ^{13}C-NMR (CD_3OD / TFA-d, 95/5): δ = 173.8 (C_2), 170.2 (C_7), 168.2 (C_9), 160.2 ($C_{4'}$), 154.4 (C_4), 134 ($C_{2'}$, $C_{6'}$), 133.9 (C_5), 122.3 (C_6), 121.2 ($C_{1'}$), 120.0 (C_{10}), 118.6 ($C_{3'}$, $C_{5'}$), 113.4 (C_3), 103.7 (C_8). UV/VIS (0.01 M HCl in MeOH): ε(470 nm) = 59700 M^{-1} cm^{-1}.The purity of **P7** was checked by UPLC-DAD-MS: t_R = 1.38 min, λ_{max} = 465 nm, *m/z* (M^+) = 239.1.

4.2.8. 7-Hydroxy-4'-methoxyflavylium chloride (**P8**)

Equimolar amounts (1 mmol) of 2,4-dihydroxybenzaldehyde and 4-methoxyacetophenone were reacted in the same conditions as for **P7**. **P8** was obtained as a dark red powder. Yield = 90%, R_f = 0.18 (EBFW). ^{1}H-NMR (CD_3OD / TFA-d, 95/5): δ = 9.10 (1H, *d*, *J* = 8.7, H_4), 8.47 (2H, *dd*, *J* = 7.6 and 2.2, $H_{2'}$, $H_{6'}$), 8.35 (1H, *d*, *J* = 8.7, H_3), 8.15 (1H, *d*, *J* = 9.0, H_5), 7.51 (1H, *d*, *J* = 2.2, H_8), 7.42 (1H, *dd*, *J* = 9.0 and 2.2, H_6), 7.25 (2H, *dd*, *J* = 7.6 and 2.0, $H_{3'}$, $H_{5'}$), 3.99 (3H, OCH_3). ^{13}C-NMR (CD_3OD / TFA-d, 95/5): δ = 173.5 (C_2), 170.7 (C_7), 168.6 (C_9), 160.5 ($C_{4'}$), 154.9 (C_4), 134.0 (C_5), 133.4 ($C_{2'}$, $C_{6'}$), 122.7 (C_6), 122.5 ($C_{1'}$), 120.4 (C_{10}), 117.1 ($C_{3'}$, $C_{5'}$), 113.5 (C_3), 103.7 (C_8), 56.8 (OCH_3). UV/VIS (0.01 M HCl in MeOH): ε(467 nm) = 57500 M^{-1} cm^{-1}. The purity of **P8** was checked by UPLC-DAD-MS: t_R = 2.3 min, λ_{max} = 465 nm, *m/z* (M^+) = 253.1.

4.2.9. 4'-Hydroxy-7-methoxyflavylium chloride (**P9**)

Equimolar amounts (1 mmol) of 2-hydroxy-4-methoxybenzaldehyde and 4-hydroxyacetophenone were reacted in the same conditions as for **P7**. **P9** was obtained as a dark red powder. Yield = 85%, R_f = 0.18 (EBFW). ^{1}H-NMR (CD_3OD / TFA-d, 95/5): δ = 9.10 (1H, *d*, *J* = 8.8, H_4), 8.46 (2H, *dd*, *J* = 7.5 and 2.0, $H_{2'}$, $H_{6'}$), 8.39 (1H, *d*, *J* = 8.8, H_3), 8.15 (1H, *d*, *J* = 9.0, H_5), 7.8 (1H, *d*, *J* = 2.2, H_8), 7.49 (1H, broad *d*, *J* = 9.0, H_6), 7.1 (2H, *dd*, *J* = 7.5 and 2.0, $H_{3'}$, $H_{5'}$), 4.15 (3H, *s*, OCH_3). ^{13}C-NMR (CD_3OD / TFA-d, 95/5): δ = 174.3 (C_2), 170.4 (C_7), 168.6 (C_9), 160.2 ($C_{4'}$), 154.4 (C_4), 134.4 ($C_{2'}$, $C_{6'}$), 133 (C_5), 121.1 ($C_{1'}$), 122.3 (C_6), 120.5 (C_{10}), 118.8 ($C_{3'}$, $C_{5'}$), 114.4 (C_3), 101.5 (C_8), 58.0 (OMe). UV/VIS (0.01 M HCl in MeOH): ε(467 nm) = 50400 M^{-1} cm^{-1}. The purity of **P9** was checked by UPLC-DAD-MS: t_R = 1.95 min, λ_{max} = 465 nm, *m*/*z* (M^+) = 253.1.

4.2.10. 4',5,7-Trihydroxyflavylium chloride (apigeninidin)

A solution of 2,4,6-trihydroxybenzaldehyde (1 mmol) and 4-hydroxyacetophenone (2 equiv.) in 3 mL of AcOEt / MeOH (2/1, v/v) was cooled to 0°C and TMSCl (20 equiv.) was added. After 60 min of stirring, complete precipitation of APN was achieved. Crystallization in MeOH / AcOEt afforded APN as a red powder. Yield = 34%, R_f = 0.83 (BAW). ^{1}H-NMR (CD_3OD / TFA-d, 95/5): δ = 9.10 (1H, *d*, *J* = 8.7, H_4), 8.33 (2H, *dd*, *J* =8.9 and 2.0, $H_{2'}$, $H_{6'}$), 8.05 (1H, *d*, *J* = 8.7, H_3), 7.08 (2H, *dd*, *J* = 8.9 and 2.0, $H_{3'}$, $H_{5'}$), 6.95 (1H, *d*, *J* = 2.1, H_8), 6.66 (1H, *d*, *J* = 2.1, H_6). ^{13}C-NMR (CD_3OD / TFA-d, 95/5): δ = 172.9 (C_2), 172.3 (C_7), 167.3 (C_9), 160.4 (C_5), 160.1 ($C_{4'}$), 149.6 (C_4), 133.2 ($C_{2'}$, $C_{6'}$), 121.4 ($C_{1'}$), 118.4 ($C_{3'}$, $C_{5'}$), 113.8 (C_{10}), 110.4 (C_6), 103.1 (C_3), 96.1 (C_8). UV/VIS (0.01 M HCl in MeOH): ε(480 nm) = 38400 M^{-1} cm^{-1}.The purity of APN was checked by UPLC-DAD: t_R = 5.5 min, λ_{max} = 475 nm. HRMS-ESI: *m/z*(M^+) calcd = 255.0652, found = 255.0651.

4.2.11. 3',4',5,7-Tetrahydroxyflavylium chloride (luteolinidin)

Equimolar amounts (1 mmol) of 2,4,6-trihydroxybenzaldehyde and 3,4-dihydroxyacetophenone were dissolved in 3 mL of AcOEt / MeOH (2/1, v/v). After cooling to

0°C, TMSCl (20 equiv.) was added and the solution stirred for 30 min at 0°C. LTN was totally precipitated by adding AcOEt. After filtration, LTN was isolated as a red powder (yield = 65%). To remove the yellow xanthylium contaminant (*ca*. 5%), LTN was crystallized in EtOH / AcOEt. R_f = 0.83 (BAW). ^{1}H-NMR (CD_3OD / TFA-d, 95/5): δ = 9.02 (1H, *d*, *J* = 8.7, H_4), 7.97 (1H, *d*, *J* = 8.7, H_3), 7.88 (1H, *dd*, *J* = 8.7 and 2.3, $H_{6'}$), 7.73 (1H, *d*, *J* = 2.3, $H_{2'}$), 7.04 (1H, d, *J* = 8.7, $H_{5'}$), 6.89 (1H, *d*, *J* = 2.1, H_8), 6.62 (1H, *d*, *J* = 2.1, H_6). ^{13}C-NMR (CD_3OD / TFA-d, 95/5): δ = 173.6 (C_2), 173.1 (C_7), 161.3 (C_9), 160.8 (C_5), 157.2 ($C_{4'}$), 149.9 (C_4), 149.1 ($C_{3'}$), 126.1 ($C_{6'}$), 122.6 ($C_{1'}$), 118.7 ($C_{5'}$), 116.8 ($C_{2'}$), 114.5 (C_{10}), 111.4 (C_6), 104.0 (C_3), 96.9 (C_8). UV/VIS (0.01 M HCl in MeOH): ε(500 nm) = 24000 M^{-1} cm^{-1}. The purity of LTN was checked by UPLC-DAD: t_R = 4.5 min, λ_{max} = 485 nm. HRMS-ESI: *m/z*(M^+) calcd=271.0601, found = 271.0603.

*4.2.12. 4-Benzyloxy-2,6-dihydroxybenzaldehyde (**5**) and 2-benzyloxy-4,6-dihydroxy-benzaldehyde (**5'**)*

A solution of 2,4,6-trihydroxybenzaldehyde (3g, 19.5 mmol) and dry K_2CO_3 (2.69 g, 1 equiv.) in 20 mL of anhydrous DMF was cooled to 0°C and stirred for 15 min. Then, benzyl bromide (2.31 mL, 1 equiv.) was added dropwise and the mixture was kept at 0°C under vigorous stirring during 2.5h. Glacial 0.1 M HCl (100 mL) was added and the aqueous phase extracted with AcOEt (3×100 mL). The combined organic phases were dried over Na_2SO_4, then concentrated. The crude product was purified by column chromatography on silica gel (cHex / AcOEt, 7/3, v/v) to afford the mixture of two regioisomers **5** and **5'** (1/4 molar ratio) as a white amorphous powder. Total yield = 45%, R_f = 0.57 (cHex / AcOEt, 6/4, v/v). **5**. ^{1}H-NMR(CD_3OD): δ = 10.05 (1H, *s*, CHO), 7.41 (5H, *m*, Ph), 5.97 (2H, *s*, H_3, H_5), 5.09 (2H, *s*, CH_2). ^{13}C-NMR (CD_3OD): δ = 191.1 (CHO), 167.5 (C_2, C_6), 163.5 (C_4), 136.2 ($1C_{Ph}$), 128.3, 128.2, 127.2 ($5C_{Ph}$), 95.1 (C_3, C_5), 70.2 (CH_2). **5'**. ^{1}H-NMR (CD_3OD): δ = 10.08 (1H, *s*, CHO), 7.41 (5H, *m*, Ph), 6.01 (1H, *d*, *J* = 2.0, H_5), 5.86 (1H, *d*, *J* = 2.0, H_3), 5.07 (2H, *s*, CH_2). ^{13}C-NMR (CD_3OD): δ = 191.9 (CHO), 165.9 (C_6), 164.2 (C_4), 163.5 (C_2), 136.3 ($1C_{Ph}$), 128.2, 127.9, 127.8 ($5C_{Ph}$), 105.6 (C_1), 93.3 (C_5), 91.8 (C_3), 69.8 (CH_2).

*4.2.13. 2-Benzyloxy-6-hydroxy-4-(2',3',4',6'-tetra-O-acetyl-β-D-glucopyranosyloxy)-benzaldehyde (**6**)*

A solution of tetra-*O*-acetyl-α-D-glucopyranosylbromide (**2**, 2.03 g, 1.5 equiv.) in distilled CH_2Cl_2 (10 mL) was added to a solution of **5** and **5'** (1 g, 3.28 mmol) and tris[2-(2-

methoxyethoxy)ethyl]amine (TMEA) (1.58 mL, 1.5 equiv.) in a saturated aqueous K_2CO_3 solution (10 mL). The mixture was refluxed for 18 h. After the same treatment as for **3**, the syrupy residue was purified on silica gel (cHex / AcOEt, 65/35, v/v), then crystallized in CH_2Cl_2 / Et_2O to afford **6** as white crystals. Yield = 49%, R_f = 0.52 (cHex / AcOEt, 6/4, v/v). ^{1}H-NMR($CDCl_3$): δ = 12.36 (1H, *s*, OH), 10.19 (2H, *s*, CHO), 7.39 (5H, *m*, Ph), 6.59 (1H, *d*, *J* = 2.2, H_5), 6.54 (1H, *d*, *J* = 2.2, H_3), 5.10 (2H, *s*, CH_2), 5.06-5.28 (4H, *m*, $H_{1'}$, $H_{2'}$, $H_{3'}$, $H_{4'}$), 4.15-4.22 (2H, 2*dd*, *J* = 12.1 and 6.1, *J* = 12.1 and 2.1, $H_{6'A}$, $H_{6'B}$), 3.87 (1H, *m*, $H_{5'}$), 2.02-2.07 (12H, *m*, 4Ac). ^{13}C-NMR ($CDCl_3$): δ = 192.5 (CHO), 169.6-170.2 (4 C=O), 166.1 (C_2), 165.9 (C_6), 164.3 (C_4), 135.5 ($1C_{Ph}$), 128.8, 128.5, 128.1, 127.9, 127.1 ($5C_{Ph}$), 107.3 (C_1), 95.7 ($C_{1'}$), 97.5 (C_5), 93.3 (C_3), 72.6 ($C_{3'}$), 72.4 ($C_{5'}$), 70.9 ($C_{2'}$), 70.7 (CH_2), 68.2 ($C_{4'}$), 61.9 ($C_{6'}$), 20.6 (4Me).

4.2.14. 2,6-Dihydroxy-4-(2',3',4',6'-tetra-O-acetyl-β-D-glucopyranosyloxy)benzaldehyde (**7**)

Compound **6** (1 g, 1.74 mmol) was dissolved in 10 mL of THF / MeOH (4/1, v/v) and 10% Pd on activated charcoal (0.124 g, 0.12 mmol) was added. Debenzylation was carried out in a hydrogenation reactor under 2 bars of H_2 for 30 min. The mixture was diluted in AcOEt (30 mL), filtered over celite, concentrated and purified on silica gel (AcOEt / cHex, 45/55, v/v). After crystallization in AcOEt / n-hexane, **7** was obtained as white crystals. Yield = 90%, R_f = 0.27 (cHex / AcOEt, 6/4, v/v). ^{1}H-NMR ($CDCl_3$): δ = 12.36 (2H, *s*, OH), 10.19 (1H, *s*, CHO), 6.01 (2H, *s*, H_3, H_5), 5.28-5.33 (2H, *m*, $H_{3'}$, $H_{4'}$), 5.13-5.20 (2H, *m*, $H_{1'}$, $H_{2'}$), 4.18-4.33 (2H, 2*dd*, *J* = 11.0 and 5.7, 11.0 and 2.0, $H_{6'A}$, $H_{6'B}$), 3.92 (1H, *m*, $H_{5'}$), 2.07-2.13 (12H, *m*, 4Ac). ^{13}C-NMR ($CDCl_3$): δ = 192.5 (CHO), 169.8-171.3 (4C=O), 164.2 (C_2, C_4, C_6), 106.8 (C_1), 97.4 ($C_{1'}$), 95.6 (C_3, C_5), 72.6 ($C_{3'}$), 72.3 ($C_{5'}$), 71.0 ($C_{2'}$), 68.3 ($C_{4'}$), 62.0 ($C_{6'}$), 20.6 (4Me).

2.2.15. 7-(2'',3'',4'',6''-Tetra-O-acetyl-β-D-glucopyranosyloxy)-3',4',5-trihydroxy-flavylium chloride (**8**)

Condensation between equimolar quantities (1 mmol) of **7** and 3,4-dihydroxyacetophenone in the presence of TMSCl (20 equiv.) was achieved in 5 mL of AcOEt / MeOH (4/1, v/v). After 30 min at 0°C, **8** was isolated by filtration as a red powder. ^{1}H-NMR (CD_3OD): δ = 9.13 (1H, *d*, *J* = 8.6, H_4), 8.20 (1H, *d*, *J* = 8.6, H_3), 8.00 (1H, d, *J* = 8.9 and 1.9, $H_{6'}$), 7.84 (1H, d, *J* = 1.9, $H_{2'}$), 7.31 (1H, broad *s*, H_8), 7.06 (1H, *d*, *J* = 8.9, $H_{5'}$), 6.73 (1H, broad *s*, H_6), 5.73 (1H, *d*, *J* = 7.8, $H_{1''}$), 5.46 (1H, *t*, *J* = 9.3, $H_{3''}$), 5.27 (1H, *dd*, *J* = 9.3 and 7.8, $H_{2''}$), 5.18 (1H, *t*, *J* = 7.8, $H_{4''}$), 4.22-4.36 (3H, *m*, $H_{5''}$, $H_{6''A}$, $H_{6''B}$), 2.07-2.13 (12H, *m*, 4 Me).

2.2.16. 5-(β-D-glucopyranosyloxy)-3',4',7-trihydroxyflavylium chloride (LTN-5Glc) and 7-(β-D-glucopyranosyloxy)-3',4',5-trihydroxyflavylium chloride (LTN-7Glc).

The same deacetylation procedure as for **P2** was carried out. UPLC-MS analysis of the red powder obtained showed a mixture of two deprotected isomers and several less polar partially acetylated pigments. Purification over TSK gel with elution by 1% aqueous HCl afforded the two inseparable deprotected isomers. The overall yield (condensation + deprotection + purification) was 6%. The purity of the LTN-Glc mixture was checked by UPLC-DAD-MS. LTN-7Glc (60%): t_R = 1.85 min, λ_{max} = 485 nm, *m/z* (M^+) = 433.1. LTN-5Glc (40%): t_R = 1.90 min, λ_{max} = 485 nm, *m/z* (M^+) = 433.1. The peak assignment was confirmed by co-injection with a sample of pure LTN-7Glc obtained by reduction[20] of the corresponding flavone luteolin7-O-β-D-glucoside. LTN-7Glc (major). ^{1}H-NMR (CD_3OD / TFA-d, 95/5): δ = 9.15 (1H, *d*, *J* = 8.8, H_4), 8.10 (1H, *d*, *J* = 8.8, H_3), 7.91 (1H, *dd*, *J* = 9.2 and 2.2, $H_{6'}$), 7.74 (1H, *d*, *J* = 2.2, $H_{2'}$), 7.06 (1H, broad *s*, H_8), 7.01 (1H, *d*, *J* = 9.2, $H_{5'}$), 7.00 (1H, *d*, *J* = 1.5, H_6), 5.18 (1H, *d*, *J* = 7.2, $H_{1''}$), 3.98 (1H, broad *d*, *J* = 11.9, $H_{6''B}$), 3.76 (1H, *dd*, *J* = 11.9 and 5.4, $H_{6''A}$), 3.64 (1H, *m*, $H_{5''}$), 3.51-3.61 (2H, *m*, $H_{2''}$,$H_{3''}$), 3.43 (1H, *t*, *J* = 9.4, $H_{4''}$). ^{13}C-NMR (CD_3OD / TFA-d, 95/5): δ = 171.4 (C_2), 169.1 (C_7), 158.1 (C_9), 157.5 (C_5), 157.1 ($C_{4'}$), 149.1 (C_4), 148.4 ($C_{3'}$), 126.0 ($C_{6'}$), 121.5 ($C_{1'}$), 117.8 ($C_{5'}$), 116.2 ($C_{2'}$), 113.5 (C_{10}), 111.9 (C_3), 105.0 (C_6), 101.8 ($C_{1''}$), 98.1 (C_8), 78.7 ($C_{3''}$), 77.8 ($C_{5''}$), 74.6 ($C_{2''}$), 71.2 ($C_{4''}$), 62.5 ($C_{6''}$). LTN-5Glc (minor). ^{1}H-NMR (CD_3OD / TFA-d, 95/5): δ = 9.09 (1H, *d*, *J* = 8.8, H_4), 8.14 (1H, *d*, *J* = 8.8, H_3), 7.96 (1H, *dd*, *J* = 9.2 and 2.2, $H_{6'}$), 7.79 (1H, *d*, *J* = 2.2, $H_{2'}$), 7.28 (1H, broad *s*, H_8), 7.03 (1H, *d*, *J* = 9.2, $H_{5'}$), 6.90 (1H, *d*, *J* = 1.5, H_6), 5.24 (1H, *d*, *J* = 7.2, $H_{1''}$), 3.98 (1H, broad *d*, *J* = 11.9, $H_{6''B}$), 3.76 (1H, *dd*, *J* = 11.9 and 5.4, $H_{6''A}$), 3.64 (1H, *m*, $H_{5''}$), 3.51-3.61 (2H, *m*, $H_{2''}$,$H_{3''}$), 3.43 (1H, *t*, *J* = 9.4, $H_{4''}$). ^{13}C-NMR (CD_3OD / TFA-d, 95/5): δ = 173.3 (C_7), 171.4 (C_2), 159.6 (C_5), 158.1 (C_9), 157.1 ($C_{4'}$), 149.5 (C_4), 149.0 ($C_{3'}$), 126.5 ($C_{6'}$), 121.5 ($C_{1'}$), 118.0 ($C_{5'}$), 116.5 ($C_{2'}$), 114.0 (C_{10}), 112.7 (C_3), 103.8 (C_6), 101.8 ($C_{1''}$), 97.7 (C_8), 78.7 ($C_{3''}$), 77.7 ($C_{5''}$), 74.6 ($C_{2''}$), 71.1 ($C_{4''}$), 62.4 ($C_{6''}$).

5. References

1. Cavalcanti, R. N.; Santos, D. T.; Meireles, M. A. A. *Food Res. Int*. **2011**, *44*, 499-509.
2. McCann, D.; Barrett, A.; Cooper, A.; Crumpler, D.; Dalen, L.; Grimshaw, K.; Kitchin, E.; Lok, K.; Porteous, L.; Prince, E.; Sonuga-Barke, E.; Warner, J. O.; Stevenson, J. *The Lancet* **2007**, *370*, 1560-1567.
3. Yoshida, K.; Mori, M.; Kondo, T. *Nat. Prod. Rep*. **2009**, *26*, 857-964.
4. Kähkönen, M. P.; Heinonen, M. J. *J. Agric. Food Chem*. **2003**, *51*, 628-633.
5. Goupy, P.; Bautista-Ortin, A. B.; Fulcrand, H.; Dangles, O. *J. Agric. Food Chem*. **2009**, *57*, 5762-5770.
6. Fleschhut, J.; Kratzer, F.; Rechkemmer, G.; Kulling, S. E. Eur. J. Nutr. **2006**, *45*, 7-18.
7. Sadilova, E.; Carle, R.; Stintzing, F. C. *Mol. Nutr. Food Res*. **2007**, *51*, 1461-1471.
8. Taylor, J. R. N.; Belton, P. S.; Beta, T.; Duodu, K. G. *J. Cereal Sci*. **2014**, *59*, 257-275.
9. Petti, C.; Kushwaha, R.; Tateno, M.; Harman-Ware, A. E.; Crocker, M.; Awika, J.; DeBolt, S. *J. Agric. Food Chem*. **2014**, 62, 1227-1232.
10. Mazza, G.; Brouillard, R. *J. Agric. Food Chem*. **1987**, *35*, 422–426.
11. Pina, F.; Melo, M. J.; Laia, C. A. T.; Parola, A. J. Lima, J. C. *Chem. Soc. Rev*. **2012**, *41*, 869-908.
12. Yang, L.; Dykes, L.; Awika, J. M. *Food Chem*. **2014**, *160*, 246-254.
13. Iwashina, T.; Kitajima, J.; Matsumoto, S. *Bull. Natl. Mus. Sci*. **2010**, *36*, 61-64.
14. Tsuda, T. *Mol. Nutr. Food Res*. **2012**, *56*, 159-170.
15. Del Rio, D.; Rodriguez-Mateos, A.; Spencer, J. P. E.; Tognolini, M.; Borges, G.; Crozier, A. *Antioxid Redox Signal*. **2013**, *18*, 1818-1892.
16. Sweeny, J.G.; Iacobucci, G.A. *Tetrahedron* **1981**, *37*, 1481-1483.
17. Carbonneau, M. A.; Cisse, M.; Mora-Soumille, N.; Dairi, S.; Rosa, M.; Michel, F.; Lauret, C.; Cristol, J. P.; Dangles, O. *Food Chem*. **2014**, *145*, 701-709.
18 Mora-Soumille, N.; Al Bittar, S.; Rosa, M.; Dangles, O. *Dyes Pigments* **2013**, *96*, 7-15.
19. El Hajji, H.; Dangles, O.; Figueiredo, P.; Brouillard, R. *Helv. Chim. Acta* **1997**, *80*, 398-413.
20. Bjoroy, O.; Rayyan, S.; Fossen, T.; Kalberg, K.; Andersen, O. M. *Phytochemistry* **2009**, *70*, 278-287.
21. Sousa, A.; Mateus, N.; De Freitas, V. *Tetrahedron Lett*. **2012**, *53*, 1300-1303.

22. Kueny-Stotz, M.; Isorez, G.; Chassaing, S.; Brouillard, R. *Synlett* **2007**, 1223-1226.

23. Chassaing, S.; Kueny-Stotz, M.; Isorez, G.; Brouillard, R. *Eur. J. Org. Chem.* **2007**, 2438-2448.

24. Dangles, O.; El Hajji, H. *Helv. Chim. Acta* **1994**, *77*, 1595-1610.

25 Dangles, O.; Brouillard, R. *New J. Chem*. **1994**, *18*, 287-296.

26. Cruz, L.; Mateus, N.; De Freitas, V. *Tetrahedron Lett*. **2013**, *54*, 2865-2869.

27. Pina, F. *J. Agric. Food Chem*. **2014**, *62*, 6885–6897.

28. Petrov, V.; Gavara, R.; Dangles, O.; Al Bittar, S.; Mora-Soumille, N.; Pina, F. *Photochem. Photobiol. Sci*. **2013**, *12*, 576–581.

Appendix II

NMR and UPLC-DAD-MS spectra of synthesized pigments

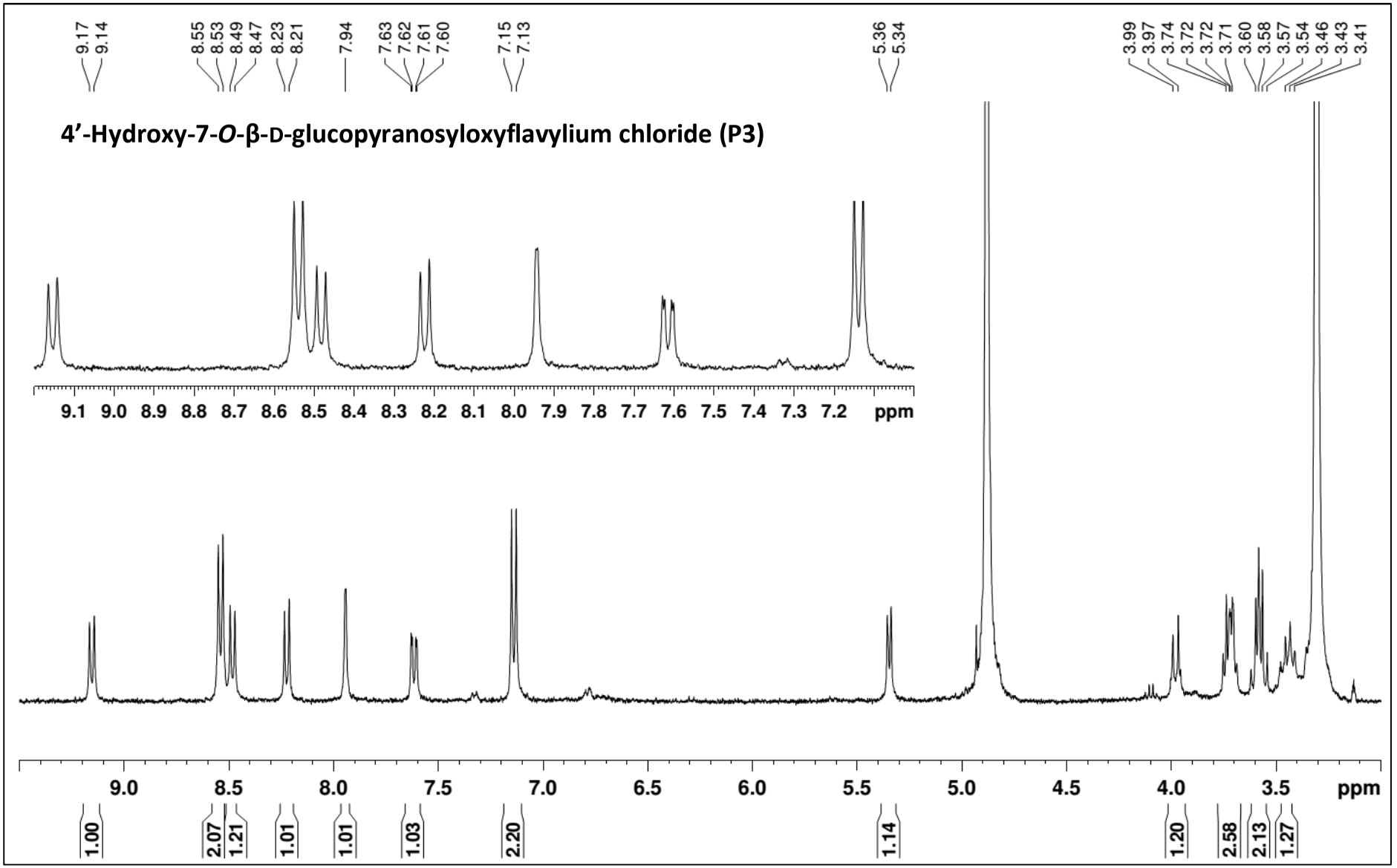
9.17
9.14
8.55
8.53
8.49
8.47
8.23
8.21
7.94
7.63
7.62
7.61
7.60
7.15
7.13
5.36
5.34
3.99
3.97
3.74
3.72
3.72
3.71
3.60
3.58
3.57
3.54
3.46
3.43
3.41
4’-Hydroxy-7-O-β-D-glucopyranosyloxyflavylium chloride (P3)
9.1 9.0 8.9 8.8 8.7 8.6 8.5 8.4 8.3 8.2 8.1 8.0 7.9 7.8 7.7 7.6 7.5 7.4 7.3 7.2 ppm
9.0 8.5 8.0 7.5 7.0 6.5 6.0 5.5 5.0 4.5 4.0 3.5 ppm
1.00
2.07
1.21
1.01
1.01
1.03
2.20
1.14
1.20
2.58
2.13
1.27

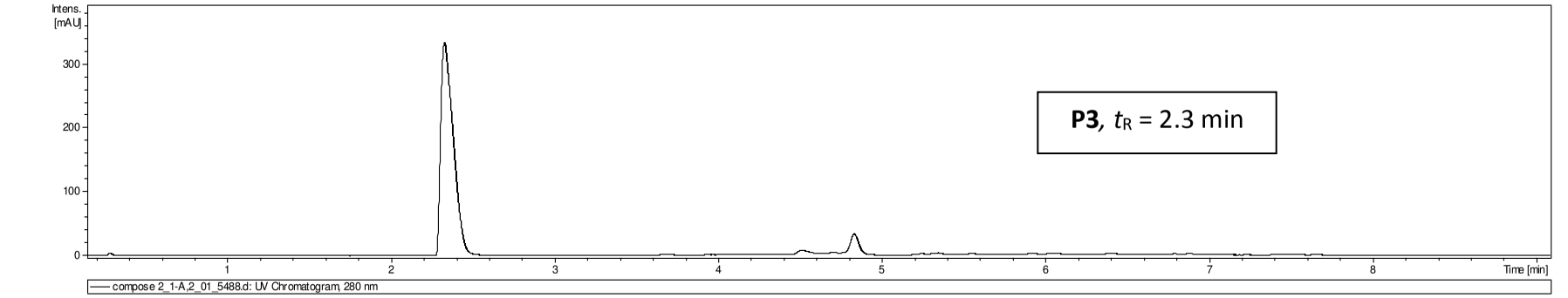
Intens.
[mAU]
300
200
100
0
1
2
3
4
5
6
7
8
Time [min]
P3, t_R = 2.3 min
compose 2_1-A,2_01_5488.d: UV Chromatogram, 280 nm

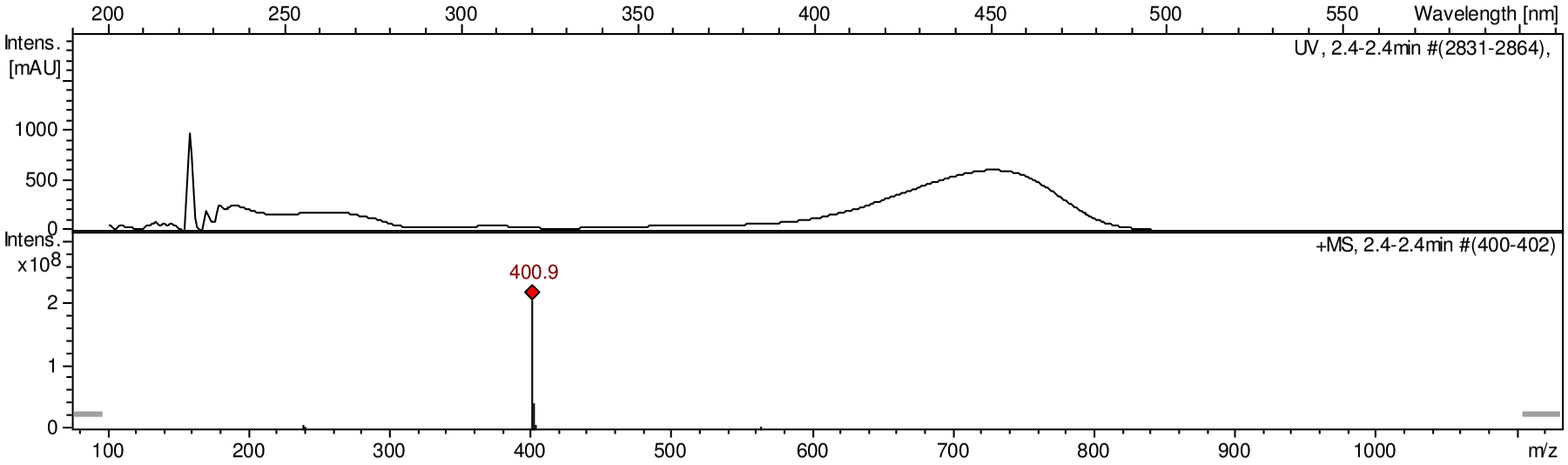
200
250
300
350
400
450
500
550
Wavelength [nm]
Intens.
[mAU]
1000
500
0
UV, 2.4-2.4min #(2831-2864),
Intens.
x10^8
2
1
0
+MS, 2.4-2.4min #(400-402)
400.9
100
200
300
400
500
600
700
800
900
1000
m/z

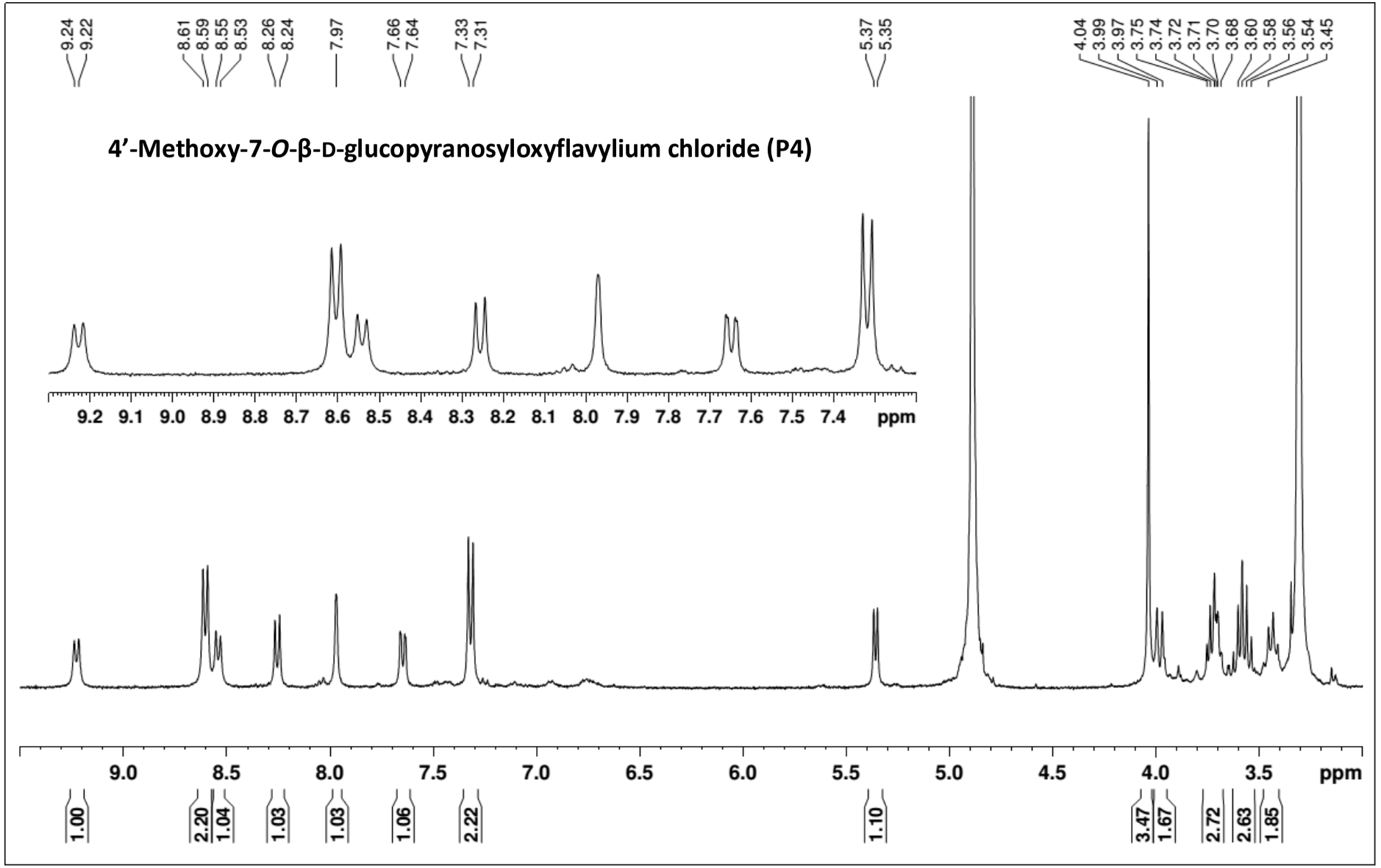
9.24
9.22
8.61
8.59
8.55
8.53
8.26
8.24
7.97
7.66
7.64
7.33
7.31
5.37
5.35
4.04
3.99
3.97
3.75
3.74
3.72
3.71
3.70
3.68
3.60
3.58
3.56
3.54
3.45
4'-Methoxy-7-O-β-D-glucopyranosyloxyflavylium chloride (P4)
9.2 9.1 9.0 8.9 8.8 8.7 8.6 8.5 8.4 8.3 8.2 8.1 8.0 7.9 7.8 7.7 7.6 7.5 7.4 ppm
9.0 8.5 8.0 7.5 7.0 6.5 6.0 5.5 5.0 4.5 4.0 3.5 ppm
1.00
2.20
1.04
1.03
1.03
1.06
2.22
1.10
3.47
1.67
2.72
2.63
1.85

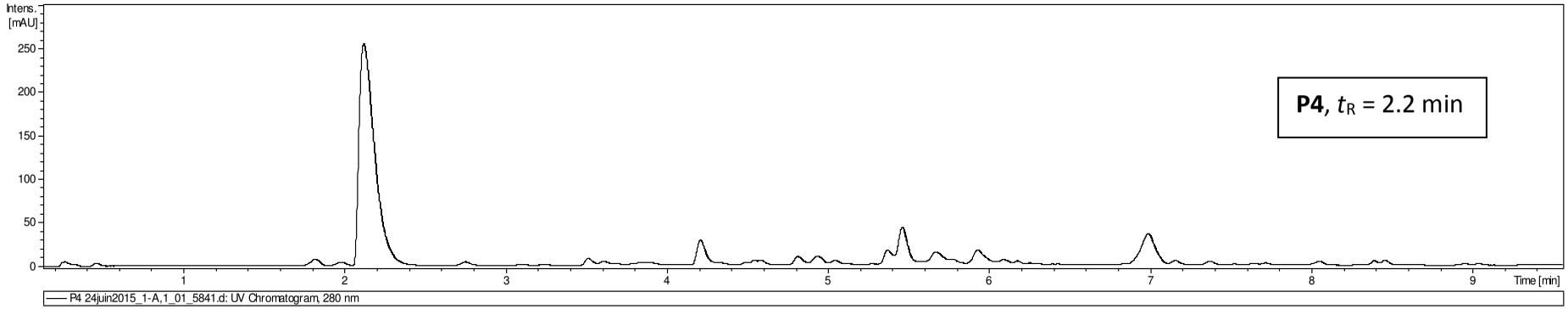
Intens.
[mAU]
250
200
150
100
50
0
1
2
3
4
5
6
7
8
9
Time [min]
P4, t_R = 2.2 min
P4 24juin2015_1-A,1_01_5841.d: UV Chromatogram, 280 nm

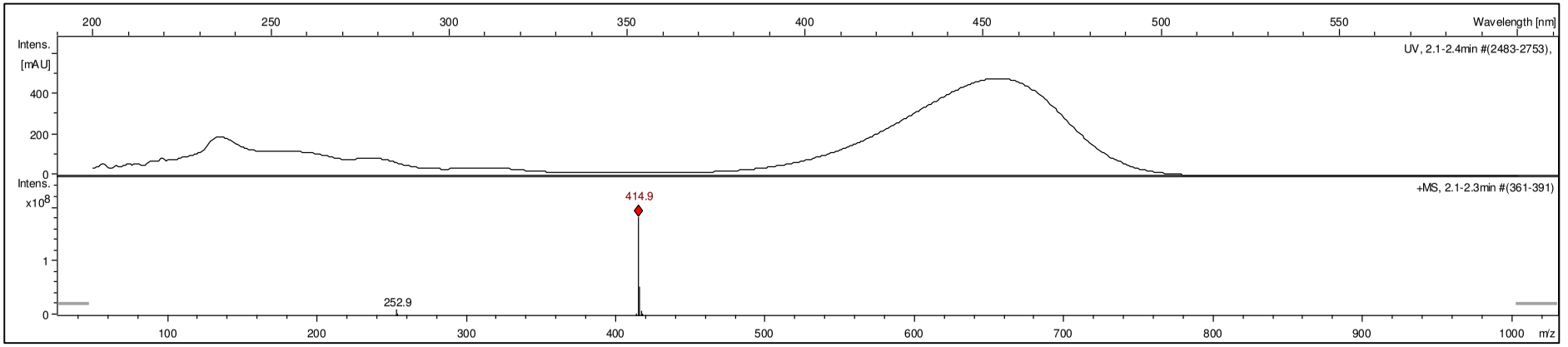
200
250
300
350
400
450
500
550
Wavelength [nm]
Intens.
[mAU]
400
200
0
UV, 2.1-2.4min #(2483-2753),
Intens.
x10^8
1
0
414.9
252.9
+MS, 2.1-2.3min #(361-391)
100
200
300
400
500
600
700
800
900
1000
m/z

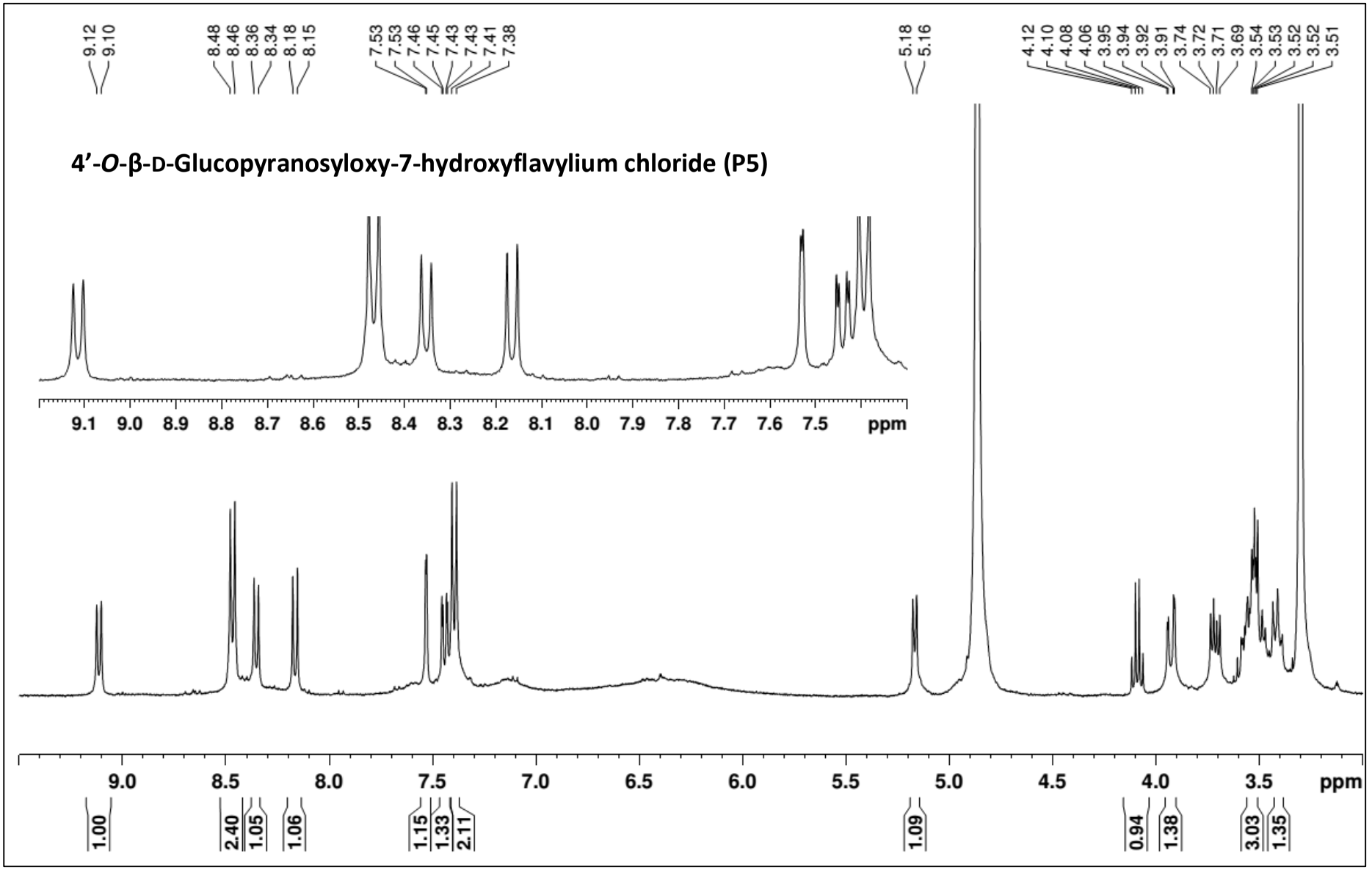
9.12
9.10
8.48
8.46
8.36
8.34
8.18
8.15
7.53
7.53
7.46
7.45
7.43
7.43
7.41
7.38
5.18
5.16
4.12
4.10
4.08
4.06
3.95
3.94
3.92
3.91
3.74
3.72
3.71
3.69
3.54
3.53
3.52
3.52
3.51
4'-O-β-D-Glucopyranosyloxy-7-hydroxyflavylium chloride (P5)
9.1 9.0 8.9 8.8 8.7 8.6 8.5 8.4 8.3 8.2 8.1 8.0 7.9 7.8 7.7 7.6 7.5 ppm
9.0 8.5 8.0 7.5 7.0 6.5 6.0 5.5 5.0 4.5 4.0 3.5 ppm
1.00
2.40
1.05
1.06
1.15
1.33
2.11
1.09
0.94
1.38
3.03
1.35

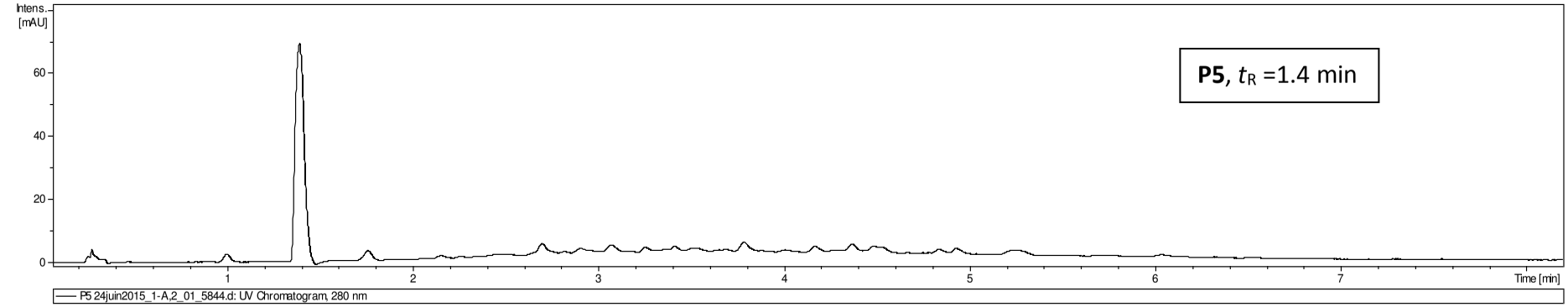
Intens.
[mAU]
60
40
20
0
1
2
3
4
5
6
7
Time [min]
P5 24juin2015_1-A,2_01_5844.d: UV Chromatogram, 280 nm

P5, t_R =1.4 min

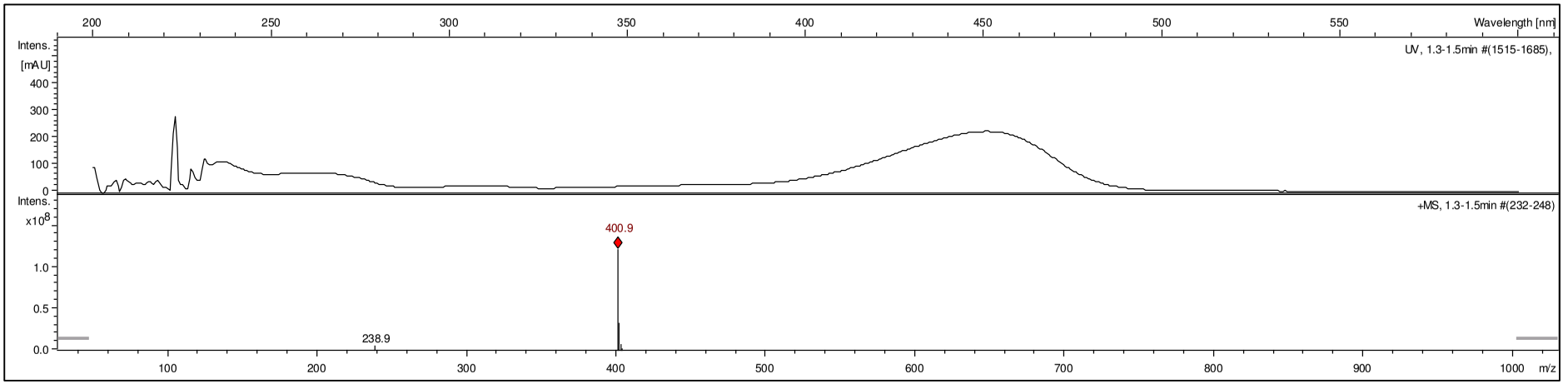
200
250
300
350
400
450
500
550
Wavelength [nm]
Intens.
[mAU]
400
300
200
100
0
UV, 1.3-1.5min #(1515-1685),
Intens.
x10^8
1.0
0.5
0.0
400.9
238.9
+MS, 1.3-1.5min #(232-248)
100
200
300
400
500
600
700
800
900
1000
m/z

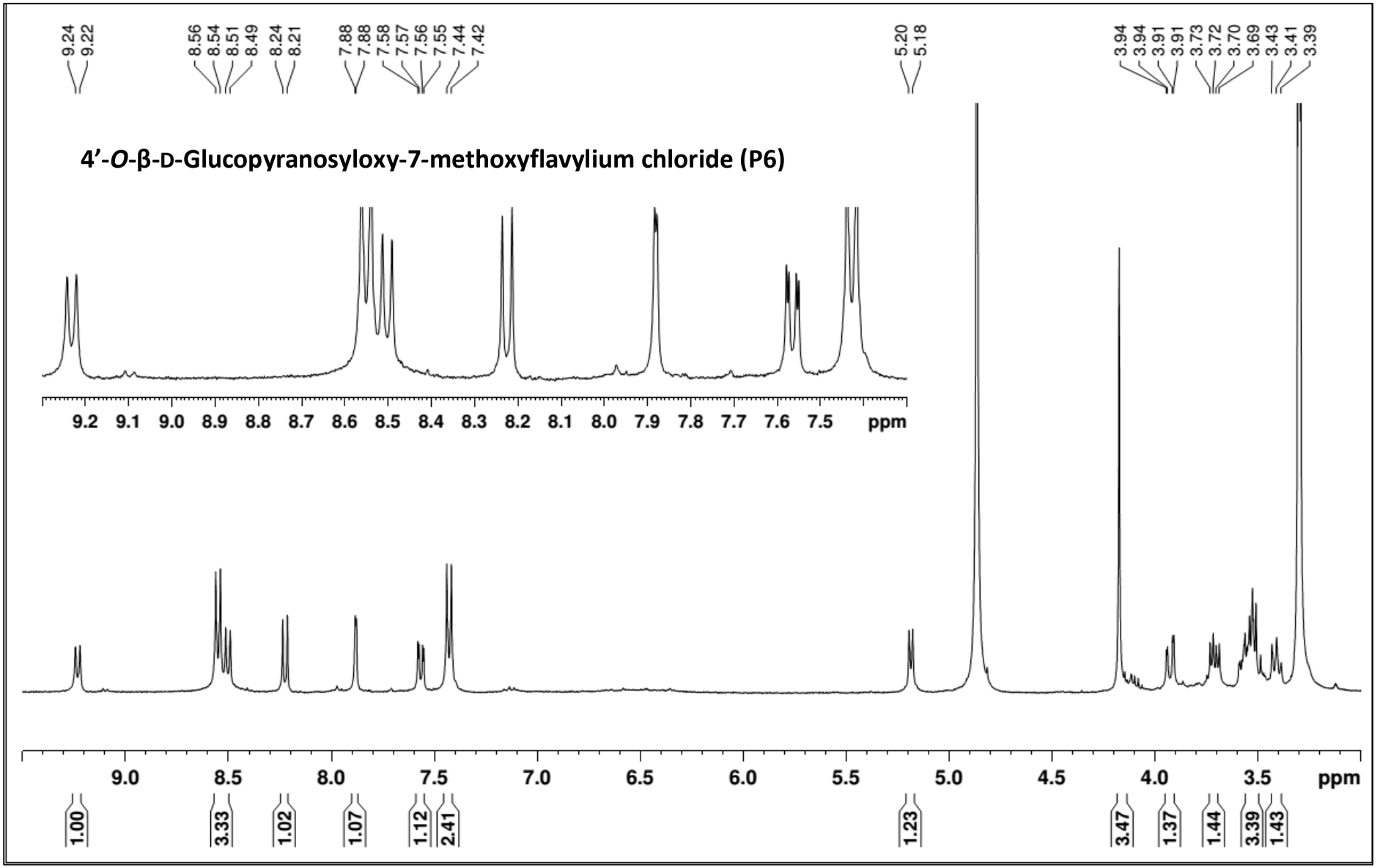
9.24
9.22
8.56
8.54
8.51
8.49
8.24
8.21
7.88
7.88
7.58
7.57
7.56
7.55
7.44
7.42
5.20
5.18
3.94
3.94
3.91
3.91
3.73
3.72
3.70
3.69
3.43
3.41
3.39
4'-O-β-D-Glucopyranosyloxy-7-methoxyflavylium chloride (P6)
9.2 9.1 9.0 8.9 8.8 8.7 8.6 8.5 8.4 8.3 8.2 8.1 8.0 7.9 7.8 7.7 7.6 7.5 ppm
9.0 8.5 8.0 7.5 7.0 6.5 6.0 5.5 5.0 4.5 4.0 3.5 ppm
1.00
3.33
1.02
1.07
1.12
2.41
1.23
3.47
1.37
1.44
3.39
1.43

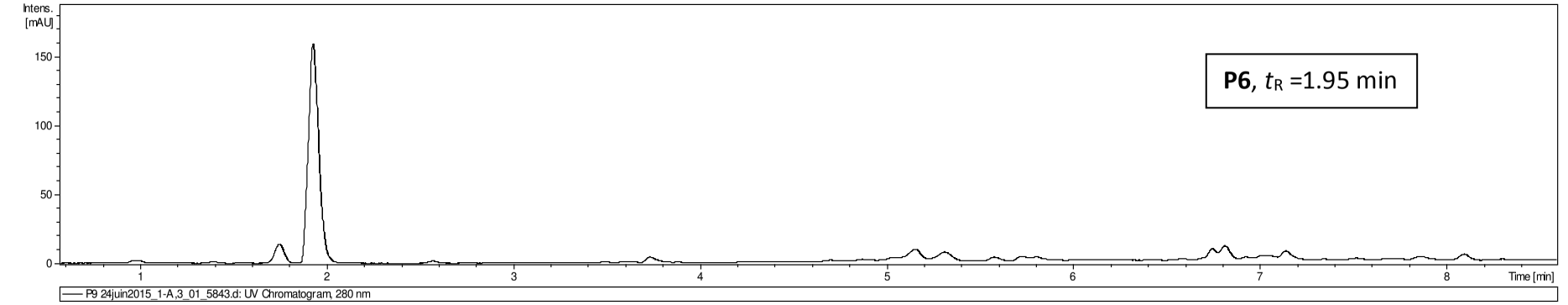
Intens.
[mAU]
150
100
50
0
1
2
3
4
5
6
7
8
Time [min]
P9 24juin2015_1-A,3_01_5843.d: UV Chromatogram, 280 nm
P6, t_R =1.95 min

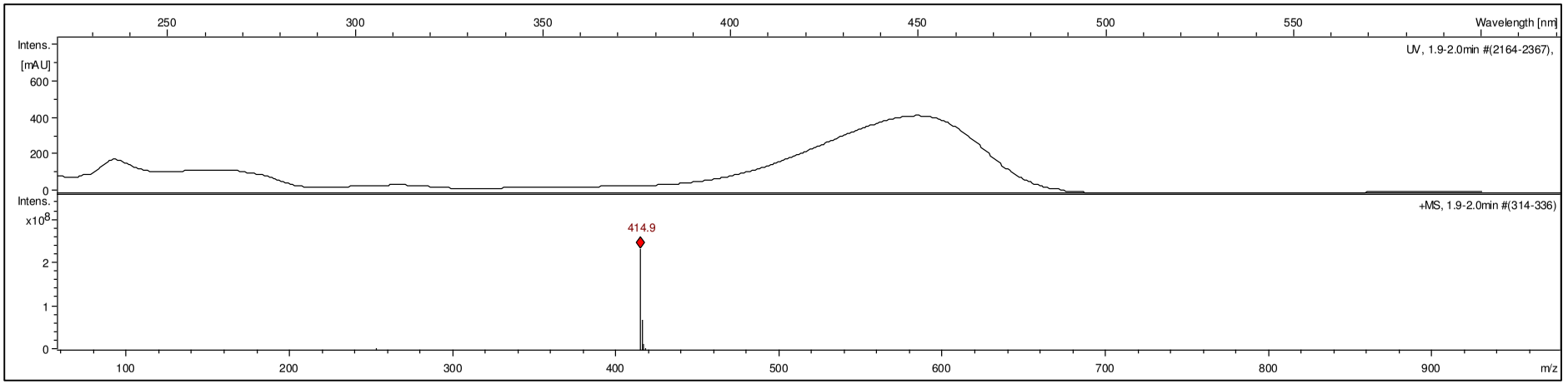
250
300
350
400
450
500
550
Wavelength [nm]
Intens.
[mAU]
600
400
200
0
UV, 1.9-2.0min #(2164-2367),
Intens.
x10^8
2
1
0
414.9
+MS, 1.9-2.0min #(314-336)
100
200
300
400
500
600
700
800
900
m/z

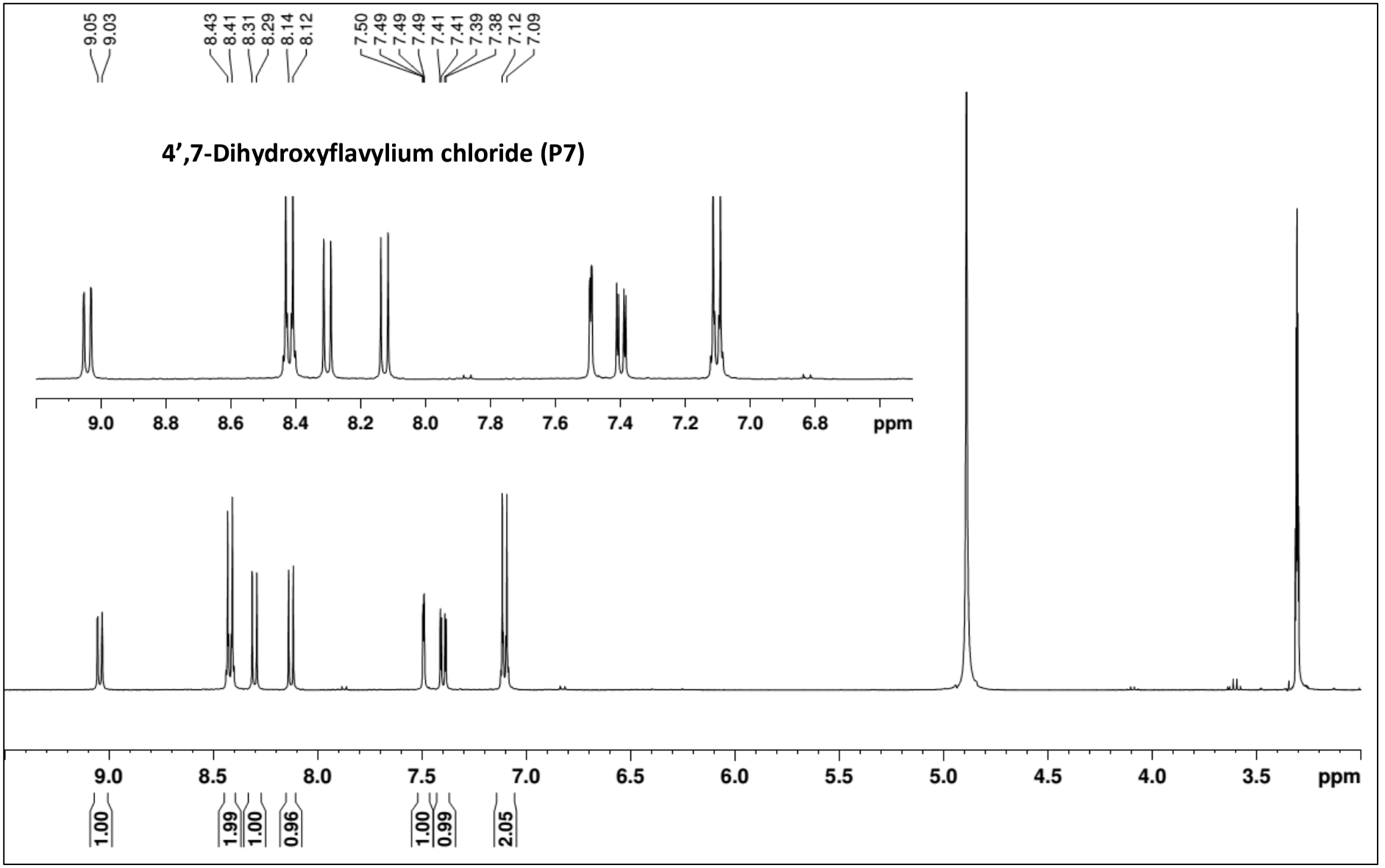
9.05
9.03
8.43
8.41
8.31
8.29
8.14
8.12
7.50
7.49
7.49
7.49
7.41
7.41
7.39
7.38
7.12
7.09
4’,7-Dihydroxyflavylium chloride (P7)
9.0
8.8
8.6
8.4
8.2
8.0
7.8
7.6
7.4
7.2
7.0
6.8
ppm
9.0
8.5
8.0
7.5
7.0
6.5
6.0
5.5
5.0
4.5
4.0
3.5
ppm
1.00
1.99
1.00
0.96
1.00
0.99
2.05

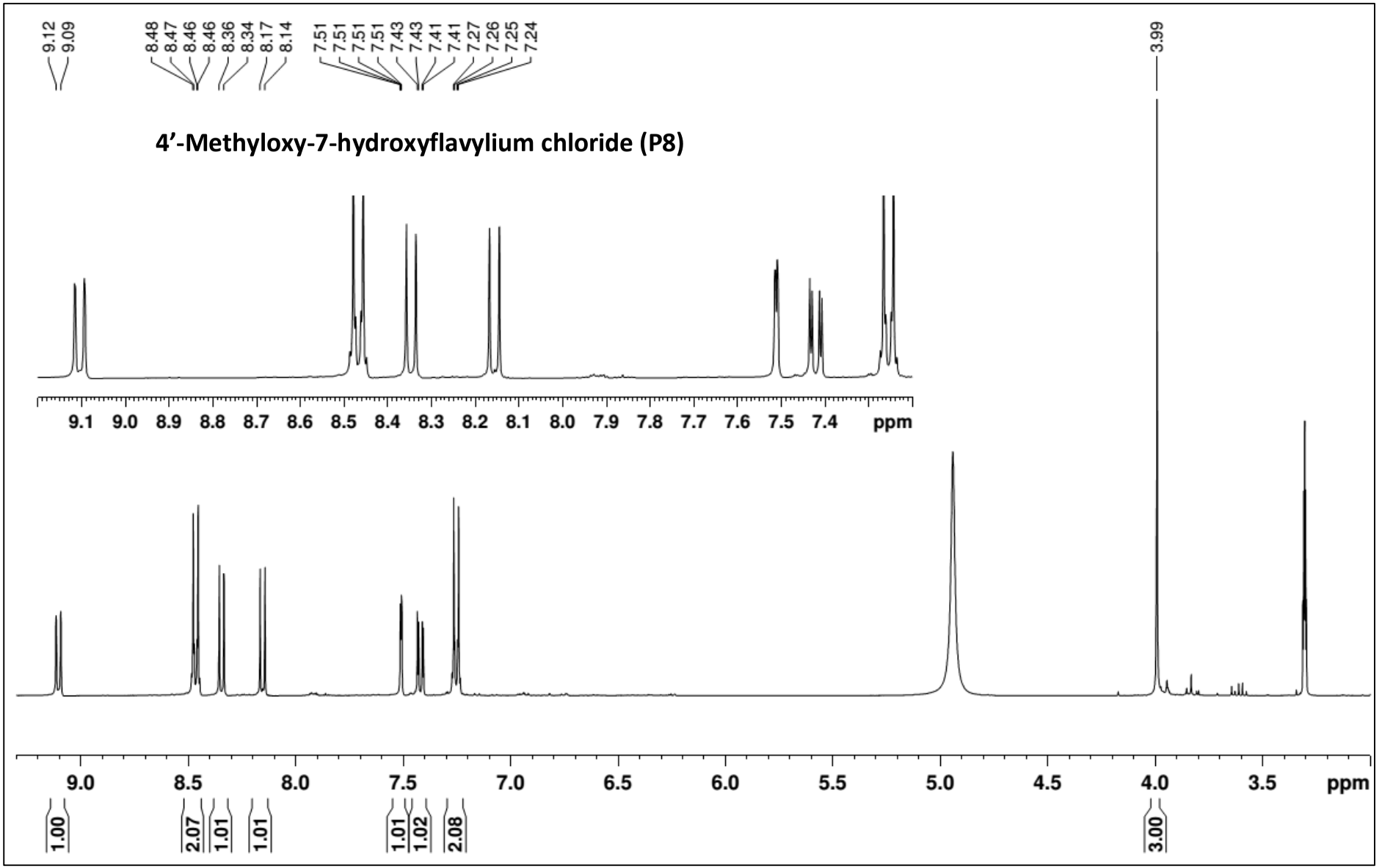
9.12
9.09
8.48
8.47
8.46
8.46
8.36
8.34
8.17
8.14
7.51
7.51
7.51
7.51
7.43
7.43
7.41
7.41
7.27
7.26
7.25
7.24
3.99
4’-Methyloxy-7-hydroxyflavylium chloride (P8)
9.1 9.0 8.9 8.8 8.7 8.6 8.5 8.4 8.3 8.2 8.1 8.0 7.9 7.8 7.7 7.6 7.5 7.4 ppm
9.0 8.5 8.0 7.5 7.0 6.5 6.0 5.5 5.0 4.5 4.0 3.5 ppm
1.00
2.07
1.01
1.01
1.01
1.02
2.08
3.00

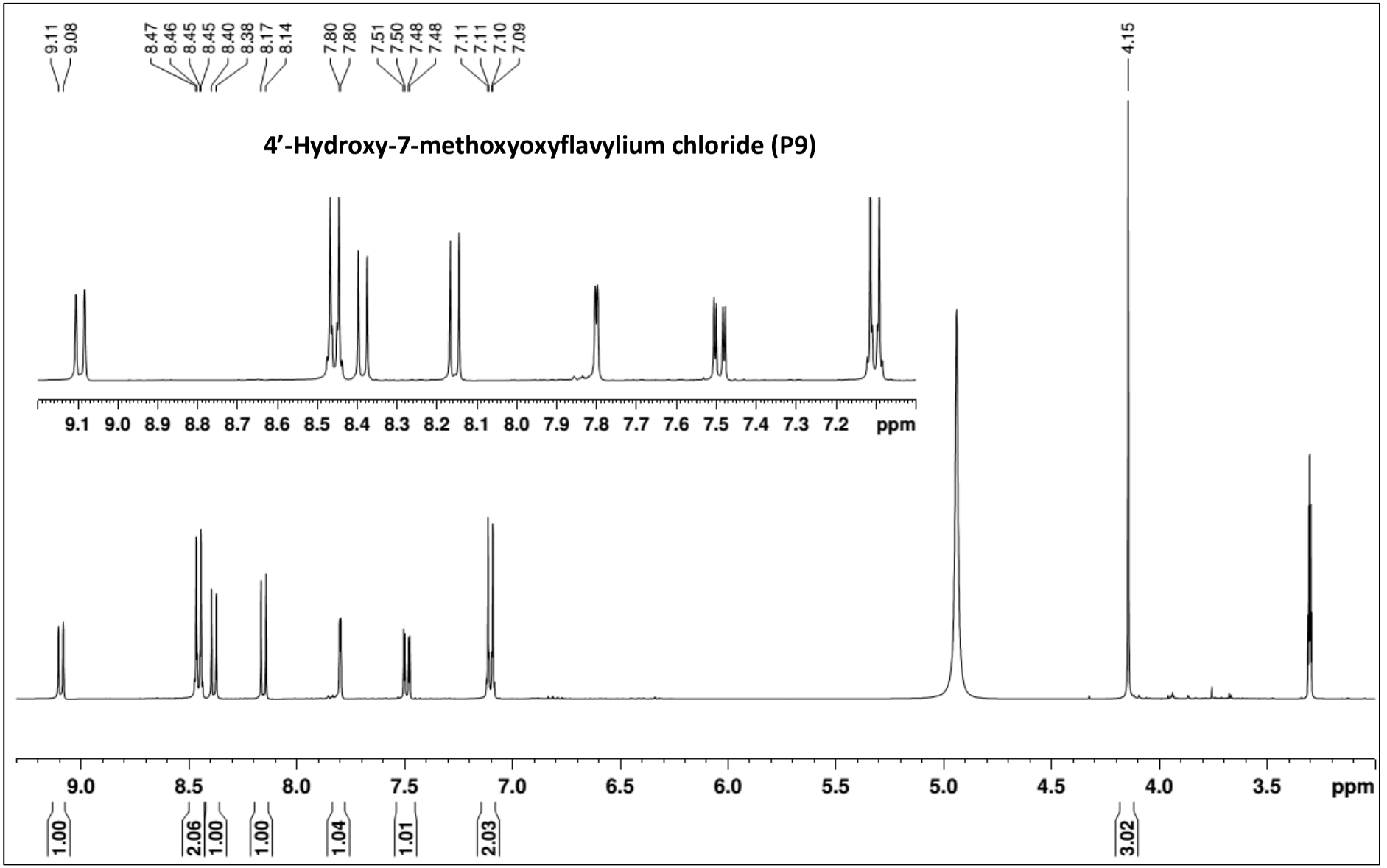
9.11
9.08
8.47
8.46
8.45
8.45
8.40
8.38
8.17
8.14
7.80
7.80
7.51
7.50
7.48
7.48
7.11
7.11
7.10
7.09
4.15
4’-Hydroxy-7-methoxyoxyflavylium chloride (P9)
9.1 9.0 8.9 8.8 8.7 8.6 8.5 8.4 8.3 8.2 8.1 8.0 7.9 7.8 7.7 7.6 7.5 7.4 7.3 7.2 ppm
9.0 8.5 8.0 7.5 7.0 6.5 6.0 5.5 5.0 4.5 4.0 3.5 ppm
1.00
2.06
1.00
1.00
1.04
1.01
2.03
3.02

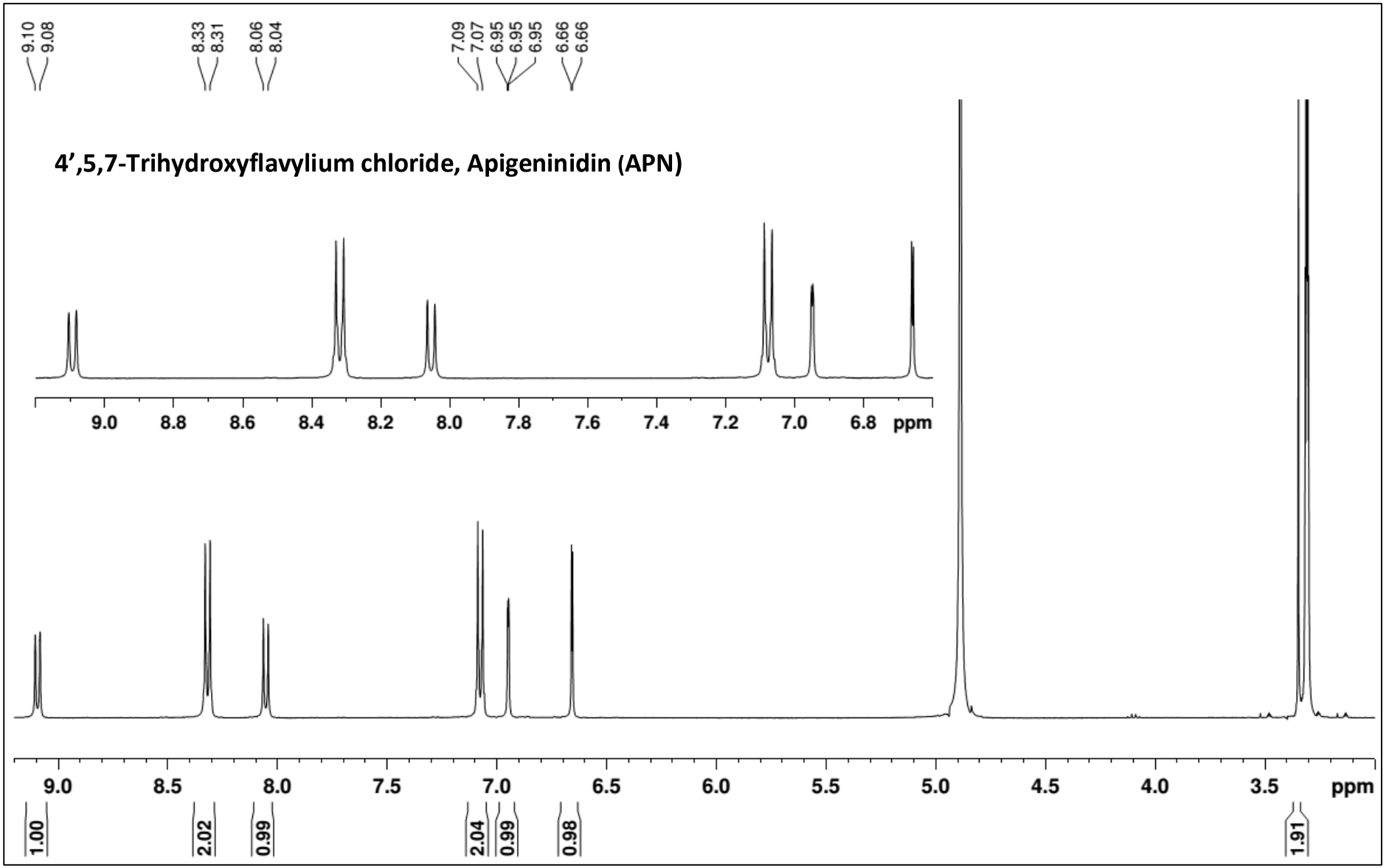
9.10
9.08
8.33
8.31
8.06
8.04
7.09
7.07
6.95
6.95
6.95
6.66
6.66
4’,5,7-Trihydroxyflavylium chloride, Apigeninidin (APN)
9.0
8.8
8.6
8.4
8.2
8.0
7.8
7.6
7.4
7.2
7.0
6.8
ppm
9.0
8.5
8.0
7.5
7.0
6.5
6.0
5.5
5.0
4.5
4.0
3.5
ppm
1.00
2.02
0.99
2.04
0.99
0.98
1.91

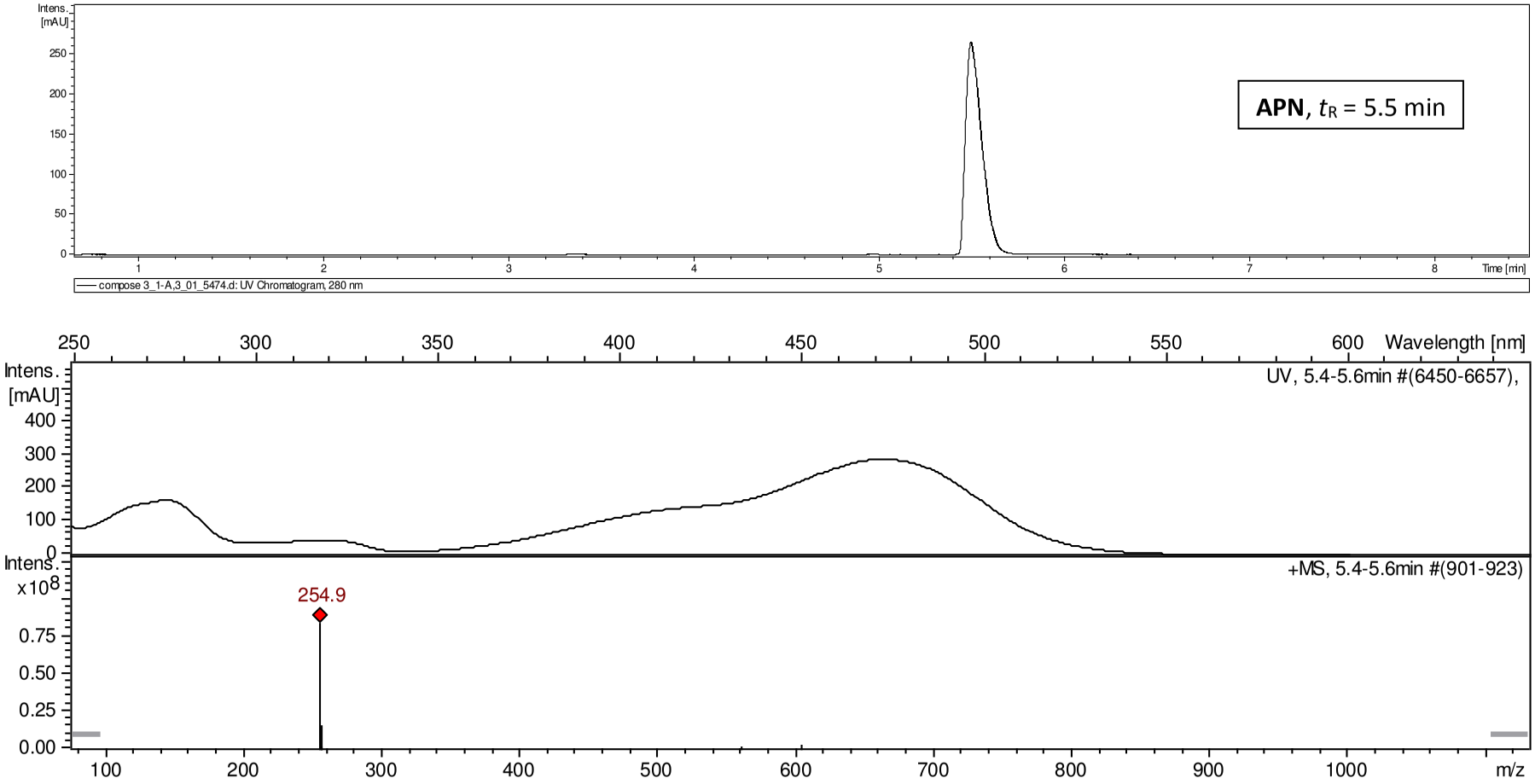
Intens.
[mAU]
250
200
150
100
50
0
1
2
3
4
5
6
7
8
Time [min]
APN, t_R = 5.5 min
compose 3_1-A,3_01_5474.d: UV Chromatogram, 280 nm
250
300
350
400
450
500
550
600
Wavelength [nm]
Intens.
[mAU]
400
300
200
100
0
UV, 5.4-5.6min #(6450-6657),
Intens.
x10^8
0.75
0.50
0.25
0.00
254.9
+MS, 5.4-5.6min #(901-923)
100
200
300
400
500
600
700
800
900
1000
m/z

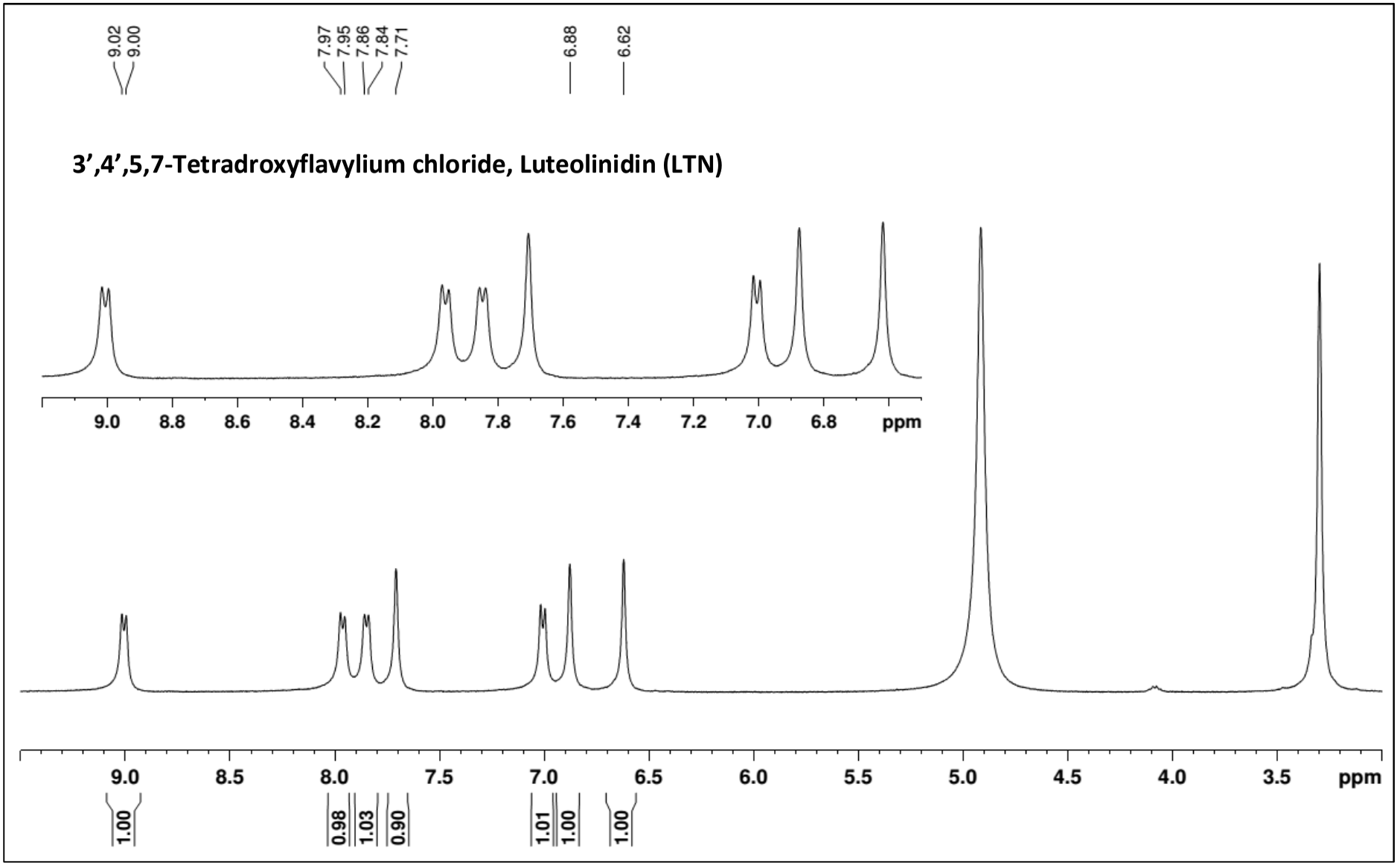
9.02
9.00
7.97
7.95
7.86
7.84
7.71
6.88
6.62
3',4',5,7-Tetradroxyflavylium chloride, Luteolinidin (LTN)
9.0
8.8
8.6
8.4
8.2
8.0
7.8
7.6
7.4
7.2
7.0
6.8
ppm
9.0
8.5
8.0
7.5
7.0
6.5
6.0
5.5
5.0
4.5
4.0
3.5
ppm
1.00
0.98
1.03
0.90
1.01
1.00
1.00

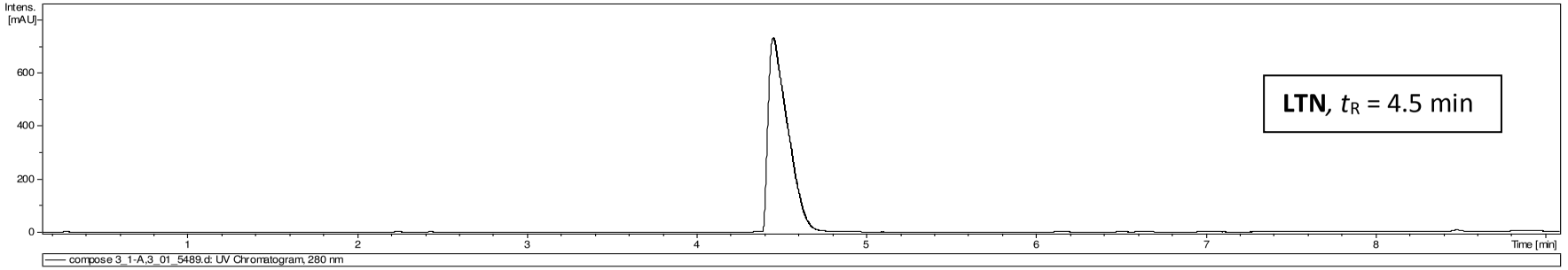
Intens.
[mAU]
600
400
200
0
1
2
3
4
5
6
7
8
Time [min]
compose 3_1-A,3_01_5489.d: UV Chromatogram, 280 nm
LTN, t_R = 4.5 min

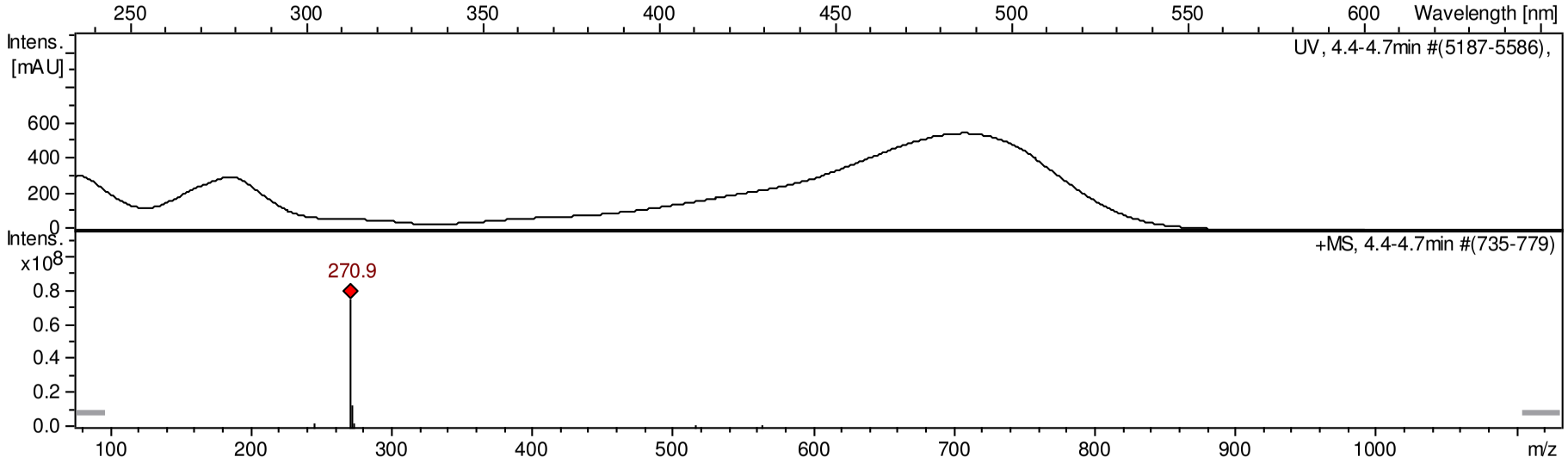
250
300
350
400
450
500
550
600
Wavelength [nm]
Intens.
[mAU]
UV, 4.4-4.7min #(5187-5586),
600
400
200
0
Intens.
x10^8
+MS, 4.4-4.7min #(735-779)
270.9
0.8
0.6
0.4
0.2
0.0
100
200
300
400
500
600
700
800
900
1000
m/z

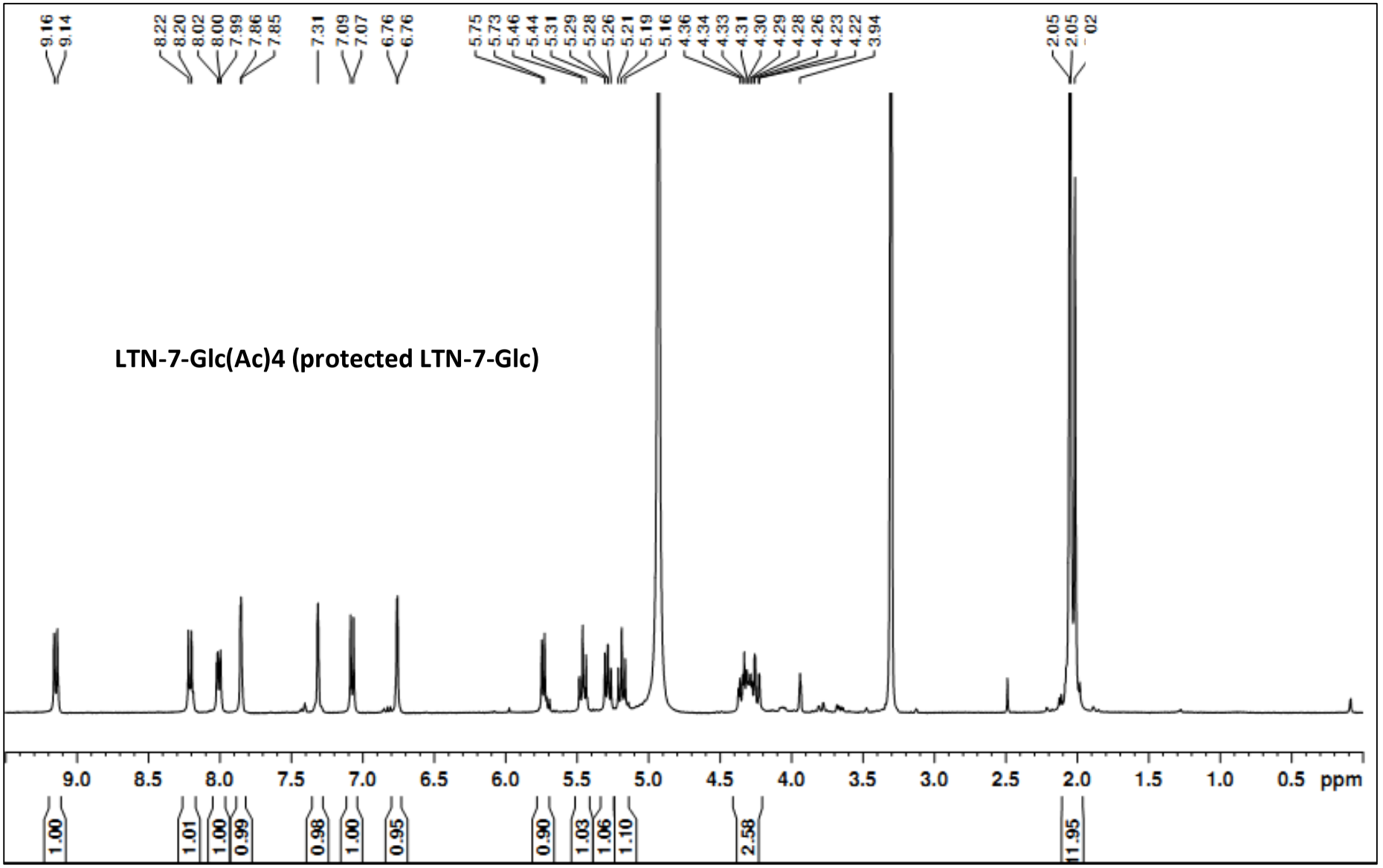
9.16
9.14
8.22
8.20
8.02
8.00
7.99
7.86
7.85
7.31
7.09
7.07
6.76
6.76
5.75
5.73
5.46
5.44
5.31
5.29
5.28
5.26
5.21
5.19
5.16
4.36
4.34
4.33
4.31
4.30
4.29
4.28
4.26
4.23
4.22
3.94
2.05
2.05
LTN-7-Glc(Ac)4 (protected LTN-7-Glc)
9.0
8.5
8.0
7.5
7.0
6.5
6.0
5.5
5.0
4.5
4.0
3.5
3.0
2.5
2.0
1.5
1.0
0.5
ppm
1.00
1.01
1.00
0.99
0.98
1.00
0.95
0.90
1.03
1.06
1.10
2.58
11.95

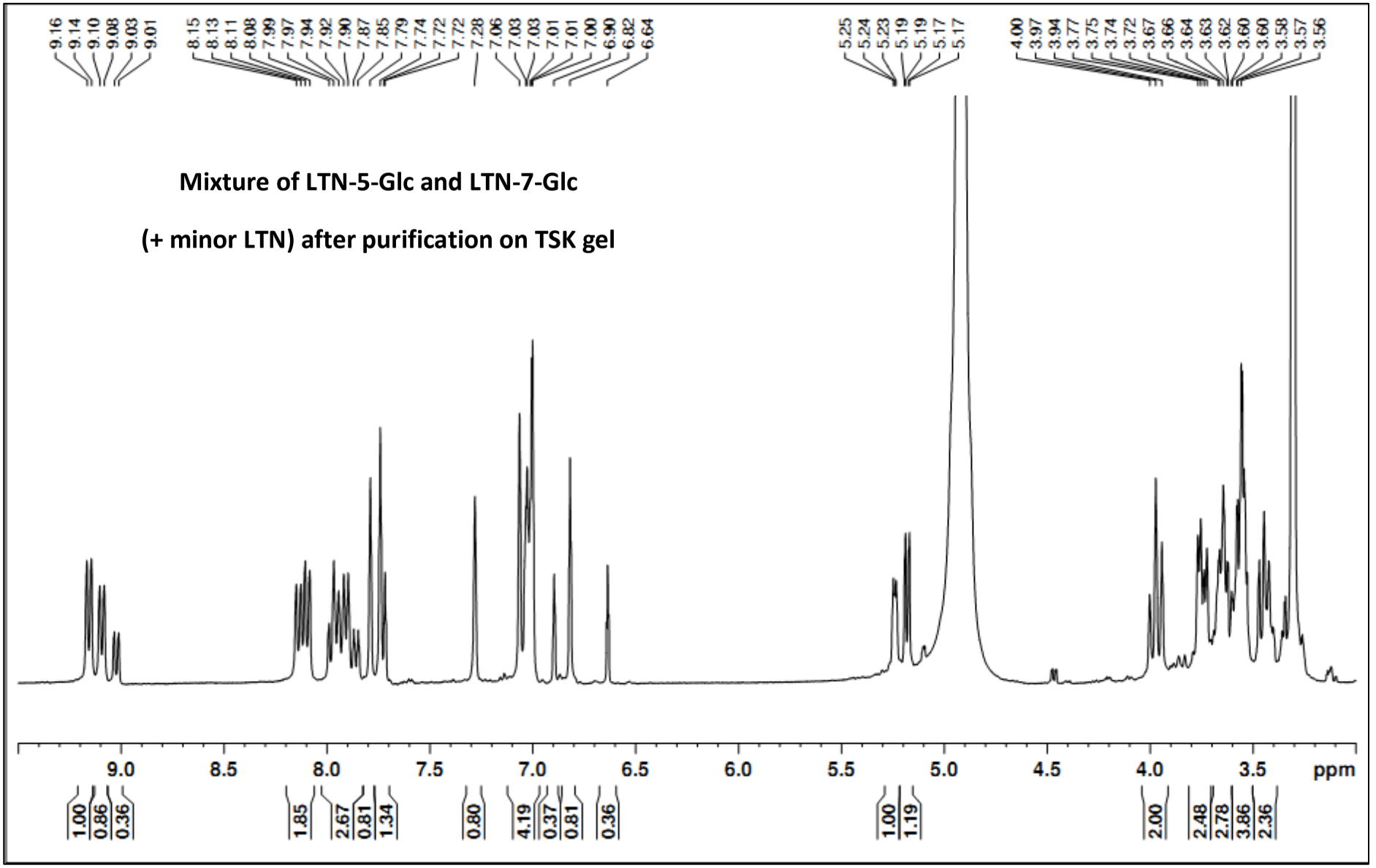
9.16
9.14
9.10
9.08
9.03
9.01
8.15
8.13
8.11
8.08
7.99
7.97
7.94
7.92
7.90
7.87
7.85
7.79
7.74
7.72
7.72
7.28
7.06
7.03
7.03
7.01
7.01
7.00
6.90
6.82
6.64
5.25
5.24
5.23
5.19
5.19
5.17
5.17
4.00
3.97
3.94
3.77
3.75
3.74
3.72
3.67
3.66
3.64
3.63
3.62
3.60
3.60
3.58
3.57
3.56
Mixture of LTN-5-Glc and LTN-7-Glc
(+ minor LTN) after purification on TSK gel
9.0
8.5
8.0
7.5
7.0
6.5
6.0
5.5
5.0
4.5
4.0
3.5
ppm
1.00
0.86
0.36
1.85
2.67
0.81
1.34
0.80
4.19
0.37
0.81
0.36
1.00
1.19
2.00
2.48
2.78
3.86
2.36

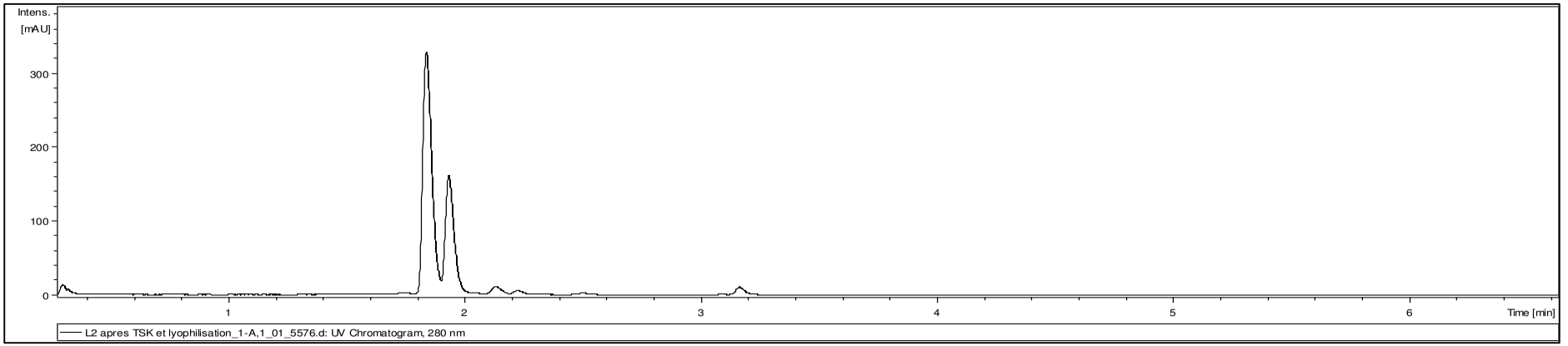
Intens.
[mAU]
300
200
100
0
1
2
3
4
5
6
Time [min]
L2 apres TSK et lyophilisation_1-A,1_01_5576.d: UV Chromatogram, 280 nm

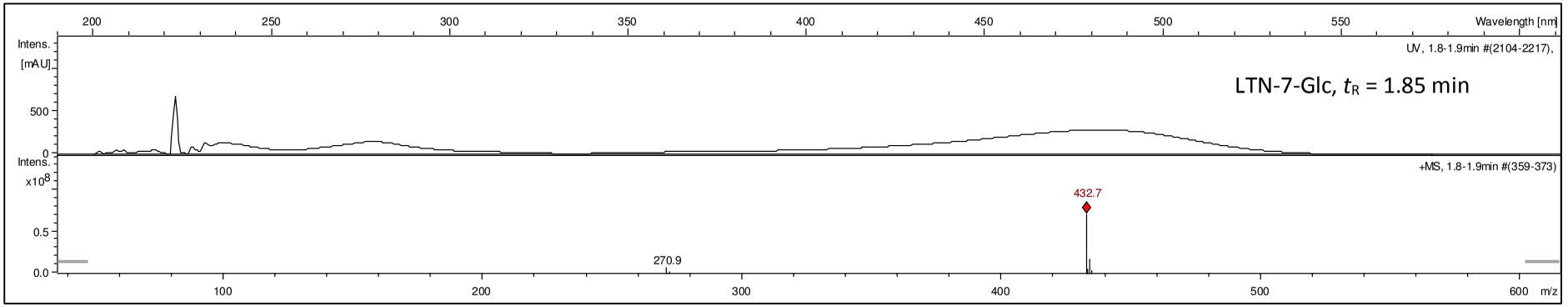
200
250
300
350
400
450
500
550
Wavelength [nm]
Intens.
[mAU]
UV, 1.8-1.9min #(2104-2217),
LTN-7-Glc, t_R = 1.85 min
500
0
Intens.
x10^8
+MS, 1.8-1.9min #(359-373)
432.7
0.5
270.9
0.0
100
200
300
400
500
600
m/z

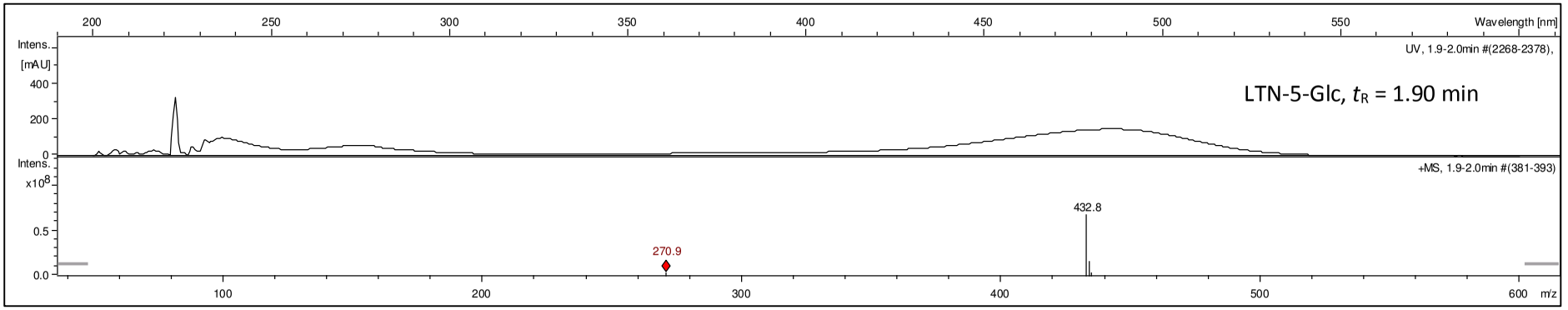
200
250
300
350
400
450
500
550
Wavelength [nm]
Intens.
[mAU]
UV, 1.9-2.0min #(2268-2378),
LTN-5-Glc, t_R = 1.90 min
400
200
0
Intens.
x10^8
+MS, 1.9-2.0min #(381-393)
432.8
0.5
270.9
0.0
100
200
300
400
500
600
m/z

Appendix III

Physicochemical properties of synthesized Luteolinidin

Introduction

Luteolinidin (**LTN**), the main 3-deoxyanthocyanidin identified in red and black sorghum [1], has a particular interest: it is a relatively stable aglycone in aqueous solution contrary to common anthocyanidins. In addition to its coloring properties, **LTN** can express a potent antioxidant activity (due to its catechol B-ring) and thus a beneficial role in food oxidative stability and human health. Successful luteolinidin synthesis is described in article 3 and its physicochemical properties as well as its antioxidant activity will be studied in this complementary work.

Materials and methods

The same as for the investigation of **P1** and **P2**, except for some modifications specified in the text.

Proton transfer and hydration reactions

The structural transformation of **LTN** in aqueous solution was studied using the same method of pH variation as described in our previous work [2]. However, its additional OH group at C5 (in comparison with **P1**) markedly lowers its water-solubility, possibly by favoring hydrogen bonding in the solid state. Thus, experiments were carried out in the presence of the non-ionic surfactant Brij®35 (4 mM). Thermodynamic constants were reevaluated for **P1** in the same conditions for comparison.

When the pH is increased from 2 to 6, flavylium ions (AH^+) are typically converted into neutral quinonoid bases by proton transfer (thermodynamic constant K_a) and into a mixture of colorless forms by water addition at C2 (overall thermodynamic constant K'_h). The typical UV-visible spectra of AH^+, A and C_E are shown in Figure 1.

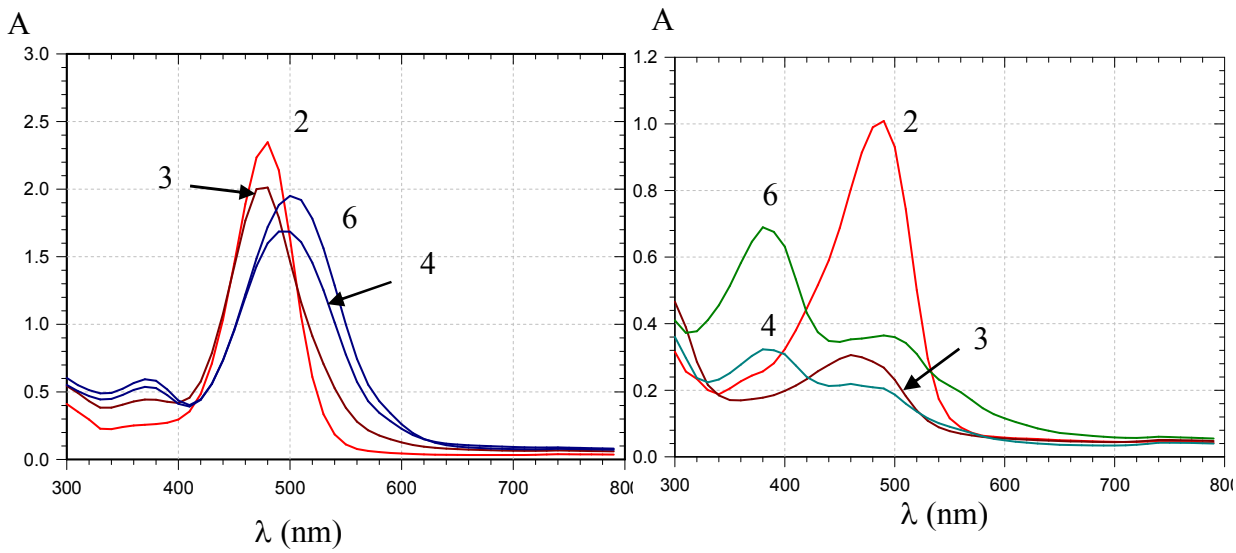

Figure 1. pH-Dependence of the UV-visible spectra of **LTN**. *Left*: Spectral measurements immediately after addition of pigment to buffer (pH 2.0, pH 3.0, pH 4, pH 6.0). *Right*: Spectral measurements on solutions equilibrated overnight (pH 2.0, pH 3.0, pH 4.0, pH 6.0).

As shown in (Table 1) **LTN** is slightly more acidic than **P1** (lower pK_a value). This is explained by the contribution of an additional quinonoid base (5-keto tautomer), which is absent in the case of **P1** (see Figure 2). However, the additional OH group of **LTN** has no impact on the overall thermodynamics of water addition. The latter suggest that it does not modify the partial positive charge at C2. Nevertheless, comparing **P1** data in the absence [2] or presence of Brij®35 shows that pK_a value is unchanged while pK'_h is lower in the presence of Brij®35. Therefore, the colorless forms (essentially, the *trans*-chalcone here) have a higher affinity for the Brij®35 micelles than the colored forms, thus making water addition thermodynamically more favorable.

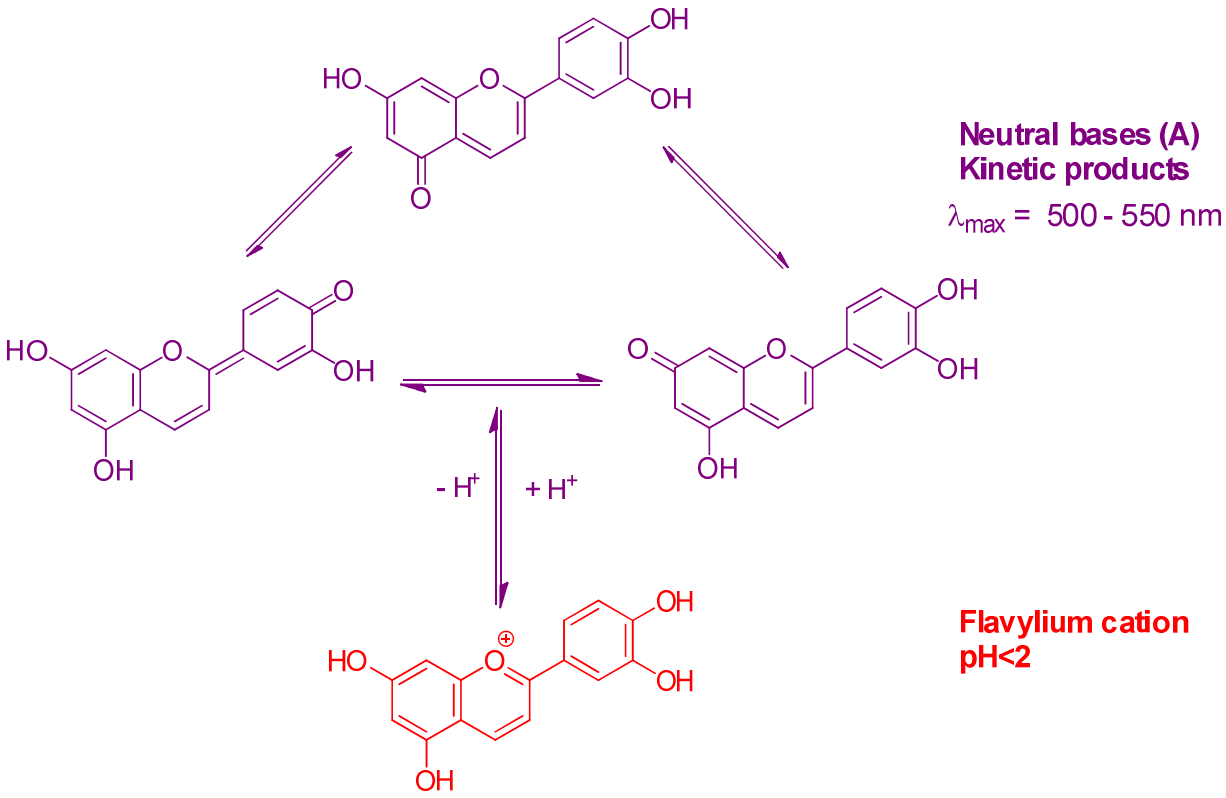

Figure 2. The different quinonoid tautomers obtained by proton loss from LTN

Table 1. Thermodynamic constants of **LTN** and **P1** measured in the presence of 4 Mm Brij®35.

	pK_a	A_0, r_A, r	pK'_h	A_0, r
LTN	3.97 ± 0.07	0.07, 5.59 ± 0.58[a)], 0.994	2.65 ± 0.15	1.5, 0.962
P1	4.43 ± 0.08	0.04, 8.86 ± 1.26[a)], 0.993	2.63 ± 0.08	1.3, 0.988

[a)] $r_A = \varepsilon_A/\varepsilon_{AH}$ (ratio of the molar absorption coefficients of quinonoid bases and flavylium ion).

Iron binding

Regarding the poor solubility of **LTN**, experiments for iron binding investigation can't be realized as described in article 2. Moreover, enhancing **LTN** solubility by adding Brij®35 as we did in the precedent experiment is not possible here as Brij®35 in large excess competes with **LTN** for metal ions and no evidence of iron – **LTN** complexes could be gained. A brief study was carried out with Fe^{III} and Fe^{II} in a mixture of acetate buffer / MeOH (3:1) at a final pH of 4. The successive addition of **LTN** and Fe^{III} (5 equiv.) to the precedent buffer solution results in a fast decay of A (485 nm) and a fast development of a broad visible band in the range 450–750 nm with an absorption maximum at *ca*. 550 nm. The corresponding UV-visible spectrum evidenced the same band of charge transfer to Fe^{III} registered in the case of **P1**-Fe^{III} binding (Figure 3).

In the same conditions, a slower **LTN** binding of Fe^{II} (5 equiv.) was registered with the same charge transfer band and a simultaneous slow chalcone formation. As shown in Table 2, lower values of binding constants were obtained in **LTN** binding of both Fe^{III} and Fe^{II} comparing to those obtained with the model **P1** (P1-iron binding results are shown in article 2). In a general understanding, we proved that natural occurring pigments binds iron by its catechol ring via similar mechanisms of Fe - **P1** binding.

Table 2**.** Kinetic analysis of **LTN** binding of Fe^{III} and Fe^{II}. Simultaneous curve-fitting of the A (485 nm) and A (550 nm) *vs.* time curves according to a simple model assuming irreversible 1:1 binding (rate constant k_b) followed by first-order rearrangement of complex 1 into complex 2 in the case of Fe^{II} because of its later autoxidation (rate constant k_r), (acetate buffer/MeOH (3:1) final pH = 4.0, 25 °C, pigment concentration = 50 μM).

	M_t/L_t, λ / nm	**K_b / M^{-1} s^{-1}**	**10^3 k_r / s^{-1}**	**ε/ M^{-1} cm^{-1}**
LTN - Fe^{III}	5, 485 (r = 0.992) 550 (r = 0.992)	1170 (± 11)	-	7650 (± 5) 6300 (± 5)
LTN - Fe^{II}	5, 485 (r = 0.999) 550 (r =0.998)	440 (± 10)	7.9 (±0.5)	11750 (± 24) 4900 (± 12)

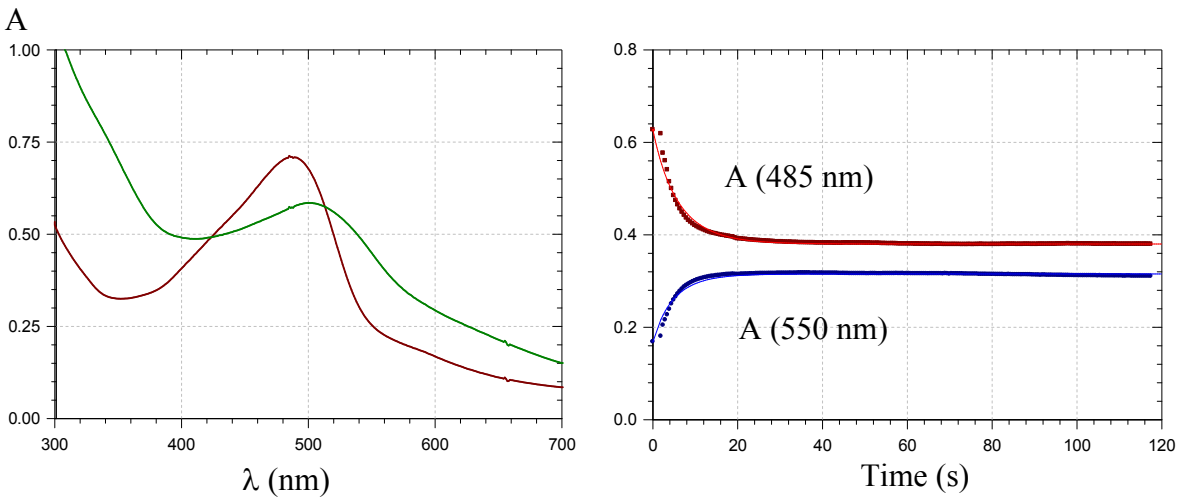

Figure 3. *Left*: UV-visible spectra of **LTN** (—) and the **LTN**-Fe^{III} complex (—) (*ca*. 30 s after addition of 5 equiv. Fe^{III}). *Right:* Time-dependence of the UV-visible absorbance of **LTN** and **LTN**-Fe^{III} complex in a final pH 4.0 [acetate buffer/MeOH (3:1)], 25 °C, Fe^{III} - **LTN** molar ratio = 5 (the solid lines are the result of exponential curve-fittings).

Scavenging of the DPPH radical

As all polyphenols with a catechol group, **LTN** is a potent electron or H-atom donor to radicals due to the relative stability of the **LTN** semiquinone formed. The capacity of **LTN** to scavenge the colored DPPH radical was investigated and analysed by the same method as for **P1** [2]. A fast decrease of the DPPH visible absorption band was observed followed by a slower one, in agreement with a fast transfer of the most labile H-atoms (B-ring OH groups) and a residual H-donating activity in the oxidation products thus formed [3].

As shown in Table 3, the kinetic analysis of the fast step permitted the estimation of the rate constant of first H-atom transfer (k_1) and the partial stoichiometry n (number of DPPH radicals reduced per pigment molecule during the fast step) [4]. From the total amplitude over the whole kinetics (fast + slow steps), the total stoichiometry n_{tot} (total number of DPPH radicals reduced per pigment molecule) was evaluated.

It is noteworthy that the kinetic analysis had to be conducted at 650 nm so as to avoid interference with the visible absorption of the pigment at the onset of the reaction.

As already evidenced [2], the catechol group was not sufficient to fully interpret the H-donating activity of 3-deoxanthocyanins. Indeed, with its additional C5-OH group, **LTN** transfers a first H-atom to DPPH *ca.* 4 times as rapidly as **P1**. Regarding precedent results, **LTN** is more acidic than **P1** in the same conditions (Brij®35 micelle solution). It can thus be assumed that in the mildly acidic conditions of the DPPH test (final pH = 4.4) the percentage of neutral base (more reducing than the flavylium ion) is higher with **LTN** than with **P1**, which favors the first H-atom transfer to DPPH. Alternatively, the total stoichiometry reflects the fate of the antioxidant during oxidative degradation. In particular, the **P1** *o*-quinone was shown to undergo water addition to the C- and A-rings with regeneration of catechol nuclei for further H-donation [5]. As n_{tot} values are different for **P1** and **LTN**, it may be assumed that the oxidation pathways of both pigments are not similar.

Table 3: DPPH-scavenging by **P1** and **LTN** in MeOH / pH 3.5 acetate buffer (1:1).

Pigment, conc. (µM)	k_1 **x10^{-3} (M^{-1} s^{-1})**[a)]	n[b)]
P1, 10	4.3(±0.1)	2.22(±0.01)
LTN, 10	14.3(±0.4)	3.06 (±0.03)
LTN, 10	13.8 (±0.2)	3.52 (±0.02)
LTN, 12.5	15.1(±0.4)	2.73 (±0.02)
LTN, 12.5	17.0(±0.4)	3.63 (±0.02)

[a)] Curve-fitting of A(650 nm)*vs*. time curves (see model [2]) over the 10 first seconds following LTN addition (40s for **P1**). Initial DPPH concentration = 0.1 x 10^{-3} M.

[b)] From the absorbance amplitude at 515 nm: total number of DPPH radicals reduced per pigment molecule n_{tot} = 4.0 (±0.2) for **P1**, 7.3 (±0.4) for **LTN** (means from triplicates).

HSA Binding

As mentioned in our previous work [6], human serum albumin (HSA) is a potential carrier for anthocyanins in the blood stream. Contrarily of common anthocyanidins, luteolinidin is a relative stable aglycone in neutral conditions and should thus be more resistant to chemical and enzymatic degradation along its transfer from food to the blood circulation. Although this point remains undocumented, it can thus be speculated that **LTN** may be present in higher concentration in plasma.

In neutral conditions, **LTN** must be a mixture of neutral and anionic bases. This distribution could be affected by binding to HSA as the typical binding site of flavonoids (sub-domain IIA, [7]) is a hydrophobic pocket lined by positively charged amino acid residues (Arg, Lys).

To distinguish between the colored forms and the *trans*-chalcone, **LTN** - HSA binding was studied with or without a preliminary overnight incubation of **LTN** in the neutral buffer (leading to the conversion of most colored forms into the *trans*-chalcone).

Part of the HSA fluorescence quenching by the ligand can be ascribed to the absorption of the ligand at the excitation and emission wavelengths. This inner filter effect was corrected.

As already observed with **P1** and **P2**, the linear *trans*-chalcone has more affinity for HSA than the corresponding colored forms. Compared with **P1**, the additional OH group at C5 destabilizes both **LTN** – HSA complexes (Figure 4, Table 4).

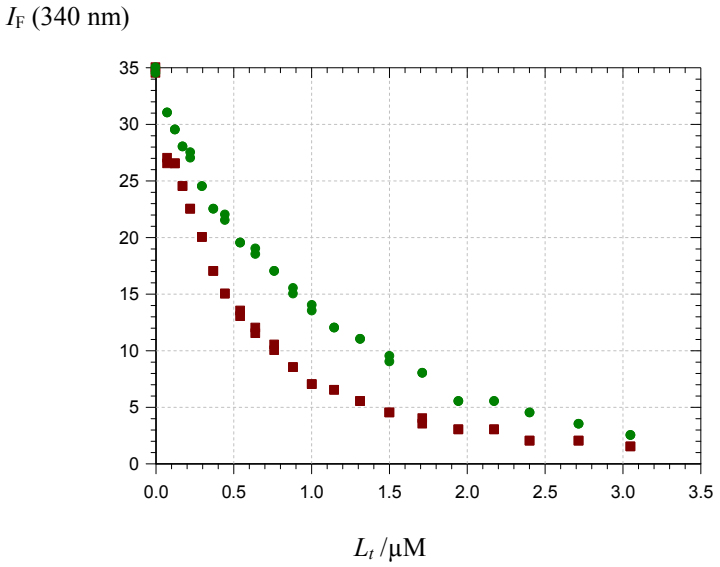

Figure 4. Quenching of the HSA fluorescence by the **LTN** quinonoid bases (■) and *trans*-chalcone (●). HSA concentration = 2 µM, pH 7.4 phosphate buffer, 37°C, excitation at 295 nm.

Table 4. Binding constant (K_b) of pigments and their *trans*-chalcones to HSA (2µM) in a pH 7.4 phosphate buffer at 25°C(*n*=2).

	$10^3 K_b/M^{-1}$	$10^6 f_p/M^{-1}$	$\varepsilon_L/M^{-1}cm^{-1}$ [a]	*r*
LTN colored forms	66.6 (±2.4)	17.3 (±0.2)	8600+3700	0.997
LTN chalcone	146.5 (±4.9) [b]	16.9 (±0.2)	10500+5500 [b]	0.998
P1 colored forms	273 (± 7)	15.5 (± 0.1)	8900 + 5800	0.998
P1 chalcone	344 (± 12) [b]	14.2 (± 0.1)	15800 + 16400 [b]	0.997

[a] First value at 295 nm (excitation wavelength), second value at 340 nm (emission wavelength);

[b] Apparent values including a minor contribution of residual colored forms present at equilibrium.

By analogy with flavonols and anthocyanins, a large part of LTN could circulate in the blood as more polar conjugates (O-glucuronides and O-sulfo forms) of LTN and 3'-O-methyl-LTN [8][9]. Even if conjugation could lower the affinity of LTN to HSA, it is unlikely to cancel the preference of HSA for the trans-chalcone. It may thus be speculated that most LTN could circulate in the blood as (conjugated) trans-chalcone – HSA complexes. This is an important point to take into account in assessing the total bioavailability of LTN. In particular, a careful acidification of plasma samples with subsequent incubation over a few hours could be required to revert the whole trans-chalcone pool into the corresponding flavylium ions.

Inhibition of lipid peroxidation

In mildly acidic conditions (pH 5 – 6) typical of the stomach acidity at the beginning of digestion and in the presence of heme iron (from red meat), the accumulation of conjugated dienes (CDs, absorption at 234 nm), the common primary oxidation products of polyunsaturated fatty acids (PUFAs), is fast. CDs are mainly PUFA hydroperoxides formed according to the mechanism in Scheme 1 (LH = PUFA with one of its labile *bis*-allylic H atom):

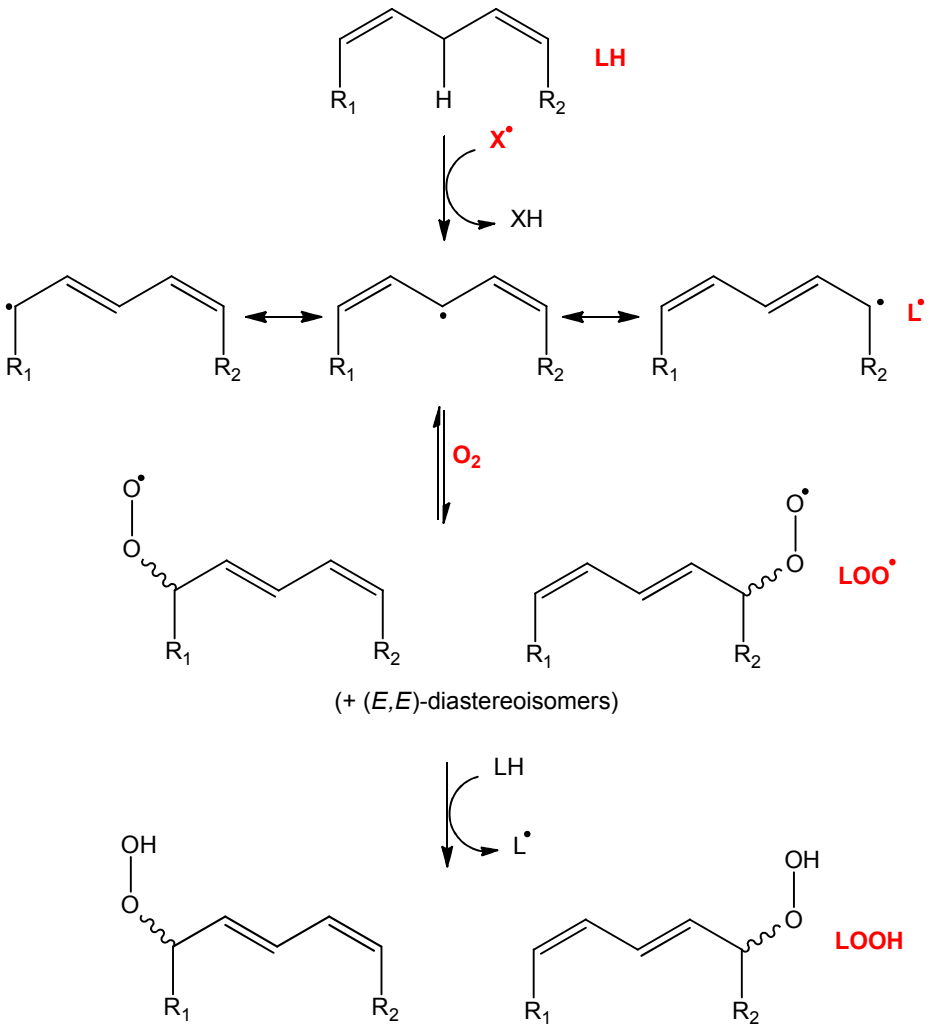

Scheme 1. PUFA (Linoleic acid par example) oxidation mechanism.

In the case of the heme-induced lipid peroxidation, the initiating species $X^{\bullet}$ are the $LOO^{\bullet}$ radicals themselves formed according to a $Fe^{III} – Fe^{IV}$ redox cycle ($MbFe^{III}$ = metmyoglobin):

$MbFe^{III} + LOOH + H^{+} \rightarrow MbFe^{IV} + LO^{\bullet} + H_2O$ ($LO^{\bullet} + O_2 \rightarrow \rightarrow$ketodienes)

$MbFe^{IV} + LOOH \rightarrow MbFe^{III} + LOO^{\bullet} + H^{+}$

Heme cofactor and its protein environment (globin).

Polyphenols, including anthocyanins, delay CD accumulation, mostly by entering the heme crevice to reduce the Fe^{IV} center [10].

As seen in the Figure 5, both the colored and *trans*-chalcone forms of LTN efficiently inhibit the metmyoglobin-induced peroxidation of linoleic acid.

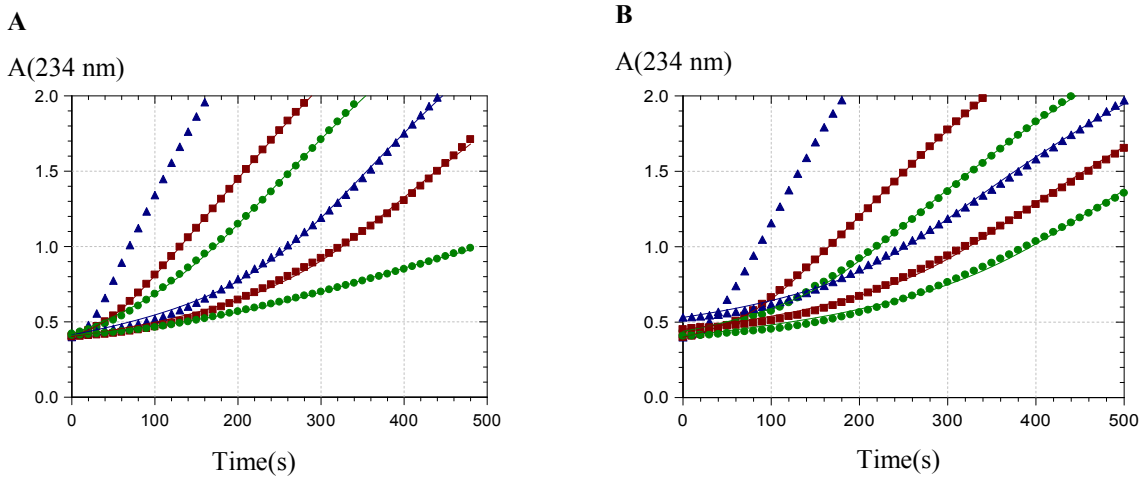

Figure 5**.** CD accumulation during the metmyoglobin-induced peroxidation of linoleic acid in the presence of luteolinidin. LTN concentration (from left to right) = 0, 0.5, 1.0, 1.5, 2.0, 2.5 µM, **A**: colored forms, **B**: *trans*-chalcone (pH 5.8 phosphate buffer + Brij®35, 37 °C).

The kinetic analysis of the peroxidation curve (shown in Table 5) allows the determination of 3 parameters:

- The lipid oxidizability (r_2), typical of the lipid and its environment and quantifying the efficiency of the propagation (*vs*. termination) reaction,

- The antioxidant efficiency $AE_1 = k$ (**LTN** + $MbFe^{IV}$) / k (LOOH + $MbFe^{IV}$),

- The antioxidant stoichiometry n= number of $MbFe^{IV}$ reduced per LTN molecule.

Given the relatively high variability in the parameters depending on the antioxidant and its concentration, only general trends can be outlined. The colored forms and *trans*-chalcone are roughly as efficient in the inhibition. Their persistent protection of linoleic acid is manifested by high stoichiometries (n = 5 – 6). Compared to **P1**, the additional OH group of **LTN** seems to improve the antioxidant activity of the colored forms ($n \approx 3$ for **P1**), while having little impact on the *trans*-chalcones.

Table 5. Kinetic analysis of the metmyoglobin-induced peroxidation of linoleic acid in the presence of luteolinidin. Curve-fitting of the *A* (234 nm) *vs.* time curves (CD accumulation). Rate constant of lipid hydroperoxide cleavage by metmyoglobin (estimated from control experiment): $k_{i1} = 3x10^3\ M^{-1}\ s^{-1}$.

Pigment / μM	r_2 / $M^{-1/2}\ s^{-1/2}$	AE_1	n
Colored forms			
0.5	2.41 (± 0.01)	60 (± 4)	2.7 (± 0.1)
1.0	2.29 (± 0.02)	15 (± 2)	4.7 (± 0.4)
1.5	2.30 (± 0.02)	22 (± 1)	5.9 (± 0.2)
2.0	2.02 (± 0.03)	21 (± 1)	5.0 (± 0.2)
2.5	1.18 (± 0.01)	13 (± 1)	2.7 (± 0.1)
***Trans*-Chalcone**			
0.5	2.27 (± 0.01)	46 (± 4)	4.9 (± 0.1)
1.0	2.04 (± 0.01)	29 (± 2)	5.1 (± 0.2)
1.5	1.92 (± 0.01)	24 (± 1)	5.8 (± 0.2)
2.0	1.86 (± 0.01)	22 (± 1)	4.9 (± 0.1)
2.5	1.80(± 0.01)	18 (± 1)	4.7 (± 0.1)

This preliminary study confirms that **LTN** is a potent radical-scavenger and an efficient inhibitor of heme-induced lipid peroxidation. Its possible use as a food colorant could thus provide the additional advantage of improving the oxidative stability of food products.

References

1. Wu, L.; Hsu, H.-W.; Chen, Y.-C.; Chiu, C.-C.; Lin, Y.-I.; Ho, J. A. Antioxidant and antiproliferative activities of red pitaya. *Food Chem.* **2006**, *95*, 319–327.

2. Soumille, N. M.; Al Bittar, S.; Rosa, M.; Dangles, O. Analogs of anthocyanins with a 3', 4'-dihydroxy substitution: Synthesis and investigation of their acid-base, hydration, metal binding and hydrogen-donating properties in aqueous solution. *Dyes Pigments* **2012**, *96*, 7–15.

3. Dangles, O. Antioxidant activity of plant phenols: chemical mechanisms and biological signficance. *Curr. Org. Chem.* **2012**, *16*, 1–23.

4. Goupy, P.; Bautista-Ortin, A.-B.; Fulcrand, H.; Dangles, O. Antioxidant Activity of Wine Pigments Derived from Anthocyanins: Hydrogen Transfer Reactions to the DPPH Radical and Inhibition of the Heme-Induced Peroxidation of Linoleic Acid. *J. Agric. Food Chem.* **2009**, *57*, 5762–5770.

5. Dangles, O.; Fargeix, G.; Dufour, C. Antioxidant properties of anthocyanins and tannins: a mechanistic investigation with catechin and the 3',4',7-trihydroxyflavylium ion. *J. Chem. Soc. Perkin Trans.* **2000**, *2*, 1653–1663.

6. Al Bittar, S.; Mora, N.; Loonis, M.; Dangles, O. Chemically Synthesized Glycosides of Hydroxylated Flavylium Ions as Suitable Models of Anthocyanins: Binding to Iron Ions and Human Serum Albumin, Antioxidant Activity in Model Gastric Conditions. *Molecules* **2014**, *19*, 20709–20730.

7. Dufour, C.; Loonis, M.; Dangles, O. Inhibition of the peroxidation of linoleic acid by the flavonoid quercetin within their complex with human serum albumin. *Free Radic. Biol. Med.* **2007**, *43*, 241–252.

8. Kay, C. D. Aspects of anthocyanin absorption, metabolism and pharmacokinetics in humans. *Nutr. Res. Rev.* **2006**, *19*, 137–146.

9. De Ferrars, R. M.; Czank, C.; Zhang, Q.; Botting, N. P.; Kroon, P. A.; Cassidy, A.; Kay, C. D. The pharmacokinetics of anthocyanins and their metabolites in humans. *Br. J. Pharmacol.* **2014**, *171*, 3268–3282.

10. Goupy, P.; Vulcain, E.; Caris-Veyrat, C.; Dangles, O. Dietary antioxidants as inhibitors of the heme-induced peroxidation of linoleic acid: Mechanism of action and synergism. *Free Radic. Biol. Med.* **2007**, *43*, 933–946.

Appendix IV

UPLC-MS identification of oxidation products of 3-deoxyanthocyanins by activated heme iron

Introduction

Myoglobin ($MbFe^{II}$) or metmyoglobin ($MbFe^{III}$) is a major protein in red meat and a major source of dietary iron. Its activation by hydrogen peroxide has been largely studied as a phenomenon responsible of meat deterioration [1].

Further studies showed the implication of (met)myoglobin in oxidative stress through protein and lipid modifications [2]. Those modifications result in anti-nutritional effects through two viewpoints: first, by decreasing the bioavailability of essential lipids and proteins for cell functionality, second, by producing potentially harmful oxidation products (e.g., lipid-derived hydroperoxides and aldehydes) [3].

We have studied the ability of some 3-DAs to inhibit the metmyoglobin-induced oxidation of linoleic acid in mildly acidic micelle solution, as a model of antioxidant activity in the gastric compartment [4]. In this work, we try to identify some of the 3-DA oxidation products formed in such conditions. In the lipid peroxidation experiment, hypervalent heme iron (the initiating species) is formed by reaction between $MbFe^{III}$ and the lipid hydroperoxides (LOOH). To simplify the analysis, the reaction was repeated in the absence of lipid and surfactant by mixing $MbFe^{III}$ and H_2O_2. The oxidation products of the 3-DA colored forms and chalcone are characterized by UPLC-DAD-MS.

Material & Methods

UPLC-MS analyses. Performed on an Acquity Ultra Performance LC™ (UPLC™) apparatus from Waters, equipped with an UV-visible diode array detector (DAD) and coupled with a Bruker Daltonics HCT ultra ion trap mass spectrometer with negative electrospray ionization (ESI) mode. Separation was conducted on a 1.7 µm (2.1 - 50 mm) Acquity UPLC BEH C18 column thermostated at 30°C. Mass spectra were generated in the Ultrascan mode in the m/z

range 100-1000. The ion source parameters were: nebulizer pressure, 50 psi; capillary 2000V, drying gas flow, 9 L min-1; drying gas temperature, 365°C.

The mobile phase consisted of H_2O / HCO_2H (99:1, v/v) (eluent A) and MeCN / HCO_2H (99:1) (eluent B). The flow rate was 0.5 mL/min. The elution program was as follows: 10–100% B (0–10 min); 100–10% B (10–10.5 min); 10–10% B (10.5-12 min).

Heme-induced oxidation of 3-DAs. To 2 mL of 30 µM $MbFe^{III}$ solution in a pH 5.8 phosphate buffer ($MbFe^{III}$ concentration standardized using $\varepsilon = 7700\ M^{-1}\ cm^{-1}$ at 525 nm), 2 µL of pigment solution in MeOH / 0.01 M HCl (1 equiv., pigment concentration in the cell ca. 30 µM) was added. For flavylium oxidation product identification, 20 µL of aqueous H_2O_2 solution (3 equiv., *ca.* 90 µM in the cell, concentration determined spectrophotometrically using $\varepsilon = 39.4\ M^{-1}\ cm^{-1}$ at 240 nm) was rapidly added and the mixture was analyzed by UPLC-MS. By contrast, for identification of the chalcone oxidation products, the mixture ($MbFe^{III}$ + pigment) was incubated for one night at 37°C for complete conversion of the pigment into the chalcone before H_2O_2 addition and UPLC-MS analysis.

Results & Discussion

The mechanism of metmyoglobin activation by H_2O_2 can be simplified as follow: Hydrogen peroxide triggers two-electron oxidation on $MbFe^{III}$ with simultaneous formation of an iron-oxo center (Fe^{IV}=O) and a protein radical located on Tyr-103 or Trp-14 [5]. The activated form of metmyoglobin is named perferrylmyoglobin ($Mb^{\bullet}Fe^{IV}$=O) and ferrylmyoglobin ($MbFe^{IV}$=O) (its autoreduction product) in the absence of external source of electrons. In acidic conditions, $MbFe^{III}$ activation by hydrogen peroxide also leads to the inert green pigment ($GMbFe^{III}$) formation via a covalent bond between the porphyrin nucleus and Tyr-103. The presence of bovine serum albumin (BSA) quenches this pathway, thus favoring $MbFe^{IV}$=O formation [1]. In the presence of external sources of electrons (antioxidants, polyunsaturated lipids, proteins), both ($Mb^{\bullet}Fe^{IV}$=O) and ($MbFe^{IV}$=O) can be reduced.

The complex redox chemistry of (met)myoglobin in aerobic conditions is summarized on Sheme 1.

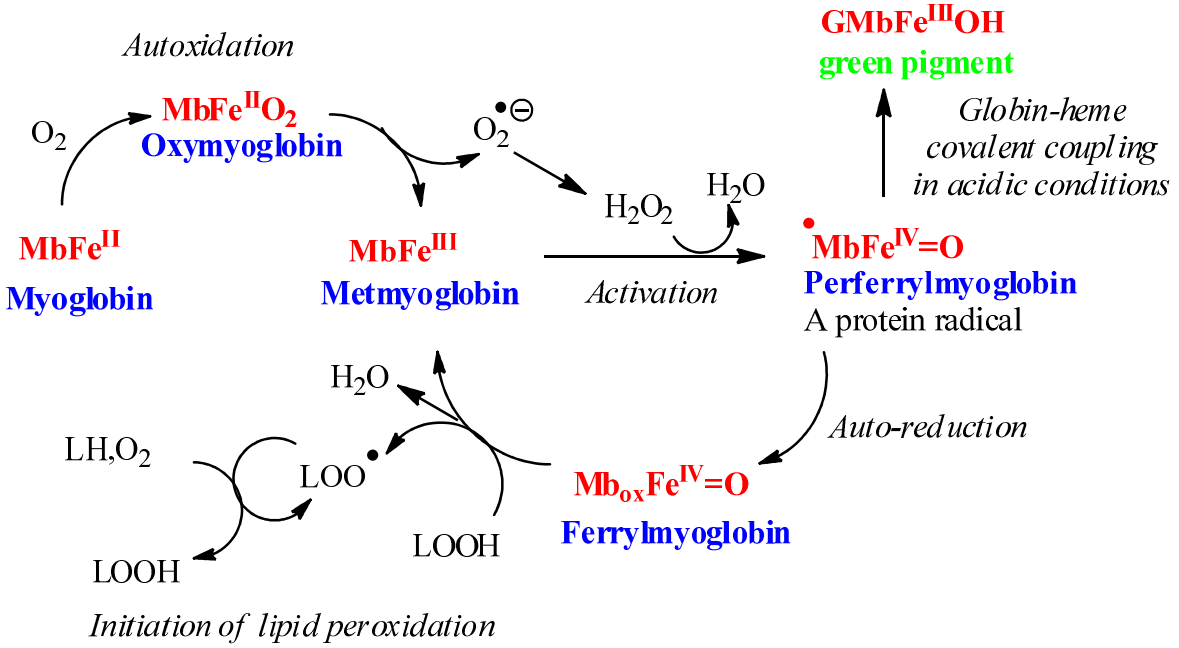

Scheme 1. The chemistry of (met)myoglobin redox chemistry adapted form [6].

In mildly acidic conditions, the ability of polyphenols to reduce perferrylmyoglobin ($MbFe^{III}$ + polyphenol, then H_2O_2) and ferrylmyoglobin, pre-formed by reaction between $MbFe^{III}$ and H_2O_2 ($MbFe^{III}$ + H_2O_2, then polyphenol), has been established [7]. The former reaction is now repeated with 3-DAs bearing an electron-donating catechol B-ring (**P1**, **P2** and LTN).

In article 2, the antioxidant capacity of 3-DAs (in colored or chalcone forms) was evidenced by their ability to inhibit CD accumulation during metmyoglobin-induced oxidation of linoleic acid. As a complement, 3-DA oxidation products are investigated in the present work through two methods: i) successive pigment and H_2O_2 additions to the $MbFe^{III}$ solution in a 5.8 pH buffer to generate oxidation products of colored form, ii) one-night incubation of pigment in the $MbFe^{III}$ solution to ensure total chalcone formation before H_2O_2 addition.

The following comments can be made:

1) Control experiments in the absence of H_2O_2 did not lead to significant oxidation.

2) The second method did not permit to identify oxidation products of chalcones although the starting compounds were clearly consumed.

3) The first method allowed the identification of oxidation products, suggesting two-electron oxidation followed by nucleophilic attack of a water molecule and/or a second pigment molecule (dimerization). The sequence of two-electron oxidation / water addition (already evidenced in the reaction of **P1** with DPPH [4] and, in this thesis, with Cu^{2+}, see Scheme 2 in Annex 1) could also be repeated or the dimers further oxidized.

Interestingly, glycosidation of C7-OH apparently quenches dimerization (no dimer detected with **P2**) while an additional OH group at C5 favors it (no water addition observed with LTN), possibly because of the increased nucleophilicity of the A-ring. With **P1**, both routes were evidenced.

A

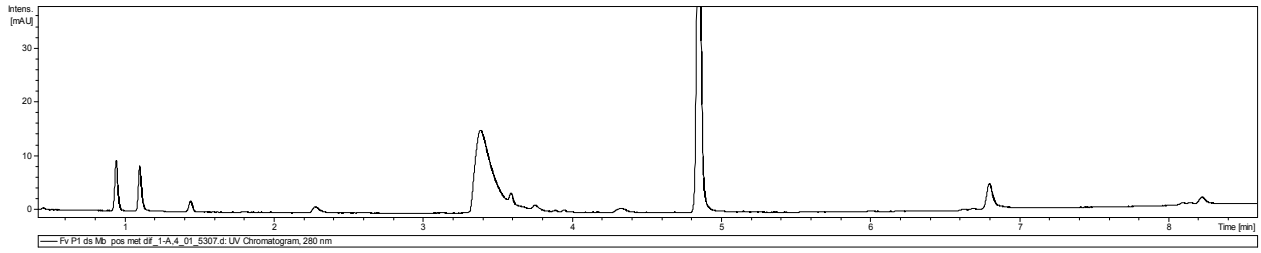
Intens.
[mAU]
Time [min]
Fv P1 ds Mb pos met dif_1-A,4_01_5307.d: UV Chromatogram, 280 nm

B

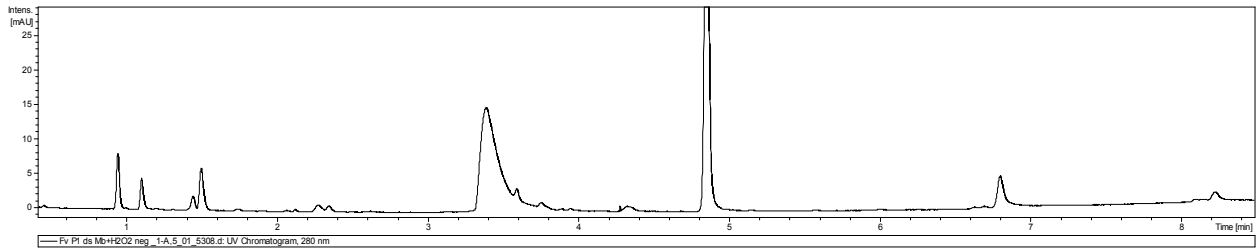
Intens.
[mAU]
Time [min]
Fv P1 ds Mb+H2O2 neg_1-A,5_01_5308.d: UV Chromatogram, 280 nm

C

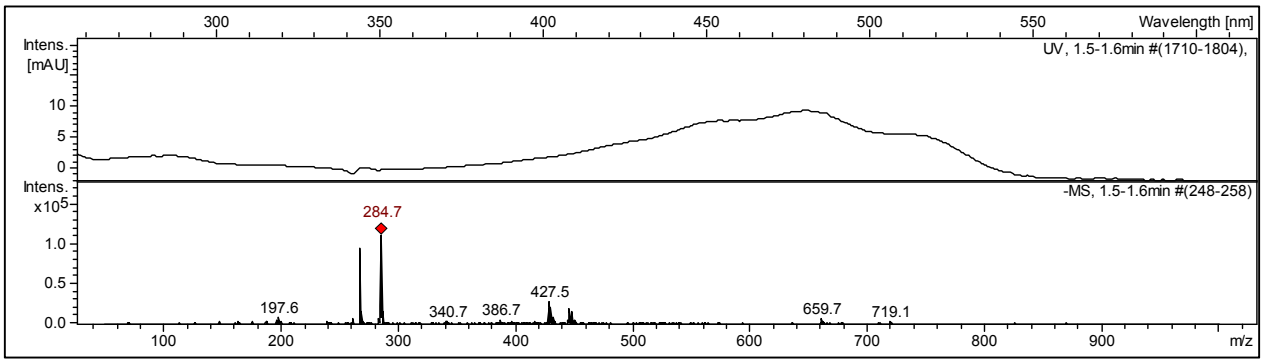
Wavelength [nm]
Intens.
[mAU]
UV, 1.5-1.6min #(1710-1804),
-MS, 1.5-1.6min #(248-258)
284.7
197.6
340.7
386.7
427.5
659.7
719.1
m/z

D

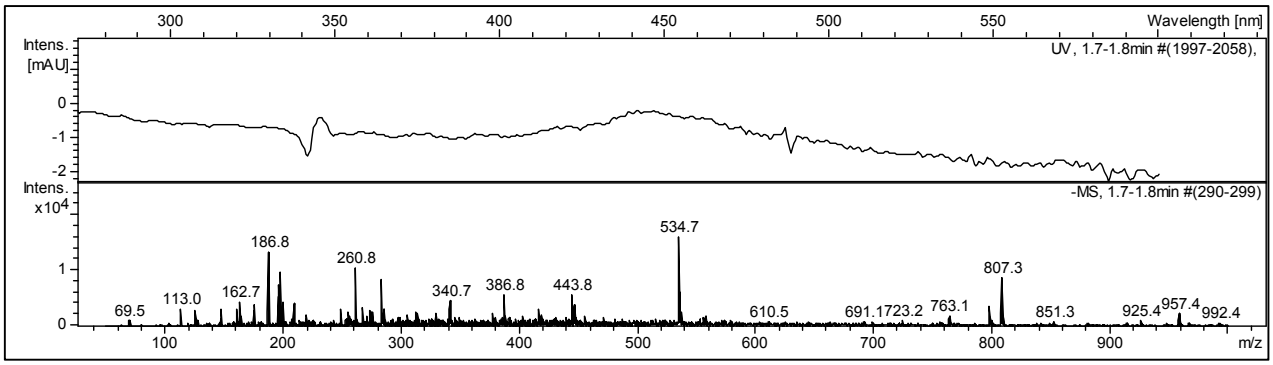
Wavelength [nm]
Intens.
[mAU]
UV, 1.7-1.8min #(1997-2058),
-MS, 1.7-1.8min #(290-299)
534.7
186.8
260.8
807.3
69.5
113.0
162.7
340.7
386.8
443.8
610.5
691.1723.2
763.1
851.3
925.4
957.4
992.4
m/z

E

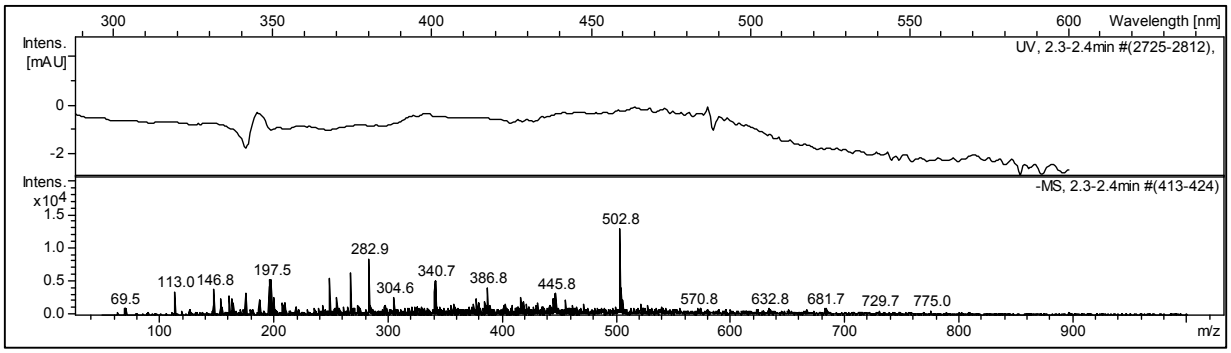

Figure 1. UPLC –DAD – MS analysis of perferrylmyoglobin reduction by P1 (pH 5.8 phosphate buffer, 25°C)

A: Chromatograms (280, 350 and 520 nm) of the **P1 -** $MbFe^{III}$

B: Chromatograms (280, 350 and 520 nm) of the **P1 -** $MbFe^{III}$ - H_2O_2

C: UV-vis and mass spectra of compound at t_R = 1.50 min, *m/z* (ES^-) = 285.

D: UV-vis and mass spectra of compound at t_R = 1.74 min, *m/z* (ES^-) = 535.

E: UV-vis and mass spectra of compound at t_R = 2.34 min, *m/z* (ES^-) = 503.

A

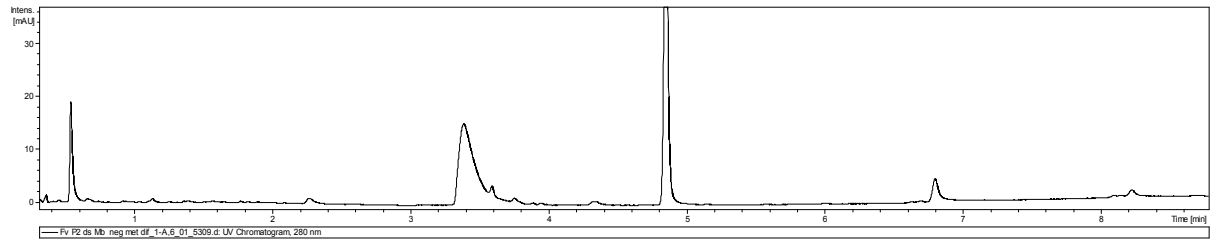

B

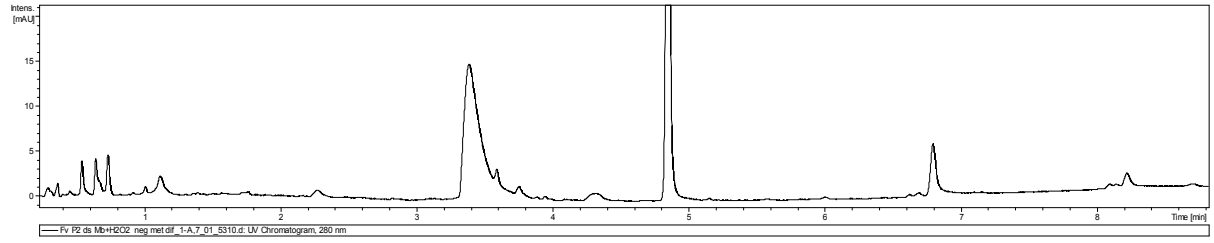

C

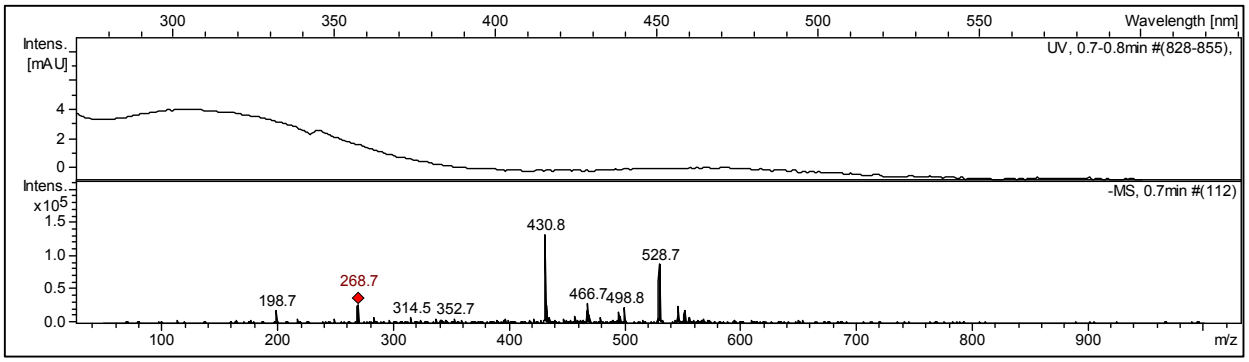

D

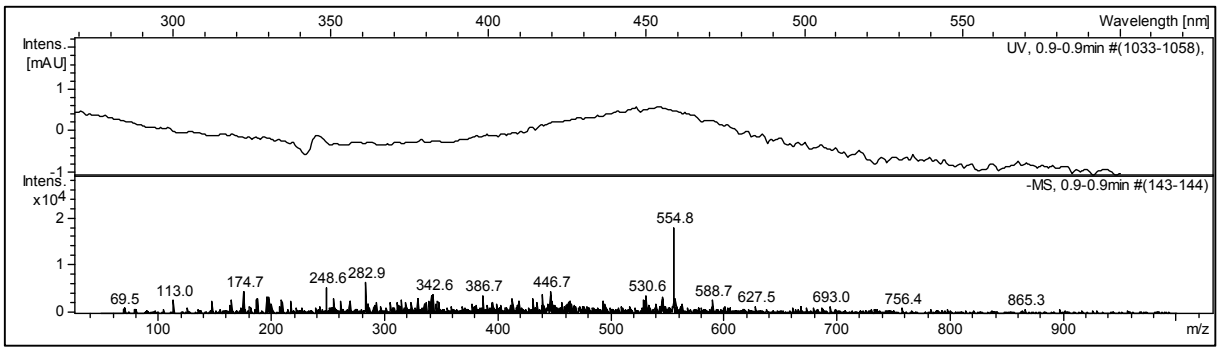

E

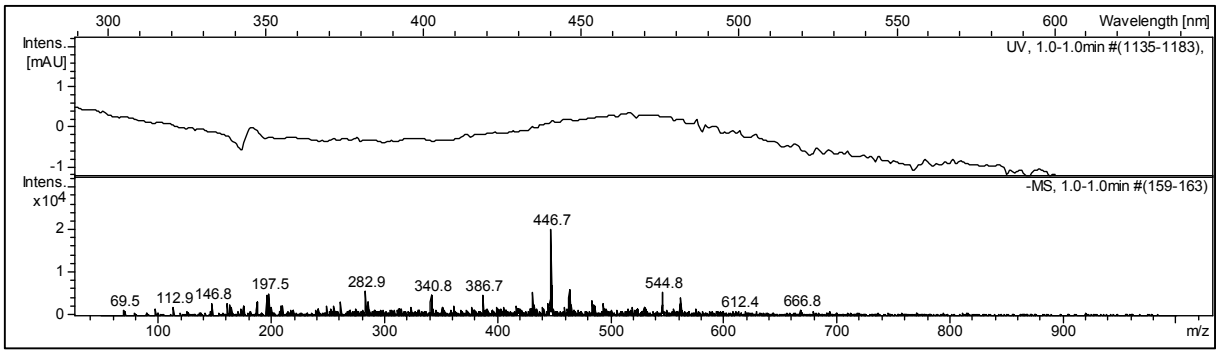

Figure 2. UPLC –DAD – MS analysis of perferrylmyoglobin reduction by P2 (pH 5.8 phosphate buffer, 25°C)

A: Chromatograms (280, 350 and 520 nm) of the **P2 -** $MbFe^{III}$

B: Chromatograms (280, 350 and 520 nm) of the **P2 -** $MbFe^{III}$ - H_2O_2

C: UV-vis and mass spectra of compound at t_R = 0.75 min, *m/z* (ES^-) = 431.

D: UV-vis and mass spectra of compound at t_R = 0.95 min, *m/z* (ES^-) = 555.

E: UV-vis and mass spectra of compound at t_R = 1.05 min, *m/z* (ES^-) = 447.

A

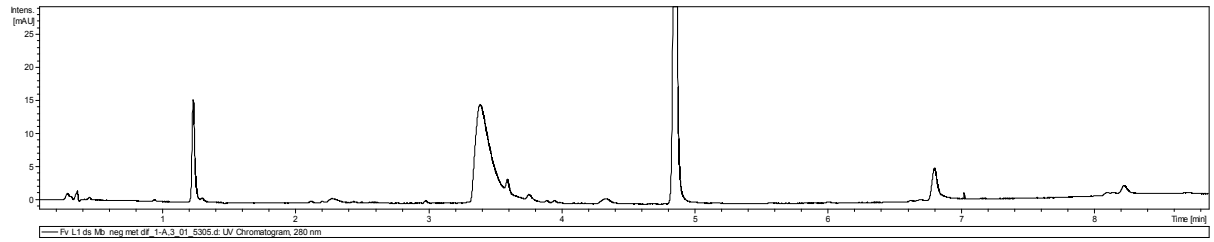

B

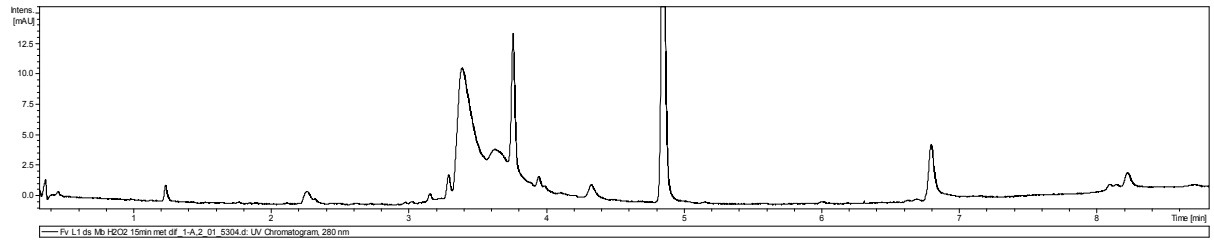

C

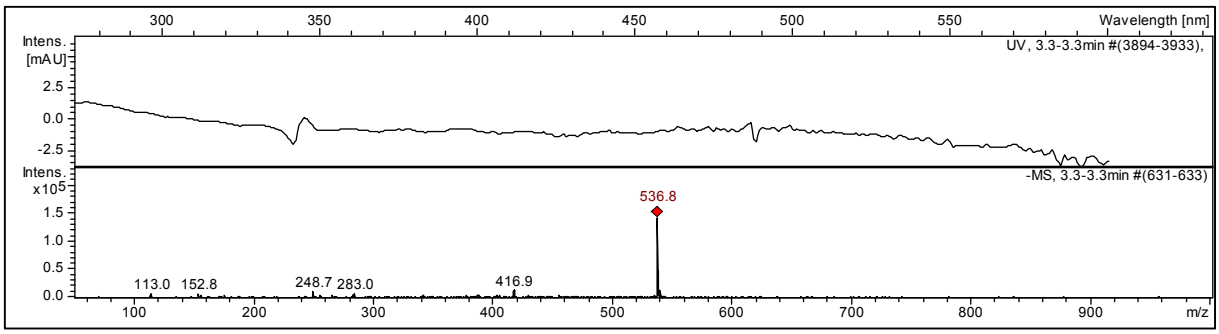

D

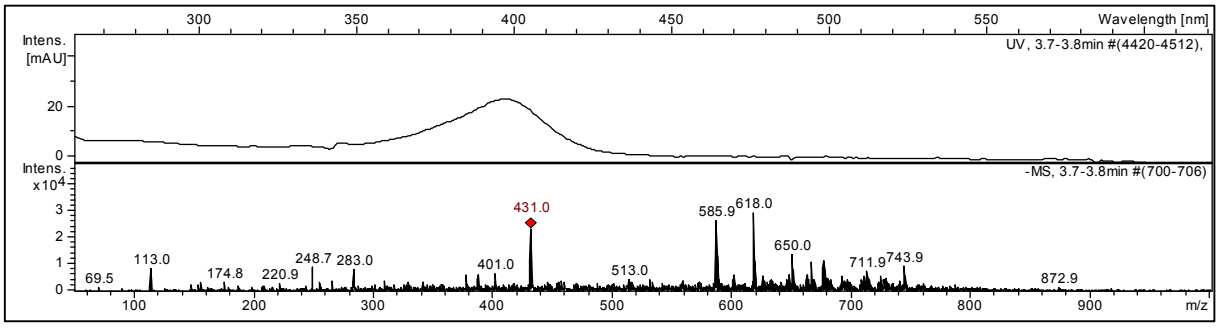

Figure 3. UPLC –DAD – MS analysis of perferrylmyoglobin reduction by LTN (pH 5.8 phosphate buffer, 25°C)

A: Chromatograms (280 nm) of the **LTN -** $MbFe^{III}$

B: Chromatograms (280 nm) of the **LTN -** $MbFe^{III}$ - H_2O_2

C: UV-vis and mass spectra of compound at t_R = 3.29 min, *m/z* (ES^-) = 537.

D: UV-vis and mass spectra of compound at t_R = 3.75 min, *m/z* (ES^-) = 431.

Table. UPLC-DAD-MS analysis of 3-DA oxidation products

Conditions	t_R (min)	λ_{max} (nm)	m/z (ES^-)	Structure proposed
All samples	3.40	280	ND	Globin
	4.85	400	660	Hematin
P1 + $MbFe^{III}$	1.10	470	253	**P1** (A^- ion)
P1 + $MbFe^{III}$ + H_2O_2	1.16	ND	269	**P1** - 2H + H_2O
	1.50	470	285	**P1** – 4H + $2H_2O$
	1.74	440	293, 535	2**P1** - 8H + $2H_2O$
	2.34	440	251, 503	2**P1** - 4H (ox. dimer)
P2 + $MbFe^{III}$	1.10	380	271, 433	**P2** (C_t anion)
P2 + $MbFe^{III}$ + H_2O_2	0.65	330	269, 431	**P2** - 2H + H_2O
	0.75	330	269, 431	**P2** - 2H + H_2O
	0.92	450	347, 555	NI
	1.05	470	241, 447	**P2** - 4H + $2H_2O$
LTN + $MbFe^{III}$	1.20	485	269	LTN (A^- ion)
LTN + $MbFe^{III}$ + H_2O_2	3.29	350	308, 411, 537	2LTN - 2H (dimer)
	3.75	390	431	NI

ND: non- detected

NI: non-identified

Reference:

1. Falowo, A. B.; Fayemi, P. O.; Muchenje, V. Natural antioxidants against lipid–protein oxidative deterioration in meat and meat products: A review. *Food Research International* **2014**, *64*, 171–181.

2. Kanner, J.; Lapidot, T. The stomach as a bioreactor: dietary lipid peroxidation in the gastric fluid and the effects of plant-derived antioxidants. *Free Radical Biology and Medicine* **2001**, *31*, 1388–1395.

3. Dangles, O. Antioxidant activity of plant phenols: chemical mechanisms and biological signficance. *current organic chemistry* **2012**, *16*, 1–23.

4. Al Bittar, S.; Mora, N.; Loonis, M.; Dangles, O. Chemically Synthesized Glycosides of Hydroxylated Flavylium Ions as Suitable Models of Anthocyanins: Binding to Iron Ions and Human Serum Albumin, Antioxidant Activity in Model Gastric Conditions. *Molecules* **2014**, *19*, 20709–20730.

5. Lorrain, B.; Dufour, C.; Dangles, O. Influence of serum albumin and the flavonol quercetin on the peroxidase activity of metmyoglobin. *Free Radical Biology & Medecine* **2010**, *48*, 1162–1172.

6. Baron, C. P.; Andersen, H. J. Myoglobin-induced lipid oxidation. *Journal of Agricultural & Food Chemistry* **2002**, *50*, 3887–3897.

7. Vulcain, E.; Goupy, P.; Caris-Veyrat, C.; Dangles, O. Inhibition of the metmyoglobin-induced peroxidation of linoleic acid by dietary antioxidants: Action in the aqueous vs. lipid phase. *free radical research* **2005**, *39*, 547–563.

General discussion

and

Conclusions

Our work can be discussed through two axes:

1. Chemical synthesis of 3-deoxyanthocyanin(di)ns

Two pigments, 3',4',7-trihydroxyflavylium (**P1**) and its 7-*O*-glucoside (**P2**) were synthesized by aldol condensation in acidic conditions in a precedent work by our team. However, it was difficult to control the quantity of gaseous HCl generated and directly bubbled in the reaction flask. Highly variable yields led us to search an alternative HCl source and TMSCl was proposed. Several methods were tested such as the preliminary preparation of HCl solutions by mixing TMSCl with protic solvent such as AcOH or MeOH, from which defined HCl equivalents were injected in the reaction flask. Finally, optimized yields of **P1** were obtained by injecting TMSCl directly in a closed flask containing equimolar quantities of reagents solubilized in EtOAc.

Concerning luteolinidin synthesis, two difficulties arouse:

- The 2,4,6-trihydroxybenzaldehyde reagent has a poor solubility in AcOEt and the condensation has to be carried out in AcOEt / MeOH (2:1). However, the MeOH content must be kept at a minimum to not compromise the precipitation of LTN.

- 2,4,6-Trihydroxybenzaldehyde is prone to acid-catalyzed dimerization (possibly, oligomerization) by electrophilic aromatic substitution, leading to yellow – orange xanthylium pigments difficult to separate from LTN (Sheme 1). From the NMR and UPLC-DAD-MS analyses, the loss of carbon monoxide is clear but remains difficult to explain.

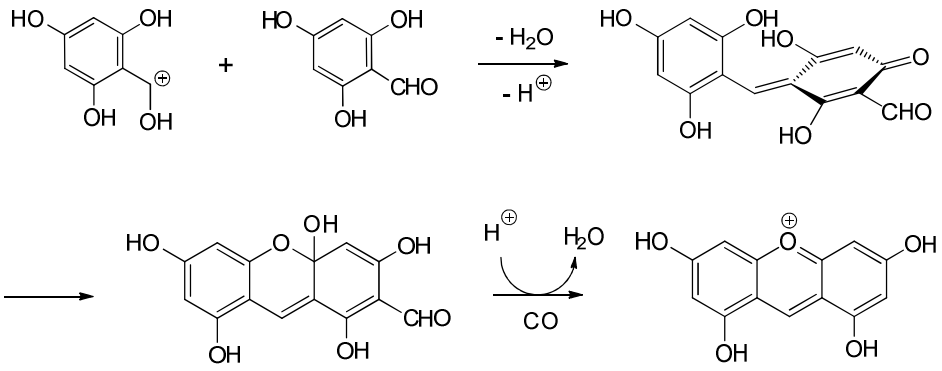

Sheme 1. Proposed mechanism of 2,4,6,8-tetrahydroxyxanthylium formation.

The reaction duration has to be carefully checked to minimize xanthylium formation (6%). In our most recent optimizations, using 3,4-dihydroxyacteophenone in excess led to the total disappearance of 2,4,6,8-tetrahydroxyxanthylium.

These general conditions for the condensation step were adapted for the other flavylium ions synthesized in this work. The MeOH / AcOEt ratio ranged from 25 to 70% depending on the solubility of the reagents. Aglycones **P7**, **P8** and **P9** were all obtained in good yields.

Preliminary desacetylation of protected 4-β-glucosyloxyacetophenone and subsequent condensation with 2,4-dihydroxybenzaldehyde or 2-hydroxy-4-methoxybenzaldehyde was possible and afforded pure **P5** and **P6**. By contrast, desacetylation of protected 2-hydroxy-4-β-glucosyloxybenzaldehyde could not be led to completion, even in the presence of MeONa in excess, possibly because of the deprotonation of the phenolic OH group at C2 and the charge repulsion occurring between the phenolate and methoxide anions. Hence, deacetylation was conducted after the condensation step and a final purification on a C18 cartridge was necessary to obtain pure **P2**, **P3** and **P4**.

Our challenge was to synthesize the naturally occurring luteolinidin 5-O-glucoside. The chemical synthesis was imagined as: protection of 2,4,6-trihydroxybenzaldehyde at C4-OH, glucosidation at C2-OH, then deprotection of C4-OH before condensation and final deacetylation. Unfortunately, benzylation occurred at C2-OH instead of C4-OH and shifted the synthesis toward luteolinidin 7-O-glucoside (see NMR spectrum of the protected pigment in Appendix II).

Moreover, the final deacetylation turned out to be very slow and remained largely incomplete despite prolonged reaction time and MeONa in large excess. UPLC-MS analysis confirmed the presence of LTN-Glc in addition to partially acetylated pigments. Later purification on TSK gel afforded a mixture of LTN-7-Glc and naturally occurring LTN-5-Glc.

To our knowledge, this unexpected isomerization in alkaline conditions has no equivalent in the literature. It might occur through a stabilized 6-C-glucosyl intermediate (Scheme 2).

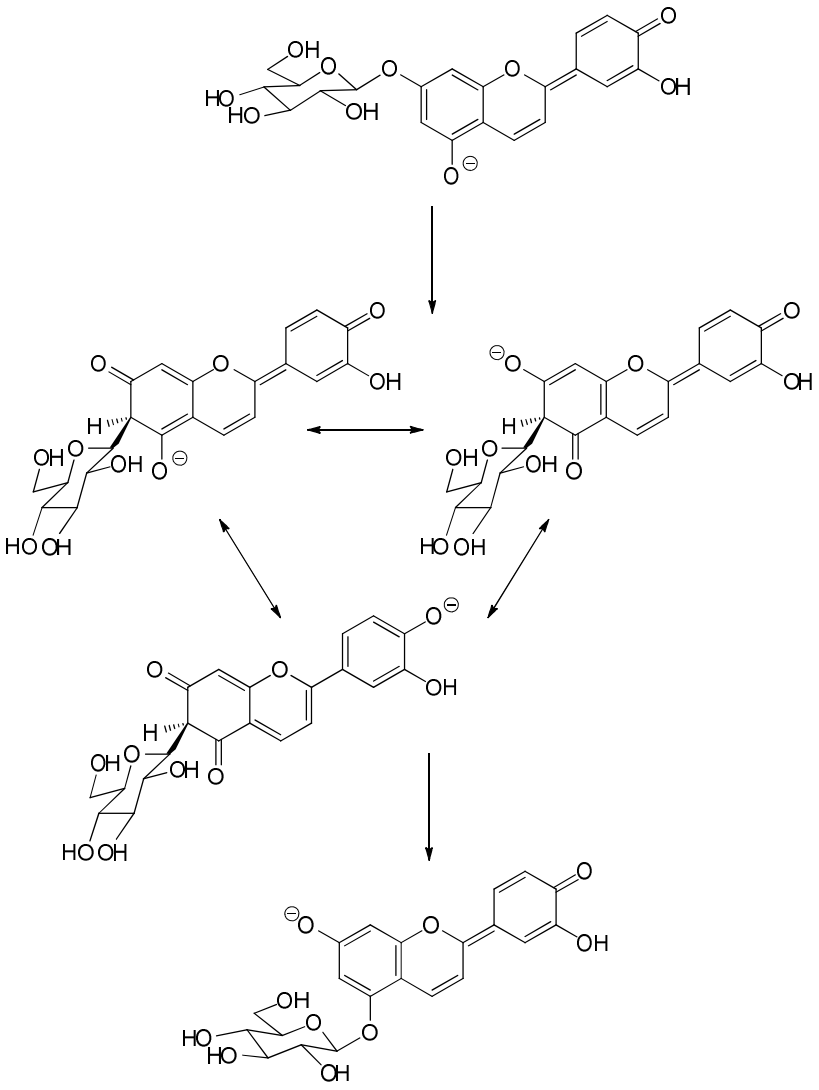

Scheme 2. Proposed mechanism for the isomerization of LTN-7-Glc to LTN-5-Glc under alkaline conditions.

2. Physicochemical properties of synthesized pigments

2.1. Proton transfer and water addition

P1 vs. P2 *(effect of C7-OH glucosidation):* **P2** appears significantly less acidic than **P1** as a consequence of the replacement of the acidic proton at C7-OH by the β-*D*-glucosyl moiety. The close pK'_h values show that the thermodynamics of the overall hydration-ring opening (*Z*, *E*) isomerization process is not affected by the β-*D*-glucosyl moiety.

P1 vs. LTN *(effect of C5 hydroxylation):* LTN is more acidic than **P1**, which is explained by a contribution of C5-OH (formation of 5-keto quinonoid base A5) to the overall acidity. Otherwise, hydroxylation at C5 doesn't affect the thermodynamics of water addition.

P3 vs. P5 *(C7-OH glucosidation vs. C4'-OH glucosidation):* Comparing the two regioisomers **P3** and **P5**, it seems clear that the glucosidation site has a considerable influence on the resulting color and its stability in aqueous solution. **P5** has probably a higher K_a value due to proton loss being much more favorable from C7-OH than from C4'-OH, which is in agreement with the literature [1] and with **P1** being more acidic than **P2**. Moreover, our preliminary study shows that **P5** is much more resistant to color loss than **P3** in neutral conditions. In the case of **P5**, we may have the situation where K_a is higher than K_h, meaning that the quinonoid base is both the thermodynamic and kinetic product of the flavylium ion.

More work is needed to understand the stability of **P5** and the detailed physical chemistry of the synthesized pigments. For this task, a collaboration with Pr. Fernando PINA and its team (Lisbon University) is under way.

2.2. Metal binding

P1, **P2** and LTN having a 1,2-dihydroxy substitution in their B-ring can bind metal ions such as Al^{III}, Fe^{II}, Fe^{III} Cu^{I} and Cu^{II} in mildly acidic solutions (pH 4 - 5) with concomitant removal of the phenolic protons. The kinetics and thermodynamics of metal binding were studied by UV-visible spectroscopy. As transition metal – polyphenol binding may be a first step toward

autoxidation [2], the presence or absence of oxidation products was checked by UPLC-DAD-MS analysis.

Unfortunately, LTN-metal binding could not be studied in aqueous solution because of insufficient solubility of LTN. So, the experiments were carried out in a buffer containing 30% of MeOH. So, only **P1** and **P2** can be directly compared for their metal-binding properties.

Al^{III} - binding: It is faster with **P1** than with **P2** but the Al^{III} - **P1** complex appeared much less stable as accumulation of free chalcone was observed in much higher concentration with **P1**. In other words, the Al^{III} - **P1** complex is much more prone to water addition than the Al^{III} - **P2** complex. From this viewpoint, glycosidation at C7-OH can be regarded as an efficient way to increase the stability of the Al^{III} complex in mildly acidic aqueous solution.

Fe- binding: Fe^{III} rapidly binds both **P1** and **P2** in mildly acidic solutions, thereby quenching their conversion into the corresponding chalcones. Again, glycosidation at C7-OH is an efficient way to increase the stability of the Fe^{III} complex in mildly acidic aqueous solution. Kinetically, Fe^{III} - **P2** binding is faster than Al^{III} - **P2** binding but the thermodynamic constants are almost identical, meaning that **P2** has the same affinity for both trivalent metals. Moreover, **P2** interacts with Fe^{II} faster than **P1**. Both pigments promote Fe^{II} autoxidation with subsequent fast binding of Fe^{III} as inert complexes. As free Fe^{II} is involved in the Fenton reaction, the latter sequence can be regarded as an antioxidant mechanism.

Cu- binding: **P1** binds Cu^{I} rapidly without chalcone formation. With **P2**, the binding is partial and chalcone is formed (confirmed by UPLC-DAD-MS). Here, glucosidation is not efficient at stabilizing the complexes and preventing chalcone formation. Otherwise, oxidation products are detected for both pigments in the presence of Cu^{II}. Again, water addition is obvious within the **P2** - Cu^{II} mixture and some oxidation products could actually be produced from the chalcone.

2.3. DPPH radical-scavenging

This test is a first simple assessment of the intrinsic H-atom/electron-donating activity of antioxidants. It is especially useful when a complete data analysis is carried out, so as to extract rate constant and stoichiometry values.

When the pigments **P1, P2** and LTN are added to the DPPH solution, a fast decrease of the DPPH visible absorption band is observed featuring the transfer of the labile H-atoms of the catechol OH groups. Then, a slower decay follows that reflects the residual H-donating activity of some oxidation products. **P1** transfers a first H-atom to DPPH *ca*. 4 times as rapidly as **P2**, but also the total number of DPPH radicals reduced by **P1** is *ca*. 3 times as high as by **P2**. It is suggested that quinonoid base A7 makes a major contribution to the radical-scavenging activity of **P1** via H-transfer from C4'-OH or even that the anionic quinonoid base in low concentration makes a contribution by electron-transfer to DPPH. On the other hand, LTN transfers a first H-atom to DPPH *ca*. 4 times as rapidly as **P1** and a higher total stoichiometry (more than 7 for LTN *vs*. ca. 4 for **P1**) was obtained. Thus, quinonoid base A5 and/or a mixture of anionic quinonoid bases (deprotonation of C7-OH + C4'-OH and/or C5-OH) in low concentration probably make a major contribution to the radical-scavenging activity of LTN.

2.4. HSA-binding

Although the bioavailability of 3-DAs is unknown, these pigments (more probably, their O-glucuronyl and O-sulfo conjugates) are likely to travel in the blood as complexes with human serum albumin. The affinity for HSA of **P1**, **P2** and LTN in their colored and colorless forms has been studied. The glucose moiety strongly destabilizes the complexes, especially for the colored forms. Moreover, the chalcones, having an open linear structure, display a higher affinity for HSA than the corresponding colored forms. Artificial **P1** in both its colored and chalcone forms has a higher affinity for HSA than natural occurring LTN. This study suggests that 3-DAs could travel in the blood mostly as chalcones (and their conjugates). Hence, careful reacidification and incubation for at least 2h can be recommended to convert the chalcones into the corresponding colored forms. Otherwise, the bioavailability of 3-DAs could be greatly underestimated.

2.5. Inhibition of lipid peroxidation

Although possibly higher than for anthocyanins (notoriously less chemically stable than 3-DAs), the bioavailability of 3-DAs in their original (colored or colorless) forms is probably low, as extensive catabolism by the microbiota and subsequent conjugation by human enzymes in the intestine and liver are very likely, based on the current knowledge on the bioavailability of polyphenols [3]. Moreover, these enzymatic transformations all concur to lower the electron-donating activity. In other words, the antioxidant activity of 3-DAs after intestinal absorption

is probably a minor contribution to their health-promoting effects. Hence, a simple model for assessing the antioxidant activity of 3-DAs prior to intestinal absorption was selected [4]. In this model of postprandial oxidative stress (heme iron + oxidizable lipids in the stomach), **P1**, **P2** and LTN were shown to inhibit the metmyoglobin-induced peroxidation of linoleic acid in mildly acidic micelle solution. Appropriate experimental conditions enabled us to distinguish between the colored and chalcone forms for their inhibitory capacity. In agreement with the DPPH test, **P2**, whether in its colored or chalcone form, is a poorer antioxidant than **P1**. Moreover, the chalcone forms came up as more potent inhibitors than the corresponding colored forms. Similar results were obtained with LTN, although its chalcone remained less efficient than the **P1** chalcone. The kinetic analysis of the peroxidation curves was consistent with 3-DAs acting by reducing hypervalent heme iron (formed by reaction between metmyoglobin and lipid hydroperoxides). This is consistent with the oxidation products detected by UPLC-DAD-MS in the reaction between 3-DAs and ferrylmyoglobin (formed by reaction between metmyoglobin and H_2O_2). Unfortunately, the large spectral interferences between ferrylmyoglobin and the pigments prevented the kinetic analysis of the reaction.

Overall, 3-DAs (aglycones) are potent inhibitors of heme-induced lipid peroxidation and could act as such within the dietary bolus in the stomach, thereby protecting essential lipids from alteration. To our knowledge, this is also the first work outlining the contribution of the colorless forms to their overall antioxidant activity of anthocyanins.

Reference

1. Pina, F. Chemical Applications of Anthocyanins and Related Compounds. A Source of Bioinspiration. *J. Agric. Food Chem.* **2014**, *62*, 6885–6897.

2. Nkhili, E.; Loonis, M.; Mihai, S.; El Hajji, H.; Dangles, O. Reactivity of food phenols and copper ions: binding dioxygen activation and oxidation mechanisms. *Food Funct.* **2014**, *5*, 1186–1202.

3. Del Rio, D.; Rodriguez-Mateos, A.; Spencer, J. P. E.; Tognolini, M.; Borges, G.; Crozier, A. Dietary (poly)phenolics in human health: structures, bioavailability, and evidence of protective effects against chronic diseases. *Antioxid. Redox Signal.* **2013**, *18*, 1818–1892.

4. Dangles, O. Antioxidant activity of plant phenols: chemical mechanisms and biological signficance. *Curr. Org. Chem.* **2012**, *16*, 1–23.

Perspectives

1) Improving the chemical synthesis of luteolinidin O-glucosides

Luteolidin 5- and/or 7-O-glucosides are interesting water-soluble derivatives of luteolinidin that keep a free catechol B-ring for metal chelation and antioxidant activity. Unfortunately, our synthesis of these pigments largely failed because of the low yield of the final condensation / deprotection steps.

The following sequence could be tested: a) deacetylation of 2-benzyloxy-6-hydroxy-4-(2',3',4',6'-tetra-O-acetyl-β-D-glucopyranosyloxy)-benzaldehyde, b) condensation with 3,4-dihydroxyacetophenone, c) debenzylation, autoxidation (Scheme).

Keeping the benzyl group until the final step could ease the deacetylation by limiting the formation of phenolate anions and maintain the adequate solubility for the condensation step. However, debenzylation will likely lead to a mixture of flavenes, thus requiring a final step of autoxidation in the air for the recovery of the pigment.

Alternatively, the more labile *p*-methoxybenzyl group could be used for removal in the acidic conditions of the condensation step [1].

2) 3-Deoxyanthocyanin stability and antioxidant activity in food

3-DAs have not been sufficiently studied as food colorants. In particular, little information is available about color preservation during food processing and storage. More research is needed about their thermal and photochemical stability and how to improve it by an appropriate environment (influence of copigments, metal ions and biopolymers).

The antioxidant potential of 3-DAs with a 3',4'-dihydroxy substitution has been demonstrated in this work. It would be interesting to confirm it in more relevant food models, *i.e*. in oil-in-water emulsions stabilized by phospholipids and/or proteins, as already carried out in our team with other polyphenols [2] [3].

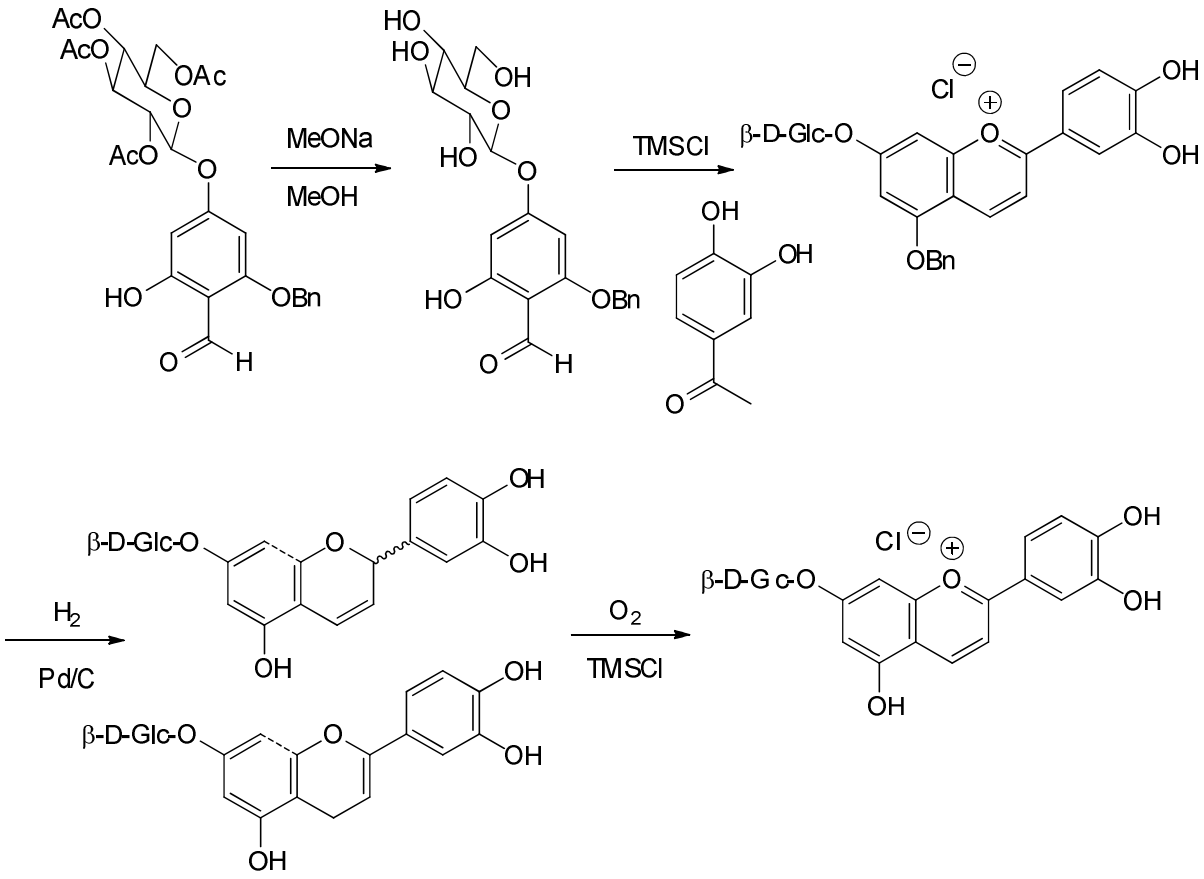

Scheme: proposal for an improved synthesis of LTN-7Glc

3) 3-Deoxyanthocyanin formulation for stable red to blue colors

The production of stable natural blue color for application in candies and beverages is the aim of extensive research. Luteolinidin, easily accessible by chemical synthesis, could serve as a basis for blue colorants in combination with other ingredients (copigments, iron ions, biopolymers such as food proteins and polysaccharides) increasing the pigment's stability and solubility.

4) 3-Deoxyanthocyanin bioavailability

The bioavailability of 3-DAs in humans is unknown but, given their much higher chemical stability, we can speculate it may be higher than for common anthocyanins. Our expertise in 3-DA synthesis and physical chemistry (in particular, our capacity to synthesize luteolinidin at a 100 mg scale) could open up interesting collaborations with biologists investigating the bioavailability and health effects of polyphenols. From our experience, 3-deoxyanthocyanidin identification in blood samples must follow a relatively long step on incubation after acidification to ensure a complete conversion of the *trans*-chalcone form into the flavylium ion.

Phenolic phytochemicals encapsulated in nanoparticles (1 - 100 nm) were shown to more easily cross the intestinal barrier, either by para-cellular or by trans-cellular pathways [4]. Encapsulation could not only enhance intestinal absorption but also protect dietary phenolic compounds against degradation in the GI tract. A model of negative charged nanoparticles of protein isolate (WPI) coated with beet pectin (BP) was proposed [5]. Such strategies could be applied to 3-DAs.

References:

1. El Hajji, H.; Dangles, O.; Figueiredo, P.; Brouillard, R. 3'-(β-D-Glycopyransyloxy)flavilium Ions: Synthesis and Investigation of Their Properties in Aqueous Solutions. Hydrogen Bonding as a Mean of Colour Variation. *Helvetica Chimica Acta* **1997**, *80*, 398–413.

2. Lorrain, B.; Dangles, O.; Genot, C.; Dufour, C. Chemical modeling of heme-induced lipid oxidation in gastric conditions and inhibition by dietary polyphenols. *Journal of Agricultural & Food Chemistry* **2010**, *58*, 676–683.

3. Lorrain, B.; Dangles, O.; Loonis, M.; Armand, M.; Dufour, C. Dietary iron-initiated lipid oxidation and its inhibition by polyphenols in gastric conditions. *Journal of Agricultural & Food Chemistry* **2012**, *60*, 9074–9081.

4. Li, Z.; Jiang, H.; Xu, C.; Gu, L. A review: Using nanoparticles to enhance absorption and bioavailability of phenolic phytochemicals. *Food Hydrocolloids* **2015**, *43*, 153–164.

5. Arroyo-Maya, I. J.; McClements, D. J. Biopolymer nanoparticles as potential delivery systems for anthocyanins: Fabrication and properties. *Food Research International* **2015**, *69*, 1–8.

Other publications

Photochemical & Photobiological Sciences

RSC Publishing

PAPER

View Article Online
View Journal

Cite this: DOI: 10.1039/c2pp25329a

A flash photolysis and stopped-flow spectroscopy study of 3′,4′-dihydroxy-7-*O*-β-D-glucopyranosyl-oxyflavylium chloride, an anthocyanin analogue exhibiting efficient photochromic properties

Vesselin Petrov,[a] Raquel Gavara,[a] Olivier Dangles,*[b] Sheiraz Al Bittar,[b] Nathalie Mora-Soumille[b] and Fernando Pina*[a]

Received 2nd October 2012,
Accepted 29th November 2012

DOI: 10.1039/c2pp25329a

www.rsc.org/pps

The complete determination of all rate and equilibrium constants of the network of reversible chemical reactions involving the anthocyanin analogue, 3′,4′-dihydroxy-7-*O*-β-D-glucopyranosyloxyflavylium chloride, was achieved by means of UV-visible spectroscopy, flash photolysis and pH jumps monitored by stopped-flow. An energy level diagram containing all the data was obtained. A detailed step by step procedure illustrating all the calculations is reported.

1. Introduction

Some flavylium derivatives have been shown to exhibit very interesting photochromic properties with potential applications in several fields, from models of optical memories[1] to systems capable of mimicking elementary properties of neurons.[2] The photochromism of flavylium compounds in an acidic medium arises from the existence of a network of chemical reactions involving five species, see Scheme 1 for 4′-hydroxyflavylium.[3,4] The flavylium cation (**AH**$^+$) is stable only in a very acidic medium. When the pH increases the quinoidal base (**A**) is obtained from deprotonation of **AH**$^+$. The hemiketal (**B**) is formed by hydration of **AH**$^+$. The *cis*-chalcone (**Cc**) results from the ring opening (tautomerization) of **B**, and the *trans*-chalcone (**Ct**) from isomerization of **Cc**. The key step for the occurrence of photochromism is the formation of **Cc** from irradiation of **Ct**. The primary photochemical product, **Cc**, can give **AH**$^+$/**A** as a kinetic product, that in a further process reverts back to the initial state defining in this way a photochromic system.

The study of the network is simplified if eqn (1) is considered. Eqn (1) is equivalent to a single acid–base equilibrium between the flavylium cation and a conjugate base, **CB**, defined as the sum of the concentrations of the other species in the network,[5–8] [**CB**] = [**A**] + [**B**] + [**Cc**] + [**Ct**].

$$\mathbf{AH}^+ + H_2O \rightleftharpoons \mathbf{CB} + H_3O^+ \qquad K'_a = K_a + K_h + K_hK_t + K_hK_tK_i \tag{1}$$

In the case of anthocyanins the mole fraction of **Ct** is very small and as a consequence these natural compounds are not suitable as photochromic systems. However, some natural analogues of anthocyanin, such as 3-deoxyanthocyanidins,[9] or dracoflavylium,[10] lead to photochromic systems, as well as the flavylium cation itself[11] and many of its derivatives, Scheme 2.[3]

The photochromism of flavylium compounds is very useful not only for the practical applications mentioned above but also as a powerful tool for the calculation of the rate and equilibrium constants of the flavylium networks, shown in Scheme 1.

In this paper we report the photochromic properties of a recently described anthocyanin analogue, 3′,4′-dihydroxy-7-*O*-β-D-glucopyranosyloxyflavylium chloride (DGF), Scheme 3,[12] as well as a detailed description of the stopped-flow and flash photolysis techniques used to calculate the kinetic and thermodynamic constants of the system.

2. Experimental part

3′,4′-Dihydroxy-7-*O*-β-D-glucopyranosyloxyflavylium (DGF) was synthesized as described elsewhere.[12] All the reagents (>99%) were used without any further purification. The solutions were

[a]*REQUIMTE, Departamento de Química, Faculdade de Ciências e Tecnologia, Universidade Nova de Lisboa, 2829-516 Monte de Caparica, Portugal. E-mail: fp@fct.unl.pt*
[b]*University of Avignon, INRA, UMR408, 84000 Avignon, France. E-mail: Olivier.Dangles@univ-avignon.fr*

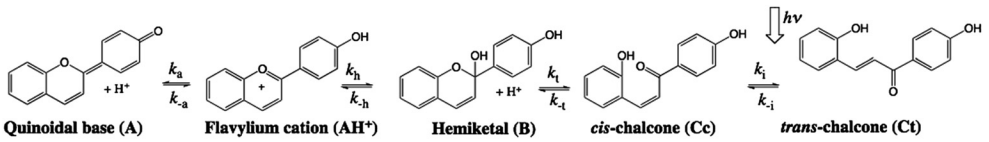

$$K_n = \frac{k_n}{k_{-n}} \quad n=a,h,t,i$$

Scheme 1 Network of reversible chemical reactions of 4′-hydroxyflavylium.

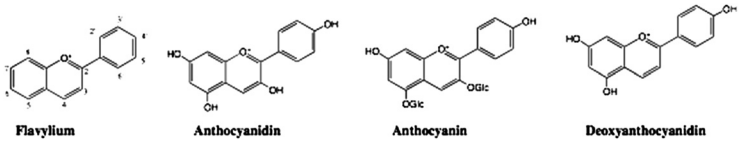

Scheme 2

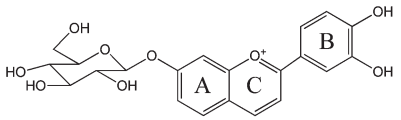

Scheme 3 3′,4′-Dihydroxy-7-*O*-β-D-glucopyranosyloxyflavylium (DGF).

prepared in Millipore water. The pH of the solutions was adjusted by the addition of HCl, NaOH or 0.05 M Universal buffer Theorell–Stenhagen† (final concentration) and was measured on a Radiometer Copenhagen PHM240 pH/ion meter. UV/Vis absorption spectra were recorded on Varian Cary 100 Bio and Varian Cary 5000i spectrophotometers. The stopped-flow experiments were conducted in an Applied Photophysics SX20 stopped-flow spectrometer provided with a PDA.1/UV photodiode array detector with a minimum scan time of 0.65 ms and a wavelength range of 200 nm to 735 nm. Photoexcitation in continuous irradiation experiments was carried out using a xenon/medium pressure mercury arc lamp, and the excitation band (365 nm) was isolated with an interference filter (Oriel). The incident light intensity was measured by ferrioxalate actinometry.[13] The flash photolysis experiments were performed on a Varian Cary 5000i spectrophotometer with a Harrick FiberMate attached to the CUV-ALL-UV 4-way cuvette holder compartment (Ocean Optics) on the external side of the sample holder in order to perform light excitation perpendicular to the analyzing beam and with the sample compartment shielded with black cardboard and black tape. As a pulsed light source a commercially available Achiever 630AF camera flash was used, placed in close contact with the sample holder. The excitation was made with the white light of the camera flash with a time resolution of *ca.* 0.05 s. Further details are described elsewhere.[14]

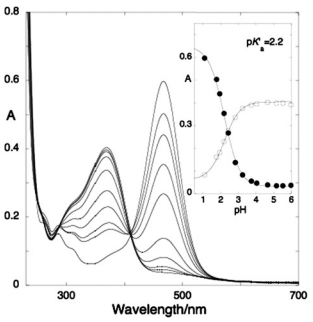

Fig. 1 Absorption spectra of equilibrated solutions of DGF, 3.3×10^{-5} M. *Insert*: pH dependence of the absorbance at 467 nm (●) and 368 nm (○) and fitting according to a single proton transfer, eqn (1).

3. Results and discussion

The determination of all the rate and equilibrium constants was obtained by a step-by-step procedure as follows.

Step 1 – Thermal equilibrium. Determination of K'_a

This important combination of equilibrium constants is obtained from the absorption spectra of equilibrated solutions of the compound, Fig. 1. Fitting was achieved considering a single acid–base equilibrium according to eqn (1); a value of $pK'_a = 2.2$ was obtained.‡

Step 2 – Direct pH jumps. Determination of K_a

Stock solutions of DGF at pH = 1.0 were submitted to pH jumps to higher pH values (direct pH jumps) and the absorption spectra measured by means of a stopped-flow apparatus, 10 ms after the mixing, Fig. 2. Inspection of Fig. 2 shows the formation of the quinoidal base during the mixing time of the

†Citric, phosphoric and boric acids and sodium hydroxide "Küster–Thiel" Tabelle per le analisi chimiche e chimico-fisiche 12° edition Ulrico Hoepli Edition spa 1985, Milano, Italy.

‡The value is lower than the one reported in N. Mora-Soumille, S. Al Bittar, M. Rosa, O. Dangles, Analogs of anthocyanins with a 3′,4′-dihydroxy substitution: Synthesis and investigation of their acid–base, hydration, metal binding and hydrogen-donating properties in aqueous solution, *Dyes and Pigments*, 2013, **96**, 7–15. In the latter work, titration was not extended to highly acidic pHs and experimental conditions (buffer, ionic strength) were different.

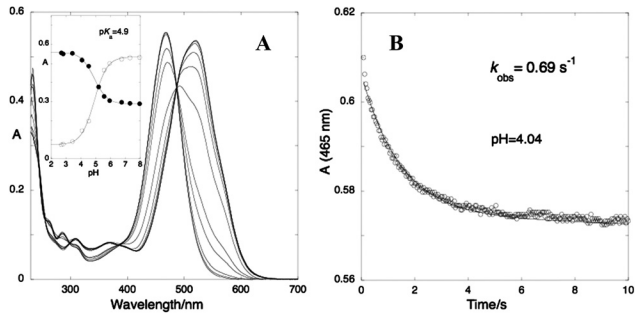

Fig. 2 (A) Spectral variations taken 10 ms after a pH jump from stock solutions of DGF, at pH = 1.0 to higher pH values monitored by stopped flow. Final concentration, 3.3×10^{-5} M. *Insert*: pH dependence of the absorbance at 465 nm (●) and 520 nm (◯) and fitting according to a single proton transfer, eqn (2). (B) Trace at 465 nm obtained upon a direct pH jump from pH = 1.1 to 4.1.

stopped-flow device, as expected from the proton transfer reaction, which is by far the fastest step of the network.

The experimental data from Fig. 2 were fitted using eqn (1) by adjusting the acidity constant, pK_a = 4.9. This corresponds to the first deprotonation in ring B (OH at C4′). A second deprotonation takes place at higher pH values (not determined).§ The spectra taken after 10 ms evolve to the equilibrium through a bi-exponential kinetics, as shown in Fig. 2B, by representing the trace at 465 nm. The first part of this step was fitted with a rate constant of 0.69 s^{-1} for a final pH = 4.1. The thermodynamic equilibrium is reached in a much slower process (the initial part also visible in Fig. 2B) with a rate constant equal to 4.3×10^{-4} s^{-1} (this last process will be analysed in step 5).

The kinetic behaviour of the 3′,4′-dihydroxy-7-*O*-β-D-glucopyranosyloxyflavylium ion is very similar to that of natural anthocyanins.[3,8] When a direct pH jump is carried out, three kinetic steps well separated in the timescale take place. The first is deprotonation according to eqn (2), Fig. 2A,

$$\mathbf{AH}^+ + H_2O \rightleftharpoons \mathbf{A} + H_3O^+ \cdots K_a \quad (2)$$

The second process corresponds to the hydration reaction to give **B**, followed by the tautomerization to form **Cc**, eqn (3) and (4) respectively,

$$\mathbf{AH}^+ + 2H_2O \rightleftharpoons \mathbf{B} + H_3O^+ \cdots K_h \quad (3)$$

$$\mathbf{B} \rightleftharpoons \mathbf{Cc} \cdots K_t \quad (4)$$

These two reactions are much faster than the *cis–trans* isomerization and as a consequence $\mathbf{AH}^+$, **A**, **B** and **Cc** (pseudo) equilibrate.

The thermodynamic equilibrium takes place upon *cis–trans* isomerization, eqn (5),

$$\mathbf{Cc} \rightleftharpoons \mathbf{Ct} \cdots K_i \quad (5)$$

§ At higher pH values DGF is not stable due to oxidation of the catechol unit, so this study was limited to acidic pHs.

The rate of proton transfer follows eqn (6) and cannot be determined unless very fast kinetic techniques, such as temperature jumps,[5] are used (not measured in the present work).

$$k_{1st} = k_a + k_{-a}[H^+] \quad (6)$$

During the second kinetic step, as in Fig. 2B (k_{obs} = 0.69 s^{-1}, pH = 4.1) the pseudo-equilibrium is attained. This process is usually controlled by the hydration reaction, unless $[H^+]$ is very high, which is not the case of the direct pH jumps, and thus eqn (7) is valid.

In eqn (7) the hydration constant (k_h) is multiplied by the mole fraction of $\mathbf{AH}^+$,[5] because in an acidic medium **A** does not directly add water to yield **B**, and the dehydration constant (k_{-h}) is multiplied by the mole fraction of **B**. In other words, in the same way that not all $\mathbf{AH}^+$ is available to give **B** (part of it is in fast equilibrium with **A**), not all **B** is available to give $\mathbf{AH}^+$, due to the establishment of the equilibrium between **B** and **Cc**.

$$k_{2nd} = \frac{[H^+]}{[H^+] + K_a} k_h + \frac{1}{1 + K_t} k_{-h}[H^+] \quad (7)$$

The final equilibrium is reached through eqn (8),

$$k_{3rd} = \frac{K_h K_t}{[H^+] + K_a + K_h(1 + K_t)} k_i + k_{-i} \quad (8)$$

In eqn (8) the term that multiplies the isomerization constant k_i corresponds to the mole fraction of **Cc** available at the (pseudo)equilibrium. This process will be described in step 5.

Step 3 – Reverse pH jumps. Determination of K_t and the respective rate constants

Useful information can be obtained by reverse pH jumps.[15,16] The experiment is constituted by a sequence of two pH jumps: (i) the stock solution of the flavylium cation at pH = 1.0 is submitted to a first pH jump to higher pH values, in the present case to pH 4.98, and after a few minutes to allow the (pseudo)equilibrium to be established (before formation of significant amounts of *trans*-chalcone), (ii) a second pH jump back to acidic pH, in this experiment to pH = 1.53, is performed and the traces of the flavylium appearance monitored by stopped flow, Fig. 3.

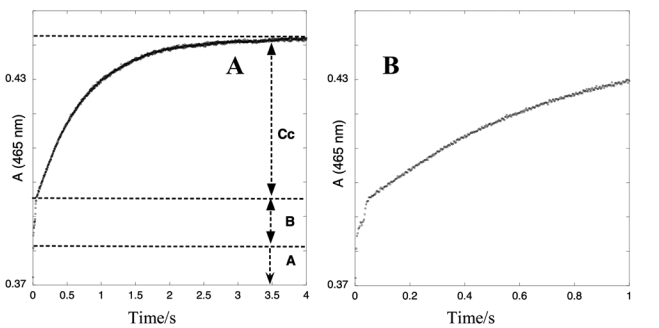

Fig. 3 (A) Reverse pH jump from "fresh" solutions of DGF at pH = 4.98 back to pH = 1.53. The first kinetic process was fitted for a first-order process with a rate constant of 100 s^{-1}, k_t = 3.3 s^{-1}; k_{-t} = 1.45 s^{-1}. (B) The same in a shorter timescale.

The procedure described above allows the formation of the (pseudo)equilibrium for $\mathbf{AH^+}$, **A**, **B** and **Cc**, and when the system reverts back to very acidic pH values, the kinetic process reflects the distribution of the species at this state.

Unlike direct pH jumps, the final pH in reverse pH jumps is very acidic so that the hydration reaction becomes faster than the tautomerization.[17] The initial absorbance change in Fig. 3 is due to the conversion of the quinoidal base present at pH = 4.98 into the flavylium cation, a process which is much faster than the mixing time of the stopped-flow device. The first observed kinetic process is the result of the conversion into the flavylium cation of the hemiketal present at the (pseudo)equilibrium. Finally the slowest process corresponds to the formation of more flavylium cation from the *cis*-chalcone (present at pH = 4.98) through the hemiketal. The observed rate constants from reverse pH jumps correlate with the kinetic rate constants of the system through eqn (9) and (10). The disappearance of **B** is faster than its formation from **Cc** and the hydration kinetics follows eqn (9), which differs from eqn (7) used in the case of the direct pH jumps because the equilibrium between **B** and **Cc** is not attained. As a consequence, k_{-h} is not multiplied by the mole fraction of **B** of the tautomerization equilibrium. On the other hand, the tautomerization kinetics follows eqn (10), which does not contain the term k_t for the same reasons.

$$k_{obs(Taut)} = \frac{[H^+]}{K_a + [H^+]} k_h + k_{-h}[H^+] \quad (9)$$

$$k_{obs(Taut)} = k_{-t} + k_{-t}^{OH}[OH^-] + k_{-t}^{H}[H^+] \quad (10)$$

In eqn (10), the last two terms account for base catalysis and acid catalysis of the tautomerization reaction as defined previously.[15,16]

Fitting of the data in Fig. 3 was achieved with k_{obs1} = 100 s^{-1} and k_{obs2} = 1.4 s^{-1}.¶

The ratio of the amplitudes of the slowest process, eqn (10), and the fastest, eqn (9), is proportional to [**Cc**]/[**B**] and equal to the equilibrium constant K_t = 3.3, and from eqn (10), $k_{-t} + k_{-t}^{H}[H^+]$ = 1.4 s^{-1}, since at acidic pH values base catalysis does not occur. The process described by eqn (9) is more properly studied from the flash photolysis experiments.

Step 4 – Data from flash photolysis. A useful complementary technique

In cases where the system exhibits photochromism it is very useful to use the data from flash photolysis in the determination of the rate and equilibrium constants of the system.

In Fig. 4 are shown the spectral changes that follow the irradiation of DGF at 366 nm and pH = 3.7. The corresponding flash photolysis trace followed at 465 nm is shown in Fig. 5A. Irradiation of **Ct** results in its disappearance and the appearance of $\mathbf{AH^+}$, with a quantum yield, Φ = 0.1. It is known that light absorption by **Ct** leads to the formation of **Cc** in picoseconds.‖ **Cc** is not thermodynamically stable and has two routes for disappearing: backward to **Ct** and forward to $\mathbf{AH^+}$/**A** *via* **B**, see the thermodynamic scheme below. Moreover, the disappearance of **Cc** *via* the forward route could occur by two different regimes according to the pH: (i) for lower pH values, hydration is faster than tautomerization and the system is controlled by the latter reaction as shown in eqn (11). In this equation the backward route is accounted for by rate constant k_i, and the forward route by rate constant k_{-t} and the respective contributions of base catalysis and acid catalysis as reported previously.[16]

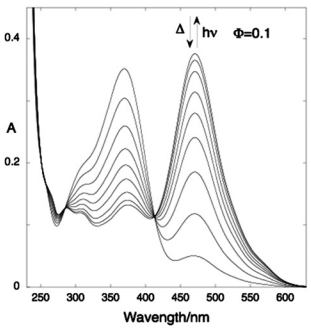

Fig. 4 Irradiation of DGF 3.3 × 10^{-5} M, at 366 nm, pH = 3.7; Φ = 0.1.

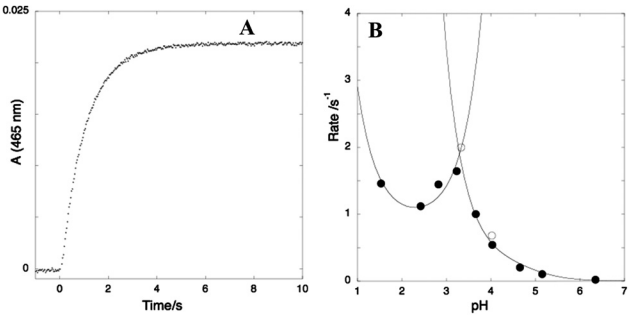

Fig. 5 (A) Flash photolysis trace for the flavylium formation (465 nm) at pH = 3.7. (B) Rate constants for the formation of DGF upon the flash photolysis experiments (●), and from the fastest step after a reverse pH jump, followed by stopped-flow UV-vis spectroscopy (○). The traced line corresponds to the fitting according to eqn (11), the full line to the fitting with eqn (12); $k_i + k_{-t}$ = 0.85 s^{-1}, k_{-t}^{OH} = 5 × 10^{10} M^{-1} s^{-1}, k_{-t}^{H} = 20 M^{-1} s^{-1}; $k_{obs(Hyd)}$ = 3.2 × 10^3 M^{-1} s^{-1} $[H^+]$ + 0.33$[H^+]$/($[H^+]$ + $10^{-4.9}$).

$$k_{obs(Taut)} = k_i + k_{-t} + k_{-t}^{OH}[OH^-] + k_t^{H}[H^+] \quad (11)$$

At higher pH values, the regime changes since hydration becomes the rate-determining step of the forward route, eqn (12).**[6,18] This equation contains the forward term, which is the same as eqn (7) for the direct pH jumps plus the backward term given by k_i in this case multiplied by the mole fraction of **Cc**, since there is time for **B** and **Cc** to equilibrate before reacting.

¶ The error of the first constant is very high, but the order of magnitude of k_{obs1} is consistent with more accurate data of the hydration constant obtained below.

‖ Leydet *et al.* work in progress.

** This equation is different from eqn (20) previously reported in Gago *et al.* (2012),[18] to take into account the quinoidal base derived from DGF.

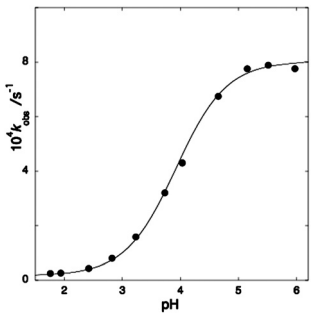

Fig. 6 pH dependence of the rate constant of the slowest process upon a direct pH jump from solutions of DGF at pH = 1.0 to higher pH values.

$$k_{obs(Hyd)} = \frac{k_i K_t}{1 + K_t} + \frac{k_h[H^+]}{[H^+] + K_a} + \frac{k_{-h}[H^+]}{1 + K_t} \quad (12)$$

The pH dependence of the observed rate constants obtained by flash photolysis is represented in Fig. 5. Fitting according to eqn (11) and (12) was achieved for the following parameters: $k_i + k_{-t} = 0.85\ s^{-1}$, $k_t^{OH} = 5 \times 10^{10}\ M^{-1}\ s^{-1}$, $k_t^H = 20\ M^{-1}\ s^{-1}$; $k_{obs(Hyd)} = 3.2 \times 10^3\ [H^+] + 0.33[H^+]/([H^+] + 10^{-4.9})\ M^{-1}\ s^{-1}$.

Having the value of k_t^H, by its substitution in the relation of step 4, $k_{-t} + k_t^H[H^+] = 1.4\ s^{-1}$, a value for $k_{-t} = 0.8\ s^{-1}$ can be obtained and finally a value for $k_t = 2.6\ s^{-1}$ using the value of K_t.

In principle comparison with the data from eqn (10) and (11) would allow us to calculate k_i. However, if the magnitude of this rate constant is small, the difference between the two observed rate constants is smaller than the experimental error, and k_i cannot be determined.

Evidence for $k_i \ll k_{-t}$ is confirmed from the fitting by eqn (12) (higher pH regime) where $k_i K_t/(1 + K_t) < 0^{-2}$, $k_h = 0.33\ s^{-1}$ and $k_{-h}/(1 + K_t) = 3.2 \times 10^3\ M^{-1}\ s^{-1}$.

These values allow us to calculate $k_{-h} = 1.4 \times 10^4\ M^{-1}\ s^{-1}$ and $K_h = 2.5 \times 10^{-5}$ M. Finally from the values of K'_a, K_a, K_h and K_t, a value for $K_i = 75$ is obtained.

Step 5 – Determination of the isomerization rate and equilibrium constants

The last step is the determination of the isomerization rate constants from the representation of the rate constant of the slowest step as a function of pH, eqn (8). The fitting was achieved using the equilibrium constants previously calculated and $k_i = 1.2 \times 10^{-3}\ s^{-1}$. There is not enough accuracy to calculate k_{-i} from the fitting but a value of $k_{-i} = 1.6 \times 10^{-5}\ s^{-1}$ can be obtained from equilibrium constant K_i (Fig. 6).

The values of the equilibrium constants and rate constants are summarized in Tables 1 and 2 respectively.

In order to have an overview of the thermodynamics and kinetics of the 3′,4′-dihydroxy-7-*O*-β-D-glucopyranosyloxyflavylium ion, it is very convenient to construct a thermodynamic energy level diagram.[1] This diagram is easily obtained from the relationship $\Delta G^0 = -RT \ln K$, where $\Delta G°$ is the standard Gibbs energy, R the gas constant, T the absolute temperature and K the equilibrium constant for the respective process, Scheme 4.

Table 1 Equilibrium constants for the structural transformations of 3′,4′-dihydroxy-7-*O*-β-D-glucopyranosyloxyflavylium chloride in a mildly acidic aqueous solution

pK_a'	pK_a	K_h/M	K_t	K_i
2.2	4.9	2.5×10^{-5}	3.3	75

Table 2 Rate constants for the structural transformations of 3′,4′-dihydroxy-7-*O*-β-D-glucopyranosyloxyflavylium chloride in a mildly acidic aqueous solution

k_h/s^{-1}	$k_{-h}/M^{-1}\ s^{-1}$	k_t/s^{-1}	k_{-t}/s^{-1}	k_i/s^{-1}	k_{-i}/s^{-1}
0.33	1.4×10^4	2.6	0.8	1.2×10^{-3}	1.6×10^{-5}

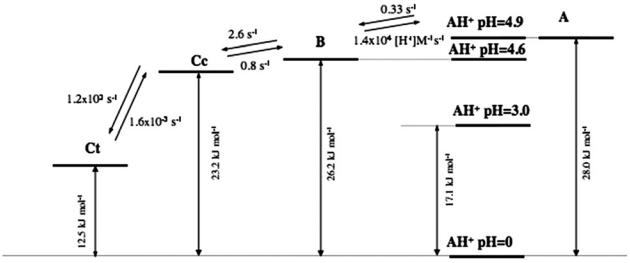

Scheme 4 Energy level diagram and rate constants for DGF.

When this energy level diagram is compared with the one of anthocyanins,[3] it is clear that **B** and **Ct** display higher and lower relative energy levels, respectively.

Conclusion

The first example of the photochromism of a water-soluble glycoside of hydroxylated flavylium ions (easily accessible by chemical synthesis) is presented. Flash photolysis proved to be an indispensable tool to determine the rate and equilibrium constants of the network. The kinetic pattern of 3′,4′-dihydroxy-7-*O*-β-D-glucopyranosyloxyflavylium chloride is quite similar to the one of anthocyanins, since three well separated kinetic steps are observed: proton transfer to form the quinoidal base, hydration and tautomerization leading to a (pseudo) equilibrium and the slowest step, *cis–trans* isomerization to attain the equilibrium. Regarding the thermodynamics, **B** is barely more stable than **A**, which is a difference with common natural anthocyanins (**B** much more stable than **A**). Most of the hemiketal's relative instability seems to be attributable to its fast dehydration into the flat highly stable flavylium ion. This could be the main reason why the colour of 3-deoxyanthocyanidins in a mildly acidic solution is much more stable than that of common anthocyanins.[19,20] It is also remarkable that C-ring opening (**B** → **Cc**) and subsequent isomerization of **Cc** (**Cc** → **Ct**) are both relatively fast. In particular, **Ct** is much

more stable than **Cc** while both stereoisomers display close stability with common anthocyanins (**Cc** even slightly more stable than **Ct**) because of the steric hindrance brought about by the bulky *O*-glycosyl moiety. Consequently, at equilibrium, the only detectable colourless form of 3′,4′-dihydroxy-7-*O*-β-D-glucopyranosyloxyflavylium chloride is the *trans*-chalcone, a favourable situation for obtaining efficient photochromic systems.

References

1 F. Pina, M. J. Melo, M. Maestri, R. Ballardini and V. Balzani, Photochromism of 4′-methoxyflavylium perchlorate. A "write-lock-read-unlock-erase" molecular switching device, *J. Am. Chem. Soc.*, 1997, **119**, 5556–5561.
2 F. Pina, M. J. Melo, M. Maestri, P. Passaniti and V. Balzani, Artificial chemical systems capable of mimicking some elementary properties of neurons, *J. Am. Chem. Soc.*, 2000, **122**, 4496–4498.
3 F. Pina, M. J. Melo, C. A. T. Laia, A. J. Parola and J. C. Lima, Chemistry and applications of flavylium compounds: a handful of colours, *Chem. Soc. Rev.*, 2012, **41**, 869–908.
4 F. Pina, V. Petrov and C. A. T. Laia, Photochromism of flavylium systems. An overview of a versatile multistate system, *Dyes Pigm.*, 2012, **92**, 877–889.
5 R. Brouillard and J.-E. Dubois, Mechanism of structural transformations of anthocyanins in acidic media, *J. Am. Chem. Soc.*, 1977, **99**, 1359–1364.
6 R. Brouillard and B. Delaporte, Chemistry of anthocyanins pigments. 2. Kinetic and thermodynamic study of proton transfer, hydration and tautomerization reactions of malvidin-3-glucoside, *J. Am. Chem. Soc.*, 1977, **99**, 8461–8468.
7 R. Brouillard, B. Delaporte and J.-E. Dubois, Chemistry of anthocyanin pigments. 3. Relaxation amplitudes in pH-jumps experiments, *J. Am. Chem. Soc.*, 1978, **100**, 6202–6205.
8 R. Brouillard and J. Lang, The hemiacetal-*cis*-chalcone equilibrium of malvin, a natural anthocyanin, *Can. J. Chem.*, 1990, **68**, 755–761.
9 M. J. Melo, S. Moura, A. Roque, M. Maestri and F. Pina, Photochemistry of luteolinidin. Write-lock-read-unlock-erase with a natural compound, *J. Photochem. Photobiol.*, 2000, **135**, 33–39.
10 M. J. Melo, M. Sousa, A. J. Parola, J. S. de Melo, F. Catarino, J. Marçalo and F. Pina, Identification of 7,4′-dihydroxy-5-methoxyflavylium in "dragon's blood". To be or not to be an anthocyanin, *Chem.–Eur. J.*, 2007, **13**, 1417–1422.
11 F. Pina, M. J. Melo, M. Maestri, P. Passaniti, N. Camaioni and V. Balzani, Photo- and pH-induced transformations of flavylium cation: "Write-lock-read-unlock-erase" cycles, *Eur. J. Org. Chem.*, 1999, 3199–3207.
12 N. Mora-Soumille, S. Al Bittar, M. Rosa and O. Dangles, Analogs of anthocyanins with a 3′,4′-dihydroxy substitution: synthesis and investigation of their acid–base, hydration, metal binding and hydrogen-donating properties in aqueous solution, *Dyes Pigm.*, 2013, **96**, 7–15.
13 C. G. Hatchard and C. A. Parker, A new sensitive chemical actinometer. 2. Potassium ferrioxalate as a standard actinometer, *Proc. R. Soc. (London), Ser. A*, 1956, **235**, 518.
14 M. Maestri, R. Ballardini, F. Pina and M. J. Melo, An easy and inexpensive flash spectroscopy experiment, *J. Chem. Educ.*, 1997, **74**, 1314–1316.
15 R. A. McClelland and G. H. McGall, Hydration of the flavylium ion. 2. The 4′-hydroxyflavylium, *J. Org. Chem.*, 1982, **47**, 3730–3736.
16 R. A. McClelland and S. Gedge, Hydration of the flavylium ion, *J. Am. Chem. Soc.*, 1980, **102**, 5838–5848.
17 Y. Leydet, R. Gavara, V. Petrov, A. M. Diniz, A. J. Parola, J. C. Lima and F. Pina, The effect of self-aggregation on the determination of the kinetic and thermodynamic constants of the network of chemical reactions in 3-glucoside anthocyanins, *Phytochemistry*, 2012, **244**, 54–64.
18 S. Gago, V. Petrov, A. J. Parola and F. Pina, Synthesis and characterization of 3′-butoxyflavylium derivatives, *J. Photochem. Photobiol., A*, 2012, **244**, 54–64.
19 R. Brouillard, G. A. Iacobucci and J. G. Sweeny, Chemistry of anthocyanin pigments.9. UV-visible spectrophotometric determination of acidity constants of apigeninidin and three related 3-deoxyflavylium salts, *J. Am. Chem. Soc.*, 1982, **104**, 7585–7590.
20 F. Nave, V. Petrov, F. Pina, N. Teixeira, N. Mateus and V. de Freitas, Thermodynamic and kinetic properties of a red wine pigment: catechin-(4,8)-malvidin-3-*O*-glucoside, *J. Phys. Chem. B*, 2010, **114**, 13487–13496.

Food Chemistry 141 (2013) 3268–3272

Contents lists available at SciVerse ScienceDirect

Food Chemistry

journal homepage: www.elsevier.com/locate/foodchem

An innovative grape juice enriched in polyphenols by microwave-assisted extraction

Sheiraz Al Bittar, Sandrine Périno-Issartier *, Olivier Dangles, Farid Chemat

Université d'Avignon et des Pays de Vaucluse, INRA, UMR408, 84000 Avignon, France

ARTICLE INFO

Article history:
Received 4 March 2013
Received in revised form 13 May 2013
Accepted 30 May 2013
Available online 11 June 2013

Keywords:
Grape
Enriched juice
By-product
Microwave hydro-diffusion and gravity
Total phenol content
Anthocyanins

ABSTRACT

The grape juice by-product obtained from grape traditional press was extracted by Microwave Hydrodiffusion and Gravity (MHG); a green extraction technique preliminarily optimized at 1 W/g. The MHG extract (MHGE) was analyzed by HPLC for identification and quantification of anthocyanins and other phenolic compounds. Then, MHGE was added to the natural juice (NJ) to produce an innovative grape juice (IJ). These three juices were evaluated for their total polyphenol content (TPC), total anthocyanin content (TAC) in addition to their sensorial characteristics. MHGE showed the highest values of TPC (21.41 ± 0.04 mg GAE/g DW), TAC (4.49 ± 0.01 μg MVGE/g DW). Moreover, IJ (grape juice enriched with MHGE) was richer in TPC (6.70 ± 0.01 mg GAE/g DW) and TAC (3.96 ± 0.01 μg MVGE/g DW) than NJ (2.90 ± 0.02 mg GAE/g DW and 3.63 ± 0.06 μg MVGE/g DW, respectively).

1. Introduction

Foods and beverages rich in polyphenols are potentially beneficial to human health due to the combination of in vitro antioxidant and cell-signalling effects expressed by these plant products (Hogan, Zhang, Li, Zoecklein, & Zhou, 2009; Luque-Rodríguez, Luque de Castro, & Pérez-Juan, 2007). As such, polyphenols could take part in the prevention of degenerative diseases, especially cardiovascular disease, brought about by diets rich in plant products (Anastasiadi, Pratsinis, Kletsas, Skaltsounis, & Haroutounian, 2010; Mulero, Pardo, & Zafrilla, 2010). Recently, many researches were aimed at developing natural polyphenols in the food industry instead of synthetic antioxidants, such as butylated hydroxytoluene (BHT) and butylated hydroxyanisole (BHA), which are suspected of carcinogenic potential (Spigno & Faveri, 2007). On the other hand, anthocyanins are natural plant pigments (expressing a diversity of bright colours from red to blue) and potent water-soluble antioxidants. Hence, anthocyanins could be also used as natural pigments in the food, cosmetic and pharmaceutical industries (Torskangerpoll & Andersen, 2005).

Grape is one of the fruits with the highest phenolic content. In fact, polyphenols are the most important constituents of grape juice after water (81–86%), sugars (glucose, fructose) and organic (tartaric, malic and citric) acids. However, most of these valuable phenolic compounds remain in by-products after juice processing in agreement with the phenolic distribution in grape as 30% in skin, 60% in seeds and only 10% in pulp (Muñoz, Mestres, Busto, & Guasch, 2008). Consequently, grape juice by-products are rich sources of anthocyanins and other phenolic compounds and have been the material of many extraction works using different grape parts, solvents, and methods (Table 1).

Moreover, it is well known that the phenolic content of grape juices is tightly related to their sensorial qualities in terms of colour and astringency (Gurak, Cabral, Rocha-Leao, Matta, & Freitas, 2010). For instance, the specific sensorial characteristics of red wine are achieved after a maceration step that drastically increases its phenolic content (Revilla & Ryan, 2000). On the other hand, many attempts were carried out to produce a grape juice richer in polyphenols (patent WO/2002/085137; ES 2177465). For example, a postharvest UV-C treatment of grape berries was combined with a maceration step to obtain high resveratrol contents without altering the sensorial properties of juice (Gonzàlez-Barrio, Vidal-Guevara, Tomas-Barberan, & Espin, 2009).

In this article, fresh grape berries were pressed and the juice by-product thus obtained was extracted by the MHG technique without solvent. The corresponding extract (MHGE) was analyzed by HPLC for its phenolic content. Then, MHGE was added to the total volume of natural juice (NJ) to produce an innovative juice (IJ) enriched in polyphenols in agreement with the European legislation (EC No. 258/97). The total polyphenol and anthocyanin contents of MHGE, NJ and IJ were compared as well as their sensorial characteristics.

* Corresponding author. Tel.: +33 0490144426; fax: +33 0490144441.
E-mail address: sandrine.issartier@univ-avignon.fr (S. Périno-Issartier).

0308-8146/$ - see front matter © 2013 Elsevier Ltd. All rights reserved.
http://dx.doi.org/10.1016/j.foodchem.2013.05.134

Table 1
Reported techniques for the extraction of polyphenols and anthocyanins from grape and grape by-products.

Samples	Solvent	Analytes	Methods	References
Grape berries	EtOH, MeOH	Pp[a]	UAE[a]	Anastasiadi et al. (2010)
	Synthetic wine[a]	Pp[a]	Maceration	Muñoz et al. (2008)
	MeOH + HCl	An[a]	SLE[a]	Abert Vian et al. (2006)
Grape skin	EtOH	Pp[a] and An[a]	SLE	Luque-Rodríguez et al. (2007)
Skin, seeds	MeOH + EtOH	Pp[a]	SLE, UAE, MAE[a], HPTE[a]	Casazza et al. (2010)
Grape seeds	MeOH + EtOH	Pp[a] and An[a]	SLE	Orak (2007) and Bozan et al. (2008)
	SC-CO_2	Seed oil	SFE	Passos et al. (2010)
Marc	EtOH + H_2O	Pp[a]	UAE[a]	Evren Oscan (2006)
	EtOH, Ac_2O	Antioxidants	Maceration	Spigno and Faveri (2007)
	Ac_2O, SC–CO_2	Antioxidants	SFE[a] CO_2	Louli et al. (2004)
	EtOH + HCl	Pp[a]	MAE[a]	Pérez-Serradilla and Castro (2011)
White wine marc	EtOH + (HCl, $C_4H_6O_6$)	Pp[a]	Maceration	Makris et al. (2007)
	H_2O	Pp[a]	HVED[a] + SLE	Boussetta et al. (2009)

[a] Pp, polyphenols; An, anthocyanins; SLE, solid–liquid extraction; SFE, supercritical fluids; UAE, ultrasound-assisted extraction; HVED, high voltage electrical discharge pretreatment; MAE, microwave-assisted extraction; HPTE, high pressure temperature extraction; synthetic wine: hydro alcoholic solution of tartaric acid (pH 3.2).

2. Materials and methods

2.1. Material and juice preparing

Two kilograms of red grape (Alphonse Lavallée, *Vitis vinifera,* South Africa) (including berries and stems) was pressed in a vertical laboratory hydraulic press (REUS, $P = 200$ bars, Contes, France). Four hundred grams of press cake was collected and put directly in the microwave reactor to extract a red microwave juice (Fig. 1). IJ was prepared by mixing Nj (86%) with MHGE (14%) which corresponds with the proportion of extracted juices (Table 3). Samples of three juices were freeze-dried before analyze.

2.2. Chemicals

All solvents used for chromatographic purposes were HPLC grade. HPLC water, acetonitrile and formic acid were from VWR (Fontenay-sous-Bois, France). The HPLC grade anthocyanin standard malvidin-3-*O*-glucoside was purchased from Extrasynthese (Lyon, France), while phenolic standards gallic acid, caffeic acid were from Alfa Aesar (Schitigheim, France). Catechin was purchased from Sigma–Aldrich (Saint Quentin Fallavier, France).

2.3. Moisture content determination

Moisture content in grape berries and grape by-product, before and after MHG extraction, was assessed by conventional Dean–Stark distillation according to the American Oil Chemist' Society (AOCS) official methods (Zill-e-Huma, Abert-Vian, & Maingonnat, 2009). A moisture content of 80.9% was determined in the grape fresh berries, vs. 43.8% and 37.0% in the grape by-product before and after extraction, respectively.

2.4. Solvent-free microwave hydrodiffusion and gravity

Microwave hydrodiffusion and gravity was performed in a Milestone EOS-G microwave laboratory oven (Sorisole Bergamo, Italy) consisting in a multimode microwave reactor operating with a frequency of 2.45 GHz and variable power (10 W increments, maximal value: 900 W). The extraction vessels are made of Pyrex and have a capacity of 1 L. During extraction, temperature was continuously monitored and recorded by sensors made of optic fibres inserted both in the plant material and in the reactor. The press cake was heated for 20 min at atmospheric pressure and at a constant power density of 1 W/g without addition of solvent. The direct interaction of microwaves with plant water triggers the release of plant cell contents and the corresponding extract moves downwards under the effect of earth gravity through a spiral condenser outside the microwave cavity. The extraction was continued until no more extract was collected or overheating was detected.

2.5. HPLC analysis

HPLC analyses were performed using a Waters HPLC system (Guyancourt, Versailles, France) consisting of a Waters 600E pump, a Waters 717+ auto sampler, a Waters 2996 photodiode-array detector. The HPLC pumps, automatic sample, column temperature and diode-array system were monitored and controlled by the Waters Empower 2 Chromatography Data software program. The chromatographic separation was carried out on a Purospher Star RP-18 end-capped column (250 × 4 mm I.D.; 5-μm particle size from Merck), with a RP18 guard column (4 × 4 mm I.D.; 5-μm particle size also from Merck). The injection volume was 20 μL. All analyses were repeated at least three times, only mean values were reported.

The wavelength for grape anthocyanin analysis was 530 nm. The end-capped column and guard column were held at 25 °C and the flow rate was set at 1 ml/min. The mobile phase consisted of (A) formic acid/water/acetonitrile (10/60/30) and (B) water/formic acid (90/10) .The solvent gradient used was: 0–40 min, (A) 20% and (B) 80%; 40–50 min, (A) 76% and (B) 24%; 50–53 min, (A) 90% and (B) 10%; 53–60 min, (A) 20% and (B) 80%; 60–65 min, (A) 20% and (B) 80%. Identification of anthocyanins was carried out by comparing their elution order and UV–visible spectra. Quantification was carried out by using malvidin-3-*O*-glucoside (MVG) as an external standard in known concentration. A linear regression of the peak area vs. concentration (0.05–0.35 mg/ml) was used to quantify the compounds in the sample. Anthocyanin concentrations were calculated in mg of malvidin-3-*O*-glucoside equivalent (MVGE)/g of extract dry weight (DW).

The wavelength for total grape phenol analysis was 280 nm. The end-capped column and guard column were held at 27 °C and the flow rate was set at 1 ml/min. The mobile phase consisted of (A) water/formic acid (94/6) and (B) water/acetonitrile/formic acid (65/30/5). The solvent gradient used was: 0–10 min, (A) 99% and (B) 1%; 10–45 min, (A) 70% and (B) 30%; 45–75 min, (A) 20% and (B) 80%; 75–80 min, (B) 100%; 80–85 min, (A) 99% and (B) 1%; 85–90 min, (A) 99% and (B) 1%. Identification of phenolic compounds was carried out by comparing the elution order and

UV–visible spectra. External standards (caffeic acid, gallic acid, catechin) of known concentration (0.1–1 mg/ml) were used for calibration through linear regressions. Final concentrations were expressed in mg/g DW.

2.6. Determination of total phenolic contents (TPC)

TPC was estimated by the Folin–Ciocalteu method (Zill-e-Huma et al., 2009) using a kit (SEPPAL (Isitec-lab), France) especially suitable for food products. This kit includes: Reagent A (modified Folin–Ciocalteu reagent), reagent B (alkaline buffer) and a gallic acid solution (3 g/L). A small volume (20 μL) of H_2O (blank), gallic acid solution (standard) or the extract (sample) was mixed with (2 ml) of reagent A. After 1 min, 1 ml of reagent B was added. The mixtures were allowed to stand for 30 min in the dark at room temperature. Then, their absorbance was measured at 760 nm with a diode-array Hewlett–Packard 8453 spectrophotometer. TPC were calculated by using the following formula:

$$TPC = 3 \times (A_s - A_0)/(A_{st} - A_0)$$

where A_s was the sample absorbance, A_0 the blank absorbance and A_{st} the standard absorbance. Results were expressed as mg gallic acid equivalent (GAE)/g DW.

2.7. Determination of total anthocyanin contents (TAC)

TAC of extracts was determined by measuring the visible absorbance at 530 nm against a blank of 10% formic acid in distilled water. A calibration curve was built with MVG solutions (25, 12.5, 6.25, 3.125 μg/ml in 10% aqueous formic acid). All samples were diluted in 10% aqueous formic acid until the absorbance was within the calibration limits. The results are expressed in mg MVGE/g DW.

2.8. Colour measurements

The colour of juices was measured by using the CIE $L^*a^*b^*$system (CIE 1986) and a Minolta CR 400/410 colorimeter equipped with a pulsed Xe lamp. The (L^*, a^*, b^*) space models the human eye perception in terms of luminance and chrominance. L^* expresses the luminance and changes from 0 for black to 100 for white, a^* and b^* represent the green–red axis and blue–yellow axis respectively and vary from −60 to +60. Any colour can be expressed in the L^*, a^*, b^* rectangular coordinate system. Hue angle h_{ab} is defined as: $h_{ab} = \arctan(b^*/a^*)$. Remarkable h_{ab} values are: 0° (red), 270° (or −90°, blue), 90° (yellow), 45° (orange) and 180° (green). Colour assessment of the samples was carried out after colorimeter calibration with a white plaque. The fresh samples (before freeze-drying) were placed in a special quartz cell for measurements in triplicate. Mean values were reported.

2.9. Sensorial analysis

The sensory analyses of the three fresh juices (MHGE, NJ, IJ) were conducted by a panel consisting of 15 graduate students from Avignon University, France. The subjects were seated in sensory booths with appropriate ventilation and lighting. The samples were presented to each panellist in polystyrene cups. For the three juices, the following attributes were evaluated: colour, smell, acidity, astringency and global acceptance. For overall quality, the scale ranged from 0 (weakest attribute) to 10 (strongest attribute) and a score of 5 corresponded to an ideal perception. The panellists gave their preferences for each sample on a hedonic scale (0–10). The average of the points was calculated for each attribute.

3. Results and discussion

3.1. Proposed MHG mechanism

In MHG extraction, the two transport phenomena, heat and mass transfer, are in the same direction from the inside of the extracted material to the bulk reactor (Abert-Vian, Tomao, Coulomb, Lacombe, & Dangles, 2006). Consequently, the microwave-assisted extraction process can be carried out without solvent. In this case, heat is dissipated volumetrically within the irradiated medium, and heat transfer occurs from the sample to the colder environment. By contrast, in conventional solvent extraction, heat is transferred from the heating medium to the interior of the sample and mass transfer occurs from the inside to the outside. In conventional heating, heat transfer depends on thermal conductivity, on the temperature gradient across the sample, on convection currents in fluids. As a result, the temperature increase is often rather slow. By contrast, in microwave heating, due to the volumetric heating effect, much faster temperature increases can be obtained, depending on the microwave power and the dielectric loss factor of the material being irradiated. The juice situated inside the cells is extracted by hydrodiffusion (extraction and diffusion) which is intensified by microwave heating.

3.2. Microwave heating and extraction kinetics

This efficient microwave absorption results in a rapid increase in temperature leading to the rupture of cells by the *in situ* water, followed by the release of crude juice and steam. The heating phenomenon proceeding in the centre of the grape by-product was detected by a temperature sensor including optic fibres. Different phases in the temperature and mass variations were distinguished (Fig. 2). During the first phase (phase A, induction period), no

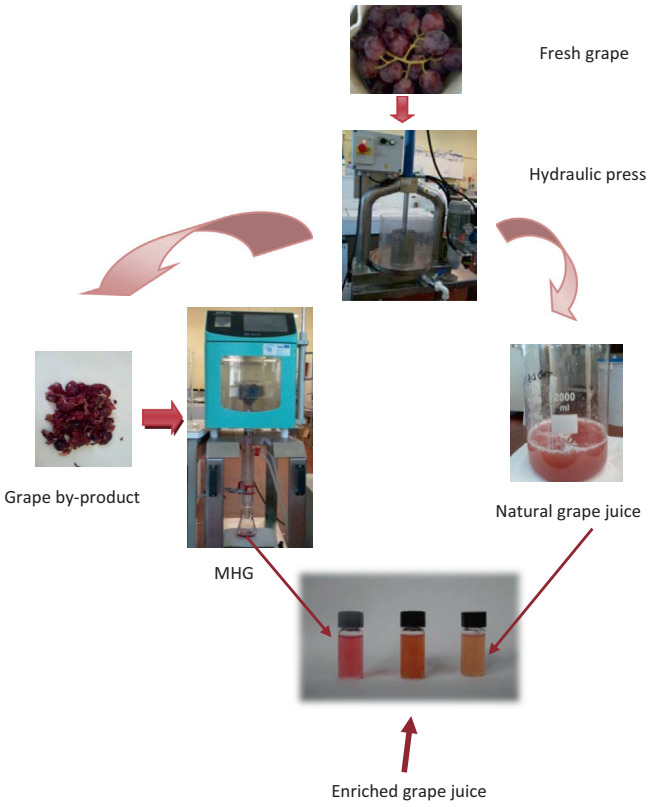

Fig. 1. The preparation process of polyphenol-supplemented grape juice.

Table 2
HPLC identification and quantification of anthocyanins and other phenols in MHGE.

Anthocyanins at 530 nm	Quantity[a]	Other phenols at 280 nm	Quantity[b]
Delphinidin-3-*O*-glucoside	0.26	Gallic acid	0.16
Cyanidin-3-*O*-glucoside	0.06	Catechin	4.70
Petunidin-3-*O*-glucoside	0.31	Caffeic acid	1.96
Peonidin-3-*O*-glucoside	0.89		
Malvidin-3-*O*-glucoside	2.15		
Malvidin-3-*O*-(6-*O*-acetyl)glucoside	ND		

[a] Anthocyanin concentration expressed in mg MVGE/DW.
[b] Phenolic acid concentration expressed in mg/g DW.

Table 3
Total comparison between MHGE, NJ and IJ in yield, Brix degree, pH, colour, TPC and TAC.

Sample	Weight (g)	Volume (ml)	Brix degree	pH	Colour: L^*, h_{ab}	TPC[a]	TAC[b]
MHGE	185.31	184	5	4.03	16.54, 11.86°	21.41 ± 0.01	4.49 ± 0.01
NJ	1397.9	1250	14	4.10	26.37, 65.5°	2.90 ± 0.02	3.63 ± 0.06
IJ	1583.21	1434	10	4.09	23.48, 12.3°	6.7 ± 0.002	3.96 ± 0.01

[a] TPC is expressed in mg GAE/g DW.
[b] TAC is expressed in mg MVGE/g DW.

increase in temperature was observed in the grape by-product (initial temperature = 0 °C). Moreover, no mass loss in of plant material was observed. This phase ended with the appearance of the first drop of water outside the microwave cavity. During the next phase (phase B), the water inside the plant material was heated up, then diffused out of plant matrix and moved downward under the influence of earth gravity. At this point, the temperature reached a plateau at 100 °C and remained constant until the complete extraction of unbound water. A sharp decline in mass of plant material was observed during this phase. At last, when there was only tightly bound water left, the temperature started to further increase, which led to the burning phase (phase C) and no further mass loss was observed.

3.3. Identification and quantification of MHGE by HPLC

HPLC analyses allowed the identification of seven different anthocyanins at 530 nm (Table 2). Whatever the microwave power used, the most abundant anthocyanin in the grape by-product extract was malvidin-3-*O*-glucoside in agreement with the literature (Abert-Vian et al., 2006). The other anthocyanins identified were peonidin-3-*O*-glucoside, petunidin-3-*O*-glucoside, delphinidin-3-*O*-glucoside and malvidin-3-*O*-(6-*O*-*p*-coumaryl) glucoside. Cyanidin-3-*O*-glucoside and malvidin-3-*O*-(6-*O*-acetyl) glucoside were also detected in traces in MHGE. The total anthocyanin content estimated by HPLC was consistent with the value determined by UV–visible spectroscopy (Luque-Rodríguez et al., 2007). In addition to anthocyanins, gallic acid, caffeic acid and catechin were the main phenolic compounds identified and quantified in MHGE at 280 nm (see Table 2).

3.4. Total juice evaluation

The Folin–Ciocalteu method allowed a good discrimination between MHGE, NJ and IJ. MHGE showed a higher TPC (21.41 ± 0.04 mg GAE/g DW) than NJ (2.90 ± 0.02 mg/g DW) and IJ (6.40 ± 0.01 mg/g DW). By contrast, no large differences in total

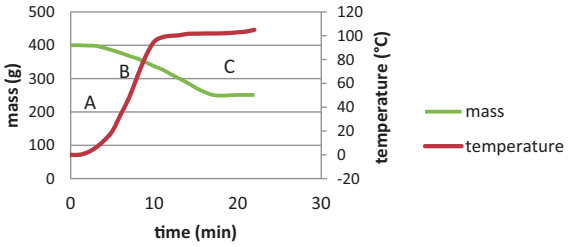

Fig. 2. Mass and temperature variations in MHG extraction at optimized power (400 W): A = heating phase, B = extracting phase and C = burning phase.

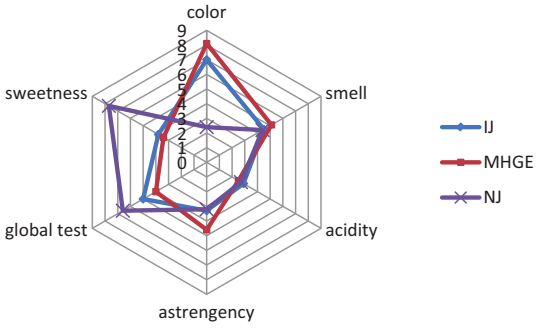

Fig. 3. Sensorial tests investigated in three jus MHGE, IN and NJ.

anthocyanin content were observed between the three juices (Table 3). In a previous works (Orak, 2007)], reported that the correlation between antioxidant activity and TPC was more significant than with TAC. Thus, a high antioxidant activity of MHGE is expected due to its high content in colourless polyphenols.

MHGE, NJ and IJ were also compared by their physical characteristics as weight, volume, Brix degree, pH and colour (Table 3). The three juices have close pH values but different sweetness values as expressed by Brix degrees. As evidenced by a h_{ab} value near 0°, the colour of the natural juice supplemented with the MHG extract was darker and redder than the natural juice ($h_{ab} \approx 45°$).

3.5. Sensorial tests

The results of sensorial tests for the three juices (Fig. 3) are correlated with their physical characteristics. The panellists found NJ sweeter than the other juices, whereas the astringency, acidity, smell and global evaluation of the three juices approximately gave the same attributes. Otherwise, the colour of the supplemented juice (IJ) was more attractive than that of the natural juice, which is an important point as colour is typically the first sensorial quality that attracts attention and influences the consumer's choice.

4. Conclusion and perspectives

MHG is a green extraction method that offers important advantages like short extraction time (20 min), low energy input and no requirements in solvents. This study proved the efficiency of MHG in the extraction of polyphenols and anthocyanins from grape by-products. Moreover, the juice supplemented in MHG extract had a more attractive colour and a higher polyphenol content while retaining acceptable organoleptic characteristics. Thus, MHG comes up as a sustainable food process that offers opportunities to meet the growing demands for healthier food products.

Acknowledgements

This scientific study was carried out as part of the Alcotra Eco-Extraction Transfrontalière project framework which brings together private and public-sector stakeholders (University of Avignon, European University of Fragrances & Flavours, FranceAgriMer, University of Turin and Technogranda). We would also like to warmly thank our co-funding partners, i.e. the European Union (FEDER), the French and Italian governments, the Piedmont region as well as ADEME and the Conseil Régional Provence-Alpes-Côtes d'Azur through the Etat-Region-ADEME framework programme. Their financial support has helped partners successfully achieve the project's scientific objectives.

References

Abert-Vian, M., Tomao, V., Coulomb, P. O., Lacombe, J. M., & Dangles, O. (2006). Comparison of the Anthocyanin composition during ripening of Syrah grapes grown using organic or conventional agricultural practices. *Journal of Agricultural and Food Chemistry, 54*, 5230–5235.

Anastasiadi, M., Pratsinis, H., Kletsas, D., Skaltsounis, A.-L., & Haroutounian, S. A. . *Food Research International, 43*, 805–813.

Boussetta, N., Lanoisellé, J.-L., Bedel-Cloutour, C., & Vorobiev, E. (2009). Extraction of soluble matter from grape pomace by high voltage electrical discharges for polyphenol recovery: Effect of sulphur dioxide and thermal treatments. *Journal of Food Engineering, 95*, 192–198.

Bozan, B., Tosun, G., & Özcan, D. (2008). Study of polyphenol content in the seeds of red grape (Vitis vinifera L.) varieties cultivated in Turkey and their antiradical activity. *Food Chemistry, 109*, 426–430.

Casazza, A. A., Aliakbarian, B., Mantegna, S., Cravotto, G., & Perego, P. (2010). Extraction of phenolics from Vitis vinifera wastes using non-conventional techniques. *Journal of Food Engineering, 100*, 50–55.

Gonzàlez-Barrio, R., Vidal-Guevara, M. L., Tomas-Barberan, F. A., & Espin, J. C. (2009). *Innovative Food Science & Emerging Technologies, 10*, 374–382.

Gurak, P. D., Cabral, L. M. C., Rocha-Leao, M. H. M., Matta, V. M., & Freitas, S. P. . *Journal of Food Engineering, 96*, 421–426.

Hogan, S., Zhang, L., Li, J., Zoecklein, B., & Zhou, K. (2009). *LWT – Food Science and Technology, 42*, 1269–1274.

Louli, V., Ragoussis, N., & Magoulas, K. (2004). Recovery of phenolic antioxidants from wine industry by-products. *Bioresource Technology, 92*, 201–208.

Luque-Rodríguez, J. M., Luque de Castro, M. D., & Pérez-Juan, P. (2007). *Bioresource Technology, 98*, 2705–2713.

Makris, D. P., Boskou, G., & Andrikopoulos, N. K. (2007). Recovery of antioxidant phenolics from white vinification solid by-products employing water/ethanol mixtures. *Bioresource Technology, 98*, 2963–2967.

Mulero, J., Pardo, F., & Zafrilla, P. (2010). *Journal of Food Composition and Analysis, 23*, 569–574.

Muñoz, S., Mestres, M., Busto, O., & Guasch, J. (2008). *Analytica Chimica Acta, 628*, 104–110.

Orak, H. H. (2007). *Scientia Horticulturae, 111*, 235–241.

Oscan, E. (2006). Ultra sound assisted extraction of phenolics from grapes pomace, The graduate school of natural and applied sciences, Middle east technical university.

Passos, C. P., Silva, R. M., Silva, F. A. D., Coimbra, M. A., & Silva, C. M. (2010). Supercritical fluid extraction of grape seed (Vitis vinifera L.) oil. Effect of the operating conditions upon oil composition and antioxidant capacity. *Chemical Engineering Journal, 160*, 634–640.

Pérez-Serradilla, J. A., & de Castro, M. D. L. (2010). Microwave-assisted extraction of phenolic compounds from wine lees and spray-drying of the extract. *Food Chemistry, 124*, 1652–1659.

Revilla, E., & Ryan, J. M. (2000). *Journal of Chromatography A, 881*, 461–469.

Spigno, G., & Faveri, D. M. D. (2007). *Journal of Food Engineering, 78*, 793–801.

Torskangerpoll, K., & Andersen, M. (2005). *Food Chemistry, 89*, 427–440.

Zill-e-Huma, M., Abert-Vian, J. F., & Maingonnat, F. (2009). Chemat. *Journal of Chromatography A, 1216*, 7700–7707.

Abstract

This work deals with the chemical synthesis of simple analogs of anthocyanins, the main class of water-soluble natural pigments. Eleven flavylium ions with hydroxyl, methoxyl and β-D-glucopyranosyloxyl substituents at positions 4', 5 and 7 have been prepared by straightforward chemical procedures. Moreover, the two main 3-deoxyanthocyanidins of red sorghum, apigeninidin (APN) and luteolinidin (LTN), have been synthesized in a one-step protocol. The physicochemical properties and antioxidant activity are investigated for 3',4',7-trihydroxyflavylium chloride (P1), its 7-O-β-D-glucoside (P2) and 3',4',5,7-tetrahydroxyflavylium chloride (LTN). Owing to their catechol B-ring, they rapidly bind Fe^{III}, Al^{III} and Cu^{I}, more weakly interact with Fe^{II} while promoting its autoxidation to Fe^{III}. Following Cu^{II} binding, the pigments undergo oxidation. Aglycones P1 and LTN are moderate ligands of human serum albumin (HSA) with chalcones having a higher affinity for HSA than the corresponding colored forms. The antioxidant activity of P1, P2 and LTN is investigated via two tests: reduction of the stable DPPH radical and inhibition of heme-induced lipid peroxidation (a model of postprandial oxidative stress in the stomach). Aglycones P1 and LTN (especially in their colorless chalcone form) are more potent than glucoside P2.

Résumé

Ce travail porte sur la synthèse chimique d'analogues simples d'anthocyanes, une classe majeure de pigments naturels solubles dans l'eau. Onze ions flavylium substitués par des groupements hydroxyl, méthoxyl et β-D-glucopyranosyloxyl en positions 4', 5 et 7 ont été préparés en utilisant des procédures simples. De plus, les deux principales 3-désoxyanthocyanidines du sorgho rouge, l'apigéninidine (APN) et la lutéolinidine (LTN), ont été synthétisées en une seule étape. Les propriétés physico-chimiques ainsi que l'activité antioxydante ont été étudiées pour le chlorure de 3',4',7-trihydroxyflavylium (P1), son 7-O-β-D-glucoside (P2) et le chlorure de 3',4',5,7-tétrahydroxyflavylium (LTN). Grâce à leur noyau catéchol, ces pigments complexent rapidement Fe^{III}, Al^{III} and Cu^{I} et ne se lient que faiblement à Fe^{II} tout en stimulant son autoxydation en Fe^{III}. Suite à la complexation de Cu^{II}, les pigments subissent une oxydation. Les aglycones P1 et LTN sont des ligands modérés de l'albumine de sérum humain (HSA) et leurs chalcones ont montré une plus grande affinité pour la HSA que leurs formes colorées. Leur capacité antioxydante a été démontrée par le test de réduction du radical stable DPPH et par l'inhibition de la peroxydation lipidique induite par le fer héminique, un modèle de stress oxydant postprandial dans l'estomac. Les aglycones P1 et LTN (particulièrement, dans leur forme incolore chalcone) sont plus efficaces que le glucoside P2.